Sergey Vasil'yevich Klyuev
Alexander Vasil'yevich Klyuev *Editors*

Proceedings of the International Conference Industrial and Civil Construction 2021

Springer

Lecture Notes in Civil Engineering

Volume 147

Lecture Notes in Civil Engineering (LNCE) publishes the latest developments in Civil Engineering - quickly, informally and in top quality. Though original research reported in proceedings and post-proceedings represents the core of LNCE, edited volumes of exceptionally high quality and interest may also be considered for publication. Volumes published in LNCE embrace all aspects and subfields of, as well as new challenges in, Civil Engineering. Topics in the series include:

- Construction and Structural Mechanics
- Building Materials
- Concrete, Steel and Timber Structures
- Geotechnical Engineering
- Earthquake Engineering
- Coastal Engineering
- Ocean and Offshore Engineering; Ships and Floating Structures
- Hydraulics, Hydrology and Water Resources Engineering
- Environmental Engineering and Sustainability
- Structural Health and Monitoring
- Surveying and Geographical Information Systems
- Indoor Environments
- Transportation and Traffic
- Risk Analysis
- Safety and Security

To submit a proposal or request further information, please contact the appropriate Springer Editor:

– Mr. Pierpaolo Riva at pierpaolo.riva@springer.com (Europe and Americas);
– Ms. Swati Meherishi at swati.meherishi@springer.com (Asia - except China, and Australia, New Zealand);
– Dr. Mengchu Huang at mengchu.huang@springer.com (China).

All books in the series now indexed by Scopus and EI Compendex database!

More information about this series at http://www.springer.com/series/15087

Sergey Vasil'yevich Klyuev ·
Alexander Vasil'yevich Klyuev
Editors

Proceedings of the International Conference Industrial and Civil Construction 2021

Springer

Editors
Sergey Vasil'yevich Klyuev
Belgorod State Technological University
Belgorod, Russia

Alexander Vasil'yevich Klyuev
Belgorod State Technological University
Belgorod, Russia

Preface

The International Scientific Conference "Industrial and Civil Construction 2021" is held from January 18 to 19, 2021, on the basis of Federal State Budgetary Educational Institution of Higher Education Belgorod State Technological University named after V.G. Shukhov. Industrial and Civil Construction 2021 is an annual conference.

The sessions organized within the framework of the conference are united by the common idea of the need to exchange experience and new knowledge between students, scientists, teachers, and representatives of the industrial sphere in the field of industrial and civil construction, organization, and production of building materials, taking into account the sustainable development of scientific achievements in the environmental aspect of their application to their further cooperation and the formation of scientific collaborations in promising areas in the field of construction and building materials science.

The conference is held on the three followings topics:

Session 1. Building Materials, Building Constructions.
Session 2. Structural Mechanics and Theory of Structures, Industrial and Civil Construction.
Session 3. Environmental Engineering and Sustainability.

The subject of the session "Building Materials, Building Constructions" is devoted to an overview of modern achievements in design issues, the organization of all types of construction work, the production of building materials, their properties, and practical application.

The session "Structural Mechanics and Theory of Structures, Industrial and Civil Construction" is focused on the latest advances and theoretical and practical results in structural mechanics applied to industrial and civil construction.

The session "Environmental Engineering and Sustainability" highlighted environmental aspects in the construction industry, building materials science, and production of building materials from the point of view of their effectiveness and sustainability.

308 participants from 27 regions of the Russian Federation and 24 participants from 7 countries of the near abroad (Iraq, Kazakhstan, the Ukraine, Uzbekistan, Tajikistan, Belarus, and Vietnam) were registered for the conference in 2021.

The reports presented at the conference contain materials both of theoretical orientation in the form of ideas, projects, concepts, and hypotheses, and experimental (results, patterns) and practical-applied (examples of the practical application and functioning of the created materials, objects, ways of their solution and optimization).

A significant proportion of research materials was prepared within the framework of implementation of state and national programs in the scientific field as a grant, federal targeted programs, decrees of the Government of the Russian Federation, and other programs.

All articles were peer reviewed by specialists with a degree. 50 best scientific manuscripts corresponding to the profile of the conference and reflecting the results of theoretical and experimental studies of the authors are recommended for publication.

Annual holding of such conferences is planned to be organized on the main topics of the construction industry.

<div align="right">

Sergey Vasil'yevich Klyuev
Alexander Vasil'yevich Klyuev

</div>

Organization

Organizing Conference Committee

Evtushenko E. I.	Doctor of Engineering Sciences (Advanced Doctor), Professor, Belgorod State Technological University named after V.G. Shukhov, Russia
Ayzenshtadt A. M.	Doctor of Chemical Sciences (Advanced Doctor), Professor, Northern (Arctic) Federal University named after M.V. Lomonosov, Arkhangelsk, Russia
Lesovik V. S.	Doctor of Engineering Sciences (Advanced Doctor), Professor, Corresponding Member of RAASN, Belgorod State Technological University named after V.G. Shukhov, Russia
Vatin N. I.	Doctor of Engineering Sciences (Advanced Doctor), Professor, Peter the Great St. Petersburg Polytechnic University, Russia

Scientific Conference Committee

Amir Abdulrahman	Iraq—Doctor of Engineering, Professor, Anbar University
Ali Belloush	Morocco—Ph.D., Professor, Rector, Funtius Institute
Kovtun M. A.	Australia—Ph.D.
Kozhukhova M. I.	The USA—Ph.D., University of Wisconsin-Milwaukee
Loganina V. I.	RF—Doctor of Engineering Sciences (Advanced Doctor), Professor, Penza State University of Architecture and Construction

Lukuttsova N. P.   RF—Doctor of Engineering Sciences (Advanced
                           Doctor), Professor, Bryansk State Engineering
                           Technological University
Nevzorov A. L.   RF—Doctor of Engineering Sciences (Advanced
                           Doctor), Professor, Northern (Arctic) Federal
                           University named after M.V. Lomonosov
Nenad Stoykovich   Serbia—Ph.D., Nish Higher Technical School
                           of Vocational Education
Naumov A. E.   RF—Candidate of Engineering Sciences (Ph.D.),
                           Associate Professor, Belgorod State
                           Technological University named after
                           V.G. Shukhov
Elyan Issa Jamal Issa   Jordan—Ph.D., Amman University
Salyamova K. D.   Uzbekistan—Doctor of Engineering Sciences
                           (Advanced Doctor), Professor, Institute
                           of Mechanics and Seismic Stability of
                           Structures of the Academy of Sciences of the
                           Republic of Uzbekistan
Sovann Chin   Cambodia—Ph.D.
Strokova V. V.   RF—Doctor of Engineering Sciences (Advanced
                           Doctor), Professor, Belgorod State
                           Technological University named after
                           V.G. Shukhov
Suleymanova L. A.   RF—Doctor of Engineering Sciences (Advanced
                           Doctor), Professor, Belgorod State
                           Technological University named after
                           V.G. Shukhov
Tabet Salem Al-Azab   Yemen—Ph.D.
Fisher H. B.   Germany—Professor, Bauhaus-University
                           of Weimar
Hisham Almama   Syria—Ph.D., Damascus University
Hussein Motawi   Egypt—Ph.D., Professor, Vice-Rector,
                           Damanhour University
Eknik Jürgen   Switzerland—Ph.D., Professor, Executive
                           Director of a Swiss Company, Perfomance
                           Selling Academy Zurich Area GmbH
Shakarna Mahmoud   Palestine—Ph.D.
  Husni Ibrahim

All conference participants express deep gratitude to the science team.

Contents

The Choice of Filler in the Formulation of Sol-Silicate Paints

V. I. Loganina[1]([envelope]) [ID], S. V. Klyuev[2] [ID], and Y. B. Mazhitov[3] [ID]

[1] Penza State University of Architecture and Construction,
440028 Penza Street Titova, Russia
loganin@mail.ru
[2] Belgorod State Technological University named after V.G. Shukhov,
Kostyukov Street, 46, Belgorod 308012, Russia
[3] West Kazakhstan Agrarian Technical University named after Zhangir Khan,
Uralsk, Kazakhstan

Abstract. It is proposed to apply thermodynamic criteria when choosing a filler in paint formulations - critical surface tension, Hamaker constant. The values of the critical surface tension of a liquid (ethanol solutions with different water content) at the interface with a solid (different fillers) are calculated. The energy of interaction between the filler particles was estimated by the value of the Hamaker constant. Determined that microcalcite has a higher critical surface tension, compared to other fillers. It is shown that when calcite is used as a filler, the inter particle interaction is enhanced. It was found that the use in sol silicate paints as a filler of calcite contributes to obtaining a higher cohesive strength of coatings due to an increase in the contribution of dispersion forces. Based on the study, the numerical values of the Hamaker constant and the critical value of the surface tension of various fillers were obtained. It allowed makes it possible to choose the optimal type of filler. It has been established that there is a linear relationship between the value of the interaction energy between the filler particles (Hamaker constant) and the tensile strength of the coatings. A mathematical model of cohesive strength is obtained depending on the value of the Hamaker constant.

Keywords: Sol- silicate paint · Filler · Critical surface tension · Hamaker constant · Cohesive strength

1 Introduction

Silicate paints are widely used for finishing exterior and interior walls of buildings [1–3]. Given the increasing requirements for the quality of finishing and the fact that coatings based on silicate paints have insufficient crack resistance, it is urgent to develop methods for modifying liquid glass, which will allow you to obtain coatings with higher protective and decorative properties. The analysis of patent and scientific and technical literature shows the prospects of using polysilicate solutions as a film-forming agent, which provides higher performance properties of coatings [4–6]. In works [7, 8] it is indicated that solutions of sodium polysilicate with a modulus of 6–8 can be obtained by adding a solution of water glass to a concentrated silica sol. In this case, gelation is observed at the

initial stages of the process. Such solutions do not withstand long-term storage. The peculiarities of obtaining polysilicate solutions impose certain restrictions and requirements for the development of paint and varnish compositions based on it.

The technological process of creating sol-silicate paint is complicated and it is not always possible to achieve the required characteristics. In this regard, the development of the development of a formulation of a sol-silicate paint, the coatings on the basis of which are characterized by increased physical, technological and operational characteristics, is urgent. When developing a formulation of a sol-silicate paint, the question of choosing a filler is of particular importance.

Fillers must have a certain particle size distribution, particle shape. Fillers should have good wettability, dispersibility, low hardness and density, low oil absorption and high whiteness. However, in our opinion, when developing the formulation of paints and varnishes, the energetic characteristics of the filler should also be taken into account - surface tension and the energy of interaction between filler particles [12].

2 Materials and Research Methods

During the development of the sol-silicate paint, we used the sol of silicic acid Nanosil 20 and Nanosil 30, liquid glass with a silicate modulus M = 2.78–3.29. A polysilicate solution was obtained by mixing water glass with a silicic acid sol [9–11].

Since the surface properties of the filler particles will have an important influence on the physical and mechanical characteristics of paint and coatings based on it, the choice of the filler was based on thermodynamic criteria (critical surface tension, Hammaker constant) [13, 14].

As fillers used microcalcite MK-2, microtalk MT-GSHM, - marshalite brand "A". The value of the surface tension of the solid (filler) was determined using the critical surface tension of the liquid (K) at the boundary with the solid (G. A. Zisman's method) [15, 16]. The averaged curve $\cos\theta = f(\sigma_{lig})$ was extrapolated to $\cos\theta = 1$ and the critical value of surface tension c was determined, which is an characteristic of the surface energy of filler [17–19].

The energy of interaction between the filler particles was estimated by the value of the Hamaker constant calculated by the equation:

$$\cos\theta - 1 = \frac{A^*}{12 h_{min} \sigma_{lig}} \tag{1}$$

where h_{min} is the smallest film thickness that corresponds to the Van der Waals distance (0.24 nm);

σ_{lig} - liquid surface tension;

A * is the complex Hamaker constant for the interaction of a liquid with a solid at the boundary with air.

To determine the Hamaker constant, the graphical dependence $\cos\theta - 1 = f(1/\sigma_{lig})$ was built.

Ethanol solutions with different water fraction content were used as liquid. The angle of wetting of the filler surface was measured at a temperature of 20 °C on a KRUSS Easy Drop installation. Samples were prepared by pressing the corresponding filler under a load of 1.5 kPa into a metal mold 10 mm in diameter.

The determination of the surface tension of a liquid was carried out by the method of counting drops (stalagmometric method) [20]. All experiments were carried out at a temperature of 22 ± 1 °C.

The work of adhesion of the binder to the filler was calculated in accordance with the thermodynamic equation of Dupre – Young

$$W_a = \sigma(1 + cos\theta) \tag{2}$$

where W_a is the work of adhesion

σ is surface tension;

θ - equilibrium contact angle

The wetting work W_{wet} was determined by the ratio:

$$W_{wet} = \sigma cos\theta \tag{3}$$

In the course of further research, the tensile strength of the coatings was determined. Tensile strength (cohesive strength) was determined in accordance with GOST 18299-72 * "Paints and varnishes. Method for determining ultimate tensile strength, elongation at break and elastic modulus" on a tensile testing machine IR 5057-50. The method is based on stretching a test specimen $0.7 \times 10 \times 50$ mm in size to rupture at a deformation rate of 1 mm/min. The film samples were fixed in the clamps of the tensile testing machine so that its longitudinal axis was located in the direction of tension, and the applied forces acted uniformly over the entire section of the sample. The tests were carried out at air temperature = 20 ± 2 °C and relative air humidity = 65%. The calculation of the ultimate tensile strength was carried out according to the test results of at least five samples of each composition. Tensile strength, MPa (N/mm^2) for each sample was calculated by the formula:

$$R = \frac{F_{pi}}{S_{oi}} \tag{4}$$

where F_{pi} is the tensile load at the moment of rupture, N;

S_{oi}- initial cross-sectional area of the sample, m^2.

3   Research Results

The research results showed that for all the samples under study, there is a linear dependence $cos\theta = f(\sigma_{lig})$ (Fig. 1).

Analysis of the data (Table 1) indicates that microcalcite has a higher critical surface tension, equal to $\sigma = 28.8$ mN/m, compared to other fillers. The value of the

Hamaker constant for microcalcite is A = 3.15 · 10^{-20} J, which characterizes a stronger interparticle interaction in the "microcalcite - microcalcite" system (Fig. 2).
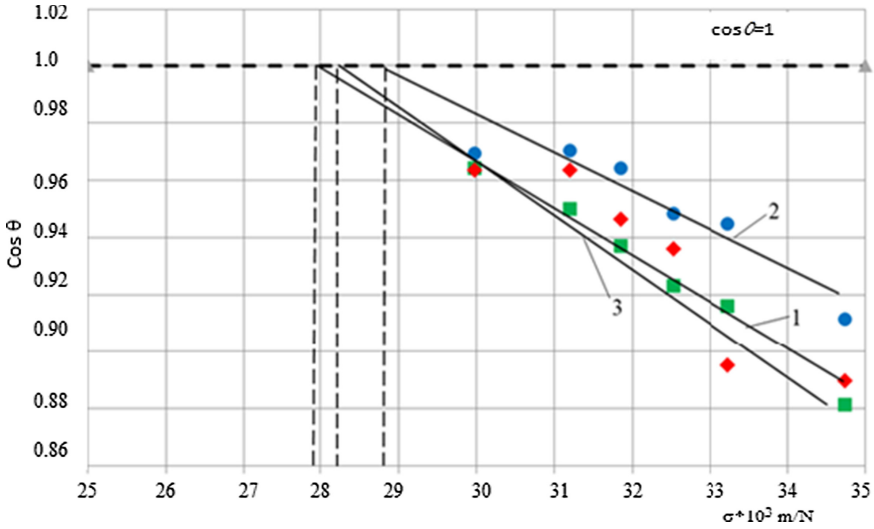
Fig. 1. Dependence $\cos\theta = f(\sigma_{lig})$: 1 - microtalc; 2- microcalcite; 3 – marshalite.
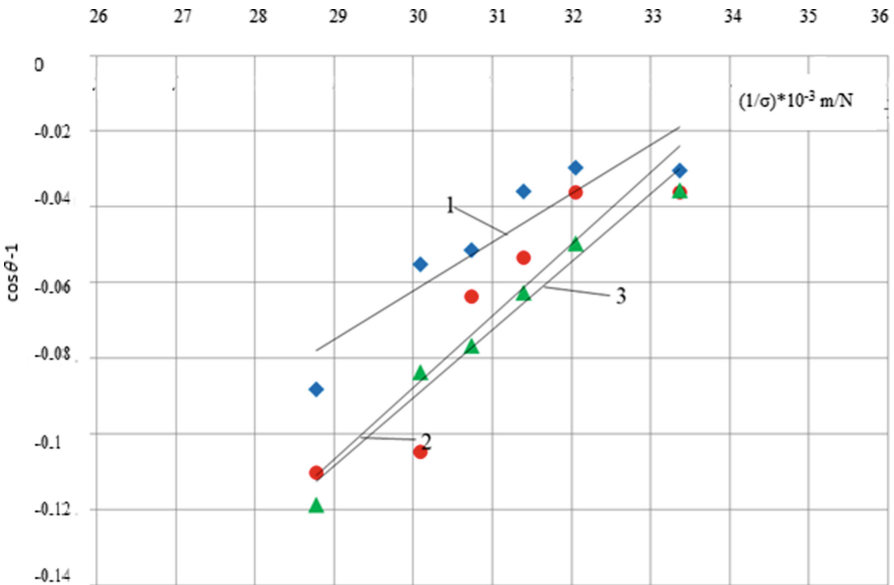
Fig. 2. Functional dependence $\cos\theta-1 = f(1/\sigma_{lig})$:1 - microtalcum; 2- microcalcite; 3 – marshalite.

Table 2 shows the values of the tensile strength of the coatings depending on the type of filler.

Table 2. Tensile strength values of coatings depending on the type of filler.

Filler type	Tensile strength of coatings, MPa
Microcalcite	1.83
Microtalc	0.36
Marshalite	1.23

It was found that there is a linear relationship between the value of the Hamaker constant and the tensile strength (cohesive strength) of the coatings (Fig. 3). A mathematical model of cohesive strength was obtained depending on the value of the Hamaker constant, which has the form

$$\sigma_{cog} = -5.72 + 2.41 * 10^{20} x \tag{5}$$

where x is the Hamaker constant.

The correlation coefficient is R = 0.9933. Thus, the cohesive strength of coatings is largely determined by the strength of the interparticle "filler-filler" interaction and can be determined using the Hamaker constant.
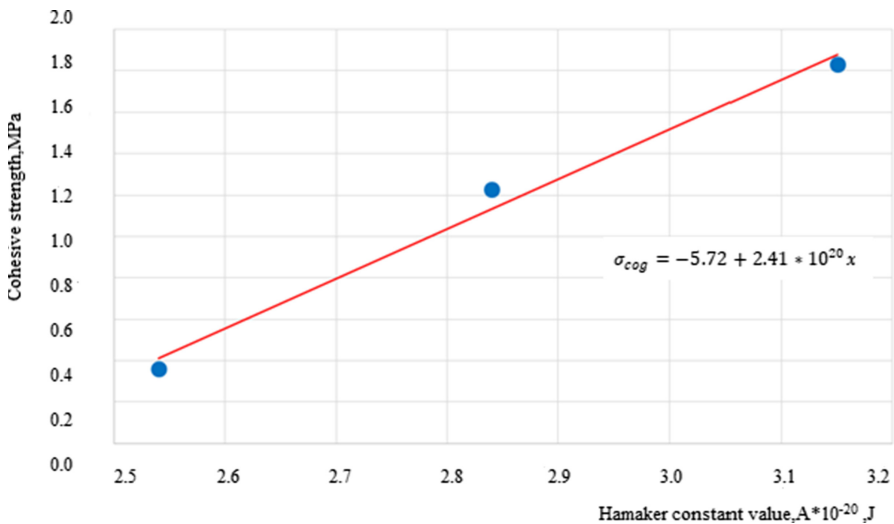
Fig. 3. Dependence of the cohesive strength of the coating on the force of interparticle interaction "filler-filler" - the Hamaker constant.

Table 3 shows the values of the work of adhesion and wetting of the filler surface of the potassium polysilicate solution. The surface tension of the potassium polysilicate solution was 59 mN/m.

Table 3. Influence of the type of filler on the work of adhesion of a polysilicate solution.

Filler name	Contact angle, ^{o}C	Work of adhesion, mJ/m^2	Wetting work, mN/m	Wetting coefficient
Microcalcite	47.2	99.08	40.09	0.839
Microtalc	49.0	97.78	38.71	0.829
Marshalite	53.0	94.51	35.51	0.801

The analysis of the data (Table 3) shows that the value of the work of adhesion of the polysilicate solution to the fillers is 94.51–99.087 mJ/m^2. It was not possible to reveal the correlation between the cohesive strength of coatings and the work of adhesion of the binder to the filler.

4   Conclusion

Thus, the cohesive strength of coatings is largely due to the strength of the interparticle "filler-filler" interaction. The choice of the filler should also be determined using the criterion for assessing the strength of interparticle interaction - the Hamaker constant. It has been established that the use in sol-silicate paints as a filler of calcite contributes to obtaining a higher cohesive strength of coatings, due to an increase in the contribution of dispersion forces.

The formulation of sol-silicate paint has been developed, the coatings on the basis of which are characterized by decorative expressiveness and have an even matte surface [21].

References

1. Figovsky, O.L., Beilin, D.: improvement of strength and chemical resistance of silicate polymer concrete. Int. J. Concrete Struct. Materials **3**(2), 97–101 (2009)
2. Figovsky, O.L., Karchevsky, V., Romm, F.: Conductive coatings based on quaternary ammonium silicates. organic-inorganic hybrids II. Science, Technology, Applications, University of Surrey 11 (2002)
3. Figovsky, O., Borisov, Y., Beilin, D.: Nanostructured binder for acid-resisting building materials. J. Sci. Israel-Technol. Advantages **14**(1), 7–12 (2012)
4. An-Peng, T.: A theory for polymerization of silica acid. Sci. Sinica **9**, 1311–1320 (1963)
5. Ayler, P.: Chemistry of silica. In 2 volumes. World, Moscow (1982)
6. Korneev, V.I., Danilov, V.I.: Liquid and Soluble Glass. SPb, Stroyizdat (1996)
7. Belton, D.J., Deschaume, O., Perry, C.C.: An overview of the fundamentals of the chemistry of silica with relevance to biosilicification and technological advances. FEBS J. **279**(10), 1710–1720 (2012)

8. Brinker, C.J., Scherer, G.W.: Sol → gel → glass: I. Gelation and gel structure. J. Non-Crystalline Solids **70**(3), 301–322 (1985)
9. Loganina, V.I., Mazhitov, Y.: Estimation of rheological properties of ash silicate paint. Materials Sci. Forum **992**, 569–573 (2020)
10. Loganina, V.I., Kislitsyna, S.N., Mazhitov, Y.B.: Development of sol-silicate composition for decoration of building walls. Case Stud. Construct. Materials **9**, e00173 (2018)
11. Loganina, V.I., Kislitsyna, S.N., Mazhitov, Y.B.: Properties of polysiylate binders for sol-silicate pains. Adv. Materials Res. **1147**, 1–4 (2018)
12. Tong, J., Liu, C.H., Jing, L.Q., Liu, H.C., Zhang, D.: The molar surface Gibbs energy and its application 3: The aqueous solution of ionic liquids [C(n)mim][OAc](n = 3, 5). J. Chem. Thermodyn. **127**, 1–7 (2018)
13. Frolova, M.A., Tutygin, A.S., Aizenshtadt, A.M., Makhova, T.A., Lesovik, V.S.: Non-destructive quality control of concrete building composites. Build. Materials **3**, 21–23 (2012)
14. Romm, F.: Thermodynamics of microporous material formation. Surfactant Science Series "Interfacial forces and fields: Theory and applications". Monographic series. CRC Press, New York (1999)
15. Ferreira, D.J.S., Bezerra, B.N., Collyer, M.N., Garcia, A., Ferreira, I.L.: The use of computational thermodynamics for the determination of surface tension and Gibbs-Thomson coefficient of multicomponent alloys. Continuum Mech. Thermodyn. **30**(5), 1145–1154 (2018)
16. Zisman, G.A.: The Course of General Physics. Chemistry, Moscow (1968)
17. Frolova, M.A., Aizenshtadt, A.M., Makhova, T.A., Pospelova, T.A.: Application of the thermodynamic approach to assessing the energy state of the surface of dispersed materials. Nanotechnol. Construct. Sci. Internet J. **3**(6), 13–25 (2011)
18. Veshnyakova, L.A., Frolova, M.A., Aizenshtadt, A.M., Lesovik, V.S., Mikhailova, O.N., Makhova, T.A.: Assessment of the energy state of raw materials for obtaining building materials. Build. Materials **10**, 53–55 (2012)
19. Drozdyuk, T.A., Aizenshtadt, A.M., Frolova, Rama Shanker Verma, M.A.L.: Mineral composite with the use of saponite-containing waste of the mining industry. Construction Materials Prod. **3**(3), 21–27 (2020)
20. Schuster, J.M., Schvezov, C.E., Rosenberger, M.R.: Construction and calibration of a goniometer to measure contact angles and calculate the surface free energy in solids with uncertainty analysis. Int. J. Adhesion Adhesives **87**, 205–215 (2018)
21. Loganina, V.I., Smirnov, V.A, Kislitsyna, S.N., Zakharov. O.A., Khristolyubov, V.G.: Evaluation of decorative properties of paint and varnish coatings. Paintwork Mater. Appl. **8**, 10–12 (2004)

Thermokinetic Processes of Hydration of Binders Based on Scrap Concrete

Ahmed Ahmed Anees Ahmed[(✉)] and R. V. Lesovik

Belgorod State Technological University named after V.G. Shukhov,
Belgorod, Russia
Civileng85@yahoo.com

Abstract. The object of research is the hydration of binders obtained from scrap concrete of destroyed buildings and structures. We used fractions of scrap concrete 0.00–0.16 mm and 0.16–0.315 mm, as x-ray phase analysis of various fractions of scrap concrete showed that these fractions have the highest content of non-hydrated alite and belite particles.

As a result of thermokinetic studies, it was found that the highest value of the heat release rate is observed in a binder based on scrap concrete with a specific surface of 964 m^2/kg: 2.4 times higher than with a specific surface of 555 m^2/kg; 1.3 times higher than with a specific surface of 1255 m^2/kg; 1.6 times higher than with a specific surface of 1431 m^2/kg. This fact reflects its higher reactivity. The results obtained are consistent with the physical and mechanical characteristics of binders based on scrap concrete in the initial period of hardening and are of practical interest from the point of view of controlling the structural and mechanical properties of concrete mixtures on the developed binders. Thus, with a specific surface area of 964 m^2/kg, the best conditions are created for the formation of the primary framework and its further fouling with various calcium crystal hydrates, which provide optimal density and strength. This composite binder composition, with a specific surface area of 964 m^2/kg, is characterized as the most energy-efficient.

Keywords: Effective Composites · Fragments of Destroyed Buildings and Structures · Construction Waste · Green Construction

1 Introduction

Currently, one of the problems in some states is the use of fragments of destroyed buildings and structures for the production of building materials. Production of binders based on technogenic raw materials with improved, and sometimes with fundamentally new performance properties and a certain pre-set structure is possible by controlling the processes of structure formation in the hardening system [1–3].

The production of such binders is based on the principle of purposeful management of the technology at all its stages: the development of optimal compositions, the use of mechanic and chemical activation of components, the use of active mineral additives, and some other techniques. Numerous studies conducted on the use of construction waste and demolition of various objects for the manufacture of concrete products and

structures have confirmed its high efficiency [4–9]. However, the question of the possibility of obtaining multicomponent binders using scrap concrete has not been sufficiently studied yet, although the available data suggest its high value in this quality. These questions are very important and serve as the goals of this study to establish the actual role that fraction sizes play in the production of concrete scrap binders. It is expected that this study will also provide more information to understand the interaction of new generation building materials and empirical evidence for promoting a green environment, and its overuse in mass concrete structures such as pedestrian walkways and blinding to the foundation of reinforced concrete structures among other applications.

In this paper, we studied the effect of the specific surface area on the degree of hydration of binders from the powder fraction of concrete scrap dropout. The fractions 0.0–0.16 and 0.16–0.315 mm were used in the experiment. The positive results of using recycled waste as a binder allow using it and solving a negative environmental problem [10–15].

2   Methods and Materials

For the use of scrap concrete in the production of building materials, it is necessary to select carefully and control the used raw materials. In this regard, its influence on the processes of structure formation in concrete and on the performance properties of composites, such as porosity, crack resistance, and frost resistance, was established. The paper used dropouts of rubble fragments of destroyed buildings and structures (Fig. 1).

Fig. 1. Fragments of destroyed buildings and structures.

To study the effect of the size of concrete scrap fractions on the properties of the resulting binder, crushed fragments of different fractions were used. Concrete scrap was crushed on a laboratory jaw crusher, dispersed into fractions of 0.00–0.16 mm; 0.16–0.315 mm; 0.315–0.63 mm; 0.63–1.25 mm; 1.25–2.5 mm; 2.5–5 mm (Table 1).

Table 1. Granulometric composition of concrete scrap crushing dropouts.

Indicator	Size of sieve holes, mm					
	2.5	1.25	0.63	0.315	0.16	<16
Weight of residues on the sieve, g	350	83	113	133	155	166
Particular residues, %	35	8.3	**11.3**	13.3	15.5	16.6
Full residues, %	35	43.3	54.6	67.9	83.4	100

The granulometric composition of concrete scrap crushing dropouts shows that the maximum amount of 35% is a fraction of 2.5–5 mm. The content of other fractions is more or less uniform. When performing experimental work, the methodological foundations of the system-structural approach in construction materials science "composition – technology – structure – properties" were used.

3   Results and Discussion

Identification of various phases in their mixture based on the analysis of the diffraction pattern given to the samples under study is the main task of x − ray phase analysis (XRD) (Table 2).

Table 2. The intensity of the diffraction reflections $C_3S + C_2S$.
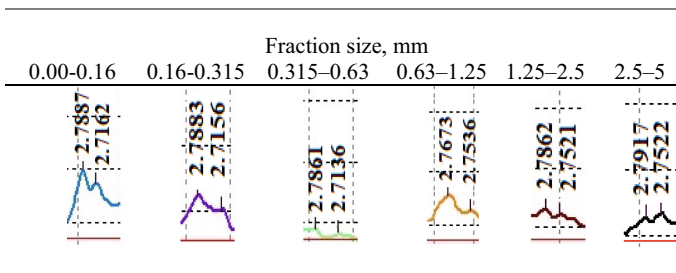
It was found that their main components are: non-hydrated clinker minerals C_3S – (d = 2.77; 2.19 Å); C_2S – (d = 2.75; 2.74; 2.19… Å); quartz – (d = 4.24; 3.34; 2.45; 2.280;…Å) portlandite $Ca(OH)_2$ – (d = 4.93; 3.11; 2.63; 1.93; 1.79 A); calcite $CaCO_3$ – d = 3.85; 3.35; 3.04; 2.78; 2.49; 2.28 Å); partially crystallized tobermorite-like calcium hydrosilicate CSH(II) – d = 9.8; 4.9; 3.07; 2.85; 2.80; Å); calcium hydroferrite and solid solutions of complex compounds etc.

It should be noted that the number of C_3S and C_2S decreases with the transition from the 0.00–0.16 fraction. At the same time the amount of quartz and minerals characteristic of a large aggregate increases. The smallest fractions of scrap concrete (pulverized and 0.16–0.316 mm) contain the maximum amount of C_3S and C_2S that can harden when interacting with water, compared to larger fractions.

For further studies, fractions of 0–0. 315 mm were crushed to specific surfaces of 555, 964, 1255, 1431 m^2/kg. Grinding kinetics (Figure 2).
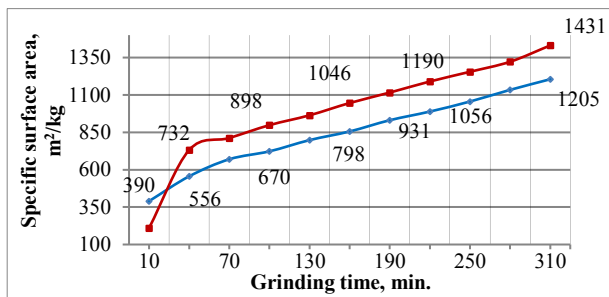
Fig. 2. Changes in the specific surface area of binders depending on the grinding time: ◆- PC; ■- scrap concrete.

To clarify the complex mechanism of the early stages of hydration of binders based on scrap concrete, thermokinetic studies of its components were carried out. Table 3 shows the heat release kinetics of binders with different specific surfaces (555, 964, 1255 and 1431 m^2/kg) compared to conventional Portland cement (with a specific surface area of 330 m^2/kg). The weight of the samples is 10 g, the ratio of W/B = 0.5.

Table 3. Characteristics of thermokinetic parameters of binders.

Components of binders	Reaction beginning, s	Exoeffect			Heat release max. for 72 h, W/g
		Achievement moment, h : min : s	Maximum value, J/g·h	Heat release, J/g	
PC (330 m^2/ kg)	15	00:03:09	58.07	1.97	263.65
		08:11:00	12.35	73.09	
CB (555 m^2/ kg)	27	00:00:37	7.81	0.03	26.5
		67:56:00	0.15	25.99	
CB (964 m^2/ kg)	15	00:04:31	18.73	1.16	74.35
		07:17:00	1.38	18.13	
CB (1255 m^2/kg)	13	00:04:58	14.27	0.93	52.54
CB (1431 m^2/kg)	16	00:04:49	12.08	0.77	73.2
		38:01:00	1.69	44.44	

Interesting features of the initial heat release after contact with water and the manifestation of reactivity in the binder based on scrap concrete.

The binder with a dispersion of 555 m^2/kg shows two peaks of energy release (Fig. 3) in the interval between which the intensity of heat release is approximately constant. This behavior of the system allows saying that there are two periods of hydration, taking into account the induction period. As a result of initial contact with the mixing liquid at 37 s, the system under study has a first burst of heat release of 7.81J/g·h with a total amount of released energy of 0.03 J/g, which is primarily due to water adsorption and early chemical interaction. In the future, the level of heat release drops to 0.15 J/g·h, which is a sign of the beginning of the induction period.

a)   b)
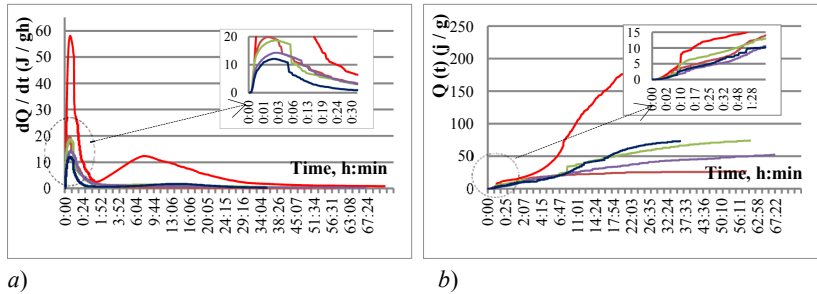
Fig. 3. Kinetics of heat release during hydration of binders: a – heat release rate, b – heat hydration -PC;-555 m^2/kg;-964 m^2/kg;-1255 m^2/kg;-1433 m^2/kg.

The binder with a higher dispersion of 964 m^2/kg (Fig. 3) also shows hydraulic activity almost immediately after mixing. The first spike in the intensity of specific heat release (18.73 J/g·h) occurs at about 4 minutes. The total amount of released energy at this point reaches 1.16 J/g. In the future, the intensity of heat generation decreases to the level of 1.38 J/g·h and the hardening system enters the induction period.

A further increase in the specific surface area of the composite binder to 1255 m^2/kg leads to a single peak in the intensity of heat release with a level of 14.27 J/g·h, after which the system enters the induction period characterized by a low average heat output level of 0.93 J/g.

The interaction with water of the binder with a dispersion of 1431 m^2/kg in the early period is characterized by a single peak of heat release intensity of 12.08 J/g·h at the time corresponding to 5 minutes after closing. The integral value of heat evolution at this point is 0.77 J/g. A repeated burst of heat release with a maximum value of 1.69 J/g·h is observed at the time corresponding to 38 h from the beginning of hydration. The total specific amount of energy released by the hardening system for the specified period is 44.44 J/g.

The research made it possible to formulate the theoretical basis for improving the efficiency of binders, which consists in establishing the features of their structure formation, and the use of multicomponent binders to improve the efficiency of concrete.

4   Conclusion

As a result of thermokinetic studies, it was found that the highest value of the heat release rate is observed in binders based on scrap concrete with a specific surface of 964 m^2/kg: 2.4 times higher than with a specific surface of 555 m^2/kg; 1.3 times higher than with a specific surface of 1255 m^2/kg; 1.6 times higher than with a specific surface of 1431 m^2/kg. This fact reflects its higher reactivity. The results obtained are consistent with the physical and mechanical characteristics of binders based on scrap concrete in the initial hardening period and are of practical interest from the point of view of controlling the structural and mechanical properties of concrete mixtures on the developed binders.

References

1. Lesovik, V.S., Zagorodnyuk, L.H., Shamshurov, A.V., Belikov, D.A.: Composite binder based on a complex organomineral modifier for dry repair mixtures. Bull. BSTU named after V.G. Shukhov **4**, 25–31 (2014)
2. Tan, M.D., Gyeongo, K., Young-sang, K.: Development of a new cementless binder for controlled low strength material (CLSM) using entirely by-products. Construction Build. Materials **206**, 576–589 (2019)
3. Tan, M.D., Gyeongo, K., Ngan, V., Young-sang, K.: Development of a new cementless binder for marine dredged soil stabilization: strength behavior, hydraulic resistance capacity, microstructural analysis, and environmental impact. Construction Build. Materials **186**, 263–275 (2018)
4. Klyuev, S.V., Khezhev, T.A., Pukharenko, Y.V., Klyuev, A.V.: Experimental study of fiber-reinforced concrete structures. Materials Sci. Forum **945**, 115–119 (2018)
5. Klyuyev, S.V., Klyuyev, A.V., Lesovik, R.V., Netrebenko, A.V.: High strength fiber concrete for industrial and civil engineering. World Appl. Sci. J. **24**(10), 1280–1285 (2013)
6. Lesovik, R.V., Tolypina, N.M., Alani, A.A., Al-bo-ali-W.S.J.: Composite binder on the basis of concrete scrap. Lecture Notes in Civil Eng. **95**, 307–312 (2020)
7. Keun-Hyeok, Y., Jin-Kyu, S., Ashraf, F., Eun-Taik, L.: Properties of cementless mortars activated by sodium silicate. Construction Build. Materials **22**, 1981–1989 (2008)
8. Lesovik, R.V., Klyuev, S.V., Klyuev, A.V., Tolbatov, A.A., Durachenko, A.V.: The development of textile fine-grained fiber concrete using technogenic raw materials. Res. J. Appl. Sci. **10**(10), 696–701 (2015)
9. Zagorodnjuk, L.H., Lesovik, V.S., Volodchenko, A.A., Yerofeyev, V.T.: Optimization of mixing process for heat-insulating mixtures in a spiral blade mixer. Int. J. Pharmacy Technol. **8**(3), 15146–15155 (2016)
10. Lesovik, V.S., Chulkova, I.L., Zagordnyuk, L.K., Volodchenko, A.A., Yurievich, P.D.: The role of the law of affinity structures in the construction material science by performance of the restoration works. Res. J. Appl. Sci. **9**(12), 1100–1105 (2014)
11. Klyuev, S.V., Khezhev, T.A., Pukharenko, Y.V., Klyuev, A.V.: To the question of fiber reinforcement of concrete. Materials Sci. Forum **945**, 25–29 (2018)

12. Karpikov, E.G., Lukuttsova, N.P., Soboleva, G.N., Golovin, S.N., Cherenkova, Y.S.: Effect of microfillers based on natural wollastonite on the properties of fine-grained concrete. Construction Mater. Products **2**(6), 20–28 (2019)
13. Khezhev, T.A., Pukharenko, Y.V., Khezhev, K.A., Klyuev, S.V.: Fiber gypsum concrete composites with using volcanic tuffsawing waste. ARPN J. Eng. Appl. Sci. **13**(8), 2935–2946 (2018)
14. Klyuev, S.V., Khezhev, T.A., Pukharenko, Y.V., Klyuev, A.V.: The fiber-reinforced concrete constructions experimental research. Materials Sci. Forum **931**, 598–602 (2018)
15. Lesovik, R.V., Klyuyev, S.V., Klyuyev, A.V., Netrebenko, A.V., Kalashnikov, N.V.: Fiber concrete on composite knitting and industrial sand KMA for bent designs. World Appl. Sci. J. **30**(8), 964–969 (2014)

Efficient Construction Composites
for Construction in the North and the Arctic

Alexander Tolstoy$^{(\boxtimes)}$, Anatoly Gridchin , Evgeny Glagolev ,
Ruslan Lesovik , and Nikolay Shapovalov

Belgorod State Technological University named after V.G. Shukhov, Kostyukov
Street, 46, Belgorod 308012, Russia
{Alexandertolstoy,Anatolygridchin,Evgenyglagolev,
Ruslanlesovik,Nikolayshapovalov}@uni-hannover.de

Abstract. Construction in the North and the Arctic associated with certain features characteristic of the polar territories, with a low level of population density, difficulties in implementing technological methods for the production of building materials and construction, as well as with the requirements for increased protection of construction sites from the harmful effects of the environment. In this regard, the development of effective building composites and methods of protecting structures based on new principles of transdisciplinarity is relevant. The article discusses the problem of improving the technology of new generation composites with increased strength while maintaining high strength indicators to protect against natural environmental influences, as well as the development of a new method for self-healing of concrete structures during operation in the Arctic.

Thus, new methods of obtaining porous composites of increased strength and self-healing of concrete structure using internal and external factors are shown. The essence of the method lies, firstly, in creating a high-density and high-strength structure of the material and, secondly, in the introduction of a reactive mineral, which is part of a fine filler (iron sulfide). This combination provides the appearance of ettringite-like iron-containing calcium hydrates in the thickness of the concrete stone during cracking, which occurs with an increase in the volume of solid and condensed phases.

Keywords: Fine-Grained concrete · Porous concrete of increased strength · Mineral and technogenic raw materials · Composite binder · Self-Healing structures

1 Introduction

As you know, construction in the Arctic Circle is carried out with the preservation of permafrost soil on special supports. At the same time, the structure must be durable and, at the same time, energy efficient in terms of heat loss. Arctic construction depends to a large extent on high-quality construction materials manufactured using efficient technologies that retain their operational properties over time. In this regard, porous fine-grained concrete of increased strength is a popular material for special structures.

This concrete differs from the traditional one with increased porosity, but, at the same time, with increased strength.

In the conditions of the Far North, the durability of the applied building structures, its forecasting and maintenance is important. A significant step in the development of the methodology for ensuring durability and corrosion resistance was the emergence of a wide range of methods for self-healing of concrete during the operation of structures [1, 2].

The theoretical basis for the creation of high-quality composites is a new scientific direction of geonics and geometry, which use the results of the study of geological processes and rocks to create materials of a new generation [3, 4].

One of the limiting factors in the development of high-strength fine-grained concretes is the cost of their manufacture, associated with a large number of mixture components, the accuracy of adherence to technological regulations, and can exceed the cost of traditional concretes several times. Therefore, based on the needs of the region, it is important to research new types of raw materials, including technogenic ones, which will provide construction with effective structural materials [6–13].

2   Materials and Methods

According to the current Interstate Standard GOST 25820–2014 "Light Concrete. Specifications "lightweight structural concrete includes concrete with an average density of less than 2100–2200 kg/m3, obtained by various technologies and with various aggregates or without them. When concrete strength exceeds 20 MPa, they are classified as high-strength lightweight composites [5].

The raw materials used to obtain high-performance porous concrete are mainly aggregates with high open porosity, which provides a low average density (up to 1000 kg/m3 and high strength - up to 50 MPa). In this regard, it is important to obtain building material at the same time, with high porosity with high strength. The porosity must be characterized by spherical pores, which must be closed throughout the material.

The prototypes of high-strength porous concrete were $10 \times 10 \times 10$ cm in size and were made on the basis of ordinary Portland cement and a complex modifier. After 1 day of exposure, they were subjected to steaming according to the mode of 2–5–2 h at a temperature of 85 °C. After 3 days of hardening, the samples were tested for strength and to determine other properties.

The durability of building materials and structures in the Arctic, especially high-strength ones, created on new principles of transdisciplinarity, is currently the most important task. The practice of operating critical structures in harsh climatic conditions, such as high or low temperatures, shows, unfortunately, the insufficient durability of reinforced concrete, from which these structures are built. Internal corrosion processes, as a rule, are supplemented by external aggressive influences (temperature and humidity drops, changes in the gas composition of the ambient air, etc.). Therefore, self-healing of the concrete structure during operation is important. In high-strength hardening systems, the acceleration of the process of self-organization of the structure and its strengthening leads to an early risk of destruction of this system. To avoid a

decrease in the construction and technical properties of high-strength concrete, it is necessary to make additional efforts to "pump" energy into the system to maintain the previously acquired state.

This paper proposes a new method of concrete self-healing by overgrowing the formed cracks with new formations expanding in volume, i.e. due to the physico-chemical process due to the oxidation of the reactive element of the aggregate, and the subsequent interaction of the products of this oxidation with the hydration products of Portland cement, for example, iron sulfide. With the interaction of aluminates of cement stone and sulfate ions, not only the filling of cavities with crystals of new formations occurs, but also some tension of the entire structure of concrete as a result of their expansion in the volume of pores and capillaries of concrete. The destruction products contain calcium trisulfohydroaluminate and gypsum.

Until now, the influence of the mineral composition of aggregates on the properties of concrete has not been fully investigated, especially in those cases when they are industrial waste. There is no consensus on the issue of the reactivity of iron sulfides, in particular pyrite (FeS_2), the inclusions of which are most often found in rocks, in relation to the hydrated minerals of hardening cement.

3   Results and Discussion

As a result of the complex of the studies carried out, the following results were obtained (Table 1).

Table 1. Physical and technical properties of the obtained lightweight concrete.

No	(R_{com}), MPa at the age of 3 day	(ρ_{av}), кг/м^3	(λ_0), V$_t$/м·°C	F	W
1	32.0	1840	0.35	20	4
2	33.1	1850	0.36		
3	33.4	1860	0.37		
4	34.2	1870	0.38	30	
5	34.4	1880	0.39	30	

The data obtained indicate that in 1 day after demoulding and TVO the test specimens have Rczh = 20 MPa, and after 7 days of hardening - equal to 30 MPa. In other words, the obtained porous concrete has a tempering strength equal to 75% of the brand one after 1 day.

Such high characteristics of construction and technical properties are obtained due to the optimization of the structure with combined pores, which makes it possible to increase the protective properties of the enclosing structure in terms of thermal insulation and acoustic properties while maintaining high strength characteristics. Such a structure was obtained on special multicomponent hardening systems due to the preparation of a mixture, where the effect of gas evolution is manifested upon stirring without adding a gas generator. This effect manifests itself after an increase in the amount of the component of the mixture - an aluminate mineral additive, which

interacts with the minerals of Portland cement with the release of gas, swelling the structure "Portland cement - mineral modifier - hyperplasticizer - water". Correct selection of the composition of the raw mix made it possible to obtain lightweight high-strength concrete.

The structure of the pore walls (interporous partitions) ensures the preservation of the "feeding" fluid, which allows the growth of the number of neoplasms inside the pore. By the 28th day, the concrete pores are completely filled with gel-like calcium hydrosilicates, and the joints of the contact zone provide strong adhesion between the formed crystalline hydrates. At high magnification, a tight contact between the crystalline hydrates of the structure of the porous composite is visible (Fig. 1).
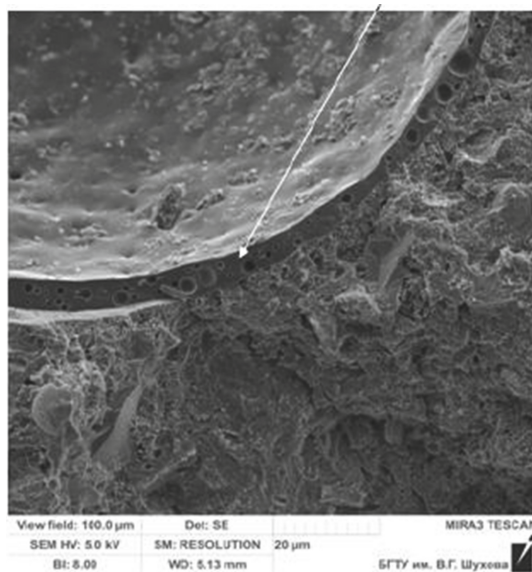
Fig. 1. Partitions of air pores of lightweight composite with increased strength.

The concrete healing process is "frontal". In the depth of the crack, where high alkalinity and pH reaches 11.5–12, the conditions are favorable for the formation of ettringite-like phases, which occurs with an increase in the solid phase and "advances" the process to the beginning of the crack. When emerging from the crack, the pH of the medium decreases, which leads to the decomposition of calcium trisulfohydroaluminate. Gypsum is formed in large quantities on the crack surface (Fig. 2).

In this study, the principle of self-healing was used with the use of both internal and external activator (substance) of the self-healing process of concrete: internal - iron sulfide of the aggregate, external - persulfate solution. In this way, a "smart" system was created that reproduces the process of natural self-healing biological systems, just like most materials in nature self-repair by a transdisciplinary mechanism.

The samples were subjected to compression tests at the age of 14 and 28 days of hardening under normal conditions. The test results are presented in Table 2.

Table 2. Dynamics of self-healing of strength indicators of high-strength composite samples.

No	Controlled parameter	Q (FeS$_2$), %	P (50 кg/sm^2)	
			14 days	28 days
1	Rcom, MPa	0.4	35.6	77.1
		1.4	36.0	77.8
		2.4	36.4	78.1
2	V ultrasound, м/s	0.4	4810	4920
		1.4	4860	4980
		2.4	4920	5040
3	K durability	0.4	0.94	0.97
		1.4	0.96	0.98
		2.5	0.97	0.99
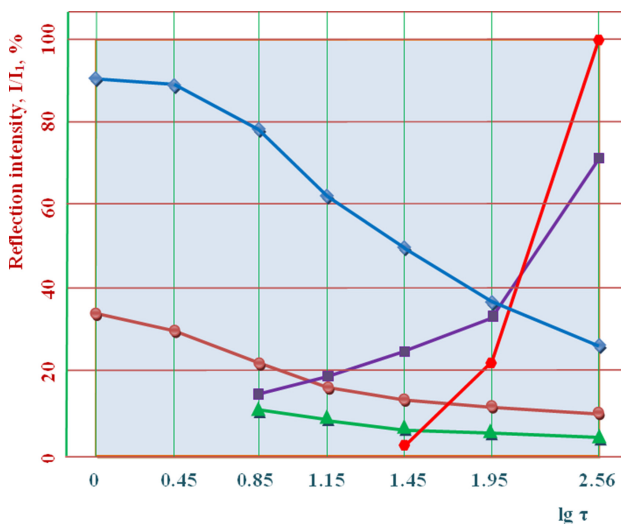
Fig. 2. Kinetics of phase formation in the CaO – FeS$_2$ – H$_2$O$_2$–H$_2$O system. Intensity of lines on X-ray diffraction patterns: ◆- CH with d = 2.63 Å; ●- FeS$_2$ with d = 3.13 Å; ▲- C$_3$F (Cs, CH) H$_{12}$ with d = 10.3 Å; ■- CsH$_2$ with d = 7.62 Å; ●- CsFCs$_3$H$_{32}$ with d = 0.972 Å.
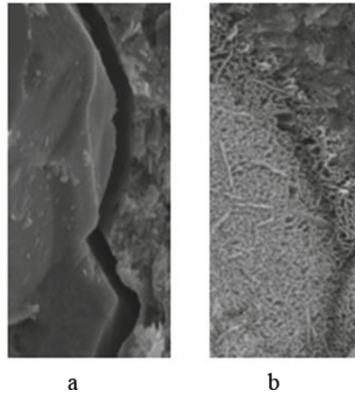
Fig. 3. "Healing" of cracks in concrete according to the proposed method under load: a - crack formed in concrete under load; b - crack overgrown with crystalline interaction products (ettringite-like phases and gypsum) of iron sulfide filler (internal factor) with a persulfate solution (external factor).

The degree of self-healing was established according to the results of testing the resistance coefficient of pre-loaded samples, as well as the velocity of the ultrasonic pulse.

The data obtained show that up to 28 days of age, there is a steady increase in the mechanical properties of high-strength concrete samples under load, which indicates a decrease in the degree of concrete permeability for an aggressive reagent as a result of an intensive process of self-healing of cracks.

The results of "self-healing" of cracks are confirmed by the data of scanning electron microscopy (Fig. 3).

"Healing" of microcracks in concrete according to the proposed method under load: a - microcrack formed under load; b - microcrack overgrown with crystalline products of the interaction of iron sulfide filler (internal factor) and persulfate solution (external factor) - ettringite-like phases and gypsum)

After 28 days of testing under load, almost all opening microcracks are completely filled with crystalline new formations, the growth of which is due to the presence of sulfides inside the concrete, and sulfates in the surrounding solution.

4   Conclusion

Thus, the obtained high-strength porous concrete can be classified as structural and heat-insulating, and it can be recommended for special construction purposes - protection against sound and temperature effects. This material may well provide special acoustic protection. facilities, for which preparatory work has begun and a cooperation agreement has been concluded with one of the units of the RF Ministry of Defense.

The patterns of structure formation during hardening of a multicomponent composite were observed during the formation and optimization of the structure parameters at all technological stages of manufacturing.

For the conditions of the Arctic, the composition was obtained, the conditions of hardening and the characteristics of structural and soundproof concrete were determined, which are within the recommended ones, which are within the limits established by regulatory documents. The possibility of using them in the manufacture of products for sound insulation of special structures has been confirmed. The resulting composite showed an average compressive strength of 30 MPa after 3 days of hardening, and 45 MPa after 7 days, the average density was 1850–1900 kg/m^3.

The use of the developed self-healing technique will ensure the formation of a crystalline framework in the thickness of the concrete stone, at the site of the cracks formed. This frame perceives internal stresses arising from deformation of the structure during the hardening period, due to shrinkage, contraction, or during operation - temperature and humidity deformations. This frame relieves stress and extends the service life of the product tenfold compared to deformations in ordinary concrete.

References

1. Aldia, C.-M., Singes, U.-G., Popovich, S.Y., Chah, S.P.: Degree of crack healing in normal strength concrete. English Materials J. **12**, 92–96 (2000)
2. Hern, H., Morly, S.: Self-compacting property of concrete: experimental data. Structura of Mater. **30**, 404–411 (1997)
3. Lesovik, V.S.: Geonika (geomimetics). examples of implementation in building materials science. BSTU, Belgorod (2014)
4. Tolstoy, A.D., Lesovik, V.S., Kovalev, I.A.: Organomineral high-strength decorative compositions. Bulletin of the BSTU named after V.G. Shukhov **5**, 67–69 (2014)
5. Gridchin, A.M., Korolev, N.V., Shukhov, V.N.: Overburden KMA in Road Construction. Tsentralno-Chenozemnoe Publishing House, Voronezh (1983)
6. Zvezdov, A.I., Falikman, V.R.: High-strength light concrete in construction and architecture. Hous. Construction **7**, 106–109 (2008)
7. Lesovik, R.V., Klyuyev, S.V., Klyuyev, A.V., Netrebenko, A.V., Yerofeyev, V.T., Durachenko, A.V.: Fine-grain concrete reinforced by polypropylene fiber. Res. J. Appl. Sci. **10**(10), 624–628 (2018)
8. Glagolev, E.S.: High-strength fine-grained concrete on composite binders and man-made sands for monolithic construction: dis. … Cand. tech. Sciences: 05.23.05. Moscow (2010)
9. Lesovik, R.V., Klyuev, S.V., Klyuev, A.V., Tolbatov, A.A., Durachenko, A.V.: The development of textile fine-grained fiber concrete using technogenic raw materials. Res. J. Appl. Sci. **10**(10), 696–701 (2015)
10. Tolstoy, A.D.: Sulfate resistance of concrete with pyrite-containing aggregate, determined by the accelerated method: dis. … Cand. Tech. Sci. 05.23.05. BSTU, Belgorod (1987)

11. Klyuyev, S.V., Klyuyev, A.V., Lesovik, R.V., Netrebenko, A.V.: High strength fiber concrete for industrial and civil engineering. World Appl. Sci. J. **24**(10), 1280–1285 (2013)
12. Lesovik, R.V., Klyuyev, S.V., Klyuyev, A.V., Netrebenko, A.V., Kalashnikov, N.V.: Fiber concrete on composite knitting and industrial sand KMA for bent designs. World Appl. Sci. J. **30**(8), 964–969 (2014)
13. Klyuev, S.V., Khezhev, T.A., Pukharenko, Y.V., Klyuev, A.V.: To the question of fiber reinforcement of concrete. Mater. Sci. Forum **945**, 25–29 (2018)

Color Control of Portland Cement Clinker by Separate Input of Mineralizers

S. V. Kovalev[✉] and D. A. Mishin

Belgorod State Technological University named after V. G. Shukhov,
Belgorod, Russia
k-ws@mail.ru

Abstract. The color control of Portland cement clinker was regulated by separate insertion of calcium fluoride in the presence of Na_2O. Studies were carried out on a raw mixture of pure reagents with a Fe_2O_3 content equal to 2.93%. The mixture has the following characteristics: KH = 0.93; AM = 1.24; SM = 2.18. Calcium fluoride was inserted as a CaF_2 reagent of the "pure" qualification. Na_2O was inserted as a "pure" Na_2CO_3 reagent. The samples were roasted in a laboratory furnace at 1300 °C with an isothermal exposure time of 20 min. The heating speed of the furnace is 10 °C/min. The color change was determined by measuring the brightness coefficient on a reference polished barium sulfate plate using an FB-2 gloss meter. The content of free calcium oxide was determined by the ethyl-glycerate method. It was found that the optimal approach for increasing the clinker whiteness is to insert 1.5% CaF_2 separately in the presence of 3.5% Na_2O. The amount of 3.5% Na_2O is sufficient to bind stoichiometric all aluminum in $Na_2O \cdot Al_2O_3$. The binding of Al_2O_3 to sodium aluminate prevents the formation of calcium aluminoferrites. At the same time, the whiteness of the compound with a mineralizer is 49.5%. In the compound without a mineralizer, it reaches 39%. An increase in the clinker whiteness to the maximum is accompanied by a decrease in the content of free calcium oxide. In the compound without a mineralizer, it is 20.1%. The compound with a mineralizer has a free calcium oxide content of 5.28%.

Keywords: Separate input · Clinker whiteness · Mineralizer · Fluorspar CaF_2 · Na_2O

1 Introduction

In [1], the Department of Cement and Composite Materials Technology of BSTU named after V.G. Shukhov (Russia, Belgorod) studied the possibility of controlling the color of Portland cement clinker by changing the Na_2O content in the clinker. When the Na_2O content increases, calcium aluminoferrites are destroyed. Calcium aluminoferrites are the most coloring phase of clinker [2]. The destruction of calcium aluminoferrites occurs due to the formation of sodium aluminoferrites and is accompanied by a change in the clinker whiteness. The resulting clinker is characterized by an increased content of free calcium oxide. Therefore, controlling the color of the clinker in this way is impractical. Color control and intensification of the white cement roasting process

are possible due to the insertion of various mineralizing additives, such as ZnO, BaSO$_4$ [3], CaF$_2$ and CaSO$_4$ [4]. Mineralizing additives can get into the raw material mixture as part of alternative sources of raw materials [5, 6]. The use of calcium fluoride is more appropriate.

However, in modern furnace systems, there is a phenomenon of circulation and accumulation of alkali metal salts [7–9]. Therefore, it is difficult to create conditions in which the furnace system would contain only calcium fluoride without alkali metal salts. The traditional (in the raw mix) insertion of calcium fluoride in the presence of alkali metal salts in the raw mix leads to a mutual weakening of their properties [10]. Therefore, the aim of this work is to study the possibility of controlling the color of Portland cement clinker by separate insertion of mineralizers.

2   Methods and Materials

As the initial raw material mixture, a raw material mixture prepared from reagents of the "pure" qualification was used: CaCO$_3$, SiO$_2$, Al$_2$O$_3$, Fe$_2$O$_3$ (Table 1). The raw mixture has the following characteristics: AM = 1.24; SM = 2.18; saturation coefficient (according to Kind) KH = 0.93.

Table 1. Chemical composition of the raw material mixture based on pure reagents, % wt.

LOI[a]	SiO$_2$	Al$_2$O$_3$	Fe$_2$O$_3$	CaO
34.81	13.59	3.64	2.93	44.31

[a]LOI – loss on ignition.

Na$_2$CO$_3$ and CaF$_2$ reagents of the "pure" qualification were used as mineralizers. All concentrations are taken in mass percentages for clinker.

Simulation of the circulation and accumulation of alkali metal salts was carried out by introducing a mineralizer Na$_2$CO$_3$ in the amount of 1; 2; 3; 3.5; 4; 5; 6; 7% Na$_2$O

The CaF$_2$ mineralizer was inserted separately [11]. Modeling of separate input of the mineralizer under conditions of circulation and accumulation of alkali metal salts was carried out in a laboratory furnace as follows. Na$_2$CO$_3$ was added to the initial raw mixture in the required amount in terms of Na$_2$O. Tablets were formed from the resulting mixture and roasted at a temperature of 1100 °C. The roasting product was crushed and the required amount of calcium fluoride was inserted into it. Tablets were re-formed from this material and returned to a preheated temperature of 1100 °C, after which they were fired at the required temperature and time of isothermal exposure.

The samples were roasted in a laboratory furnace at a temperature of 1300 °C, with an isothermal holding time of 20 min. The heating speed of the furnace is 10 °C/min.

Determination of the free calcium oxide (CaO$_{free}$) content in clinker was performed by the ethyl-glycerate method.

The degree of whiteness (brightness coefficient BC) of the clinker was determined using an FB-2 gloss meter based on a standard polished barium sulfate plate.

3 Results and Discussion

To achieve this goal, it is necessary to determine the effect of separate insertion of calcium fluoride in the absence of alkali metal salts, i.e. individually. At roasting temperature of 1300 °C (Fig. 1), starting with the insertion of 1% calcium fluoride, the brightness coefficient of the clinker increases. The maximum value of the brightness coefficient is reached at 1.5% CaF_2 and is 48%, while the composition without additives is 46.5%. The content of free calcium oxide is 5.96% lower than that of the composition without additives. After 1.5% CaF_2, the brightness coefficient decreases as the mineralizer concentration increases. The minimum value of the brightness coefficient is observed when inserting 3.5% CaF_2.

The value of the brightness coefficient is fully correlated with the content of free calcium oxide. Therefore, we can conclude that the determining factor when changing the brightness coefficient is the change in the number of white crystals of free calcium oxide.
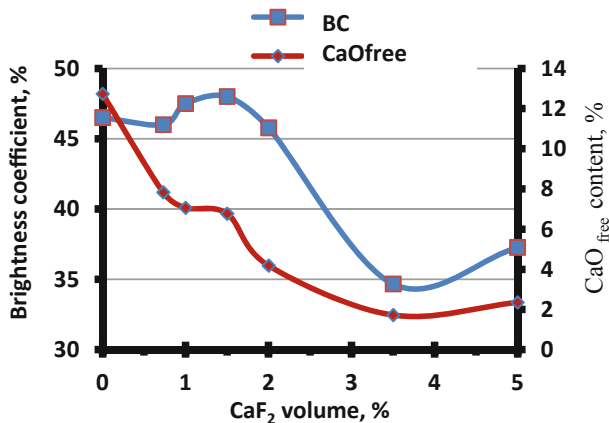
Fig. 1. Effect of calcium fluoride on the whiteness of Portland cement clinker.

The optimal amount of calcium fluoride from the position of clinker whiteness is 1.5% CaF_2. Further increase in the amount of calcium fluoride in order to reduce the content of free calcium oxide is impractical. In addition, an increase in the concentration of calcium fluoride over 1.5% can lead to deterioration of the lining in the sintering zone.

Separate insertion of calcium fluoride under conditions of circulation and accumulation of alkali metal salts was carried out in the previously established amount of 1.5% CaF_2 (Fig. 2). When the Na_2O content increases to 3.5%, the clinker brightness coefficient gradually increases to a maximum value of 49.5%. This is 10.5% higher than the composition without additives. The maximum value of the brightness coefficient of 49.5% was achieved with 6% Na_2O.

The amount of 3.5% Na_2O is sufficient to bind stoichiometric all aluminum in $Na_2O \cdot Al_2O_3$. The amount of 6% Na_2O is sufficient to bind all the aluminum and iron contained in the clinker in $Na_2O \cdot Al_2O_3$ and $Na_2O \cdot Fe_2O_3$:

When inserting more than 6% Na_2O, a sharp drop in the brightness coefficient of the clinker occurs.
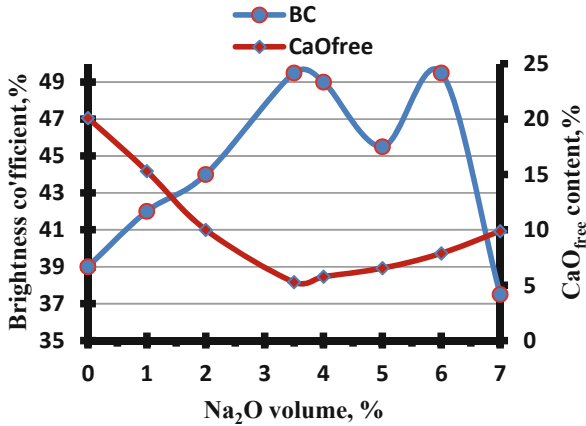
Fig. 2. Effect of Na_2O on the whiteness of Portland cement clinker with separate insertion of 1.5% CaF_2.

The minimum content of free calcium oxide is observed with the introduction of 3.5% Na_2O and is 5.28%. The insertion of more than 3.5% Na_2O causes an increase in the content of free calcium oxide. No correlation was found between the CaO_{free} content and the clinker brightness coefficient. Therefore, in this case, the content of free calcium oxide is not a determining factor when changing the clinker whiteness. The change in clinker whiteness occurs due to the formation of sodium compounds with Fe_2O_3 and Al_2O_3 instead of calcium aluminoferrites.

4   Conclusion

Separate insertion of 1.5% calcium fluoride in the presence of 3.5% Na_2O increases the clinker whiteness by 10.5% in relation to the compound without additives. The content of free calcium oxide decreases from 20.1% to 5.28%. The increase in the clinker whiteness with a decrease in the number of white crystals of free calcium oxide indicates the interaction of Na_2O with the aluminoferrite phase of the clinker.

References

1. Mishin, D., Kovalyov, S.: Influence of sodium oxide on brightness coefficient of Portland cement clinker. In: Glagolev, S. (ed.) ICAM 2019. SPEES, pp. 352–355. Springer, Cham (2019). https://doi.org/10.1007/978-3-030-22974-0_85
2. Zubekhin, A.P., Golovanova, S.P., Kirsanov, P.V.: White Portland cement. (ed.) In: Proceedings of Universities of North Caucasus Region, Rostov on/D (2004)
3. Timoshenko, T.I., Zalogina, A.V., Khudasov, V.I.: Influence of ZnO and BaSO$_4$ additives on construction and technical properties of low-base white cements. Constr. Mater. Prod. **1**(3), 17–24 (2018)
4. Blanco-Varela, M.T., Palomo, A., Puertas, F., Vázquez, T.: CaF$_2$ and CaSO$_4$ in white cement clinker production. Adv. Cem. Res. **9**(35), 105–113 (1997)
5. Zhanikulov, N.N., Taimasov, B.T., Borisov, I.N., Dauletiyarov, M.S., Aitureev, M.Z., Dzhanmuldaeva, Z.K.: Preparation low-energy content cement from technogenic raw materials. Refract. Ind. Ceram **61**(2), 163–169 (2020). https://doi.org/10.1007/s11148-020-00449-5
6. Novoselova, I.N., Novosyolov, A.G.: Peculiarities of physical and chemical processes of clinker formation in raw mixes with increased content of magnesium oxide in presence of barite waste. In: IOP Conference Series: Materials Science and Engineering, vol. 327 no. 3, p. 032042 (2018)
7. Luginina, I.G.: Selected Articles. Publishing House of BSTU named after V.G. Shukhov, Belgorod (2002)
8. Klassen, V.K., Ermolenko, E.P., Michin, D.A., Novosyolov, A.G.: Problem of impurity of salts of alkali metals in cement raw materials. Middle East J. Sci. Res. **17**(8), 1130–1137 (2013)
9. Cortada Mut, M.D.M., Nørskov, L.K., Frandsen, F.J., Glarborg, P., Dam-Johansen, K.: Review: circulation of inorganic elements in combustion of alternative fuels in cement plants. Energy and Fuels **29**(7), 4076–4099 (2015)
10. Mishin, D.A., Kovalev, S.V., Chekulaev, V.G.: Reason for reduced efficacy of mineralizers for burning Portland cement clinker. Bull. BSTU named after. V. G. Shukhov **1**(5), 161–166 (2016)
11. Patent No 2633620 Russian Federation, IPC C04B 7/42 (2006.01), C04B 7/06 (2006.01). Method for intensifying the process of roasting Portland cement clinker with mineralizers (options): No 2016127078: application 05.07.2016: publ. 16.10.2017/ Mishin D.A, Kovalev S.V., Chekulaev V.G., applicant BSTU

Cement Hydratation and Curing Cycles

V. A. Lotov, N. P. Gorlenko$^{(\boxtimes)}$ ⓘ, Yu. S. Sarkisov ⓘ,
and T. S. Shepelenko ⓘ

Tomsk State University of Architecture and Building, Tomsk, Russia
gorlen52@mail.ru

Abstract. The paper investigates the heat formation and absorption processes in the cement-water system. The temperature gradient in a cement composition is one of the mainsprings of cement hydration and curing and the formation of final properties of the cement-water system. The differential calorimetric analysis based on measuring the temperature difference between dry and wet cement shows the reciprocal, cyclic heat formation. The observed effects are caused by the processes of dispersion and hydration of cement particles and crystallization of cement hydration products. Three types of harmonic frequencies are detected for the heat formation, viz. 1–3 vibrations per minute, ~ 12 h, and a several days vibration period. The heat formation-based analysis of phenomena observed in the cement-water system shows self-excited vibrations during the cement hydration and curing. The reaction continues owing to the energy release during hydration of clinker minerals and dispersion of the initial cement particles. The high sensitivity of the differential calorimetry as against the integral methods provides the deeper understanding of the phenomena observed and allows improving the cement potential in the production of a wide range of building materials.

Keywords: Cement · Hydration · Particle dispersion · Hardening · Heat generation · Induction period · Microcalorimetry

1 Introduction

Cement is a unique building material; its potential is used to a small extent due to no fundamental approach to the development of its hydration and curing processes. Despite numerous studies in the field [1, 2], the hydration and structure formation mechanisms are usually based on Le Chatelier's principle, Michaelis and Baikov theories, whose followers reasonably develop, clarify and stick with these hypotheses by using all up-to-date violent physicochemical methods.

The complexity of the processes which run in the cement-water system is conditioned by its high sensitivity to different transition factors from the initial, paste structure and low strength to the final, high-order structure and strength. The high sensitivity of the cement-water system is conditioned rather by the physicochemical than chemical interaction between the components. Any external influence (thermal, mechanical, electrochemical, electrophysical) on the cement-water system or change in its inner energy properties (dispersibility, chemical potential, surface free energy) causes an adequate response of its physicochemical process [3–5]. In the case of no

external influence, the energy sources causing the physicochemical process are the surface free energy and the chemical potential of the system.

It is known that the driving force of spontaneous processes is the system transition to the lowest energy state, with the heat formation or, most probably, to the highly disordered state with maximum entropy. Entropy of hydrated compounds significantly increases during hydration of clinker minerals, which is confirmed by the data summarized in Table 1 [6].

Table 1. Standard values of entropy S and heat capacity C of unhydrated and hydrated clinker minerals.

Unhydrated clinker minerals			Hydrated clinker minerals		
Compounds	S_{298}^{ij}, kJ/(mol· K)	C_{298}, kJ/(mol · K)	Compounds	S_{298}^{ij}, kJ/(mol· K)	C_{298}, kJ/(mol· K)
β-2CaO. SiO$_2$	127.79	128.74	$2CaO \cdot 3SiO_2 \cdot 2{,}5H_2O$	268.16	295.46
$3CaO.SiO_2$	168.5	171.70	$4CaO \cdot 3SiO_2 \cdot 1{,}5H_2O$	330.80	309.80
$3CaO.Al_2O_3$	205.73	209.60	$5CaO \cdot 6SiO_2 \cdot 5{,}5H_2O$	612.36	699.40
$CaO.SiO_2$ $3CaO.Al_2O_3$ + $3CaSO_4$	145.39 –	153.90 –	$3CaO \cdot Al_2O_3 \cdot 6{,}0H_2O$ $3CaO \cdot Al_2O_3 \cdot 3CaSO_4 \cdot 31H_2O$	405.17 1710.36	447.30 1965.45
CaO	39.80	42.87	$Ca(OH)_2$	83.50	92.39

According to Table 1, the heat capacity of compounds changes similarly to entropy, the numerical values for the normal conditions being the same. The Gibbs free energy ($\Delta G = \Delta H - T\Delta S$) at cement hydration is negative throughout the spontaneous process, as its development is provided not only by entropy $T\Delta S$ (bound heat), but also enthalpy ΔH (the binding energy between cation and anion during the compound transition from the initial to hydrated state).

If entropy is caused by the dispersion of cement particles in water, the change in ΔH enthalpy is predetermined by changes in the temperature and heat capacity of the cement-water system. The heat capacity continues to grow due to the formation of the primary solid hydration products having the true density of ~ 1.5 g/cm^3, which is lower than that of unhydrated cement (2.9–3.1 g/cm^3). Water having the abnormally high heat capacity, significantly contributes to the heat capacity of hydrated cement products. The energy changes in the developing cement-water system cause an adequate change in its temperature. This phenomenon is widely used in thermokinetic studies of the cement-water system using calorimeters of various design [7–9]. The analysis of the operating principles of these calorimeters shows that they are capable of recording the integral heat formation of the cement-water system in the first 1–7 days. The most distinct are two peaks of the heat formation, namely: in cement wetting and between 7 and 12 h of the hydration process. It is clear that these data do not provide a real assessment of the processes running in the system. The proposed highly sensitive differential method of the temperature control provides the deeper understanding of

phenomena developing in the cement-water system and can be used to enhance the cement potential in the development of modern construction technologies.

2 Methods and Materials

The type CEM I 42.5B Portland cement was investigated in this experiment. Temperature measurements were performed by using a differential microcalorimeter containing two calorimeter cells for reference and test material, respectively. The reference weighted portion of 1.35 g dry cement was placed in the first cell, and the test weighted portion of 1.0 g was placed in the second cell. After the weigh temperature equalization, 35 ml of distilled water was introduced in the calorimeter cell with the test weigh to achieve the mass balance in both calorimeter cells. The cells were equipped with miniature resistance temperature detectors, that gave signals to a computer for processing the data obtained. Measurement results were then displayed as temperature-time dependences, *viz.* $\Delta T = f(\tau)$.

The proposed technique allows recording the temperature difference between the calorimeter cells immediately after the water-cement contact in the cell with the test weigh during its temperature change and diverse thermochemical processes [8, 9].

3 Results and Discussion

The kinetic curves of temperature fluctuations in the cement-water system are given in Figs. 1 and 2 for the hydration and curing processes during 3 days and the latent period.
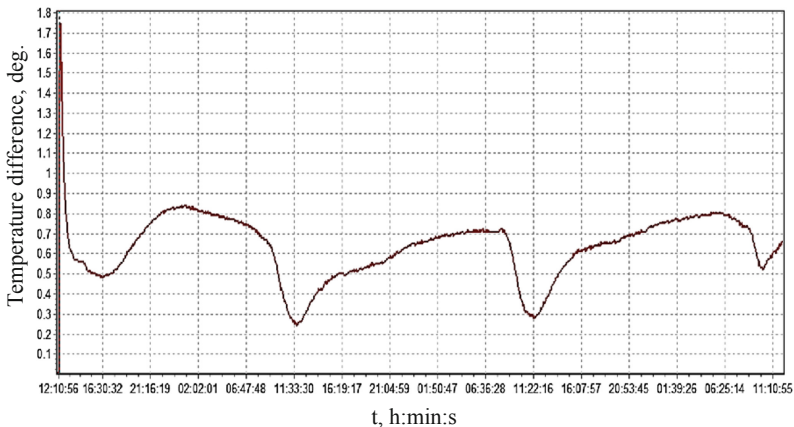
Fig. 1. Kinetic curve of temperature fluctuations in the cement-water system during 3-day hydration and curing.
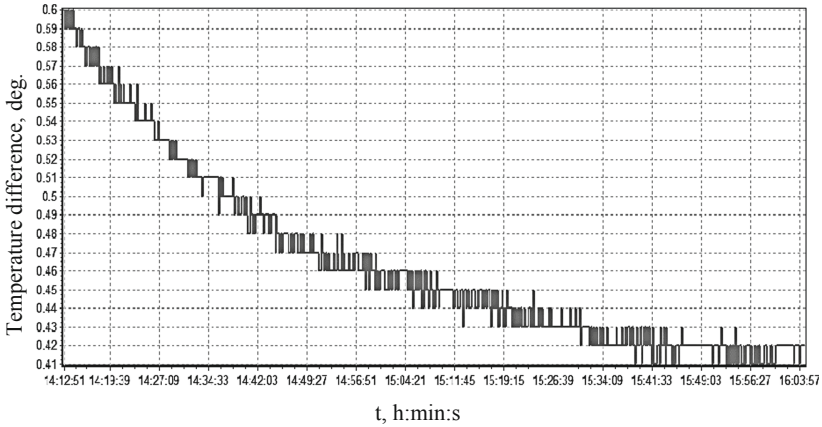
Fig. 2. Kinetic curve of temperature fluctuations in the cement-water system during the latent period of hydration and curing.

Based on the analysis of the experimental data the following conclusions can be drawn.

1. Heat formation is wavy in the cement-water system (see Fig. 1). This can be explained by the unity and opposition of the two main processes observed during the cement hydration and curing, namely the particle dispersion of the initial cement (entropy, heat absorption) and crystallization of hydration products (enthalpy, heat formation).

2. The intense heat formation during cement wetting promotes hydrolysis of tricalcium silicate and hydration of clinker minerals. These processes are accompanied by continuous binding of free water. Spontaneous dispersion of the cement particles predominates during the latent period also.

3. As can be seen from Fig. 2, the harmonic frequency of ~ 12 h for the heat formation, is the second, as its development is predetermined by the fundamental frequency of 1–3 vibrations per minute. In turn, the second harmonic is the basis for the third harmonic frequency of several days of vibration.

4. The total thermal effect Q_c from the cement-water interaction includes three components: heat dispersion Q_d of the cement crystal lattice into the structural elements, hydration heat Q_h of these elements, and crystallization heat Q_{cr} of hydrated products. The crystal lattice dispersion is always accompanied by the heat absorption, whereas hydration of the structural elements and crystallization of hydrated products are accompanied by the heat formation:

$$Q = Q_h + Q_{cr}$$

5. The fundamental harmonic of the heat formation indicates that the heat dispersion and hydration heat make the main contribution to the exothermic process.

6. The extreme values of the released or absorbed heat during the second harmonic are predetermined either by dispersion or hydration and recrystallization of the primary hydration products with their transition to a more compact state.

Our experiments show that the vibration processes of the heat formation last for 27 days of the cement curing, and then transfer to the endothermic process with increasing vibration period from 3 to 4 days.

It should be noted that the cement particle dispersion with water occurs not only in the surface layer, but also in the crystal lattice volume. This is because the implantation of H_3O^+ having a smaller size than the crystal lattice parameters for minerals. As a result, the crystal amorphization occurs with formation of hydrated compounds, which adsorb free water on their effective surface.

The fundamental harmonic is observed already on the right side of the heat formation curve during cement wetting, with the dispersion process also dominating in the latent period for 3 or 4 h. When pH $\approx$ 12 in the cement-water system, recrystallization of mostly primary portlandite units occurs with the heat-formation maximum observed after 10 or 12 h of the cement-water interaction and matching the time of cement setting. By this time, almost all mixing water transfers from the free to the adsorbed state. Mixing of cement at the initial hydration stage is confirmed by Vyrodov [10]. During the formation of jelly-like hydration products of 1.5 g/cm^3 density, 75% of water and 25% of cement form a mixture. According to [25], these products occupy 90% of the initial porosity (the density of dry cement is 1.35 g/cm^3, the volume fraction of the solid phase K_{T1} is 0.45, and the porosity is 1 − K_{T1} = 0.55). At the initial cement concentration of 0.45 in the solid phase K_{T1}, the water film thickness retained by the particle surface can be obtained from

$$\delta = \frac{1 - k_{T1}}{k_{T1}} / S_m \rho_m = \frac{0.45}{0.55} / 283 \cdot 1350 = 3.2 \cdot 10^{-6} m = 3.2 \mu m,$$

where S_m is the specific surface of the cement unit mass (m^2/kg); ρ_m is the density of the dry cement (kg/m^3).

Consequently, in the initial state of the cement-water system, the neighbor particles interact through the liquid film with a thickness of 2δ = 6.4 μm. Calcium hydroxide releasing during tricalcium silicate hydrolysis increases the specific surface of the solid phase by more than an order of magnitude. As a result, the thickness of the liquid layers between the particles lowers to a fraction of a micrometer. In chemical and adsorption binding of the liquid phase, free water almost completely disappears already in the first hours of interacting with cement. In the absence of free water, it is not quite correct to speak about any dissolution of clinker minerals.

In cement wetting, unstable dissipative structures appear, when the heat formation reaches the maximum. The presence of such structures is confirmed by the fundamental harmonic of the heat formation, that performs a kind of motor function of self-excited vibrations of the dispersion and hydration processes. These processes run in the local equilibrium state and are continuously and extremely economically fed by the energy and substance flows in the system. The formation and destruction of dissipative structures accompanied by a continuous entropy, serve as a driving force of the hydration process.

The formation of highly-dispersive hydration products and the intense binding of mixing water most likely occur during the latent period, when the increment ΔF of the surface free energy in the water-cement system is calculated as

$$F = H - PV - TS = + Q_h,$$

where $\Delta\sigma$ is the increment of the surface free energy in forming the new surface, Q_h is the absorbed or latent heat of the new surface formation.

The system constant temperature in the latent period indicates to the phase transition resulting in the formation of highly-dispersive hydration products. This is also supported by the exothermic process which follows by the latent period, during which the pores in the cement layer are completely filled with primary hydration products. Due to the restricted porosity, the latter partially transfer to a more compact crystalline state with a density of 2.23–2.5 g/cm^3. The crystallization process is accompanied by the heat formation, solid phase reduction, new free volume formation, and release of free water which interacts topochemically with unhydrated cement grains and disperses their surface, thereby absorbing a significant amount of the system energy. Free water releasing during crystallization, weakens the particle interaction, enabling periodic changes in the mechanical properties of the system. Thus, during the cement hydration the liquid phase goes through the solid phase but not vice versa.

The temperature increase after 1-day curing is probably caused by the ettringite crystal deposition accompanied by binding of a significant amount of free water. Due to quantitative changes in the system, it acquires new qualities after 42–48 h of the cement-water interaction. First of all, this is a change in the strength generation mechanism caused by the modified phase composition of the system. At the initial volume fraction of 0.45 of the solid phase K_{T1}, its content increases to $K_{T2} = 0.65$–0.67, including that one with 1.5 g/cm^3 density. The hydration products occupy the initial pore volume of $1 - K_{T1}$ by 0.55 degree, the porosity N occupies $K_{T2} - K_{T1}/1 - K_{T1} = 0.37$–0.40, and the cement hydration is $\alpha = K_{T2} - K_{T1}/1 - K_{T2} = 0.45$–0.48 [12]. At $N = 0.37$–0.40, the nodal point of quantitative and qualitative changes in the system is a conventional border, where the cement curing mechanism changes. Until this state is reached, the dispersion and hydration processes dominate in the system. After that, the porosity significantly reduces due to the formation of the primary crystalline structure of hydrated cement. The pore volume is filled with primary hydration products to achieve the restricted volume according to Sychev [13] with their subsequent crystallization.

The analysis of cement hydration based on the obtained heat formation kinetics allows us to identify two types of the restricted volume in the system. The first type is observed at an early hydration stage as a result of filling the initial pores with colloidal hydration products, which form the coagulation structure. This structure contains the primary, separate microcrystalline formations, which represent crystal seeds for subsequent crystallization of colloidal hydration products. The second type is observed after 42–48 h of cement hydration, during the formation of the continuous crystallization structure of hydrated cement. In cooperation with colloidal products, this structure occupies 37–40% of free pores.

The system temperature lowers after 3 days, and the heat formation harmonics change to endothermic. The line connecting the mean values of endo- and exothermic processes of the second harmonics forms the path integral for the third-harmonic heat formation. As the primary hydration products accumulate in the pore volume and the next restricted volume is achieved, the vibration period from 3 to 4 days can be identified in the cement system.

4   Conclusion

Based on the obtained results of the heat formation in the cement-water system for more than 28 days, it can be concluded that the cement hydration process was based on continuous self-excited vibrations maintained by the energy released during the transition of clinker minerals to hydrated state. A part of this energy stored by the system during the first hours of hydration, was used for dispersion of the initial cement particles. That process was accompanied by the solid phase growth to a certain critical value, due to the formation of colloidal products low in density and high in adsorbed water content. The development of the dispersion process in the restricted pore volume led to the increase in the inner pressure that caused recrystallization of the primary hydration products. The increase in their density was accompanied by the free water release and the porosity formation. The heat formation during recrystallization increased the total energy stored in the system, which was again consumed by the cement particle dispersion, and the hydration cycle repeated. The reciprocal cement hydration process provided a gradual pore filling with crystallized hydration products.

The analysis of the cement hydration and curing mechanisms showed that of all known theories describing these phenomena, the most reliable was the Baikov theory based on the water-cement topochemical interaction with the formation of colloidal products and subsequent crystallization of the primary hydration products. It is worth clarifying that these processes in the cement-water system kept periodicity and cycling for a long time.

Purposeful efforts to affect the processes of hydration, dispersion, and crystallization in cement systems through the introduction of accelerating or retarding admixtures for cement curing, crystal seeds for crystallization of colloidal hydration products, and the external influence (mechanical, thermal, electrophysical, electromagnetic) on the cement-water system will provide an effective control for cement operating properties to meet the specific needs of modern construction technologies.

References

1. Bourchy, A., Barnes-Davin, L., Bessette, L., et al.: Effect of cement composition on fresh state and heat of hydration of portland cement with limestone and slag. ACI Mater. J. **117**(1), 153–165 (2020)
2. Vovk, A.I.: C3S hydration and C-S–H-phase structure: new approaches, hypotheses, and data. Cement i ego Primenenie **3**, 89–92 (2012)

3. Fedyuk, R.S., Mochalov, A.V., Lesovik, V.S.: Modern activation methods for binder and concrete mixtures (review). FEFU School Eng. Bull. **37**(4), 85–99 (2018)
4. Ibragimov, R.A., Pimenov, S.I.: Influence of mechanochemical activation on the cement hydration features. Mag. Civ. Eng. **2**, 3–12 (2016)
5. Gorlenko, N.P., Sarkisov, Y.S.: Low-energy activation of water-dispersed systems. Tomsk: izd-vo Tomsk. gos. un-ta. 264 (2011)
6. Babushkin, V.I., Matveev, G.M., Mchedlov-Petrosyan, O.P.: Thermodynamics of Silicates. Stroizdat, Moscow (1986)
7. Königsberger, M., Carette, J.: Validated hydration model for slag-blended cement based on calorimetry measurements. Cem. Concr. Res. **128**, 105950 (2020)
8. Lotov, V.A., Ivanov, Y.A.: Differential microcalorimeter and method for measuring heat release. Patent RF № 2475714
9. Lotov, V.A.: The use of a new design differential microcalorimeter in the study of heat release in dispersed systems. In: Conference on Thermal Analysis and Calorimetry in Russia (RTAC-2016). St. Petersburg: SPbPU, vol. 2, pp. 428–431 (2016)
10. Vyrodov, I.P.: On the physical and chemical essence of the processes of hydration of mineral binders in the early stages. J. Appl. Chem. **49**(2), 309–3124 (1976)
11. Lotov, V.A.: Periodicity of processes of hydration and hardening of cement. Build. Mater. 55–59 (2018)
12. Lotov, V.A.: Change in the phase composition of the cement-water system during hydration and hardening. Bull. Tomsk Polytechn. Univ. **321**(3), 42–45 (2012)
13. Sychev, M.M.: Formation of hardening structures and the nature of hydration processes. Cement **2**, 19–20 (1989)

Decoration of Non-ferrous Metals

N. I. Bondarenko[✉] , Z. V. Pavlenko , and D. O. Bondarenko

Belgorod State Technological University named after V.G. Shukhov,
Belgorod, Russia
bondarenko-7l@mail.ru

Abstract. Enamel is a thin glassy coating obtained by high-temperature treatment. Technical enamels are applied to products made of cast iron, steel, aluminum and light metal alloys. The metal-enamel combination successfully combines the molding ability and strength of the metal with the chemical resistance and stability of the glass. The aim of this study is to develop methods for decorating non-ferrous metals. Based on the literature analysis, a composition with similar values of the thermal coefficient of linear expansion (TCLE) of enamel ($\alpha = 159 \cdot 10^{-7}$ K^{-1}) and copper ($\alpha = 162 \cdot 10^{-7}$ K^{-1}) was selected as enamel for decorating copper. The compositions of glass coatings containing fractions of 0.071 mm and 0.1 mm were modeled. The optimal composition of glass coatings was determined experimentally, which contains 70% of the 0.071 mm fraction and 30% of the 0.1 mm fraction. The TCLE of the glass-enamel stack was determined by the dilatometric method with a measurement accuracy of $\pm 1.5\%$, the TCLE curve was constructed according to the experimental data. The fusibility of the samples was determined in a laboratory muffle silite furnace SNOL-1.6. The frit was made at a temperature of 1250 °C for 0.5 h. The slip was prepared from each composition according to the classical scheme and applied by dipping.

Keywords: Coating · Slip · Frit · TCLE · Firing temperature

1 Introduction

Currently, enameled products are used in many areas of everyday life: food industry, agriculture and forestry, construction, transport, chemical, petrochemical, pharmaceutical and other sectors of the national economy [1–5].

The quality of artistic enameling will be determined by practical experience, which allows eliminating errors in new experiments and tests. Coatings can be applied by such methods as ion-plasma, atmospheric-plasma, thermal diffusion, slip, etc. [6–9].

Complex problems of enamel composition, firing and bonding, as well as other technical issues have not been fully studied yet, but there are already significant scientific achievements that make it easier to understand the processes that occur during enameling, allowing us to judge the causes of errors. Copper has separate physical and chemical properties that allow it to have a good adhesion to enamel [10]. The high melting point of 1084 °C ensures the stability of the metal when melting enamel. Consequently, copper plays an important role in artistic enameling, as does sheet steel in industrial enameling.

2 Methods and Materials

As the main raw materials for the production of copper enamels, materials were used, the chemical composition of which is presented in Table 1.

Table 1. Chemical composition of raw materials.

Material	Content of components, wt%											
	SiO_2	Al_2O_3	CaO	MgO	B_2O_3	Na_2O	K_2O	TiO_2	P_2O_5	S	Fe_2O_3	BaO
Quartz sand	96.68	1.5	0.13	0.11		0.92					0.2	
Boric acid					56.2							
Soda ash						54.69						
Potash							66.27					
Alumina	0.03	99.0				0.5					0.035	
Chalk		0.215	52.7	0.43							0.113	
Barium oxide												97
Bentonite clay	52.3	16.55	5.49	3.03		1.92	0.92	0.95	0.12	0.12	5.92	

Raw components were weighed on electronic scales of the OHAUS model with a weighing accuracy of 0.01 g. The charge was tableted using a punch with a diameter of 0.01 m. The fusibility of the samples was determined in a laboratory muffle silicate furnace SNOL-1.6.

The frit was made in a laboratory electric silicate furnace at a temperature of 1250° C for 0.5 h, then the crucible was removed from the furnace and sharply cooled. A metal mortar and ball mill were used to grind the frit.

Copper plates were chosen as the substrate. The coating was applied by dipping. Dipping is the most universal method of applying enamel coatings, and for certain types of products – sometimes the only possible one.

Based on the literature analysis, a composition with similar values of TCLE of enamel ($\alpha = 159 \cdot 10^{-7}$ K^{-1}) and copper ($\alpha = 162 \cdot 10^{-7}$ K^{-1}) was selected as enamel for decorating copper. Chemical composition of enamel, wt%: SiO_2 – 45.6; $Al_2O_{3-7}.0$; CaO – 5.0; Na_2O – 13.1; K_2O – 10.1; B_2O_3 – 11.2; BaO – 8.0.

3 Results and Discussion

The made frit was produced by casting in the form of a flat cake on a metal plate and a stack was cast to determine the TCLE. The frit was ground by hand in a metal mortar to obtain pieces of size ≤ 5 mm, then ground in a porcelain ball mill with a diameter of 0.15 m using mixed-shape porcelain grinding media (cylindrical and spherical) for 6 h. After grinding, the frit was sifted through sieves № 0071 and № 01.

The TCLE of the glass-enamel stack was determined by dilatometric method. The accuracy of TCLE measurement by the quartz dilatometer method is $\pm 1.5\%$.

For the test, a well-made and non-flawed sample was used. A sample of a glass-enamel stack, measured with an accuracy of ± 0.1 mm, was installed in a quartz block holder so that it had a common axis with a quartz push rod. They lowered carefully the quartz block holder into the furnace. During 15–20 min, the metal parts of the dilatometer were thermostated, the required heating speed of the furnace was set, and the experiment was started.

At a sample heating rate of 3 deg/min in the furnace, it took about 3 h to construct the temperature curve for the expansion of the glass-enamel stack. Temperature and elongation measurements were carried out at least 5 min later. Based on the experimental data, the TCLE curve of the glass-enamel stack was constructed, shown in Fig. 1.
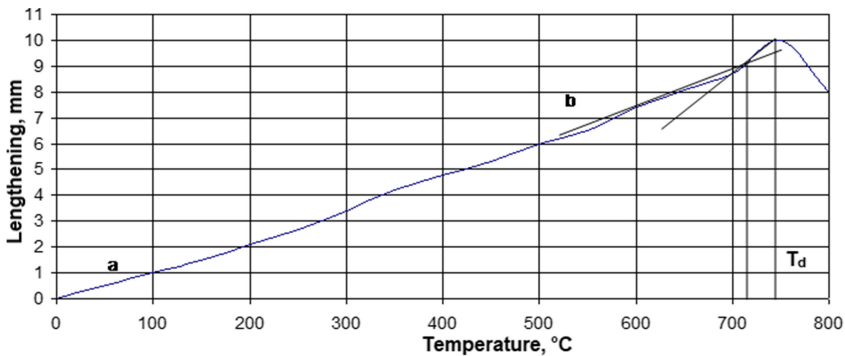
Fig. 1. TCLE glass enamel billet.

During the work, 7 compositions of glass coatings were modeled, consisting of fractions of 0.071 mm and 0.1 mm, in which the fraction content varied from 20 to 80 wt% in increments of 10% (Table 2).

Table 2. Compositions of glass coatings.

№ of composition	Number of fractions, wt%	
	0.071 mm	0.1 mm
1	80	20
2*	70*	30*
3	60	40
4	50	50
5	40	60
6	30	70
7	20	80

* – optimal composition

From each composition, a slip was made according to the classical scheme. Aging of the slip lasted at least 2 h with constant stirring. Substrates for applying the slip were prepared as follows. Copper was cut into plates of the same size, and then subjected to straightening by "smoothing" with a flattening hammer without striking. Then the plates were degreased with acetone and treated in an etching solution of the following composition, g/l H_2O: HNO_3 (conc) – 92, H_2SO_4 (conc) – 8. The slip was applied on copper by dipping, evenly distributed over the entire surface. The samples were placed on a refractory substrate and allowed the slip to dry. Then they put it in a cold electric furnace, heated it to a temperature of 850 °C and kept for 6 min at maximum temperature (Fig. 2).
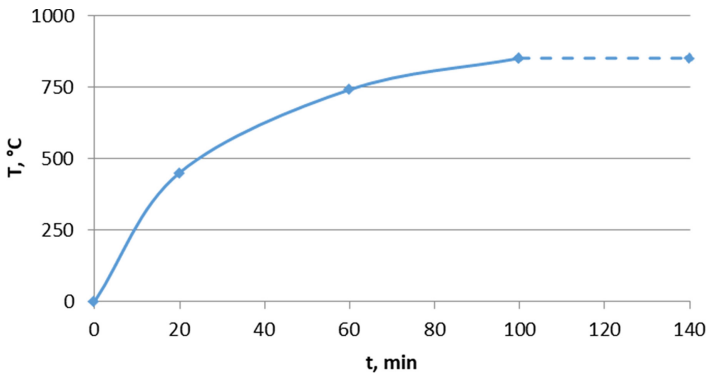
Fig. 2. Temperature-time interval of coating firing.

Figure 3 shows samples whose fractional composition corresponds to the values of Table 2.
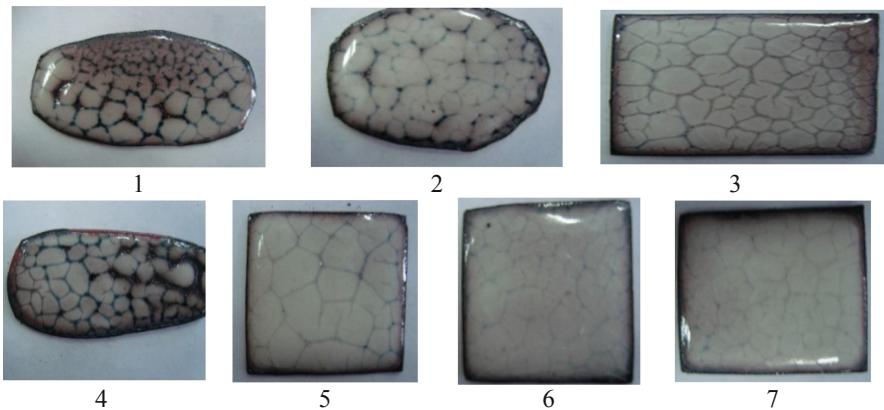
Fig. 3. Coated copper samples, heat-treated at T = 850 °C.

As a result of heat treatment, numerous burnouts and exposed metal sections were formed on samples № 1, № 3, and № 4, which indicates a violation of the surface continuity. The surface of samples № 5, № 6, and № 7 was riddled with microcracks, which indicates poor resistance to water and chemical reagents. There were no visible surface defects on sample №2, and from this we can conclude that the fractional composition was chosen correctly, which will allow it to be used as the main composition of the glass coating in the future.

4 Conclusion

During the experiment, it was found that the rational composition is composition №2, which contains 70% of the 0.071 mm fraction and 30% of the 0.1 mm fraction. The TCLE of the glass-enamel coating was determined experimentally.

5 Acknowledgements

References

1. Emelianov, AYu., Petrova, S.G., Kanyukov, N.V.: Traditions of hot enamelling in the Near East and Central Asia: from the Maghreb to Iran. Design. Materials. Technology **1**(26), 84–85 (2013)
2. Fedyayeva, T.N., Emelianov, AYu., Petrova, S.G.: Design of the decorative art objects made with the use of cloisonne technique. Design. Materials Technology. **2**(17), 95–97 (2011)
3. Fedyaeva, T.N., Emelianov, AYu., Petrova, S.G.: Use of glass forming materials as a basis for a painted enamel. Design. Materials. Technology **1**(16), 53–55 (2011)
4. Kovalchenko, N.A., Pavlenko, Z.V.: Waste-bearing decorative glazes for facade ceramics. Glass Ceram. **63**(1–2), 26–28 (2006)
5. Rodtsevich, S.P., Eliseev, SYu., Lukashevich, G.F.: Jewelry enamels with a decreased lead oxide content. Glass Ceram. **8**, 27–28 (2001)
6. Bondarenko, N.I., Bondarenko, D.O., Kochurin, D.V., Bragina, L.L., Yakovenko, T.A.: Sheet construction glass with protective and decorative coatings. Construction Materials and Products **2**(4), 11–16 (2019)
7. Bondarenko, N.I., Bondarenko, D.O.: Processes of forming protective and decorative coatings on concrete at plasma treatment. IOP Conference Series: Materials Science and Engineering **945**, 012038 (2020)
8. Bessmertnyy, V.S., Sokolova, O.N., Bondarenko, N.I., Bondarenko, D.O., Bragina, L.L., Makarov, A.V., Kochurin, D.V.: Plasmachemical modification of thermal insulated blocks with decorative coating. Bulletin of BSTU named after V.G. Shukhov 3, 85–92 (2019)

9. Bondarenko, D.O., Strokova, V.V.: Operating properties of the coating, depending on the composition during plasma-chemical modification. IOP Conference Series: Earth and Environmental Science. 341, 012141 (2019)
10. Zubekhin, A.P., Yatsenko, E.A., Klimenko, E.B.: Pb-free boroalumosilicate enamels for decorative articles made of coppers. Glass Ceram. **4**, 24–25 (2001)

Research of Black Soldier Fly (Hermetia Illucens) Maggots Zoocompost's Influence on Soil Fertility

E. A. Pendyurin[(✉)] , S. Yu. Rybina , and L. M. Smolenskaya

Belgorod State Technological University named after V. G. Shukhov,
46 Kostyukova St., Belgorod 308012, Russia
pendyrinea@yandex.ru

Abstract. At present the soil covering is systematically exposed to adverse factors, which have a negative impact on its fertility. One of the ways of maintaining soil fertility is the application of composts. In this research zoocompost of black soldier fly (Hermetia illucens) maggots was used as a fertility amendment. The zoocompost under study was a loose, slightly moving, fine-grained mass of brown color, with a faint smell of ammonia, with a predominant particle size of 1–3 mm. The main nutrients of the zoo compost are in the form of various humic acid compounds, contain the necessary macro-and microelements, biogenic Ca^{2+}, Mg^{2+}, Fe_2O_3. The zoocompost is rich in saprophytic microflora useful for soil and plants. It has been determined that such zoocompost can be used as an organic fertilizer, as its parameters meet the requirements of GOST 33830-2016. The carried-out field research has demonstrated the positive dynamics of growth and development of cucumber fruits, variety «Dalnevostochny 27». The crop yield from one cucumber plant increased from 22.16 to 240.59 g, the yield from a plot from 63.75–692.68 g. The optimal amount of application was considered to be 2 t/ha, added in spring.

Keywords: Zoocompost · Black soldier fly (Hermetia illucens) maggot · Field experiment · Crop yield · Cucumbers

1 Introduction

In the recent decade the contradictions between the possibilities of nature and the needs of humanity have escalated considerably. Each year the ecological factors have more and more influence on the economic development of countries and regions, becoming key factors at taking important decisions. Ignoring the nature protection requirements more and more often results in disasters and considerable material losses [1]. One of such losses is the decrease of soil fertility.

Soil is the historically natural body of the natural environment in conditions of the Earth; it is the main instrument and object of labor in agricultural industry, the source of the people's wealth and the human life [2].

At present soil covering is systematically exposed to adverse factors. Due to the human economic activities agricultural lands are disposed for constructing new

enterprises and cities, motor roads and high-voltage power lines, flooded for building hydroelectric power plants or mining industry development [3].

In the course of its development, the society daily faces the problem of dumping waste products, such as residues of animal and vegetable food. This waste makes up a substantial part of human life activity and requires special treatment. It has been determined that each city dweller produces 200–500 kg of organic waste. In its nutrients content and fertilizing properties it is close to manure and can be used in agriculture.

The Belgorod region is rightfully considered one of the leading agrarian territories in the country, with the rapidly developing agriculture and stock raising. Possessing 1.1% share of plough land, the Belgorod region produces over 4% of the national gross agricultural product.

As it is known, to maintain the self-supporting balance of the organic matter in chernozems, it is necessary to add 6–10 t/ha of litter manure. The usage of organic fertilizers in the Belgorod region in 1987 amounted to 9 mln ton (5.8 t/ha of area), the lowest usage was registered in 2006 - 912 thousand ton (0.9 t/ha), in 2019 11.9 mln ton (7.9 t/ha) was used. Since 2007, due to the intensive development of stock-raising, the amounts of using organic fertilizers in the region have begun to increase. It should be mentioned, that the issues of preserving and increasing soil fertility, its protection, ecology and sustainable utilization have the top priority.

2   Materials and Methods

The object of research was zoocompost, generated by maggots of black soldier fly (Hermetia illucens) [4, 5]. The technology under study is based on the ability of the maggots of black soldier fly, which is a species of dipteran insects, to recycle any organic matter. The fly maggots can digest such organic residues as pig and poultry manure, wastewater sludge, meat and fish residues, fruits, vegetables, the restaurants' waste and kitchen waste [6]. The organic matter doesn't need preliminary grinding, as black soldier fly maggots in the process of their life-sustaining activity (feeding and digesting) reduce the organic waste to similar fine particles. After separating maggots from the organic waste mass, its amount is reduced by 70–80%, and the waste is presented with the high-value, environmentally-clean and all-nutrient fertilizer for plants (zoohumus) [7]. The main advantage of this technology is its safety for the environment and for human.

In this research, for obtaining zoocompost a wide range of food waste was used, first of all, off-quality grain products, food waste from chain stores, sawdust. To the waste products mix the grown-up maggots were added, which were processing the substrate during several days. At the end of this period the maggots were separated from the processed waste by screening.

The zoocompost under study appears as a loose low-caking fine-grained brown mass with faint ammonia smell; the dominant particle size is 1–3 mm. The main nutrients of the zoocompost are present in the form of various humus acids' compounds, which contain necessary macronutrients and micronutrients, biogenous Ca^{2+},

Mg^{2+}, Fe_2O_3. The zoocompost is rich in saprophytic microflora, which is good for soil and plants.

To study the applicability of zoocompost as an organic fertilizer for soils, a number of research studies to evaluate its nutrient-supplying capacity were carried out: the air-oven, spectrophotometric, potentiometric, titration and conductometric methods [8].

3   Results and Discussion

At the first stage of the research the chemical analysis of zoocompost was carried out and the content of biogenic elements in it was determined. The experimental research findings of black soldier fly maggots' zoocompost are presented in Table 1.

Table 1.   Biogenic components content

Parameters of zoocompost										
NO_3^-, mg/kg	NO_2^-, mg/kg	NH_4^+, mg/kg	N_{total}, mg/kg	$C_{opr.}$, %	Humus, %	P_2O_5, mg/100 g	K_2O mg/100 g	Fe_2O_3, mg/100 g	pH_{H2O}	pH_{KCl}
656.2 ± 28.06	2.66 ± 0.20	8178.7 ± 1795.4	6871.15 ± 1473.9	17.20 ± 0.27	29.65 ± 0.27	220.33 ± 28.00	907.00 ± 25.00	26.00 ± 2.63	8.02 ± 0.06	7.92

The data in Table 1 indicate the presence of nutrient elements, necessary for growth and development of agricultural crops. Ammonium prevails among nitrogen metabolism products, which means that nitrification processes are still going on.

The obtained zoocompost can be used as an organic fertilizer, as its parameters meet the requirements of GOST 33830–2016 "Organic fertilizers on basis of waste of stock-raising. Specifications".

To confirm the findings of zoocompost's applicability as an organic fertilizer we carried out a field experiment at a specially separated plot, with the purpose of determining the quantitative effects of the cultivating conditions and methods on agricultural crops yield.

Zoocompost was added to the soil in amount of 1–5 ton per hectare in spring, evenly distributed on the surface of the plot, and buried 10–15 cm deep with the floating-blade cultivator KP1; the size of the plot was 1 m². The soil of the experimental field was presented with typical medium-humic chernozem in the Belgorod region, Belgorod district, Erik village, gardeners' non-commercial partnership "Zemledelets". At the prepared experimental plots the agricultural vegetable crops – cucumber, of the «Dalnevostochny 27» variety – were sown. The statistical analysis and processing of the obtained sampled data of the streamlined repetition was performed by means of NIRSMAIN.EXE application [9, 10].

The climatic conditions of the cucumbers development in 2020 are characterized as relatively favorable: the cold and rainy May, warm June and July with enough moisture, and the dry August, lacking moisture by 53% of the long-time average annual norm (Table 2).

Table 2. Climatic conditions of the cucumbers development

Meteorological data for 2020						
Month	Average monthly temperature	Norm	Dev. ±	Total precipitation, mm	Norm	% of the norm
May	12.5	14.6	2.1	101.2	47	215.3
June	20.4	17.9	2.5	62.2	63	98.7
July	20.7	19.9	0.8	86	69	124.6
August	20.11	18.8	1.31	29.8	56	53

To evaluate the influence of zoocompost on cucumbers, the germination ability of plants was studied (Table 3).

Table 3. The influence of zoocompost on the germination ability of cucumber plants

Germination ability of cucumber plants at the experimental plots, %					
Number of the plot (amount of the added compost, t/ha)					
1	2	3	4	5	To
71	75	80	75	70	65
75	85	75	80	75	70
71	100	85	70	70	70
Average value					
72	87	80	75	72	68
+4	+19	+12	+7	+4	Deviation from the control

experimental error: 1.446
LSD (absolute) 95% - 11.165
LSD (relative) 95% - 14.756.

According to the data in Table 3, the black soldier fly maggots' zoocompost has a positive effect on the germination ability of plants, increasing the cucumber plants emergence from 4 to 19%, the statistically significant data were obtained at adding 2 and 3 t/ha (plots 2 and 3).

The cucumbers at experimental plots were being grown from May to September without additional watering or fertilizing (Fig. 1). The first cucumber fruit was gathered at the plots with the highest amount of added zoocompost on July, 4.

Fig. 1. Experimental plots

The cucumber fruits were gathered in the course of their ripening, averagely once in 2–3 days; the size of cucumbers varied within the range 9–12 cm, the weight varied from 57.62 g to 82.84 g.

To study the influence of zoocompost on the fruit formation of cucumbers, the counting of the number of fruits on 1 m^2 was performed. The quantitative data are presented in Table 4.

Table 4. The influence of zoocompost on the quantitative data of cucumber fruits

Number of cucumber fruits, pcs/1 m^2					
Number of the plot (amount of the added compost, t/ha)					
1	2	3	4	5	к
16	24	19	14	16	15
13	23	20	19	16	12
14	24	18	17	16	13
Average value					
14	24	19	17	16	13
+1	+11	+6	+4	+3	Deviation from the control

experimental error: 0.367
LSD (absolute) 95% - 2.83
LSD (relative) 95% - 16.53.

As we can see in Table 4, from the control plot 13 cucumber fruits were gathered, and at adding zoocompost the number of cucumber fruits increased from 14 to 24, though the data of the plots 2 and 3 should be considered statistically significant.

To study the influence of zoocompost on the crop yield we researched the yield index of 1 plant and the average yield of cucumber fruits from a plot. The yield data are presented in Table 5–6.

Table 5. The crop yield of 1 cucumber plant, g.

Number of the plot (amount of the added compost, t/ha)					
1	2	3	4	5	To
335.16	555.4	408.22	300.30	349.90	320.87
290.13	500.00	435.07	425.07	350.00	257.25
303.90	529.10	381.40	376.40	351.50	284.60
Average value					
309.73	528.16	408.22	366.25	350.46	287.57
+22.16	+240.59	+120.65	+78.56	+62.89	Deviation from the control

experimental error: 8.740
LSD (relative) 95% - 17.98.

Table 6. Cucumber yield g/plot

Number of the plot (amount of the added compost, t/ha)					
1	2	3	4	5	To
1005.50	1587.15	1224.65	909.90	1049.70	962.61
870.39	1500.00	1305.21	1275.21	1050.00	780.00
911.70	1587.30	1144.20	1129.20	1054.50	853.80
Average value					
929.20	1558.15	1224.68	1104.77	1051.40	865.47
+63.75	+692.68	+359.21	+239.30	+185.93	Deviation from the control

experimental error: 24.865
LSD (relative) 95% - 17.10.

Analysis of the data from Table 5 indicates the statistically significant data of increase of the cucumber yield. It can be seen that the black soldier fly maggots' zoocompost has a positive impact on the crop yield of the plants and increases the average yield of cucumber plants from 309.73 g to 528.16 g. It should be mentioned that the highest increase of yield amounted to 240.59 g from one plant and was achieved at adding the double quantity of zoocompost (2 ton per hectare).

The data in Table 6 indicate the statistically significant data of the cucumber yield increase. It can be seen that the black soldier fly maggots' zoocompost has a positive impact on the crop yield: the average yield of cucumber fruits amounted to 929.20–1558.15, which is by 63.75–692.68 g higher than for the control plot. It should be

mentioned that the highest increase of yield amounted to 692.68 g from one plot, which is by 1.2 higher than for the control sample.

4 Conclusion

Having analyzed the research findings of the main chemical characteristics of the black soldier fly maggots' zoocompost, we can arrive to the conclusion that it meets the requirements of GOST 33830–2016 "Organic fertilizers on basis of waste of stock-raising. Specifications" in a number of parameters.

The zoocompost, generated by black soldier fly maggots, has a positive effect on the germinating ability of plants, increasing the germinating ability of cucumber plants from 4 to 19%.

The influence of zoocompost on the amount of cucumber fruits has been studied: 13 cucumber fruits were gathered from the control, while at adding the zoocompost the number of cucumber fruits increased from 14 to 24.

The average increase of crop yield from 1 cucumber plant increased from 22.16 to 240.59 g, the yield from a plot – from 63.75–692.68 g. It should be noted that the highest increase of yield was achieved at adding the double quantity of zoocompost (2 ton per hectare).

It has been experimentally proved that the zoocompost can be used as an organic fertilizer; the optimal quantity appears to be 2 t/ha, added in spring.

References

1. Baklazhenko, E.V.: Classification and zonation of streamsides in small cities through the example of Belgorod region. Bulletin Belgorod State Technol. Univ. Named After V.G. Shukhov. **5/8**, 61–68 (2020)
2. Solovichenko, V.D., Navolneva, E.V., Stupakov, A.G., Kulikova, M.A.: Soil fertility recovery as the basis of increasing the cropping capacity. Agroecological problems of soil sciences and arable farming. Collection of reports of research and practice conference of the Kursk department of IPO Soil scientists' society named after V.G. Dokuchaev, Kursk, pp. 190–194 (2015)
3. Smolenskaya, L.M., Rybina, S.Y., Pendyurin, E.A.: Studying the moisture capacity of artificial soils containing industrial byproducts in the collection: IOP Conference Series: Earth and Environmental Science C. 022008 (2019)
4. Alvarez, L.: The Role of Black Soldier Fly, Hermetia illucens (L.) (Diptera: Stratiomyidae) in Sustainable Waste Management in Northern Climates. Electronic Theses and Dissertations. 402 (2012)
5. Sheppard, D.C., Tomberlin, J.K., Joyce, J.A., Kiser, B.C., Sumner, S.M.: Rearing methods for the black soldier fly (Diptera: Stratiomyidae) in a colony. J. Med. Entomol. **39**(4), 695–698 (2002)

6. Bastrakov, A.I., Zagorinsky, A.A., Kozlova, A.A., Ushakova, N.A.: The high-efficient bioconversion of organic substrates by black soldier fly (Hermetia illucens) maggots. In: Biotechnology and Life Quality: International Research and Practice Conference, Moscow, 18–20 March 2014, pp. 418–419 (2014)
7. Udalova, Zh.V., Bastrakov, A.I., Zinovieva, S.V., Ushakova, N.A.: Application of black soldier fly, hermetia illucens, maggots for recycling potatoes, infected with phytonematodes. Theory Pract. Parasitic Diseases Control **20**, 627–632 (2019)
8. Bashkin, V.: Modern Biogeochemistry. Kluwer Academic publishers, New York (2002)
9. Dospekhov, B.A.: Methodology of field experience (with the basics of statistical processing of research results. - 5th ed. EXT. I per. Agropromizdat, Moscow (1985)
10. Sabitov, M.M., Karpovich, K.I., Kuzina, E.V.: Soil treatment – an affordable, effective agrotechnological method for preserving and restoring soil fertility. Agromir of the Volga region **2**(6), 14–18 (2012)

Effects of Sea Surf on Gabion Retaining Walls

L. I. Cherkasova[(✉)] [iD]

Moscow State University of Civil Engineering, Yaroslavskoe Shosse, 26,
Moscow 129337, Russia
CherkasovaLI@mgsu.ru

Abstract. The article presents the results of long-term observations of the destruction of a long gabion retaining wall at the base of a high coastal slope, under the influence of frontal sea waves. The destruction scheme is not consistent with the destruction scheme adopted in the normative literature as a result of stability under active soil pressure. The destruction of a stepped vertical wall occurs mainly as a result of the rupture of the metal mesh and the removal of stone material from the structure by the recoiling wave. The increasing strength of storms and the direction of the wind, in turn, are associated with global climate change. Analyzing the situation, the author comes to the conclusion that in the process of operation, the structure, despite its own destruction, made it possible to preserve the coastline and carry out work to strengthen the surface of the slope, subject to landslide and suffusion processes.

Keywords: Gabion structures · Recoil waves · Restraining structures · Shock effect of sea waves · Blurring the base

1 Introduction

In Russia, gabions are mainly used to strengthen the roadbed and bridge supports. Strengthening of sea coastal slopes was not excluded by the norms, but practically not regulated. The possibility of their use is allowed at low wave heights acting on a gentle slope up to 5 m high. The service life also varies widely. In this regard, observation of the long-term operation and destruction of gabion retaining walls at the base of the coastal high slope, subject to suffusion processes and the direct impact of sea storm waves, is a unique experience.

2 Methods and Materials

2.1 Gabion Retaining Structures. Advantages and Disadvantages

Gabions are containers made of galvanized twisted wire, filled with stone material. For retaining walls and to prevent possible erosion of slopes [1, 3, 4], box structures are often used.

Gabions are classified as erosion control and containment structures [1]. The latter include the gabion walls near the coastal slopes. In the calculation examples, a low slope of up to 5 m and the impact of waves no more than 3.5 m high are considered.

Gabions have a complex of building qualities, such as high resistance to stress; water permeability of structures; flexibility and stability characteristic.

In addition, the use of local stone materials, simplicity and environmental friendliness, and the possibility of combining with traditional types of fortifications increase the attractiveness of these structures. Together, these qualities allow gabions to effectively resist slope erosion. The construction qualities of gabions have led to a rapid expansion of the area of their application both in Russia and abroad [9, 10].

However, these designs have drawbacks that limit their use. The design flexibility limits their height, usually to 3–5 m. The wire frame can be damaged by shock loads and corrosive environments. The possibility to use gabions in the conditions of sea coastal slopes has been poorly studied, when two factors act at once that accelerate the destruction of gabions: an aggressive environment and the dynamic action of waves of great height and shock power, and the slope has a height of tens of meters.

The degree of influence of these factors can be estimated by observations of the state of gabion structures used for strengthening of the coastal line of the slopes of the Curonian Spit in the area of Svetlogorsk city.

The state of the structures was recorded according to published data [5–7] and the author's personal observations since 2016 to 2020.

2.2 Geological Conditions of the Sea Slope

The length of gabion structures along the coastal beach line is over 1400 m. In the area of city Svetlogorsk, the coastal slope descends to the beach at an angle of 20 to 60° (Fig. 1). The edge of the slope of variable height reaches 45.0 above sea level. The width of the sandy beach in front of the base of the slope varies with changing weather conditions and seasons.

Fig. 1. Coastal slope and beach in the area of city Svetlogorsk.

The range of variation in the width of the beach is from 25–30 m to the almost complete absence of the coastal line.

The upper part of the slope is composed of sandy soils. Below, at an elevation of 32.0–28.0, the coastal slope is composed of glacial loams and sandy loams with gravel, pebbles and boulders. Coniferous and deciduous trees grow along the upper part of the slope and in the area adjacent to the edge of the slope.

The soils that make up the slope, in areas not fixed by woody vegetation, are subject to partial slumping and surface erosion.

2.3   Retaining Wall Construction and Materials

The gabion wall is made in the form of a vertical 3–4-step staircase. The steps are made of 1.0 m wide gabions, which are stacked on top of each other with an offset of 0.5 m. From the back, the gabions have a continuation in the form of armopanels up to 3 m long. The bottom of the gabion and the reinforcing panel are made of a single piece of mesh. Standard sizes of mesh structures used in accordance with GOST R 52132-2003: $2.0 \times 1.0 \times 1.0$ m, $1.5 \times 1.0 \times 1.0$ m. There is practically no deepening of structures into the base [1, 3].

In all structures, including armopanels, a double-twisted galvanized wire mesh (GOST 51285-99) with hexagonal cells of 8×10 mm is used. Wire diameter: 3 mm. The diameter of the edge wire is 3.9 mm, and the wire for binding and tie is 2.2 mm.

In gabions, natural material was used, obtained by crushing igneous, sedimentary and metamorphic rocks, which possesses the necessary strength and frost resistance. The average density of the stone material was not less than 21 kN/m^3. The natural basis of the retaining wall is sands of various sizes and densities.

2.4   Particular Qualities of Exploitation Under the Influence of Sea Waves

Construction was carried out in 2008–2009. In 2010, two surveys of gabions were carried out - in January and October. Inspections showed the unsatisfactory condition of a part of the gabions; many containers of the lower stage were torn [5]. The next survey in the summer of 2011 recorded further destruction of the lower stage gabions.

It should be noted that vertical gabions, upon contact with waves, act as a wave-breaker wall, intensifying the recoil wave, and this causes the beach to erosion [6, 7]. In some places located in the immediate vicinity of the gabions, a significant decrease in the width of the beach has been noticed.

The destructive power of waves depends on the combination of the strength of the waves and the height of the sea level and the direction of the wind at the time of the storm. Waves coming from the north have the maximum acceleration length for the Baltic Sea and, accordingly, have high potential energy (Table 1).

Table 1. Average long-term and maximum characteristics of surf waves.

	Wind speed, m/s	Water surge, m	Wave height, m
Long-term mean values Curonian Spit	1–17 m/s	–	0.2–1.2 m
Average-long-term storm values	20 m/s	–	3 m
Nord-west Storm 2012	22–28 m/s	1.5 m	5–6 m
West Storm 2013	12–28 m/s		3.5–4.5 m
West Storm 2014-2015	27 m/s		
Nord Storm 2019	32–41 m/s	1.1 m	7.9–14 m

Over the past 7 years, the speed of strong winds has changed insignificantly, but there is a tendency to an increase in "northern" storms. Storm winds have a great impact on the formation of coastal relief, causing destructive processes in coastal areas. The strongest storm in its destructive power happened in 2019. At the same time, the wind speed and wave height reached their maximum values in the entire history of observations. Given the fact that there is a tendency to an increase in storm activity, a repeat of the emergency that occurred on January 2, 2019 is possible [6, 7]

3   Results and Discussion

3.1   Features of Destruction

Storm winds have a great impact on the formation of coastal relief, causing destructive processes in coastal areas. During the 2012 storm, the lower steps of the gabions suffered the most (Fig. 2).

Fig. 2. 2012 Destruction of the lower stage after a storm.

The destruction of the gabion wall is considered in [4] in the traditional framework of buckling according to the shear or overturning scheme due to active soil pressure from the side of the slope and a sharp increase in hydrostatic pressure. Under the influence of frontal storm waves, the destruction mechanism changes.

In fact, in the case of the frontal impact of sea waves, destruction occurs as a result of the wall undermining by the recoiling wave, ruptures of the wire mesh and the washing out of stones from the lower steps.

According to observations [6] carried out during the 2019 storm. the water level rose by 1.1 m (Fig. 3), and the wave height reached 7.9–14 m (Table 1). The lower steps of the wall were under water, and the waves rose to the unprotected surface of the slope.
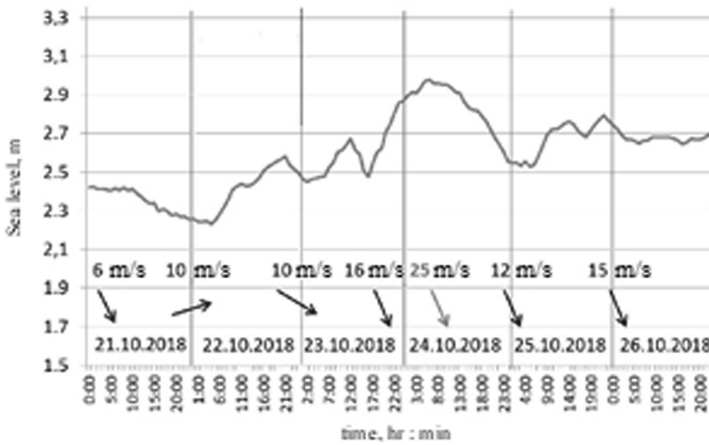
Fig. 3. Water rise graph during storm 2019. Wind direction is shown by arrows.

The lower steps, as a result of destruction, everywhere took a gentle shape, damping the shock force of the waves (Fig. 4a). practically lost their stability due to the erosion of the lower rows and the impact of water from the slope. (Figure 4b).

The widespread destruction of the 2 lower rows, the back side of the wall practically along the entire length retained its vertical position, preventing the removal of the suffusion soil removal (Fig. 4a). The outlines of the coastline of the lower part of the slope also remained practically unchanged. The slopes unprotected by gabions have undergone significant changes (Fig. 5).

The works to preserve the slope and the beach area are ongoing. Currently, gabion retaining walls are installed along the walking area above the possible level of waves.

a)

b)

Fig. 4. 2019 The coastal line of the slope is preserved by a retaining wall: a) destruction of two rows of steps; b) an area where all elements of the gabion wall are almost completely destroyed.

Fig. 5. 2019. The soils composing the slope, in areas not fixed by gabions, have undergone partial slumping and suffusion.

4   Conclusion

The gabion wall at the base of the high slope existed for 11 years in the extreme conditions of an aggressive environment and the shock impact of sea waves, the strength of which is much higher than the average storm loads for the region. Under these conditions, the retaining structure fulfilled its role as a temporary structure, maintaining the coastline of the slope despite active suffusion processes.

The destruction of the gabion wall is mainly caused by the impact of salty sea water on the metal mesh and the washout of stone material from the lower steps of the wall as a result of the recoil wave during the storm. The strength of the impact also depends on the speed and direction of the wind. These processes are not taken into account by modern standards.

When designing coastal offshore structures, it is necessary to take into account the forecast of changes in factors such as the strength of storms and the direction of waves due to climate change. The experience gained should be taken into account when developing the wall structure, the shape of the gabions and making the necessary changes to the regulatory documentation.

References

1. Technical instructions for the use of gabions to strengthen the subgrade TsPI 22/43 Approved on 30 December 1997, updated in 2020 (2020)
2. Engineering protection of territories, buildings and structures from hazardous geological processes. The main provisions of the joint venture 116.13330.2012 (2013)
3. Vodyashkin, A.S., Timokhova: ODM 218.2.049-2015 Recommendations for the design and construction of gabion structures on highways (2015)
4. Guidelines for the use of gabion structures in road and bridge construction. LLC "Organizer" FSUE "SOYUZDORPROEKT" Moscow (2001)
5. Vodyashkin, A.S., Timokhova, O.O.: Patent Gabion wall for the protection of the coastal slopes of the sea coast. RU28760 U1MPK E02B 3/06 (2006/01) Application 2010123567/21, 09 June 2010 (2010)
6. Stont, J.I., Ulyanov, M.O., Krek, E.V., Churin, D.A., Gubareva, D.E.: Storm activity in the autumn-winter period of 2019 in the southeastern part of the Baltic Sea. Sci. J. Izvestia KSTU **53** (2019)
7. Bobykina, V.P., Chubarenko, B.V.: The role of storms in the dynamics of the shores of the Southeast Baltic (on the example of the Curonian Spit. In: Proceedings of the International Scientific Conference, 13–23 June 2019 Regularities of the Formation and Impact of Marine Atmospheric Hazards and Disasters on the Coastal Zone of the Russian Federation in the Context of Global Climatic and Industrial Challenges. ("Dangerous phenomena") Rostov - on-Don (2019)
8. Perevoznikov, B.F., Selivestrov, V.L.: Road-bridge gabion structures and structures. State Road Service of the Ministry of Transport of the Russian Federation. Road Information Center (2001)
9. GEOINFO EKSPO Gabions, advantages, disadvantages and possibilities of new solutions: https://geofast.ru/stati/10-preimuschestv-gabionov. Accessed 14 Nov 2020
10. Ramli, M., Karasu, T.J., Dawood, E.T.: The stability of gabion walls for earth retaining structures. Alexandria Eng. J. **52**(4), 705–710 (2013). Alexandria: Faculty of Engineering of Alexandria University, Elsevier B.V

Effect of Clay Raw Materials on the Formation of the Microstructure of Cellular Concrete for Thermal Insulation Purposes

A. N. Volodchenko[(✉)] and V. G. Klimenko

Belgorod State Technological University named after V.G. Shukhov,
Belgorod, Russia
volodchenko@intbel.ru

Abstract. It is found that using sand and clay rocks of the incomplete stage of mineral formation as raw materials, it is possible to obtain effective autoclave cellular concretes for thermal insulation purposes. Improved rheological properties of the aerated concrete mix and a higher gas-holding capacity in comparison with lime-sand raw materials ensure the formation of a more uniform cellular structure. It is shown that the polymineral composition of raw materials provides the formation of gelled and highly crystallized phases, such as low-base calcium hydrosilicates CSH(B), hydrogranates and tobermorite, including alumina-containing ones, which optimizes the microstructure of the cementitious substance. At the same time, more dense inter-layer partitions than on lime-sand raw materials are formed, which increases the physical, mechanical and operational properties of thermal insulation materials. Increasing the number of phases in the composition of the cementing agent reduces its thermal conductivity. Micropores formed from finely dispersed highly crystallized phases also contribute to improving the thermal protection properties of heat-insulating autoclave cellular concretes on clay raw materials. The compressive strength, depending on the mineral composition of the rock at an average density of 350 kg/m^3, increases by 7–23% in comparison with lime-sand materials, and the coefficient of thermal conductivity decreases from 0.09 to 0.075–0.065 W/m·°C.

Keywords: Heat-insulating autoclave cellular concrete · Structure formation · Sand and clay rocks · Lime

1 Introduction

Cellular concretes, in particular aerated concretes that are produced under hydrothermal treatment at high pressure, differ in their properties from porous concretes obtained under normal conditions, which is due to the specifics of their synthesis hardening and structure formation. At high pressure in a saturated vapor medium, new formations are formed during the synthesis process, which are characterized by a high degree of crystallization. In addition, when using autoclave technology, it is possible to regulate the mineral composition of the cementing substance depending on the composition of cellular concrete, which allows obtaining both structural and thermal insulation materials. Due to the introduction of increased heat engineering requirements in the

construction of buildings and structures, the development, production and use of materials with increased thermal insulation properties is becoming highly relevant [1–5].

The performance properties of cellular concrete for thermal insulation purposes are mainly determined by their microstructure, which, in turn, is largely determined by the composition of the raw material. In the production technology using lime and sand, the synthesis of new formations is limited by the system $CaO–SiO_2–H_2O$ [6, 7]. Accordingly, it is possible to increase the physical and mechanical characteristics of the material only by increasing the number of new formations – calcium hydrosilicates. This can be achieved by increasing the activity of the lime-sand binder, as well as increasing the pressure and duration of hydrothermal treatment, which leads to an increase in energy costs for production.

The synthesis of the polymineral composition of new formations and the formation of the rational microstructure of the cementing substance, which determines high physical and mechanical parameters, can be achieved by using aluminosilicate rocks, for example, sand and clay rocks of the incomplete stage of mineral formation [8–14]. In addition, this raw material composition increases the plastic properties of the aerated concrete mixture, increases its gas holding capacity, forming an optimal macrostructure of cellular concrete [15].

The aim of this work is to study the formation of the microstructure of cellular concrete for thermal insulation purposes based on sand and clay raw materials.

2   Methods and Materials

To study the impact of the composition of the molding mixture on the structure formation of cellular concrete, quicklime with an activity of 78.2%, quartz sand with a grain size modulus of 1.54, and sand-clay rocks were used as raw materials. Two sandy-clay rocks of the Arkhangelsk region deposit were used in the research; each of them is classified as sandy loam. Rocks are colored yellow (rock 1) and red (rock 2). A characteristic feature of the rocks is the high content of silica (Table 1).

Table 1.   Chemical composition of sand and clay rocks.

№ of the rock	SiO_2	Al_2O_3	Fe_2O_3	CaO	MgO	K_2O	Na_2O	p.o.i.	Sum
1	76.68	8.90	4.50	4.80	0.60	0.27	0.36	2.50	98.61
2	69.45	12.12	4.95	5.55	0.59	0.06	0.18	3.69	96.59

Clay rocks of the Arkhangelsk region were formed due to weathering of igneous rocks of the main composition. This determined both the mineral and chemical composition of the rocks under study. The composition of the sand fraction of rocks is dominated by quartz. They contain calcite, feldspar, and mica in small amounts. Clay minerals of the rock 1 is represented by hydromica and montmorillonite, rock 2 – hydromica and kaolinite.

Samples of heat-insulating cellular concrete were made on the basis of sand and clay rocks and lime, as well as on the basis of traditional lime and sand raw materials. The feedstock was ground to a specific surface area of 350 m²/kg. The activity of raw mixtures was 16%. The amount of water was chosen in such a way as to ensure the spread of the raw mixture along the Suttard of 28 cm. Aluminum powder was used as a gas-forming agent. The formed products were subjected to hydrothermal treatment in an autoclave at a pressure of 1 MPa according to the mode 1.5 + 5 + 1.5 h for samples based on sand and clay rocks and 1.5 + 9 + 1.5 h based on lime and sand raw materials.

3   Results and Discussion

On the basis of the studied raw materials, cellular concretes for thermal insulation purposes with an average density of 350 kg/m³ were obtained (Table 2).

Table 2. Properties of heat-insulating cellular concrete.

Raw material	Limit of compressive strength, MPa	Mark on the average density, D	Strength class, B	Thermal conductivity, W/(m·°C)
Quartz sand	1.5	350	1	0.09
Rock 1	1.6	350	1	0.065
Rock 2	1.85	350	1	0.075

The compressive strength of lime and sand thermal insulation materials was 1.5 MPa. Replacing quartz sand with sand and clay rocks increased the strength of thermal insulation materials. For rock 1, the strength increased by 6.6% (1.6 MPa), for rock 1 – by 23% (1.85 MPa). In addition, the resulting products based on sand and clay rocks have higher thermal insulation properties. The coefficient of thermal conductivity in the dry state is 0.065−0.075 W/m·°C, which is less than the thermal conductivity of lime and sand products (0.09 W/m·°C).

In products based on lime and sand raw materials, mainly low-base calcium hydrosilicates CSH(B) are formed (exothermic effect 820 °C and reflections 3.053; 1.822 Å) (Fig. 1, *curve* 1). In addition to the CSH(B) phase, hydrogranates (endothermic effect of 350 °C and reflections of 2.774 Å) and tobermorite (reflections of 11.481–11.556 Å) are synthesized in products based on sand and clay rocks (see Fig. 1, *curves 2* and *3*). The deviation of tobermorite reflections from the value of 11 Å is probably due to the formation of non-stoichiometric compounds due to the polydisperse composition of the raw material. Increasing the number of phases in the composition of the cementing agent reduces its thermal conductivity [16].
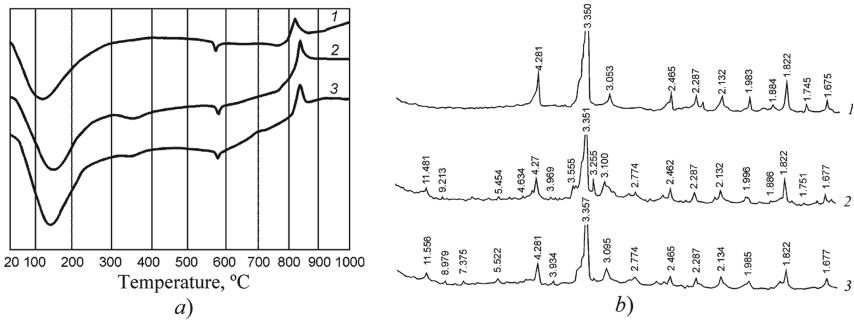
Fig. 1. Thermographic (*a*) and x-ray phase (*b*) analysis of samples based on: *1* – quartz sand; *2* – rock 1; *3* – rock 2.

The rheological properties of concrete mixtures [15] and phase composition of new formations with the use of sand and clay raw materials significantly changes in comparison with traditional lime and sand astringent nature of the formation of the pore structure of porous materials and microstructure of the cementing substance.

A scanning electron microscope study of cellular calcareous-sand materials obtained after autoclave processing showed that the interpore partitions are formed from quartz particles that are bound together by gelled calcium hydrosilicates (Fig. 2, *a*). The growth of well-crystallized new formations, which are elongated lobes of low-base calcium hydrosilicates, is observed on the pore surface (Fig. 2, *b*).
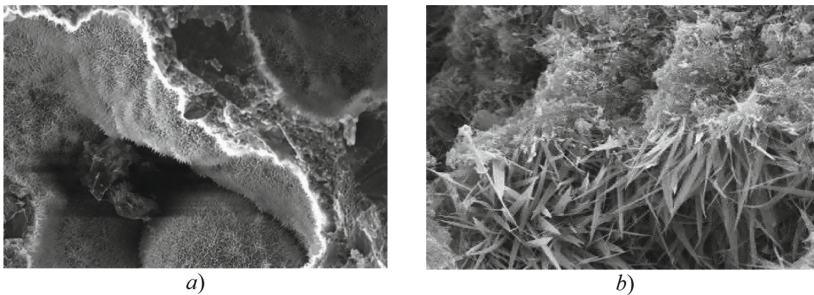
Fig. 2. Microstructure of thermal insulation materials based on traditional lime and sand raw materials, SEM: *a* – ×250; *b* – ×3000.

The cellular structure of materials based on sand and clay rocks is formed by open and closed pores (Fig. 3).
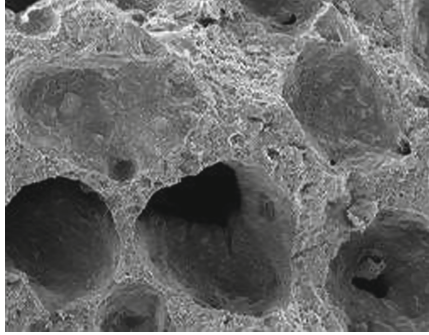
Fig. 3. Pore structure of thermal insulation materials based on rock 1, SEM: ×50.

Interporous partitions have a denser structure than in calcareous-sand materials (Fig. 4, *a*). On the surface of the pores, a layer of well-crystallized plates is formed, which are calcium hydrosilicates-tobermorite (see Fig. 4, *b* and *c*). There is also the presence of micropores, the walls of which are formed from new formations (see Fig. 4, *d*).

a)

c)

b)

d)
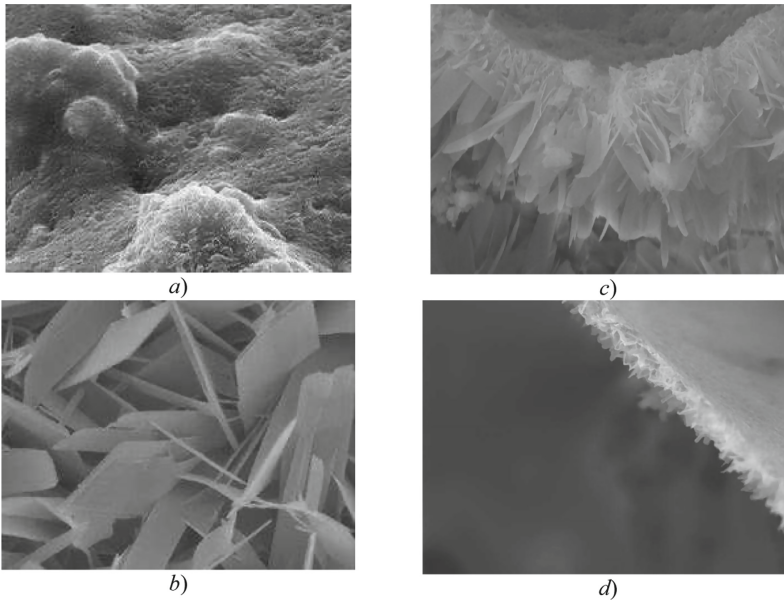
Fig. 4. Microstructure of thermal insulation materials, SEM: *a*, *b* – rock 1; *c*, *d* – rock 2; *a* – ×1000; *b*, *d* – ×20000; *c* – ×6000.

From the data obtained it can be concluded that when using rocks with unfinished stage of mineral formation due to the synthesis of gelled and well crystallized new formations of polymineral composition the rational structure of a cementing substance

is formed, which leads to improved physical-mechanical properties of aerated concrete for thermal insulation purposes.

4   Conclusion

Thus, using sand and clay rocks of the incomplete stage of mineral formation as raw materials, it is possible to obtain effective autoclave cellular concretes for thermal insulation purposes. Improved rheological properties of the aerated concrete mix and a higher gas-holding capacity in comparison with lime and sand raw materials ensure the formation of a more uniform cellular structure. The polymineral composition of the raw material provides the formation of gelled and crystalline phases, such as low-base calcium hydrosilicates CSH (B), hydrogranates and tobermorite, including alumina, which optimizes the microstructure of the cementing agent. At the same time, more dense interpore partitions than on lime and sand raw materials are formed, which leads to an increase in the physical and mechanical properties of thermal insulation materials. Increasing the number of phases in the composition of the cementing agent reduces its thermal conductivity. Micropores formed from finely dispersed highly crystallized phases also contribute to improving the thermal protection properties of aerated concrete on clay raw materials. The compressive strength in comparison with lime and sand materials increases by 7–23%, the coefficient of thermal conductivity decreases from 0.09 to 0.067–0.075 W/m·°C.

References

1. Fedin, A.A.: Scientific and technical fundamentals of the production and use of silicate cellular concrete. Publisher GASIS (2002)
2. Sazhnev, N.P., Sheleg, N.K., Sazhnev, N.N.: Production, properties and application of autoclaved cellular concrete. Constr. Mater. **3**, 2–6 (2004)
3. Vylegzhanin, V.P., Pinsker, V.A.: Aerated concrete in housing construction and prospects for its production and application in the Russian Federation. Constr. Mater. **1**, 4–8 (2009)
4. Volodchenko, A.N., Strokova, V.V.: Improving the efficiency of silicate cellular materials of autoclave hardening. Bull. North-Eastern Federal University named after M.K. Ammosov **2** (58), 60–69 (2017)
5. Nelyubova, V.V., Altynnik, N.I., Strokova, V.V., Podgorny I.I.: Rheotechnological properties of cellular concrete mix using a nanostructured modifier. Bull. BSTU named after V.G. Shukhov **2**, 58–61 (2014)
6. Hvostenkov, S.I.: On the chemistry of the interaction process in the $Ca(OH)_2$–SiO_2–H_2O system under hydrothermal synthesis conditions. Build. Mater. **5**, 76–81 (2008)
7. Klimesch, D., Ray, A.: Evaluation of phases in a hydrothermally treated CaO–SiO_2–H_2O system. J. Therm. Anal. Calorim. **70**(3), 995–1003 (2002)

8. Lesovik, V.S.: Improving the Efficiency of Production of Building Materials, Taking Into Account the Genesis of Rocks. ASV publishing house, Moscow (2006)
9. Lesovik, R.V., Klyuyev, S.V., Klyuyev, A.V., Netrebenko, A.V., Kalashnikov, N.V.: Fiber concrete on composite knitting and industrial sand KMA for bent designs. World Appl. Sci. J. **30**(8), 964–969 (2014)
10. Nelyubova, V.V., Podgorny, I.I., Strokova, V.V., Palshina, Y.: Autoclave aerated concrete with nanostructured aluminum silicate modifier. Constr. Mater. **4**, 72–75 (2016)
11. Volodchenko, A.N., Strokova, V.V.: Development of scientific bases for production of silicate autoclave materials using clay raw materials. Build. Mater. **9**, 25–31 (2018)
12. Volodchenko, A.A., Lesovik, V.S., Volodchenko, A.N., Zagorodnjuk, L.H.: Improving the efficiency of wall materials for «green» building through the use of aluminosilicate raw materials. Int. J. Appl. Eng. Res. **10**(24), 45142–45149 (2015)
13. Klyuyev, S.V., Klyuyev, A.V., Lesovik, R.V., Netrebenko, A.V.: High strength fiber concrete for industrial and civil engineering. World Appl. Sci. J. **24**(10), 1280–1285 (2013)
14. Volodchenko, A.A.: Influence of artificial calcium hydrosilicates on the hardening processes and properties of non-autoclave silicate materials based on unconventional aluminosilicate raw materials. Constr. Mater. Prod. **3**(2), 19–28 (2020)
15. Lesovik, R.V., Klyuev, S.V., Klyuev, A.V., Tolbatov, A.A., Durachenko, A.V.: The development of textile fine-grained fiber concrete using technogenic raw materials. Res. J. Appl. Sci. **10**(10), 696–701 (2015)
16. Svatovskaya, L.B., Khitrova A.V., Chernakov V.A.: Modern autoclave foam concrete. Achievements in construction materials science. In: Collection of Scientific Articles Dedicated to the 100th Anniversary of the Birth of P.I. Bozhenov, pp. 85–89. "OM-Press" publishing house, Saint Petersburg (2004)

Effect of Sleet-Proof Reagents on the Cement Stone of Concrete

I. G. Endzhievskaya[✉] , R. A. Nazirov ,
and A. S. Endzhievskiy

Siberian Federal University, Krasnoyarsk, Russia
icaend@mail.ru

Abstract. This research evaluates the effect of single-component sodium chloride solution in comparison with multicomponent commercial sleet-proof reagents (SPR) on the cement stone of side stone concretes of different compositions. Furthermore, it estimates manufacturing technologies: vibration casting - composition №1 - with a water-cement ratio of 0.4 and a strength of up to 70 MPa and №2 – W/C >0.4, strength <40 MPa. The composition №3 is manufactured using class B30 vibropress technology. Samples of each composition are saturated with salt solutions – single-component 10% NaCl or multicomponent commercial SPR of 10 or 30% concentration. Multicomponent SPR containing sodium and calcium chlorides has a greater impact on concrete in comparison with single-component salt. However, a higher concentration of the SPR solution may have a less destructive effect on the concrete. The lowest accumulation of chlorides is observed in vibropressed concrete, despite the high value of water absorption of samples. The permeability of concrete made using vibropress technology is higher than that of vibration casting ones, but destructive processes develop much more slowly. Thus, the nature of the pore space, rather than the volume, has a greater influence on their flow.

Keywords: Sleet-proof agents · Multicomponent commercial SPR · Side stones · Aggressive effect on cement concrete

1 Introduction

Modern highways are the most complex mechanisms, the condition of which is characterized by transport and operational indicators of the structural elements of the road itself, road structures and elements of arrangement. To ensure road safety conditions in the winter period, a set of measures is provided to ensure safe traffic on highways, including protection from snow drifts, snow removal, prevention and elimination of winter slipperiness. Requirements for the state of the roadway in modern cities, especially in million-plus cities, are very high, because the number of accidents and injuries to pedestrians in winter is very significant [1, 2].

Currently, the choice of commercial sleet-proof reagents is very wide, most of them are multicomponent, which, according to manufacturers, work more efficiently than single-component ones. Mainly used SPR based on chloride salts, because they are quite cheap and easy to use [3].

As practice has shown, when using multicomponent SPR on city streets, the rate of destruction of cement-concrete products, especially side stones, has a higher rate. Intensive destruction leads to their rapid decommissioning and annual replacement in some areas and, consequently, to high costs for road repairs.

The critical condition of side stones, as objects of urban infrastructure on roads, makes the study of the problem of assessing the corrosion resistance of cement stone to the action of multicomponent sleet-proof reagents very relevant [4–7].

Destruction begins at the surface and will continue at an increased rate, as easily accessible paths are formed for the penetration of aggressive salts. This process is facilitated by the impact of harvesting equipment. Cars for winter maintenance of highways equipped with such equipment as a sweeping brush with a nylon or metal pile can destroy the surface layer weakened by sleet-proof material, which loses its integrity as a result of sufficiently intense exposure, especially with such repeated manipulations.

Unfortunately, there is no universal tool for combating sleet that meets all the requirements [4–7]. According to research published by the Bulletin of the United States Transportation Research Committee, the harmful effects of chloride-based sleet-proof reagents on the cement concrete of transport structures have been studied widely, although their effectiveness in combating sleet is obvious, with calcium, magnesium and sodium chloride being the most problematic [8–11].

The aim of the study is to assess the degree of aggressiveness of the effect of solutions of single-component NaCl in comparison with multicomponent commercial SPR on the cement stone of concretes of different composition and manufacturing technologies.

2   Methods and Materials

The used materials are a multicomponent commercial SPR, the characteristics are given in Table 1, is represented by an organization engaged in the maintenance of highways in Krasnoyarsk, a single-component NaCl.

Chemical analysis methods were used to determine the salt concentration in the snow cover. The corroding of multicomponent salts solutions of 10 or 30% concentration in comparison with single-component NaCl was determined using an ultra-low-temperature Vestfrost solutions VT 407 freezer at a temperature of −50 °C. Salts are considered on the durability of cement stone of concrete, manufactured using the technology – vibration casting and vibropress. The thermogram of a multicomponent commodity SPR was obtained using a NETZSCH Yupiter STA 449 F1 synchronous thermal analysis device in an argon atmosphere.

3   Results and Discussion

The effect of solutions of single-component NaCl in comparison with multicomponent commercial SPR on the cement stone of concrete was studied. Passport data of a multicomponent SPR are presented in Table 1.

Table 1. Characteristics of a multicomponent commercial SPR.

Name of indicator	Standard	Test results
Hydrogen index	5–10	Correspond
Mass fraction of calcium chloride, %	10–30	Correspond
Mass fraction of sodium chloride, %	45–89	Correspond
Mass fraction of carbamide, %	No more than 10	Correspond

Multiple thermal analysis of the sleet-proof reagent selected at the time of the placer on the road section was performed. Data analysis showed significant variability in its composition with the main effects on the DSC curve (Fig. 1) corresponding to the decomposition processes of sodium and calcium chloride salts.
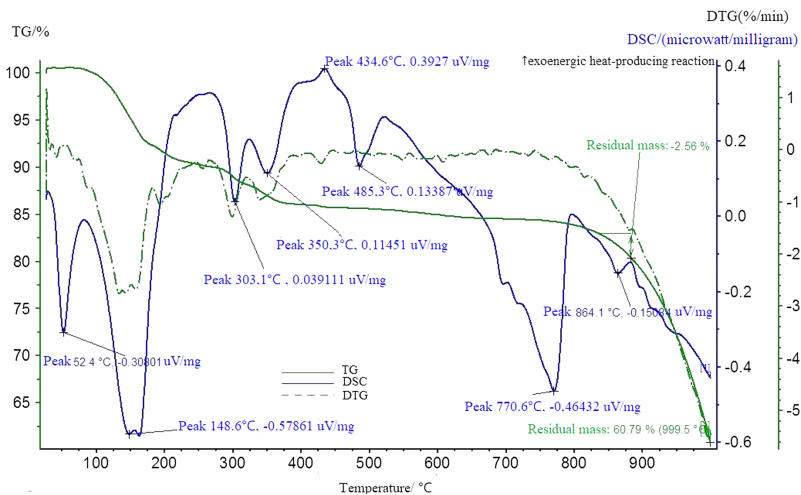
Fig. 1. Thermal analysis of commercial sleet-proof reagent (2019).

Field tests performed to determine the concentration of salt deposits in the snow cover near the side stones that form the border tray, 3 h after the road area is treated with a sleet-proof reagent, show that it reaches 30–70%. In this regard, the corroding effect measure specified in the method for determining the impact of sleet-proof materials on cement concrete - a concentration of 10% - is quite low compared to the results of field tests.

According to the method for determining the impact of sleet-proof materials on cement concrete, the ability of samples to maintain their physical condition (no cracks, chips, surface peeling) and mass during repeated variable freezing − thawing with a decrease in the freezing temperature to minus (50 ± 5) °C in a 10% NaCl solution is taken as a measure of aggressiveness.

For the study, 6 samples-cubes of concrete of three compositions were made: according to the vibration casting technology - composition № 1 - with a water-cement

ratio of 0.4 and a strength of up to 70 MPa and № 2 - W/C 0. 4, strength class B30. At W/C = 0.4, the strength of concrete is usually always significantly higher than class B30. Composition №3 is made using vibropress technology from a semi-dry mixture (VPI) of strength class B30, W/C = 0.4.

According to the GOST method, the SPR test for aggressiveness against cement concrete is carried out on samples-beams with a size of $40 \times 40 \times 160$ mm, indicating the maximum size of crushed stone 10 mm. However, the specified sample sizes do not correspond to the fraction of coarse aggregate in the production compositions of concrete side stones, and the scale of the samples is quite an important factor for studying concrete as a composite. Tests were carried out on samples-cubes with an edge of 100 mm.

After manufacturing, the samples were kept for 28 days under normal conditions to achieve the design strength. Then, the samples of each composition were saturated with salt solutions – 10% NaCl and a multicomponent commercial reagent of 10% and 30% concentration.

After 15 cycles of freezing and thawing, the indicators of aggressiveness of salt solutions on cement concrete were evaluated – specific change in mass, loss of mass and strength. The test results are shown in Table 2.

The accumulation of chlorides in the samples of three compositions was evaluated using a color test. The tested samples were split and treated first with potassium bichromate, then with silver nitrate (Fig. 2).

| Composition №1 | Composition №2 | Composition №3 |
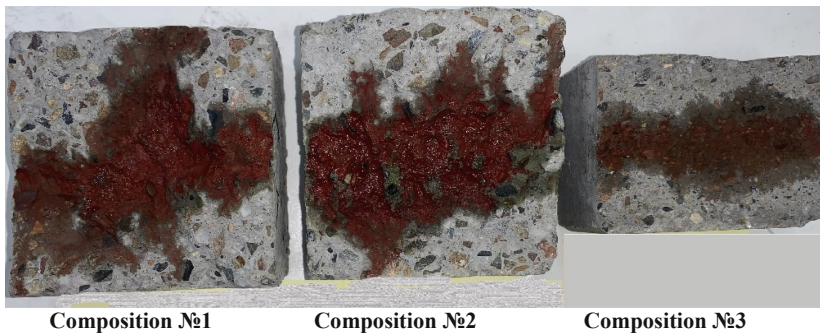
Fig. 2. Color test of samples after testing for frost resistance in a 10% solution of multicomponent commercial SPR.

A qualitative chemical reaction showed a significant accumulation of chlorides in the pore space of concrete made using vibration casting technology, especially intense coloring in the sample of composition 2.

Due to the internal pressure created in the capillaries, which is additionally caused by the formation of a large volume of calcium chloride compounds [12], the structure breaks and the samples are destroyed. The lowest accumulation of chlorides is observed in vibropressed concrete, despite the high value of water absorption.

Table 2. Results of testing samples for frost resistance in solutions of salt and commercial sleet-proof reagent.

Type of aggressive environment	Composition number	Water absorption by mass, %	Weight of samples before testing, g after	Specific change in mass of the sample, g/cm³	The strength of the samples before the testing, MPa after	Mass loss Δm, %	Reduction of compressive strength, %
GOST requirements		≤ 5	–	≤ 0.07		≤ 3	≤ 5
10% NaCl	1	5.0	$\frac{2382}{2358}$	0.030	$\frac{69.6}{70.0}$	1.01	−0.57
			$\frac{2379}{2348}$	0.024		1.30	
	2	3.2	$\frac{2372}{2342}$	0.024	$\frac{39.7}{39.5}$	1.26	0.50
			$\frac{2373}{2348}$	0.031		1.05	
	3	4.8	$\frac{1501}{1504}$	−0.004	$\frac{38.7}{39.2}$	−0.20	−1.29
			$\frac{1561}{1564}$	−0.004		−0.19	
10% SPR	1	5.0	$\frac{2395}{2344}$	0.079	$\frac{69.9}{68.8}$	2.13	1.57
			$\frac{2359}{2316}$	0.102		1.82	
	2	3.2	$\frac{2373}{2292}$	0.051	$\frac{39.3}{36.7}$	3.41	6.62
			$\frac{2379}{2274}$	0.043		4.41	
	3	4.8	$\frac{1514}{1478}$	0.004	$\frac{38.4}{38.1}$	2.38	0.78
			$\frac{1566}{1528}$	0,008		2.43	
30% SPR	1	4.9	$\frac{2419}{2372}$	0,045	$\frac{70.3}{67.2}$	1.94	1.49
			$\frac{2360}{2318}$	0.050		1.78	
	2	3.2	$\frac{2342}{2296}$	0.046	$\frac{41.4}{38.1}$	1.96	7.97
			$\frac{2338}{2288}$	0.042		2.14	
	3	4.8	$\frac{1557}{1524}$	0,007	$\frac{38.4}{37.9}$	2.12	1.30
			$\frac{1530}{1496}$	0.004		2.22	

As it can be seen from the test results, the least aggressive effect is 10% single-component NaCl, the greatest - 10% solution of multicomponent SPR. Concrete samples of composition №2 lost more than 0.07 g/cm³ in mass. The mass loss of concrete samples of composition №1 is less, but the surface peeling was observed. VPI samples have a satisfactory surface condition and insignificant mass loss.

A more concentrated 30% solution of multicomponent SPR affected concrete less destructively than 10%, but more destructively than 10% NaCl solution.

This may be due to the fact that the pores were filled with crystals that fell out of a more concentrated salt solution during freezing and for some time prevented the destructive effect of the solution on the cement stone. When freezing, the solubility of salts decreases, and the solution of a higher concentration becomes supersaturated. Salts crystallize and precipitate, covering the walls of the pores, and in the further process gradually fill them, displacing water. This leads to the fact that the crystals clog the pores of the concrete and prevent further penetration of the liquid solution deep into the concrete body. There is less water in the pores, and when the temperature freezes and further decreases, the expanding ice has a smaller volume and creates less pressure in the pores.

Concrete of composition №2 - class B30, manufactured using vibration casting technology, is most susceptible to aggressive effects of sleet-proof reagents and surface destruction due to high capillary porosity formed by an excessive amount of closing water.

Products made of vibropressed concrete were practically not subjected to destructive processes and did not accumulate chlorides, despite the higher water absorption rate [13].

4   Conclusion

The degree of aggressiveness of the effect of solutions of single-component NaCl in comparison with multicomponent commercial SPR on the cement stone of concretes made using vibration casting technology and vibropressing is estimated. Multicomponent SPR have a more aggressive effect on concrete in comparison with single-component SPR. However, a higher concentration of the SPR solution can have a less destructive effect on concrete, due to the supersaturation of the solution and the precipitation of salts with a decrease in temperature.

The permeability for concrete chlorides of different composition and manufacturing technologies was determined. The permeability of concrete made using vibropressing technology is higher than that of vibration casting one, but destructive processes develop much more slowly. Thus, the nature of the pore space, rather than the volume, has a greater impact on their flow.

References

1. Indicators of road safety. Statistics, Electron. text messages. − State Traffic Inspectorate
2. Strokova, V.V., Babaev, V.B., Markov, AYu., Sobolev, K.G., Nelyubova, V.V.: Comparative evaluation of road pavement structures using cement concrete. Constr. Mater. Prod. **2** (4), 56–63 (2019)
3. Sutter, L., Van Dam, T., Peterson, K.R., Johnston, D.: Long-term effects of magnesium chloride and other concentrated salt solutions on road surfaces and construction Portland cement concrete. Results of the first phase of research. Transportation Research Committee of the United States, 1979, Transportation Research Committee of the National Academy of Sciences of the United States. Washington, pp. 60−68 (2006)

4. Yuan, J., Zhenyu, D., Yue, W., Feipeng, X.: Freezing − thawing resistance evaluations of concrete pavements with deicing salts based on various surfaces and air void parameters. Constr. Build. Mater. **204**, 317−326 (2019)
5. Feras, A., Razaqpur, A.G.: The effect of chemical composition of deicing salts on the concrete pore structure and chloride − induced corrosion. In: CSCE 2020 Annual Conference. At Saskatoon. Saskatchewan. Canada, vol. 8 (2020)
6. Marchand, D., Sellevold, I.D., Pigeon, M.: Stratification of the concrete under action of sleet-proof salts. In: Malhotra, V.M. (ed.) Review of Publications in ACI SP-145: Strength of Concrete. American Concrete Institute, Farmington Hills, Michigan, pp. 1–46 (1994)
7. Gafuri, N., Mathis, R.P.: Delamination of the surface of concrete pavers under the influence of sleet-proof reagents. ACI Mater. J. **94**(1), 32–38 (1997)
8. Gegua, P., Revertega, E., Main, G.: Effect of chloride ions on hydrated cement paste: effect of the type of cement and long-term exposure to concentrated chlorides. Stud. Prop. Cem. Concr. **22**(2–3), 451–457 (1992)
9. Lee, X., Cody, R.D., Cody, A.M., Spry, P.G.: Effect of various sleet-proof salts on the destruction of road concrete. In: Protocol of the Mid-Continent Transport Symposium. Educational and research transport center. The University of Iowa, pp. 151–155 (2000)
10. Nikitin, A.A.: Sleet-proof materials. In search of a compromise. Bashkir Ecological Bulletin. State unitary enterprise Scientific − Research Institute of Secure of Life Activity of the Republic of Bashkortostan, pp. 3 − 4 (2013)
11. Toshin, D.S., Novikov, S.N.: Evaluation of the impact of an aqueous solution of calcium chloride on the strength of concrete. Science and Education, pp. 26−30. IE "Gulyaev G. Yu.", Penza (2019)
12. MacDonald, D.B., Perenchio, D.B.: Effect of salt type on concrete stratification. Concr. Int. **9**(7), 23–26 (1997)
13. Pshembaev, M.K.: Pore structure of the concrete road. Sci. Technol. **15**(4), 298–307 (2016)

Eco-Resource Intensity Enhancement of Residential Apartment Buildings via Optimizing Design Solutions

N. V. Bakaeva[1] , A. E. Naumov[2] , and M. O. Suvorova[2(✉)]

[1] Moscow State University of Civil Engineering,
Russian Academy of Architecture and Building Science Research Institute
of Building Physics, Moscow, Russia
[2] Belgorod State Technological University named after V.G. Shukhov,
Belgorod, Russia
marykrutilova@gmail.com

Abstract. A significant part of design decisions affecting the future maintenance and building environmental safety are made at the initial design stage. Currently, about 80% of design decisions are made by designers and architects at the initial stage of designing civil buildings, and the remaining 20% - by engineers at subsequent stages. With respect to civil buildings (namely, residential from 9 to 20 floors) the influence of various design volumetric-planning and structural parameters on the components quantity for common structural systems is strong enough. In this regard, it is crucial to have tools for quick and reliable quantitative assessment of the environmental safety of a building at the initial stages of the project – the stage of alternative design. The proposed approach will allow to establish quantitative dependencies between design solutions and used construction resources, as well as to carry out express-diagnostics of resource intensity at the pre-project stage. Using the obtained data, this will allow for comparative analysis of potential engineering (volumetric planning and organizational and technological) solutions alternative to the project and analysis primary energy use and carbon impact for the development of conventional residential buildings as well.

Keywords: Resource intensity analysis · Structural design · Eco-efficient construction development · Residential buildings

1 Introduction

Due to the global trend of energy shortages and global climate change, growing attention to energy saving and environmental safety of civil construction is being paid [1]. As the extended responsibility of businesses involved in construction has taken on relevance, the construction industry needs new eco-friendly principles of production development [2]. These principles are especially relevant for civil facilities: residential buildings, educational, health care, culture, etc., where the state is a direct participant in the construction.

Ensuring environmental safety of buildings depends on design solutions, namely, the used building materials and structures, construction and installation work performed during construction, as well as previously spent energy and resources for transportation, production of building materials, etc. [3, 4]. The environmental safety class of the materials used and the energy safety class of the construction technology used are important. Traditionally, quantitative building resources data are available when the design and estimate documentation is completed in full. Insufficient information about resources at initial stages is due to lack of the detailed project elaboration [4]. Researchers [5–7] from different countries emphasize the need for rapid analysis of resource intensity at the initial stages of design for a more accurate assessment of various technical and economic parameters, including those related to the sustainability of the project.

The authors propose to conduct express-diagnostics of resource intensity of potential engineering (volume planning, organizational and technological) solutions in the process of selection and approval of the construction project. The authors' methodology of resource intensity diagnostics allows to determine approximate volumes of construction resources and, consequently, their cost, taking into account the structural scheme and other parameters of a civil building. The effects of design parameters such as total area, number of storeys, location of structural components, etc. on the quantities of energy intensive resources for different structural systems have been presented.

2   Methods and Materials

Early resource forecasting models are particularly beneficial during the decision making phase because early stage building design decisions are more eco-sensitive compared to decisions made later in the building process [8]. This study relied on data to develop building parameters for 20 residential buildings monolithic reinforced concrete framework. Regression models were assessed to determine the best model for forecasting resource intensity using limited data during the early phases of residential building project development [9]. The research data were mainly obtained from previously constructed projects in Russia. To demonstrate the efficiency of the method, the projects were limited to groups of structural design schemes. Monolithic reinforced concrete frames were chosen for the analysis because of their wide spread in housing construction [10]. In order to test the technique, the article conducted a correlation-regression analysis of the main resource-intensive and, consequently, energy-consuming building materials: concrete and steel [11, 12]. Quantitative content of regression models is carried out by means of analysis of actual resource costs on a representative selection of considered construction projects (Table 1).

The modeling of the relationship between the source data and the final resource intensity can be performed by linear and non-linear regression dependencies. Linear dependencies are methodologically simple, easy to formalize, interpreted, however, often characterized by low quality of the resulting statistical dependence [13]. Non-linear dependencies are more complex to use, formalize and interpret, but consist of a combination of non-linear (irregular, stochastic processes) and linear (regular,

Table 1. Selection of multi-storey residential buildings with full monolithic reinforced concrete frame.

Project	Concrete, m^3	Steel, t	Total area, m^2	Volume, m^3	Number of storeys
1	4272	363	6113.36	22101.31	9
2	2573	395	6720.00	23794.00	9
3	9500	690	11734.50	37593.10	9
4	8020	543	9594.50	36675.50	11
5	10000	800	12413.00	48545.00	11
6	8750	650	12634.10	48546.00	11
7	12300	1029	15399.41	56642.00	11
8	7500	670	8647.10	36910.00	12
9	19200	1450	26998.50	88249.20	12
10	4500	398	4248.78	21787.16	13
11	10200	858	15068.18	47223.00	13
12	7453	875	9477.70	49966.00	15
13	9866	1002	10753.21	40030.49	16
14	3168	395	7697.00	27318.00	17
15	3486	400	7909.60	25196.85	17
16	10450	900	16253.00	48055.00	17
17	12400	1036	16307.60	56987.50	17
18	16010	1300	20589.50	73650.00	17
19	4000	685	10287.50	37700.00	18
20	3870	737	11223.87	38000.00	18

systematic processes) parts. In this context, the authors carried out comparative studies of the combination of applied potential and statistical quality of two types of regression dependencies:

– multiple linear regression:

$$Y = a_1 x_1 + \ldots + a_n x_n + a_0,$$

– N-degree universal K-polynomials:

$$Y = a_{-1} x^1 + a_{(0)} x^0 + a_1 x^{-1},$$

where Y – dependent variable (resource volume),
x – quantitative indicator of the building space-planning decision,
a_i – constants,

x^0 – dummy term (always equal to 1), used for structure's clearness.

The dependent variables for models were operationalized as follows: concrete volume per square meter (CSM); concrete volume per story (CS); and concrete volume per cubic meter (CCM); steel volume per square meter (SSM); steel volume per story (SS); steel volume per cubic meter (SCM).

3   Results and Discussions

The research of samples by functional and structural groups of buildings confirmed the universality and expediency of using K-polynomials for regression of volumes of basic energy-intensive building materials and quantitative indicators of volume-planning building solution. The high correlation force of the used expressions was confirmed as well, which exceeds the individual trend lines of the standard spreadsheet calculator tools by the parameter R^2 (Figs. 1 and 2).
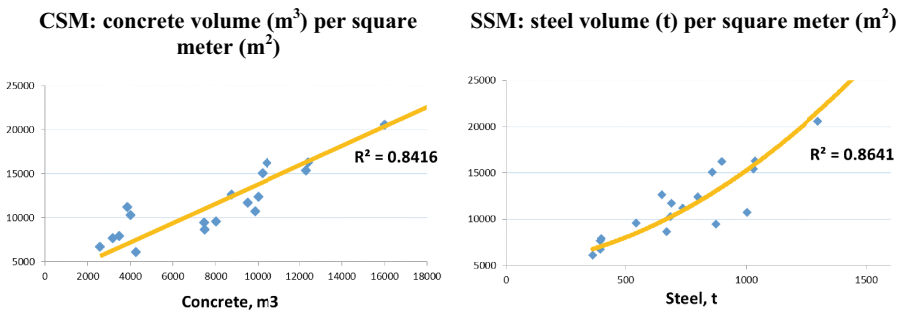

Fig. 1. Linear and non-linear regressive models of concrete and steel with total area for monolithic apartment buildings.
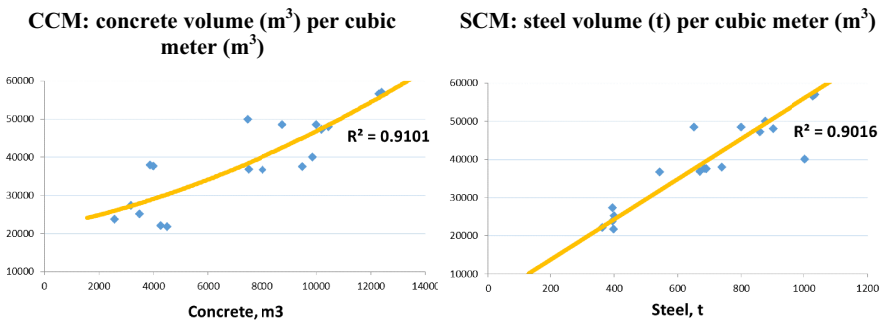
Fig. 2. Linear and non-linear regressive models of concrete and steel with building volume for monolithic apartment buildings.

$$C = 0.254A + 0.178V - 176.84N \qquad S = 0.005A + 0.014V + 4.797N$$

R square – 0.989   R square – 0,993
P-value (0.008-0.012) < 0.05   P-value (0.003-0.02) < 0.05
F (270.52) > Significance F (6,46E-14)   F (457.36) > Significance F (1.03E-15)

where C — concrete, m^3
S – steel, t
A – total building area, m^2
V – building volume, m^3
N – number of storeys.

The study of linear and nonlinear alternatives quality of regression dependence of the resource intensity investigated parameters of the construction project confirmed expediency and sufficiency of using for practical purposes linear regression equations that allow effective transition to the research level of multiple regression analysis [14, 15]. The obtained values of coefficients (P-value, Fisher, etc.) and criteria suggest that this distribution is coming best as normal distribution, which is the basis of linear multiple regression models. On the basis of the presented statistical indicators the conclusion is made about the strongly determined structure of distribution of the values of the studied dependencies. Paired regressions based on the relationship between the dependent function and the independent variable are characterized by the determination coefficient within $R^2 = 0.8-0.9$. The multiple regression based on three parameters is characterized by a higher determinacy coefficient, which confirms the reliability and, accordingly, applied acceptability of the multiple linear model [16]. Multiple regression best represents the research objectives - it contains a combination of building parameters and their correspondence through built-in internal coefficients.

4 Conclusion

The regression results can be used to analyze urban trends on a macro level in assessing the current environmental situation of urban development. Express-diagnostics is applicable for the assessment of both complex and individual housing estates, while for the assessment of individual residential buildings a high enough error is possible. The larger the amount of source data that is covered by the diagnostics, the greater the cumulative effect that will actually be achieved.

Possible directions of implementation of the obtained regression dependencies results:

- express-diagnostics of resource and energy efficiency of potential options for volume planning solutions may be applicable at the stage of feasibility studies of investments;
- allows to perform screening of resource intensity having project design data;

– the technology allows to manage urban planning policy in place a land development project by issuing a permit for construction of complex real estate from the point of view of sustainable development;
– conducting a comprehensive eco-audit of urban areas (or reconstruction of existing housing).

Using the method presented, applications for comparative eco-estimation to assess the effect of design parameters, for approximate structural assessment of an overall project given its design features have been demonstrated. This will stimulate construction of the most environmentally friendly projects by selecting the most efficient and eco-friendly materials as early as at the pre-project stage. Express-diagnostic could help to improve project planning, implementation and control strategies from an environmental perspective in the formation of urban planning policy.

References

1. Chen, Zhen, Li, Heng: Environmental Management in Construction: A Quantitative Approach. Routledge, London (2006)
2. Ilyichev, V., Kolchunov, V., Bakaeva, N., Emelianov, S.: Principles of urban areas reconstruction ensuring safety and comfortable living conditions. IOP Conf. Series: Mater. Sci. Eng. **463**(3), 032011 (2018)
3. Grabovy, P., Naumov, A., Avilova, I.: Scientific aspects of productivity management in the investment and construction sector. Int. Bus. Manage. **10**(7), 1354–1364 (2016)
4. Gangolells, M., Casals, M., Gassó, S., Forcada, N., Roca, X., Fuertes, A.: A methodology for predicting the severity of environmental impacts related to the construction process of residential buildings. Build. Envir. **44**(3), 558–571 (2009)
5. Ofori-Boadu, A..: Exploring regression models for forecasting early cost estimates for high-rise buildings. J. Technol. Manag. Appl. Eng. **31**, 1–22 (2016)
6. Trost, S.M., Oberlender, G.D.: Predicting the accuracy of early cost estimates using factor analysis and multivariate regression analysis. J. Constr. Eng. Manag. **129**(2), 198–204 (2003)
7. Edwards, P., Lawther, P., Edwards, P.: Design Cost Modelling – A Way Forward. Aust. J. Constr. Econ. Build. **1**(1) (2001)
8. Bektaş Ekici, B., Aksoy, U.: Prediction of building energy needs in early stage of design by using ANFIS. Expert Syst. Appl. **38**, 5352–5358 (2011)
9. Ilyichev, V., Emelyanov, S., Kolchunov, V., Bakaeva, N.: About the dynamic model formation of the urban livelihood system compatible with the biosphere. Appl. Mech. Mater. **725**, 1224–1230 (2015)

10. Avilova, I.P., Krutilova, M.O.: Methodology of ecooriented assessment of constructive schemes of cast in-situ RC framework in civil engineering. IOP Conf. Series: Earth Envir. Sci. **3**, 012127 (2018)
11. Oberemok, M., Naumov, A., Schenyatskaya, M.: Qualitative analysis of view characteristics of residential property. Bulletin of Belgorod State Technological University named after V. G. Shukhov **4**(3), 44–51 (2019)
12. Naumov, A.E., Koshlich, Yu., Oberemok, M.I., Belousov, A.: Comparative analyzes for increasing the energy efficiency of civil constructions. In: 19th International Multidisciplinary Scientific GeoConference SGEM 2019 Conference Proceedings. pp. 277–284 (2019)
13. Avilova, I.P., Naumov, A.E., Krutilova, M.O., Dakhova, D.D.: Low-carbon principles of eco-efficient construction development. Lecture Notes in Civil Engineering **95**, 45–51 (2020)
14. Schenyatskaya, M.A., Krutilova, M.O., Sharapova, A.V., Markova, A.A.: Enhanced technology of quantitative assessment for technological suitability of real estate for technical improvements. In: IOP Conference Series: Materials Science and Engineering. vol. 698, pp. 077050 (2019)
15. Avilova, I.P., Krutilova, M.O.: Energy efficiency tools of buildings design solutions in information and analytical management systems for construction and overhaul process. In: IOP Conference Series: Materials Science and Engineering. 4th International Scientific and Technical Conference on Energy Systems, ICES 2019, p. 012062 (2020)
16. Avilova, I., Naumov, A., Krutilova, M.: Methodology of cost-effective eco-directed structural design. International Multidisciplinary Scientific GeoConference SGEM **53**, 255–261 (2017)

Metallurgical Waste Recycling for Transport Construction

S. N. Bondarenko[(✉)] , A. N. Bodyakov , and M. S. Lebedev

Belgorod State Technological University named after V.G. Shukhov,
Belgorod, Russia
sn.bondarenko92@gmail.com

Abstract. Nowadays industrial waste recycling is the key concern for metal industry. Higher steel outputs are accompanied by increased by-products related with steel production. One of large-tonnage by-products of metallurgical production is electric arc furnace dust from arc steel furnaces. The use of metallurgical waste is therefore a promising area of research. The chemical composition of dust from arc steel furnace cleaning has been studied. The microstructural features of gas cleaning dust have been investigated. Dust formation processes have been understood. The most efficient dust clotting schemes have been selected. It has been demonstrated that it is possible to granulate dust using process water as a liquid-phase binder. It has been established that a disk pelletizer makes it possible to obtain granules up to 5 mm in diameter with sufficient strength for their transportation and further drying. When using a screw extruder it is possible to produce granules of proper cylindrical shape. Heat released from hydration of free CaO being a part of dust and bulk mixing result in screw conveyor jamming and die hole clogging. Bulk dust density has been determined for gas cleaning of arc steel furnaces. Bulk density of granules obtained by two granulation methods has been determined - with the use of a disk petellizer and a screw granulator.

Keywords: Electric arc furnace dust · Microstructure analysis · Waste granulation

1 Introduction

Waste generation in the metallurgy industry results in technogenic deposits [1, 2]. In Russia annual steel production is approximately 70 mln tonnes of steel, of which 22 mln tonnes count for electric furnace steel. Dust generated in electric arc furnace (EAF) can reach up to 30 kg per 1 ton of steel. EAF systems annually capture about 650,000 tonnes of electric furnace steel-making dust, with 99% gas purification ratio. Due to the negative impact produced by dust on the environment and human health it is essential to reduce dust generation and to develop dust reclaiming technology [3, 4].

Recycling of waste, in particular, dust, makes it possible to improve significantly production efficiency both by manufacturing additional core products and by making a new derivative product which is a recycle used to reduce consumption rates of raw materials and energy resources [5, 6]. The next step in the development of technologies

for disperse waste and mineral residues storage is disperse waste pelletizing and its subsequent warehousing [7, 8]. Unlike a particulate form the pelletized material helps to avoid during dump storage air pollution due to dust emission and to reduce or completely exclude water pollution due to waste discharge. A pelletized product is easier to handle and it is less problematic to take it from the storage place. Thus, pelletizing makes better conditions for waste disposal and increases specific material consumption for storage areas (dumps and landfills). The development and introduction of pelletizing technologies for such disperse metallurgical waste as EAF dust makes it possible to optimise waste warehousing and storage, including further returnability to the production process.

2   Methods and Materials

EAF dust samples from EAF at the Oskol Electrometallurgical Plant with a bulk density of 0.67 g/cm^3 were taken to investigate the physical, chemical and process properties. The chemical composition of the taken samples is shown in Table 1.

Table 1.   Chemical composition of EAF gas cleaning dust.

Name	Oxides content, %											
	CaO	SiO_2	$F_{e2}O_3$	MgO	Al_2O_3	MnO	Cr_2O_3	P_2O_5	ZnO	SO_3	K_2O	Na_2O
EAF dust	10.87	6.51	54.64	4.35	0.48	2.33	0.35	–	3.85	1.16	6.19	8.05

The chemical composition of the material samples used was determined with the ARL 9900 WorkStation series X-ray fluorescence spectrometer with integrated diffraction system. Scanning electron microscopy (SEM) was carried out to study the constitution and structure of particleboard EAF dust. The research was carried out on a high resolution scanning electron microscope TESCAN MIRA 3 LMU. The fraction distribution of particles in the investigated material compositions was studied on the ANALYSETTE 22 NanoTec plus laser particle size analyzer. Bulk density was determined in accordance with GOST 19440-94 Metal powders. Bulk density determination. Part 1. Funnel method.

Experiments were carried out on a laboratory disk pelletizer using water as a binding liquid to produce a finely dispersed spray through the pneumatic atomiser nozzles. The use of water as a binding liquid is due to the nozzle design features and the impossibility of obtaining a fine spray on solutions with a higher density and higher viscosity. A laboratory disk pelletizer (500 mm diameter and 300 mm height) was loaded with 2–3 kg of EAF dust. Water was injected onto the material movable layer through a pneumatic spray nozzle. After the embryos formation (granules measuring 1 ÷ 2 mm), dust was added to the material wet moving layer which led to the granules growth. After the granules had stopped growing, water was injected to lubricate the layer and again granule growth powder was added. Repeating these operations many

times, they received granules of the required size up to 5 mm, which were transferred over plate board into a receiving container. The granules received were dried in a drying cabinet at 105 °C for 24 h. The humidity was determined by drying to a constant mass. Granulation assessment was carried out visually. In order to assess the granular fraction percentage yield, the granules were scattered using the sieve method. Fractions calculation was assessed by sieved substance weight. Humidity was determined by drying in a drying cabinet at 105° C to a constant weight; the strength of wet granules (after the granulator) was determined by dropping them from 1 m height on a steel surface by the undestroyed granules yield percentage.

Experiments were also conducted on a laboratory screw extruder to produce cylindrical granules. The screw used had a diameter of 60 mm in 40 mm increments (in the moulding area) through a flat die (3 mm thick, 54 holes with a diameter of 3 mm). Screw speed is 30 rpm. By changing ratio between liquid-phase binder and powder, we achieved quality granules. The optimal ratio of liquid and solid products in the mixture was fixed, whereby quality granules were obtained during the pelletizing process. The quality of the granules received (granule side surface condition, harness flow uniformity from the die holes) was determined visually. The granules obtained were analysed for humidity by drying the sample to a constant weight in a drying cabinet at 105 °C.

3   Results and Discussion

Dust Microstructure. Steelmaking dust microstructure is shown in Fig. 1. Dust particles shape is determined by their origin. The particles generated by evaporation and oxygen blowing of bath have a shape close to spherical, which is due to droplets excess surface energy and relatively low force of gravity acting on the droplet [9, 10]. This is common in liquid dispersion or droplet vapours condensation. Electric furnace steelmaking dust tend to be generated at the fogging stage when during coalescence micro droplets run into one another and newly form a ball-shaped drop. The average droplet size is 1.5–2.5 μm and corresponds to the highest peak on particle size distribution histogram (Fig. 2).

However, in dust, there is a large number of irregularly shaped particles, spherical particle colonies sticking together. This happens when the colliding droplets consist of very viscous liquids and merging process into one spherical drop is slowed down, only the colliding droplets stick together. These "incorrect" particles also have a normal density, equal to the substance density from which they were derived. These conglomerates are 10–12 μm in size and correspond to the third peak on particle size distribution histogram.

These microphotographs also show loose particles of various shapes, so when metal vapour condensation occurs simultaneously with normal density particles, the density of which is much lower than that of metal.

For the dust generated during charging materials loading, i.e. condensate, dust particles will be sharper and more irregularly shaped [9, 10]. In addition, crystalline particles were found. Typically, the primary particles in smoke have the correct crystalline form, formed by direct transition of the vapour crystal. If smoke is produced by condensing vapour in the form of liquid droplets and then solidifying them, smoke

Fig. 1. EAF dust microphotographs.
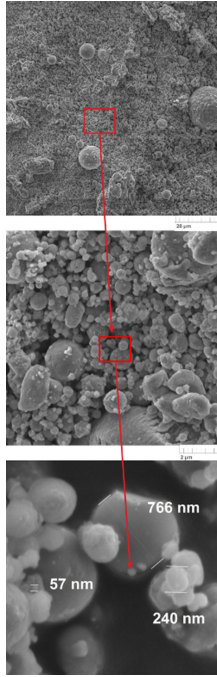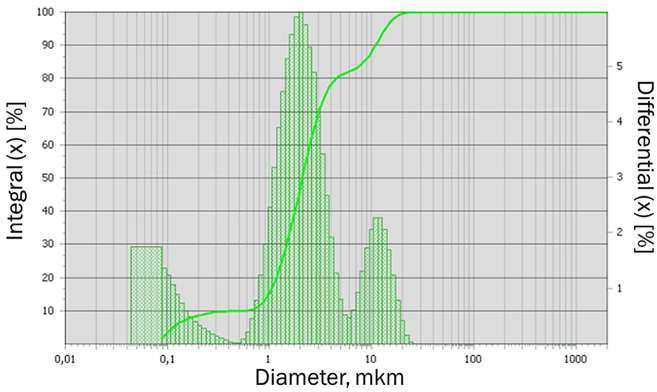

Fig. 2. EAF dust granulometry analysis.

particles may have both crystal and spherical shapes. A number of metal primary smoke particles and their oxides are small, their average size being less than 100 nm, which corresponds to the first peak on the particle size distribution histogram. Particles small size makes it difficult to determine their shape and average size.

EAF Dust Granulation. To work out metallurgical waste pelletizing methods, EAF dust was pelletized by the following two methods: with the use of disk pelletizer and screw pelletizer. The purpose of pelletizing was to produce spherical granules up to 5 mm in size from EAF dust. EAF dust pelletizing by pelletizing on a disk pelletizer to produce spherical granules from EAF dust is appropriate. Granules received had the correct spherical shape and the amount of water was 9–12% of dust mass. The high content of CaO (10–12%) quickly binds free water in a finely dispersed product, resulting in fine granules of 2–5 mm in size, which make up 80% of granules total number. Powder-shaped material is then rolled up problematically and coarse granules of 15–20 mm are formed as a result of fine granules adhesion and are spherical conglomerates. Granules with a size of 2–5 mm are optimal for future use. Granule fracture during the strength tests take place along the druse boundary. The amount of binder as well as other pelletizing process parameters have not significantly affected either structure or strength of granules. Granules humidity received is 6 ÷ 8%. After a strength test by granules dropping, 90–95% of them retained their shape and size. This allows granules to be transported directly after granulation to the dryer for dehydration. Dried granules bulk density was 1.44 g/cm^3. Installation of a pneumatic atomiser directly above the plate and a fine dust atomiser reduce the dust build-up during fine dust dispensing. The granulation rate was 40 kg/h.

For the screw type extruder, it was possible to establish an optimal ratio between liquid and solid phases during granulation. The harnesses were uniformly flown out of the die hole under 16–18% humidity. The side surface of the harnesses was smooth under this humidity. As the humidity increased, there was harnesses adhesion and water separation. When the humidity dropped, the dies were heated and the screw was jammed. During pelletizing of the optimum composition weighing more than 10 kg, there was considerable heating of the nozzles and pelletizer walls, which resulted in the screw jamming. Heating also results in a significant heat release when hydrating the free lime contained in the dust. Progressive lime also caused the mass to harden and stick to the screw and the granulator inner walls, as well as blocking the holes in the die matrix and the screw jamming. After a strength test by granules dropping, 93% of them retained their shape and size. This allows granules to be transported directly after granulation to the dryer for dehydration. Dried granules bulk density was 1.62 g/cm^3. The granulation rate was 15 kg/h.

The granules received are shown in Fig. 3.

a)   b)

Fig. 3. Granules received a) Torsion type granulator b) Screw type granulator.

4   Conclusion

The analysis found that EAF dust is a heterogeneous material with three distinct particle size distribution zones. Stable material can be produced through granulation which requires less storage space: bulk density increases from 0.67 g/cm^3 to 1.44 g/cm^3 and 1.62 g/cm^3 for the disc pelletizer and screw type granulator, respectively. The use of process water as a liquid-phase binder is sufficient to produce granules with the strength needed to transport them to the drying unit. The cylindrical granules density is higher than the density of granules obtained by pelletizing; this is due to the emergence of compression in the dies moulding matrix working area. The production of cylindrical granules in large volumes is problematic; heat is generated by hydration of free CaO, which is part of the dust, and mixing the mass leads to screw jamming and dies clogging. The rational scheme is to use a disk pelletizer. Its pelletizing speed is 2.7 times higher than that of the screw pelletizer, which is due to the time it takes for the screw pelletizer to reach its optimum composition (water/solid phase). It would be advisable to carry out further research with granular material and use it as a stabiliser to produce road-building materials that can be used both in structural elements and in the earth bed of roads and railways.

References

1. Bodyakov, A.N., Meshkova, K.V., Dukhovny, G.S.: Stabilization of metallurgical slug from arc steel-making furnaces. IOP Conf. Series: Mater. Sci. Eng. **945**(1), 012082 (2020)
2. Leontiev, L.I., Dubanov, V.G.: Technogenic wastes of ferrous and non-ferrous metallurgy and environmental problems. Ecol. Ind. **4**, 32–35 (2011)
3. Alpatova, A.A.: Investigation of the composition and properties of electric steelmaking dust and search for directions for its utilization. Physics and chemistry and technology of inorganic materials. pp. 322–323 (2016)
4. Alpatova, A.A.: Investigation of the processes of dust formation during arc heating of metal and the properties of dust for its utilization. Nauka, Moscow (2016)
5. Nevyantsev, G.I., Yurichev, A.V.: Development of installations for recycling dust from gas cleaners of metallurgical furnaces. Design Bureau **6**, 32–39 (2015)
6. Pugin, K.G.: Reducing the environmental burden of steelmaking through the use of fine iron-containing waste in metallurgy. Sci. Res. Innov. **4**(3), 64–71 (2010)
7. Sumarokova, L.S., Kapustin, F.L., Fomina, I.V.: Granulation as a method of utilization of pulverized fine-dispersed production waste. Energ. Res. Conserv. 452–455 (2016)
8. Smirnov, L.A., et al.: Modern technologies and equipment for processing and using technogenic waste of metallurgical production **34**, 69–78 (2017)
9. Belousov, V.V.: Theoretical fundamentals of gas purification. A textbook for high schools, Moscow (1988)
10. Khilko, A.A., Zubkova, S.V., Simonyan, L.M.: Studying the properties of electric steelmaking dust. News of higher educational institutions. Ferrous Metal. **7**, 68–69 (2010)

Diffraction of Harmonic S-waves into Frame Buildings

Ali Al Shemali$^{(\boxtimes)}$ [ID]

Moscow State University of Civil Engineering, Moscow, Russia
alshemali3@gmail.com

Abstract. Diffraction of seismic S-waves into multistory frame buildings is analyzed by FEA (Finite Element Analysis). The FE model consists of a ten-story superstructure rested on the slab foundation. Engineering software Abaqus/CAE 6.14 was used to analyze the interaction of seismic shear waves with the building. The explicit dynamic analysis was performed for the following seismic frequencies 0.5; 1 and 2 Hz over a time period of 5 s. Three types of columns were selected (corner- interior - edge) and the stress values were considered in monitoring points distributed over the entire height of the building at the places where these columns connect with the slabs. The analysis reveals that the arrival of the S-waves at small frequencies results in dangerous stresses in the bottom columns, especially in the corner columns, with the decreasing values of these stresses in a direction towards the last floor. Moreover, the analysis also reveals that at higher frequencies the stress magnitudes slightly decrease.

Keywords: Seismic waves · Building · Frame · Diffraction · Stress

1 Introduction

Seismic waves are acoustic waves emanating from the origin of an earthquake or undersurface explosion. They carry on the wave energy from beneath the Earth, causing surface displacements that can be recorded by seismographs. There are several different kinds of seismic waves, and they all move in different ways. The two main types of waves are body waves (P-waves, S-waves) and surface waves (Love waves, Rayleigh waves) [1]. Body waves can travel through the earth's inner layers, but surface waves can only move along the surface of the planet at a speed slower than the speed of the body's waves. Figure 1 shows the types of seismic waves and the movement of particles in each type- particles are represented by cubes in these models.

This article will be limited to S-waves and the effect of their diffraction into frame buildings. In seismology, S-waves, or shear waves are a type of elastic wave. They move by material flexing or deforming sideways from the direction of wave travel, and then returning to the original shape once the wave passes. S-wave particle motion is often divided into two components (Fig. 2): the motion within a vertical plane through the propagation vector (SV-waves) and the horizontal motion in the direction perpendicular to this plane (SH-waves).
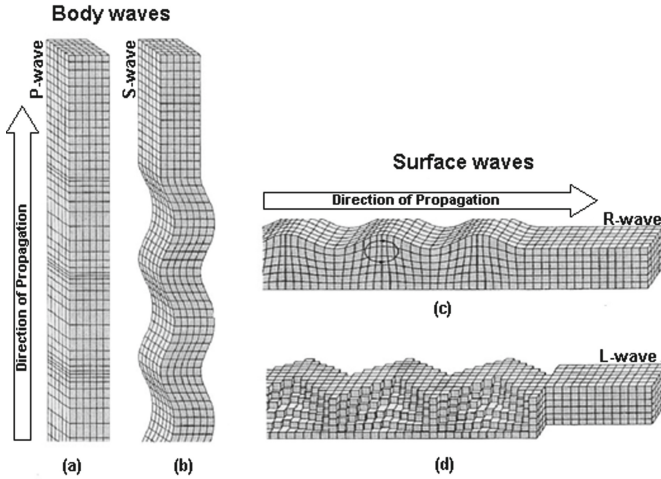
Fig. 1. Types of seismic waves propagating in the ground: (a) P-waves; (b) S-waves; (c) Rayleigh waves; and (d) Love waves.
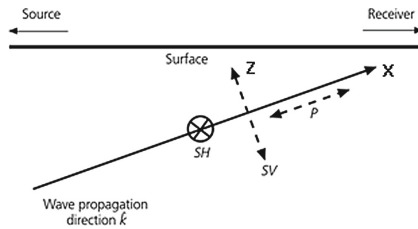
Fig. 2. Displacement fields for P and S waves propagating in the x–z plane.

More attention is paid to the effect of the SV-waves because it can also appear when P-waves are reflected [2].

The S-wave Velocity depends on the shear modulus and the density. According to the Eurocode 8 seismic shear wave speeds (C_s) are less than 100 m/s for soils that have a density of 1750 kg/m^3 while speed ranges between 180–360 m/s for density 2000 kg/m^3 [3, 4].

The term "diffraction" refers to the redistribution in space of wave intensity resulting from presence of an object. When an elastic wave meets an object or obstacle, it is diffracted due to scattering of energy of the propagating initial wave [5].

2   Methods and Materials

2.1   Basic Equation

The equation of seismic wave motion has solutions that describe the two types of propagating seismic (or elastic) waves, compressional and shear waves [1]. To obtain this equation, we start from Newton's second law F = ma, which states that the force vector equals the mass times the acceleration vector. Accordingly, the relation between the stresses in the i direction can be written as follows:

$$\sigma_{ij,j}(\mathbf{x},t) + \mathrm{f}_i(\mathbf{x},t) = \rho \frac{\partial^2 u_i(\mathbf{x},t)}{\partial t^2}. \tag{1}$$

where $\mathrm{f}_i(x,t)$ is the body force, for a homogeneous medium $\mathrm{f}_i(x,t) = 0$.

To express this in terms of displacements, we use the constitutive law for an isotropic elastic medium:

$$\sigma_{ij} = \lambda\theta\delta_{ij} + 2\mu e_{ij}, \tag{2}$$

where λ, μ are Lame's constants related to Young's modulus and Poisson's ratio.

Substituting expression (2) in Eq. 1 gives the equations of motion in terms of the displacements for isotropic homogeneous media in the x direction:

$$(\lambda + \mu)\frac{\partial\theta}{\partial x} + \mu\nabla^2(u_x) = \rho\frac{\partial^2 u_x}{\partial t^2}. \tag{3}$$

Similar equations can be obtained for the y and z components of displacement. The three equations can be combined into a single vector equation:

$$(\lambda + 2\mu)\nabla(\nabla.\mathbf{u}(\mathbf{x},t)) - \mu\nabla \times (\nabla \times \mathbf{u}(\mathbf{x},t)) = \rho\frac{\partial^2 \mathbf{u}(\mathbf{x},t)}{\partial t^2}. \tag{4}$$

We express the displacement field in terms of two other functions, and, which are known as potentials (the gradient of a scalar potential, $\phi(\mathbf{x},t)$, and the curl of a vector potential, $\psi(\mathbf{x},t)$);

$$\mathbf{u}(\mathbf{x},t) = \nabla\phi(\mathbf{x},t) + \nabla \times \psi(\mathbf{x},t). \tag{5}$$

After this substitution, the terms in Eq. 4 can be regrouped to give:

$$\nabla[(\lambda + 2\mu)\nabla^2\phi(\mathbf{x},t) - \rho\frac{\partial^2\phi(\mathbf{x},t)}{\partial t^2}] = -\nabla \times [\mu\nabla^2\psi(\mathbf{x},t) - \rho\frac{\partial^2\psi(\mathbf{x},t)}{\partial t^2}]. \tag{6}$$

One solution of the equation can be found if both terms in brackets are zero. This yields two harmonic wave equations,

For P-waves

$$\phi(\mathbf{x}, t) = A \exp(i(\omega t - \mathbf{kx})), \tag{7}$$

For S-waves

$$\psi(\mathbf{x}, t) = \mathbf{A} \exp(i(\omega t - \mathbf{kx})), \tag{8}$$

Where $\mathbf{A}$ is the oscillation amplitude, $\mathbf{k}$ is the wave vector; $\mathbf{k} = 2\pi/\lambda$, where λ is the wavelength;

2.2   Geometric and Structural Parameters of the Building

The building under study is a multi-storey flat slab concrete construction, a plan of this building is shown in Fig. 3. Geometric and structural parameters used for the design are given below.
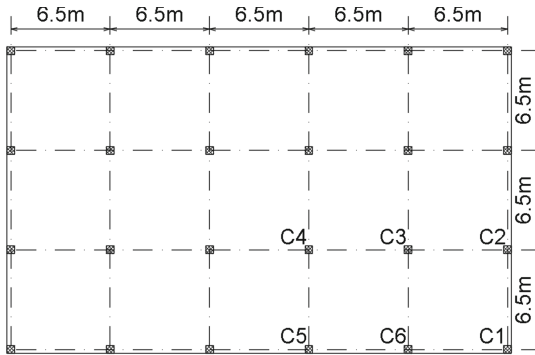

Fig. 3.   Plan of this building with column labels.

2.3   Geometric Parameters

The main parameters describing the geometry of buildings are shown in the Table 1:

Table 1.   The main parameters of the building to be modeled.

Building length, m	Building width, m	Number of storeys	Storey height, m
33	20	10	3.3

2.4   Members Properties

Square cross-section columns and flat slab in addition to the slab foundation were used for modeling. Table 2 shows the member properties of the buildings. Modulus of elasticity of concrete was taken as 30×10^9 N/m^2, poisons ratio as 0.25 and density of concrete was taken as 2200 kg/m^3.

Table 2. Cross-section of the building members.

Columns section, mxm	Slabs thickness, m	Slab foundation thickness, m
0.5 × 0.5	0.3	1.5

2.5   Boundary Conditions

For the study of general behaviour of the building, an acceleration 5 m/s^2 was applied under the foundations in two directions (x, z), considering that the construction is located in a zone of seismic intensity 9 according to the modified Mercalli scale [6]. Assuming that this acceleration changes with time according to the following periodic law:

$$f(x) = \sin(\omega\, t). \tag{9}$$

Where $\omega = 2\pi f$ is the angular frequency of seismic waves. For load-bearing structures the most dangerous seismic frequencies of body waves, which are taken into account in design, are within range $f : 0.1 - 20$ Hz [5, 7]. Considering common problems and approaches used in FE modeling it is needed to note account of energy dissipation in structures [8]; problems related to imposing non-reflecting boundary conditions at the FE modeling are discussed in [9]; problems related to the FE modeling seismic sources, causing appearance of different types of seismic waves [10]. Applications of FE modeling to seismic protection are considered in [3, 11]. Theoretical problems related to crack initiation and propagation in various elements of buildings and structures at dynamic loadings, are discussed in [12].

2.6   FE Model

Finite Element Analysis (FEA) is a computer simulation technique used in engineering analysis by using the numerical technique of finite element method (FEM). Engineering software Abaqus/CAE 6.14 was used to analyze the interaction of seismic S-waves with the building. An 8-node linear hexahedral solid element with reduced integration (C3D8R) was used for modeling the building. C3D8R has six degrees of freedom at each node. Figure 4 shows the model generated in Abaqus software.
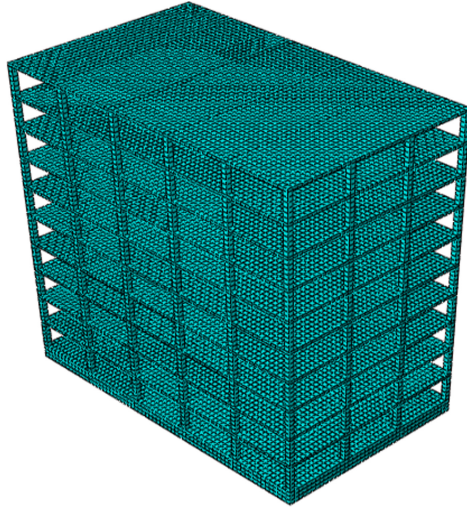
Fig. 4. 3D model of building

2.7   Type Analysis

In order to assess the state of stress in problems related to wave propagation simulation, the use of explicit dynamic analysis is most appropriate. This analysis performs a large number of small time increments efficiently. An explicit central-difference time integration rule is used. Abaqus allows to conduct this analysis to be carried out by selecting a procedure - Dynamic, Explicit step.

3   Results and Discussion

The explicit dynamic analysis was performed for the seismic frequencies $f = 0.5, 1$ and 2 Hz over a time period of 5\,s. After the analysis, the stress values that arise from diffraction of S-waves into building were considered. To facilitate the process of discussing the results, monitoring points have been set up at the places where the columns (C1, C4, C5) connect with the slabs (see Fig. 4). The locations of these points are shown in the Table 3.

Table 3. Locations of monitoring points.

Monitoring point name	Monitoring point location
monitoring point 1-(mp1)	Column connection with slab foundation
monitoring point 2 -(mp2)	Column connection with the floor of the 3rd storey
monitoring point 3 -(mp3)	Column connection with the floor of the 5th storey
monitoring point 4-(mp4)	Column connection with the floor of the 7th storey
monitoring point 5-(mp5)	Column connection with the floor of the 9th storey
monitoring point 6-(mp6)	Column connection with the slab of the 10th storey

As an example of the simulation results, several graphs are given below (Fig. 5, 6 and 7), which show the time-dependent stress change at the monitoring points.
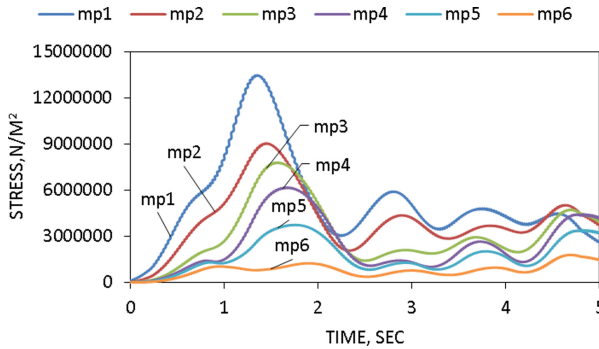
Fig. 5. Time-dependent stress for C1 at all monitoring points ($f = 0.5$ Hz).
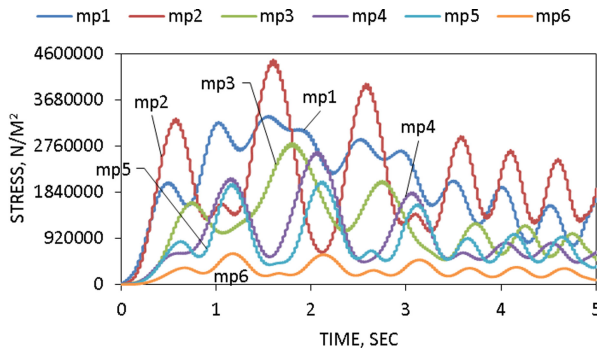
Fig. 6. Time-dependent stress for C4 at all monitoring points ($f = 1$ Hz).

Fig. 7. Time-dependent stress for C5 at all monitoring points ($f = 2$ Hz).

By looking at the stress values in the above charts, a set of results were drawn, which are listed below.

- During diffraction of S-wave into frame building, the stress values decrease from the slab foundation towards the last floor for all seismic frequencies.
- The stress values decreased with increasing the seismic frequency values for all studied columns.
- Corner columns are the most dangerous due to the high stress values in them compared to other columns.

4 Conclusion

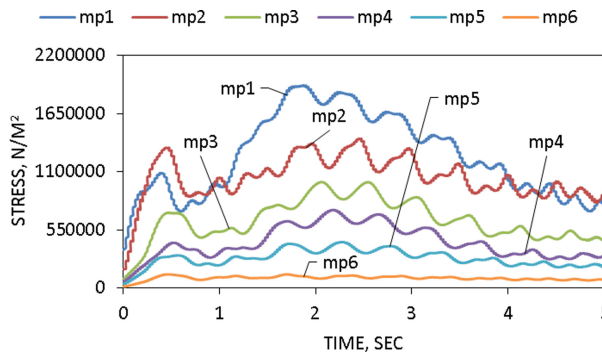A multi-storey building with the application of acceleration 5 m/s^2 under the foundations at different frequencies was modeled using the Finite Element code Abaqus. The analysis showed the places where the dangerous stresses may appear in the considered building. Moreover, to obtain more objective results, it is recommended to perform the analysis for different ground acceleration. It is also recommended to perform future studies with the presence of soil under the foundation and with different geometric and structural parameters of the building.

References

1. Stein, S., Wysession, M.: An introduction to seismology, earthquakes, and earth structure. John Wiley & Sons (2009)
2. Saini, R.: Reflection/refraction at the interface of an elastic solid and a partially saturated porous solid containing liquid filled bound pores and a connected pore space saturated by two-phase fluid. Latin Am. J. Solids Struct. **12**(10), 1870–1900 (2015)
3. Dudchenko, A.: Numerical analysis of surface Rayleigh wave interaction with seismic barriers and pile fields accounting elastic-plastic soil behaviour. PhD thesis, UJF: Grenoble (2018)
4. Code, P.: Eurocode 8: Design of structures for earthquake resistance-part 1: general rules, seismic actions and rules for buildings. Euro. Committee Standardization, Brussels (2005)
5. Arora, K., Cazenave, A. et al.: Encyclopedia of solid earth geophysics. Springer Science & Business Media (2011)
6. Jain, A.K.: Performance Based Seismic Design of Tall Buildings: Risks and Responsibilities. https://cecr.in/CurrentIssue/pages/20147
7. Semblat, J.F., Pecker, A.: Waves and vibrations in soils. Earthquakes, traffic, shocks (2009)
8. Jones, R.M.: Deformation theory of plasticity. Bull Ridge Corporation (2009)
9. Li, S., Brun, M. et al.: Numerical modelling of wave barrier in 2D unbounded medium using Explicit/Implicit multi-time step co-simulation. In: IOP Conference Series: Materials Science and Engineering. vol. 365, pp. 042062 (2018)
10. Il'yasov, K.K., Kravtsov, A.V. et al.: Exterior 3D lamb problem: Harmonic load distributed over a surface. Mech. Solids **51**(1), 39–45 (2016)
11. Kuznetsov, S.V.: Seismic waves and seismic barriers. Acoust. Phys. **57**(3), 420–426 (2011)
12. Ilyashenko, A.V., Kuznetsov, S.V.: Stress–displacement intensity factors for cracks in anisotropic media. Arch. Appl. Mech. **87**(8), 1365–1369 (2017)

Filling of Epoxy Polymers with Chemically Precipitated Chalk from Chemical Water Treatment Sludge

R. R. Galeev[1](✉) ⓘ, R. K. Nizamov[2], and L. A. Abdrakhmanova[2]

[1] Naberezhnye Chelny Institute, Kazan Federal University,
Naberezhnye Chelny, Russia
grrl98l@outlook.com
[2] Kazan State University of Architecture and Construction, Kazan, Russia

Abstract. The results of the use of chemically precipitated chalk as an active highly dispersed filler in compositions based on epoxy oligomers are presented. Used chemically precipitated chalk (original and hydrophobized), obtained by precipitation, dehydration, drying and classification of sludge from the chemical water treatment plant. To achieve the homogeneity of composites, two methods of preparing the reaction mixture for curing are considered: the introduction of the filler initially into the epoxy oligomer and the introduction of the filler into the amine hardener. Depending on the method of filler introduction and its concentration in the binder (0.5–5.0% of the mass of the epoxy oligomer), the developed formulations can be recommended for obtaining adhesives and coatings, as well as as structural composites. To study the mechanical properties, the method of determining the microhardness was used, which made it possible to evaluate the effect of the size of the filler particles and to carry out a comparative assessment of their effectiveness with small amounts of carbon-containing nanofillers (0.005–0.5%).

Keywords: Epoxy oligomer · Chemically precipitated chalk · Sludge from chemical water treatment of thermal power plants · Active filler · Microhardness

1 Introduction

Epoxy oligomers are the most common and effective thermosetting binders for creating a wide range of composite materials, and, by their functional purpose, composites based on them are almost the most numerous and diverse [1–4]. The production of epoxy polymers from oligomers is combined simultaneously with the production of composite materials based on them using a large number of different modifiers, including fillers [5–7]. The method of modification by filling, that is, the so-called prescription method of modification, at first glance, seems very simple, but from the point of view of reasonable and purposeful implementation of such modification, it is quite complex, sometimes not predictable. The fact is that the processes of formation of filled epoxy polymers depend on many factors. The most important of them [8] are:

– adsorption of oligomers by the surface of fillers and therefore the occurrence of blocking of some functional groups involved in the curing reaction;
– selective adsorption of the oligomer and hardener is possible, which can lead to changes in the stoichiometry of the components during the curing process;
– finally, the chemical nature of the filler itself can also affect the kinetics and direction of the curing reaction in different ways.

All these factors can be ambiguous depending on the size of the filler particles, their concentration, and, finally, on the degree of uniformity of the distribution of filler particles in the oligomer matrix and subsequently in the polymer composite matrix.

Most often, epoxy polymers are modified with fine mineral and organic fillers, and mineral fillers have a predominant application. Of course, fillers from technogenic waste are always attractive [9, 10] because of their low cost and energy saturation. One of the areas of interest in this regard is the sludge of chemical water treatment of thermal power plants, the volume of which is tens of thousands of tons. After certain processing, they can be effective in the production of various types of construction products of inorganic and organic nature [11]. It is obvious that the processed fine sludge of chemical water treatment can be used as a dispersed filler in the composition of epoxy building composites.

2   Methods and Materials

In this paper, we studied samples of epoxy composites with the use of chemical water treatment sludge of thermal power plants as fillers. Epoxy-bisphenol resin brand ED-20, amine hardener polyethylene polyamine (PEPA) in the ratio 100 m. p. of the resin and 15 m. p. of hardener are taken as the starting components. A two-stage mode of distraction was adopted: 24 h at a temperature of $20 \pm 2\ °C$ and 8 h at a temperature of 80 °C. Samples of different geometric sizes and shapes were prepared for the following test methods: Vickers microhardness (according to GOST R ISO 6507-1-2007; adhesive joint strength on separation ($\sigma_{breakage}$) according to GOST 14760-69. The amount of gel fraction of cured epoxy polymers was determined by extraction method according to GOST R 56782-2015. Changes in the deformation behavior of the samples were evaluated using thermomechanical compression curves (TMC) obtained on the device with the Masterscada software. Measurements were performed on samples in the form of cylinders 3 mm thick and 8 mm in diameter at a constant compressive load of 3 N and a temperature increase rate of 3 °C/min. The glass transition temperature (T_g) was estimated from the transition point on the curve from the glassy to the highly elastic state. The high-elasticity modulus (H) and the mesh density parameters (υ) were calculated based on the data of the relative deformation of samples in the high-elastic area (from TMC).

Two grades of chemically precipitated chalk (CPC) "Poly-filler" corresponding to TC 2169-001-06961628-2017, obtained by precipitation, dewatering, drying and classification of chemical water treatment sludge were used as fillers: without treatment and hydrophobized with stearic acid. In terms of mineral composition, they contain about 98% calcite. By chemical composition, the most significant oxides are CaO

(more than 46%), MgO (3.56%) and Fe_2O_3 (almost 5%). The average size of the filler particles is 15.05–15.80 microns.

In this work, two types of mixing sequences of components were used for the preparation of samples:

1. ED-20 epoxy resin + filler + PEPA hardener;
2. PEPA hardener + filler + ED-20 epoxy resin.

The amount of filler in the composition varied from 0.5 to 5% by weight of the epoxy oligomer.

3   Results and Discussion

At the first stage, the technological properties of epoxy binders were evaluated when the filler was introduced. Fillers were introduced into the binder components using two different mixing methods and mixed until they were evenly distributed in a viscous oligomeric medium. The gelation time (in hours) was estimated. As an example, in Table 1 data for the epoxy binder filled with CPC and CPC_{hydro}, combined with two options of mixing are given.

Table 1. The gelation time and the degree of conversion of the epoxy binder filled with CPC and CPC_{hydro}.

Filler content,%	Gelation time, hour		Content of the gel fraction, %	
	1 variant	2 variant	1 variant	2 variant
Control	1:32		98.7	
CPC	00:27	00:26	98.96	99.72
0.5%	00:30	00:29	98.52	99.25
1.5%	00:27	00:22	99.81	98.04
3%	00:21	00:19	98.99	93.40
5%				
CPC_{hydro}	00:35	00:30	99.18	93.51
0.5%	00:29	00:29	98.93	91.92
1.5%	00:28	00:28	98.14	94.84
3%	00:25	00:25	96.59	94.76
5%				

From these data, it follows that the gelation time during the introduction of the filler is significantly reduced, that is, the formation of the polymer mesh structure is faster. However, the conversion rate remains almost at the level of the control samples with a slight tendency towards lower values for samples with hydrophobized chalk obtained by the second combination option. It is obvious that there is a predominant adsorption of hardener molecules on the filler surface, rather than molecules of the epoxy oligomer. At the same time, the orienting influence of the filler helps to accelerate the

interaction of functional groups. However, the presence of a hydrophobizer probably leads to the formation of a structure with a lower cross-linking density.

It should also be noted that the initial viscosity of the composition after combining all the components is lower in the second variant of the binder preparation.

The main method for evaluating mechanical properties was to determine the microhardness of samples, which allowed evaluating simultaneously the uniformity of the distribution of filler particles in the matrix of the curing epoxy polymer. In Table 2 the main mechanical and thermomechanical properties of samples with an optimal concentration (3% by weight) are given according to the set of main indicators obtained for the first variant of combining components.

Table 2. Indicators of optimal formulation of epoxy composites.

Type of filler	$\sigma_{breakage}$, kPa	Microhardness, kg/mm^2	T_g, °C	H, MPa	υ, mol/g
Control	12	15.5	97	34	$2.6 \cdot 10^{-5}$
CPC	20	19.3	94	47	$3.3 \cdot 10^{-5}$
CPC$_{hydro}$	23	21.9	124	65	$6.2 \cdot 10^{-5}$

From the data in Table 2 it follows that the presence of the filler is accompanied by a decrease in the value of highly elastic deformation and, accordingly, an increase in the density of the nodes of the mesh structure of the samples. The highest values of mechanical properties of filled samples are also observed.

4   Conclusion

Thus, comparing the overall results of changes in technological properties and performance indicators, we can say that in the presence of chemically precipitated chalk and hydrophobized chemically precipitated chalk from chemical water treatment sludge, the properties of epoxy composites are at the level of control samples, and higher in a number of indicators. In the previous works of the authors [12, 13], a fairly high efficiency of using small amounts of carbon nanostructures in similar basic formulations of epoxy polymers obtained under the same temperature-time curing conditions was shown. However, taking into account the high cost of nanoadditives, as well as their tendency to aggregate in a viscous oligomer medium, it can be concluded that both from the point of view of technological modes of combining and curing the polymer, and from the point of view of ecology and economy, it is preferable to use fine chemically precipitated fillers from the sludge of chemical water treatment from thermal power stations.

References

1. Khozin, V.G.: Strengthening of epoxy polymers. 446 (2004)
2. Agrawal, A., Satapathy, A.: Mathematical model for evaluating thermal conductivity of polymer composites with hybrid fillets. Intern. J. Thermal Sci. **89**, 203–209 (2015)
3. Kasen, M.B., Schramm, R.E.: Current status of standardized nonmetalle cryogenic laminates. Adv. Cryog. Eng. **28**, 171–177 (1981)
4. Gao, B.Z., Xua, J.Z., Penge, J.J., Kanga, F.Y., Dua, N.D., Lia, J.: Experimental and theoretical studies of effective thermal conductivity made of silicone rubber and Al_2O_3 particles. Themochimica Acta **20**, 1–8 (2015)
5. Mikhaylin, Y.A.: Structural polymer composite materials. Mikhaylin-Saint Petersburg 822 (2010)
6. Xua, J., Gaoa, B., Dua, N., Kanga, F.: Statistical model for effective thermal conductivity of composite materials. Intern. J. of Thermal Sci. **104**, 348–356 (2016)
7. Kolosova, A.S., Sokolskaya, M.K., Vitkalova, I.A., Torlova, A.S., Pikalov, E.S.: Fillers for modification of modern polymer composite materials. J. Fund. Res. **10**(3), 459–465 (2017)
8. Storodubtseva, T.N., Tomilin, A.I.: Composite construction materials, methods for studying their properties. Modern High-tech Technol. **11**, 55–58 (2012)
9. Pat. 2543209 RU. Method for producing a hydrophobic polymer filler by modifying chemically precipitated calcium carbonate with stearic acid. Prokofieva L.A. Niftaliev S.I. Peregudov Yu.S.; applicant and patent holder Voronezh State University of Engineering Technologies, application 09.10.2013. publ. 02.27.2015. 6
10. Sorokin, V.V., Sharapov, O.N., Shunkin, N.M., Kiryushina, N.Y.: New polymer composites based on epoxy resin filled with technogenic waste. Bull. BSTU named after V.G. Shukhov **6**, 8–13 (2019)
11. Nikolaeva, L.A., Boroday, E.N.: Resource-saving technology for utilization of water treatment sludge at thermal power plants. Kazan. Kazan State Power Engineering University 110, (2012)
12. Abdrakhmanova, L.A., Khozin, V.G., Nizamov, R.K.: Nanomodification of epoxy binders. Nanotechnol. Const. Online Sci. J. **11**(6), 577–586 (2019)
13. Khozin, V.G., Abdrakhmanova, L.A., Nizamov, R.K., Khantimirov, A.G., Mustafina, A.R.: Possibilities of using the products of NanoTechCenter LLC for obtaining polymer nanocomposites for construction purposes. In: Proceedings of the III International scientific and practical conference "Graphene and related structures: synthesis, production and application". Tambov. pp. 241–242 (2019)

Application of Antifreezing Additives in Mortars

J. V. Denisova[(✉)]

Belgorod State Technological University named after V.G. Shuhova,
46 Kostyukova Street, Belgorod, Russia
`jdenisowa@mail.ru`

Abstract. Concrete and reinforced concrete are currently used for the construction of buildings and structures. At negative temperatures, the hydration of the binder slows down and the solidification of mortars proceeds quite slowly, and the strength set of mortars and concrete mixtures stops. As a result, to ensure a set of strength in winter conditions, it is necessary to introduce antifreezing chemical additives into the mortars, which contribute to the normal flow of cement hydration processes. In this regard, the urgent task is the correct and rational choice of raw materials, which directly affect the durability and reliability of concrete and reinforced concrete products and structures. Therefore, in the course of research, most of the time is devoted directly to the study and selection of raw materials for the preparation of concretes and mortars. It is impossible to achieve the necessary durability of concrete without introducing chemical additives into its composition. The paper presents a study of antifreezing additives that positively affect the properties and durability of concrete and mortars and work effectively in conditions of negative temperatures. Optimal dosages of the studied additives were determined and the influence of new types of additives on the strength characteristics of concrete and mortars was studied.

Keywords: Additive · Plasticizer · Antifreezing additive · Dosage · Concrete · Mortar · Strength · Cement · Sand · Water · Method for determining insoluble sediment additives · Complex additive · Antifreeze-plasticizing properties

1 Introduction

In conditions of negative temperatures the process of hydration of the binder slows down and the hardening of concretes and mortars proceeds quite slowly. At low temperatures the strength development of concrete mixtures shall be terminated. As a result, to ensure a set of strength in winter conditions, it is necessary to introduce anti-freezing chemical additives into the composition of concretes and mortars, which contribute to the normal flow of cement hydration processes. Moreover, these additives should have a positive effect on the properties and durability of concrete, as well as work effectively in conditions of negative temperatures [1]. An urgent task for technologists is the correct and rational choice of raw materials, on which the durability and reliability of concrete and reinforced concrete products and structures directly depend,

on the physical and mechanical parameters and quality of which the service life of buildings and structures under construction directly depends [2]. The solution of the problem of obtaining concretes and mortars with improved physical and mechanical properties in winter conditions can be achieved by using a complex additive that has both plasticizing ability and antifreezing properties [3].

2   Methods and Materials

Currently, in the winter period of time in the production of mortars antifreezing additive Potash (P) – salt with strong alkaline properties is widely used. During the research, most of the time is devoted directly to the study and selection of raw materials for the preparation of concretes and mortars under negative temperatures. The mineral and material composition of Portland cement PC500DO (CEM I 42.5 N according to GOST 30515), which meets the requirements of GOST 31108-2003, was studied; the optimal dosages of the studied additives were determined; the influence of new types of additives on the strength characteristics of concrete and mortars was studied. At the first stage of research, the concrete mixture with antifreezing additives introduced with the mixing water was prepared on cements of the design grade and corresponding small and large aggregates [4]. Quartz sand was used as fine aggregate: Lower-Olshansky sand quarry, Kursk and Novotavolzhanka fields. The main characteristics of the used sands are determined: the void ratio of the used sands is 35… 37%; the content of clay, silty and dusty particles is 0.5…1.5%; humidity is 4…6%. Mineralogical compositions of quartz sands were studied by x-ray phase analysis. Modern methods were used in the research to ensure the reliability of the obtained results. To study the composition and structure of raw materials, we used both high-precision instrumental research methods–x-ray diffraction, scanning electron microscopy, and standard methods for determining the properties of raw materials, mixtures, and concretes.

3   Results and Discussion

Analysis of complex additives on the market that have antifreezing and plasticizing properties showed that the most effective are the following additives – C-3 M-15, PLKP, Monolit. In the current market relations, it is important to evaluate the use of additives from an economic point of view [5]. The comparative economic efficiency of the studied additives has shown that they differ in cost, so when choosing one of the studied additives, it is necessary to be guided by storage conditions, technology and manufacturing features, as well as cost indicators. Thus, the following additives were selected for further research: LMG, Penostrom, Pyleunos, Potash, C-3M-15, PLKP, Monolit. According to the results of determining the plasticizing ability of additives, the optimal dosage for the studied additives was revealed, which is 1.5% for C-3M-15, 0.8% for PLKP, and 1.8% for Monolit by weight of cement (Fig. 1).
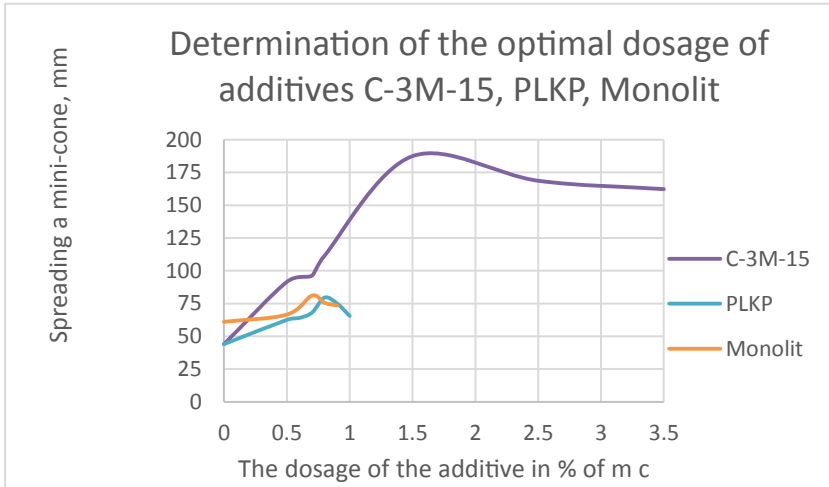
Fig. 1. Determination of the optimal dosage of additives C-3M-15, PLKP and Monolit

Alternate freezing and thawing of concrete and reinforced concrete products and structures operated in natural conditions leads to the development of destructive processes that reduce the durability of buildings and structures [6]. The reasons for the destruction of wet material under the influence of negative temperatures are internal stresses, the difference in the coefficients of expansion of ice and crystal accretion. The greatest influence is exerted by the phase transitions of moisture in the concrete body.

Increasing the frost resistance of concrete can be carried out by increasing the density of concrete by reducing the volume of macropores and their water permeability, by creating a system of reserve air pores in concrete, which are not filled with water under normal water saturation [7]. Additives C-3M-15, Potash, PLKP-S, Monolit were frozen at temperatures up to minus 18 °C. As a result, the freezing time of the additive concentrate was determined. Table 1 shows the results of the obtained tests.

Table 1. Freezing time of the additive concentrate

Freezing concentrate additive time, in hours	Ambient temperature, °C	Additive freezing time, min.			
		Potash	C-3M-15	PLKP	Monolit
	−18	110 min	80 min	80 min	Does not freeze over 240 min

It was found that among the studied antifreezing additives, the sediment is present in the PLKP additive. In this regard, in accordance with the methodology for determining the insoluble precipitate for the LMG additive, the analysis of the insoluble precipitate of the PLKP additive was carried out. In the course of research, it was found that with a constant dosage based on the mass of cement, the concrete mixture is in the

more severe conditions of hardening at a temperature below 0 °C, the higher its water-cement ratio W/C, which is not observed when adding additives to the mixing water. When any antifreezing additive is dissolved, its molecules or ions are distributed over the entire volume of water, and their chemical interaction with water molecules occurs. As a result, strong compounds of the dissolved additive particles with water molecules were formed, which led to a decrease in the freezing point of water [9].

At the next stage, the physical and mechanical properties of mortars obtained using complex additives with antifreeze-plasticizing properties are determined. Studies were carried out on mortar mixtures with a volume ratio of Sand: Cement = 1:4 and a mobility of 5…7 cm in the depth of immersion of the cone. Standard samples were formed from mortar mixtures on a porous base-cubes measuring $70.7 \times 70.7 \times 70.7$ mm. Mortar mixtures and samples with an antifreezing additive, as well as control samples without an additive, were placed directly after preparation in a freezer with a temperature of -20 ± 2 °C. Changes in their mobility were monitored for 4 h. The cube samples were stored at -20 ± 2 °C for 28 days. The compressive strength of samples previously thawed for 4 h in air at a temperature of $+18 \pm 2$ °C was monitored. Comparative selections of the M100 mortar were made, which were monitored at a negative temperature. Table 2 presents the results of the obtained tests with M100 mortars.

Mortars were selected in the following compositions (the amount and type of additive, in % by weight of cement):

1) without additives;
2) with additives: LMG 0.3% + Penostrom 0.008% + Potash 3% + Pyleunos 5%;
3) with additives: C-3 M-15 1,5% + Penostrom 0.008% + Pyleunos 5%;
4) with additives: PLKP 0.8% + Penostrom 0.008% + Pyleunos 5%;
5) with additives: Monolit 1.8% + Penostrom 0.008% + Pyleunos 5%.

Table 2. Results of the obtained tests with M100 mortars

№ compo-sition	The composition of the mortar, kg/m³			Stratification, %	Workability, cm (Π_κ3)	Compressive strength, % (days of natural storage)		
	Cement	Sand	Water, l			3 days	7 days	28 days
1	275	1405	340	3.2	10.6	18.79	41.35	71.7
2	261	1405	340	2.1	10.3	15.9	39.32	53.2
3	261	1405	296	6.7	10.0	17.35	43.08	73.4
4	261	1405	308	3.0	10.5	21.97	48.57	78.3
5	261	1405	340	3	10.5	20.63	46.07	54.6

It was found that among the studied antifreezing additives, the best strength characteristics were obtained using a complex high-performance PLKP additive. After 3 days of natural storage, the additive allows getting 50% strength with the lowest percentage of its introduction (0.8%) among the studied antifreezing additives (Potash,

C-3M-15, Monolit). However, the cost and terms of delivery suspend its application. The studied antifreezing additives allow obtaining stable strength characteristics. After 3 days of natural storage, additives allow getting about 80% of the strength of concrete while saving 10% of cement [10].

Non-heating winter concreting due to the use of antifreezing additives allows saving heat and electricity with a more flexible technology of work [12]. If it is necessary to make technical and economic comparisons with additives for other purposes, this dosage can be easily converted to cement; for the average data, it can be assumed that the water-cement ratio is 0.5. Antifreezing additives are stable substances that can be stored both in solid form and in solution for an unlimited time [13]. They perform their functions primarily by reducing the freezing point of water. Therefore, it is most reasonable and correct to assign their dosage to the mass of the mixing water, which is especially clearly manifested when the water-cement ratio (W/C) changes [14].

4   Conclusion

The introduction of antifreezing additives is 1.5 times more economical than the method of steam heating and concreting with the previous fencing of the structure and its insulation from the inside and 1.5 times more economical than electric warming and electric heating. Non-heating winter concreting due to the use of antifreezing additives allows saving heat and electricity with a more flexible technology of work [15, 16]. If the dosage is constant based on the mass of cement, the concrete mixture is in the more severe conditions of hardening at a temperature below 0 °C, the higher its W/C, which is not observed when adding additives to the mixing water [17].

Under normal hardening conditions, a stable positive kinetics of strength changes relative to the control composition was observed for concretes made of equal-moving mixtures and with W/C = const. At a negative temperature, a stable increase in strength was observed, samples that hardened outside gained up to 80% in 28 days, and those that hardened in the chamber – up to 65% of the control composition, which hardened under normal conditions for 28 days. At negative temperatures, stable strength indicators were also observed when testing using the "cold" concrete method. Thus, the use of effective complex additives that have both plasticizing and antifreezing properties in the construction industry makes it possible to obtain products that differ in higher and quality indicators.

References

1. Denisova, Y.V., Kosuhin, M.M., Popova, A.V., Shapovalov, N.A., Leshhev, S.I., Kamorova, N.D.: Vibrocompressed concrete with superplasticizer based on resorcinol-formaldehyde oligomers. Build. Mater. **10**, 32–33 (2016)
2. Poluektova, V.A., Shapovalov, N.A.: Fundamental patterns of influence of the structure and composition of the oxyphenol oligomers on the plastification of cement mixtures. Int. J. Pharm. Technol. **8**(4), 22716–22725 (2016)
3. Babkov, V.V., Sahibgareev, R.R., Kolesnik, G.S.: Rational scope of modified concrete in modern construction. Const. Mater. **10**, 20–22 (2006)
4. Bazhenov, Y.M.: Concrete Technology. ACV, Moscow (2003)
5. Gridchin, A.M., Kosuhin, M.M., Lesovik R.V.: Construction materials. Betonovedenie: laboratory practicum. 2-nd ed., revised. and extras. BSTU named after V.G. Shukhov, Belgorod (2005)
6. Alfimova, N.I., Kalatozi, V.V., Karatsupa, S.V., Vishnevskaya, Y., Sheychenko, M.S.: Mechanoactivation as a way to increase the efficiency of using raw materials of different genesis in construction materials. Bulletin of BSTU named after V.G. Shukhov **6**, 85–89 (2016)
7. Shapovalov, N.A., Denisova, J.V., Poluektova, V.A.: Biocidal research of oxyphenolic modifiers for fungicidal properties. Int. J. Pharm. Technol. **8**(4), 24976–24986 (2016)
8. Shapovalov, I.V., Ogrel, L.S., Kosuhin, M.M., Pavlenko, V.I., Popova, Y.V., Shapovalov, N.A., Slyusar, A.A.: Mineral building modifier Fungicidal compositions. RF Patent 2,235,695 (2006)
9. Shapovalov, I.V., Ogrel, L.S., Kosuhin, M.M., Pavlenko, V.I., Popova, Y.V., Shapovalov, N.A., Slyusar, A.A.: Modifier compositions. Envir Syst. Dev. **4**, 50–51 (2006)
10. Narayanan, N., Ramamurthy, K.: Structure and properties of aerated concrete: a review. Cement Concr. Comp. **22**(5), 321–329 (2000)
11. Wan-liang, Z., Jing-hua, L., Bing-gen, Z.: Further study on property of fly ashfluorogypsum-cement composite binder. J. Build. Mater. **2**, 13–18 (2008)
12. Shahova, L.D., Chernositova, E.S., Denisova, J.V.: Flowability and durability of cement containing technological additives during grinding process. AER-Adv. Eng. Res. **133**, 162–167 (2017)
13. Denisova, J.V.: Additive technology in construction. Const. Mater. Prod. **1**(3), 43–50 (2018)
14. Alfimova, N.I., Shadskiy, E.E., Lesovik, R.V., Ageeva, M.S.: Organic-mineral modifier on the basis of volcanogenic-sedimentary rocks. Int. J. Appl. Eng. Res. **10**(24), 45131–45136 (2015)
15. Klyuev, S.V., Khezhev, T.A., Pukharenko, Y.V., Klyuev, A.V.: Experimental study of fiber-reinforced concrete structures. Mater. Sci. Forum **945**, 115–119 (2018)
16. Klyuev, S.V., Khezhev, T.A., Pukharenko, Y.V., Klyuev, A.V.: To the question of fiber reinforcement of concrete. Mater. Sci. Forum **945**, 25–29 (2018)
17. Kamalova, Z.A.: Superplastifikatory in manufacturing technology of composite concrete. Herald Kazan Univ. **16**(8), 148–152 (2013)

On the Issue of Measuring the Strength of Additively Manufactured Concrete

V. S. Lesovik [ID], E. S. Glagolev [ID], M. Yu. Elistratkin[(✉)] [ID],
and D. S. Podgorniy [ID]

Belgorod State Technological University named after V.G. Shukhov,
Kostyukov Street, 46, Belgorod 308012, Russia
`mr.elistratkin@yandex.ru`

Abstract. One of the most actual issues in the development of construction printing is the development of sound methods for determining the main properties of additively obtained composites. And this applies not only to special properties, such as printability or shape stability, but also, it would seem, well-studied strength indicators. Most researchers in their works pay attention to the fact that the strength of samples obtained using molds does not correspond to the same indicator in printed structures. In this regard, this paper proposes a method for determining the strength of samples of standard sizes obtained by cutting out of a printed array. The array printing scheme assumes that each sample contains a large number of contact zones of layers, which are a weak point in the system under consideration. This approach allows considering the additively obtained composite as quasi-homogeneous, which makes it possible to simplify the calculation methods of structures and make them safer in operation. The analysis of the obtained results confirms the incorrectness of using standard methods for determining the strength indicators of additively manufactured materials when evaluating their design characteristics; the main direction for improving printing technology is the need to improve adhesion between layers; the expediency of increasing the width and thickness of tracks, which helps to reduce the number of contact zones. The proposed method is simple, accessible and does not require a special laboratory base.

Keywords: 3D additive building technology · Method for increasing strength · Test procedure · Test sample for measuring strength

1 Introduction

The characteristic features of the current stage of development of construction printing technology is the shift of researchers' focus from conceptual issues to utilitarian ones that provide technical support in the process of implementation in construction practice [1–3]. One of these issues is the normalization of key technological parameters, based on methods for measuring key properties that determine the normal course of the technological process and the quality of the final product.

Construction printing with plastic mixtures is currently most widespread and is experiencing an acute shortage of methods for measuring and normalizing the special

properties of mixtures (printability, load-bearing capacity of the molded layer, etc.) that have no direct analogues in concrete science [4–6]. However, it is more important that the definition of standard indicators, in particular strength indicators, which are responsible for the safety of additively obtained objects, also has specifics due to the peculiarities of manufacturing, the nature of work, structure, etc.

Researchers proposed a number of methods for testing the strength characteristics of concrete for 3D additive technologies. For example, in [7], to determine the strength characteristics of concrete, samples were cut out of a printed wall with a width of 60 mm-cubes with a size of 50 × 50 × 50 mm. In parallel, samples of the appropriate size were produced in standard forms. The samples were tested in three mutually perpendicular directions. In addition, using the appropriate technology, samples-beams were cut out of standard sizes 160 × 40 × 40 in two directions (vertically and horizontally along the wall). Samples of 160 × 40 × 40 were also cast in the standard way. The test of cut samples-beams was performed in the following order: vertically cut samples were tested in the direction perpendicular to the wall plane, and horizontally cut samples were tested perpendicular to the wall plane, as well as in the vertical direction. The test results showed a 12.8–21.3% reduction in the strength of printed samples during compression testing. When testing for bending, the strength decreased only for samples cut in the vertical plane, the strength reduction was 32.9–40%. For samples cut along the wall direction, a 13.1–19.5% increase in strength was observed.

In [8], molded cubic samples with a 50 mm edge and printed double-layer samples with dimensions of 20 mm in height, 40 mm in width, and 50 mm in length were also used for compression testing. Cast beams with a length of 160–200 mm and a cross section of 50 × 50 mm were also used for bending tests, as well as printed double-layer beams with a layer height of 20 mm, a width of 40 mm and a length of 160–200 mm. The compressive strength in the control samples was 48–56% higher than in the printed ones.

In [9], a similar technique was used, but the cubes were used as halves from the tested samples-beams with a size of 40 × 40 × 160 mm. Here, bending tests showed an 11% reduction in strength when applied vertically and a 5% increase in strength when applied horizontally. The compressive strength of the control sample was 33–40% higher than that of the printed samples.

In [10], cast and printed samples were also used to study the strength characteristics. The test samples were cut from printed plates of 350 × 350 × 120 mm and 500 × 350 × 120 mm in size. For the bending test, samples-beams were cut out in two directions (along and across the printing layers) with a size of 100 × 100 400 mm. Control samples were cast in standard forms. Tests for compressive strength showed the smallest decrease in strength for samples cut from 350 × 350 × 120 plates; it was 5–15%. For samples cut from a 500 × 350 × 120 plate, the strength reduction was 9–13%. The reduction in the strength of cylinders and cubes was 22–27%. Bending tests showed an increase in the strength of printed samples by 15–31% in all cases, with the exception of testing across printed layers; in this case there was a 30% decrease in strength.

Thus, the methods proposed in the literature, based on cutting out samples from a real structure, have high accuracy, but are characterized by increased labor intensity

and allow getting information only after the manufacture of a specific structure (or its model), and not at the design stage [11–13]. Printing samples with layers oriented in one direction and a limited number of contact zones allows judging the strength indicators only within the framework of the accepted method, which does not allow calculating safe cross-sections under arbitrary working conditions, which is due to their increased anisotropy.

In this regard, this paper proposes a method for correctly determining the strength indicators of printed structures from fine-grained plastic concrete mixes by extrusion.

2 Materials and Methods

2.1 Materials

Two types of CEM I 42.5 N (C1) and sulphate-resistant pozzolana CEM II/A-P 42.5 N (C2) Portland cements were used to make fine-grained concrete for construction printing. As well as two types of sand that differs in size. The modulus of sand size S1 was 1.6 (fine), and S2 - 2.5 (medium size). The ratio of cement to sand in all cases was 1:4. To make fine-grained concrete printable (extrudable), a combination of plasticizing and air-entrapping additives was used: a mixed plasticizer based on lignosulfonates and naphthalene formaldehydes + anionic foaming agent (C1/S1 compositions), which is a mixture; a plasticizer Muraplast FK 88 + an air - entrapping agent Centrament Air-202 (C2/S2 compositions).

2.2 Methods

Production of Samples. The research was carried out using a laboratory construction printer developed and manufactured at BSTU named after V.G. Shukhov, with an installed forming device for contour printing (Fig. 1 a) using the screw principle of pumping the mixture through a chamber with a diameter of 35 mm to a round nozzle with a diameter of 20 mm.
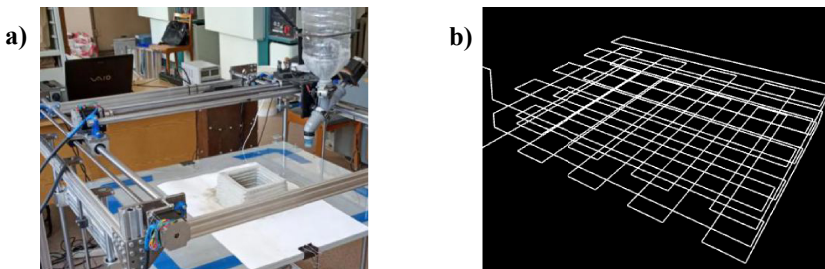

Fig. 1. Laboratory building printer for contour crafting **(a)**; Model diagram for printing **(b)**.

Determination of strength parameters of the composites for printing was carried out along two main trajectories:

Standard technology for manufacturing samples in the form of beams with dimensions of 40 × 40 × 160 mm. Two cases were considered: a) the mixture did not pass through the extruder, but immediately after making it was placed in molds; b) after making, the mixture was passed through an extruder, and then placed in molds.

Forms for obtaining samples were not used, and samples of standard sizes were made by cutting in the vertical plane of the array, printed on a laboratory construction printer.

Fig. 2. Production of printed samples for determination of strength.

When making printed samples, the array was printed on the surface of the glass plate parallel to its faces at a distance of at least 30 mm from them. A diagram of the print model is shown in Fig. 1 b. After the printing process was completed, the array was cut into a certain number of samples-beams using a ruler, square and tapping knife (Fig. 2). With this method of manufacturing samples, the cuts must be made strictly vertically; deformation, compaction and extension of the obtained samples are not allowed; the edges of the array are removed.

At the end of manufacturing, the glass plate with the samples, as well as the molded samples, were placed in a wet storage cabinet. A day later, the samples were removed from the glass plate, and the molded ones were removed from the molds and placed back in the wet storage cabinet until the test was completed.

Testing of Samples. The flexural strength was determined using the standard method, except that half of the samples for determining the printing strength were installed on the supporting elements of the device so that its faces, horizontal during manufacture, were in a vertical position-loading along the horizontal layers. The remaining samples were installed in such a way that its faces, horizontal during production, were in a horizontal position, and the marked surface (the upper face when printing) was facing up-loading across the horizontal layers. Compression tests were performed in the same way.

3   Results and Discussion

As it can be seen from Table 1, the method of manufacturing and testing samples has a significant impact on the result.

Table 1. Compositions and results of strength determination.

Method of making and testing samples	Composition	Average density, kg/m^3	Compressive strength, MPa, at the age of days				Bend, MPa
			3	7	14	28	28
1) **Printing /** loading **along** horizontal layers	S1/C1	1720	5.8	6.2	7.0	7.3	1.6
	S2/C2	1780	6.2	6.6	6.8	7.1	3.6
2) **Printing /** loading **across** horizontal layers	S1/C1	1720	5.8	6.6	6.9	7.1	2.1
	S2/C2	1780	8.2	8.8	9.0	9.3	3.5
3) **Molded** (mixture after extruder)	S1/C1	1810	14.9	18.0	19.2	19.7	3.0
	S2/C2	1880	17.9	19.2	19.6	20.1	6.7
4) **Molded**	S1/C1	1940	16.6	20.7	21.8	23.1	3.5
	S2/C2	2020	26.2	28.8	29.5	31.2	7.7

The compressive and flexural strength of the tested samples decreases in the sequence: molded → molded (mixture after the extruder) → printed.

Reduced strength of molded samples due to the passage of the mixture through the extruder (this process is actually the final stage of preparation of the mixture) the coefficient for the considered compositions is 15–35% for compression and 12–15% for bending in brand age. The main explanation for this can be a decrease in the average density of the material by an average of 6–7%, due to increased air entrainment under intense exposure to the extruder screw.

The transition to printed samples is accompanied by a more significant drop in strength indicators. In relation to those formed from the mixture passed through the extruder, the drop in compressive and flexural strength is 63 and 38% for compositions on sand S1, 59 and 47% for compositions on larger sand S2, respectively. The reasons for this situation are an even greater drop in the average density by 5–5. 5%, but the main factor is the occurrence of a large number of contact zones between the printed tracks in the sample structure. The approved scheme of printing of the array (Fig. 1 b), which assumes a layer-by-layer alternation of perpendicular tracks with a width of 20–25 mm, in each sample of the specified size ensures the presence of:

– two layers with 1–2 zones of lateral contact of tracks when they coincide with the longitudinal axis of the sample;
– two layers with 6–8 zones of lateral contact tracks perpendicular to the sample axis;
– three contact zones of layers in the horizontal plane.

This approach recreates the most complex working conditions that can be achieved with the accepted ratio of track width and standard sample size. When tested using the proposed method, an additively manufactured material can be perceived as quasi-homogeneous - contact zones are not defects with a random probability distribution or structurally weaker sections, but system elements of its structure. This can be confirmed by the low anisotropy of printed samples. Changing the direction of application of the load (along or across the horizontal layers) leads to a change in strength by only 3–15%, both in compression and bending.

4   Conclusion

The presented data do not contradict the results obtained by other researchers.

The use of standard methods for obtaining composite samples for construction printing using forms significantly overestimates the values of strength indicators of additive-manufactured structures and creates risks of accidents when using such data in structural calculations. The proposed method for determining the strength of additive composites obtained from printed samples cut from the array is characterized by comparative technical simplicity and accessibility.

The method simulates one of the most difficult cases - the presence of a large number of multidirectionally oriented contact zones of printed tracks in the sample. This makes it possible to represent an additively manufactured composite as a quasi-homogeneous object, the strength indicators of which do not depend much on the direction of application of loads. The use of such strength indicators in structural calculations will help to improve safety and simplify them, allowing calculating a multi-layer additive composite as a traditional isotropic concrete. This aspect is of the greatest importance when calculating the structural zones of printed structures that have the largest effective cross-section and perceive increased operational loads.

The strength of the contact zones in the studied system is a weak point that reduces the role of the potential strength of the solution in the formation of the strength of the additive structure as a whole. When developing and improving compositions for construction printing, attention should be paid to improving the adhesion between layers. When improving the design of forming devices, measures should be taken to counteract the decrease in the density of the mixture, but the main attention should also be focused on the implementation of technological methods for increasing the adhesion between layers.

When printing large objects, they should strive to increase the width and thickness of the tracks, which helps to reduce the number of contact zones per volume unit of the structure.

A limitation of the proposed method is the use of composites containing fiber. Cutting such arrays in the proposed way is difficult.

References

1. Vatin, N., Chumadova, L., Goncharov, I., Zykova, V., Karpenya, A., Kim, A., Finashenkov, E.: 3D printing in construction. Construction of Unique Buildings and Structures **1**(52), 27–46 (2017)

2. Klyuev, S.V., Klyuev, A.V., Shorstova, E.S.: Fiber concrete for 3-D additive technologies. Mater. Sci. Forum **974**, 367–372 (2019)

3. Demidenko, A.K., Kulibaba, A.V., Ivanov, M.F.: Prospects of 3D-printing in the building complex of the Russian Federation. Const. Unique Build. Struct. **12**(63), 71–96 (2017)

4. Elistratkin, M., Kozhukhova, M.I., Pospelova, M.A., Semernin, E.O.: Regards study of feature consolidation of building structures produced by additive technologies. Add. Fabric. Technol. **1**(1), 5–13 (2019)

5. Lesovik, V.S., Elistratkin, M.Y., Alfimova, N.I., Shurakov, I.M.: On the question of mix composition selection for construction 3D printing. Mater. Sci. Forum **945**, 218–225 (2018)

6. Inozemtcev, A.S., Korolev, E.V., Qui, D.T.: Analysis of existing technological solutions of 3D-printing in construction. Vestnik MGSU. **13, 7**(118), 863–876 (2018)

7. Rahul, A.V., Santhanam, M., Meena, H., Ghani, Z.: Mechanical characterization of 3D printable concrete. Constr. Build. Mater. **227**, 116710 (2019)

8. Alchaar, A.S., Al-Tamimi, A.K.: Mechanical properties of 3D printed concrete in hot temperatures. Constr. Build. Mater. **266**, 120991 (2021)

9. Marchment, T., Sanjayan, J.: Bond properties of reinforcing bar penetrations in 3D concrete printing. Autom. Const. 120 (2020)

10. Le, T.T., Austin, S.A., Lim, S., Buswell, R.A., Law, R., Gibb, A.G.F., Thorpe, T.: Hardened properties of high-performance printing concrete. Cem. Concr. Res. **42**(3), 558–566 (2012)

11. Lesovik, R.V., Klyuev, S.V., Klyuev, A.V., Tolbatov, A.A., Durachenko, A.V.: The development of textile fine-grained fiber concrete using technogenic raw materials. Res. J. Appl. Sci. **10**(10), 696–701 (2015)

12. Klyuyev, S.V., Klyuev, A.V., Lesovik, R.V., Netrebenko, A.V.: High strength fiber concrete for industrial and civil engineering. World Appl. Sci. J. **24**(10), 1280–1285 (2013)

13. Lesovik, R.V., Klyuyev, S.V., Klyuev, A.V., Netrebenko, A.V., Yerofeyev, V.T., Durachenko, A.V.: Fine-grain concrete reinforced by polypropylene fiber. Res. J. Appl. Sci. **10**(10), 624–628 (2018)

Assessment of the Resource of Water Protection Properties of Coatings Cement Concrete External Wall Buildings

V. I. Loganina(✉)

Penza State University of Architecture and Construction, Street Titova 28,
440028 Penza, Russia
loganin@mail.ru

Abstract. The information on the resource of water-protective properties of cement concrete coatings is given. A methodological approach is proposed for assessing the resource of water-protective properties of coatings, which consists in assessing the time to reach the maximum permissible moisture content in the contact plane "coating-concrete of the enclosing structure". It is revealed that the resource of water-protective properties depends on the initial moisture content of the structure. Bulk hydrophobization of coatings contributes to an increase in the resource of water-protective properties. The influence of the substrate porosity on the service life of the waterproofing properties of coatings is considered. It is shown that with an increase in the surface porosity of the substrate, a decrease in the time of moisture penetration through the coating is observed. The data on the influence of substrate moisture on the resource of waterproof properties and durability of protective and decorative coatings are given.

Keywords: Coatings · Resource of waterproof properties · Moisture content of the enclosing structure · Porosity of the substrate

1 Introduction

Currently, when assessing the water-protective properties of cement concrete coatings of external walls of buildings, water absorption indicators of painted samples are used as a criterion, water resistance etc. [1–3]. However, these indicators do not determine the resource of the protective properties of coatings when exposed to moisture. The resource of waterproofing properties of coatings can be estimated by the time when the moisture concentration in the protected material reaches its critical value. For outdoor enclosing structures, the resource of water-protective properties of coatings will be determined by the time it takes to reach the maximum permissible moisture content in the "coating-concrete enclosing structure" contact plane, which is determined by the maximum sorption moisture content of concrete at a relative humidity of 100% [4–6].

Moisture entering the "coating-substrate" contact area contributes to the destruction of the finishing layer [7–12]. The peculiarity of the destruction of coatings is also in the increasing role of mass transfer processes in the "coating-substrate" contact zone.

The resource of waterproof properties is a function of many factors (the type of fence material, its initial moisture content, temperature and humidity conditions of operation, etc.). In this regard, it is of interest to determine the resource of water-protective properties of coatings depending on the type of coating, initial moisture content and porosity of the substrate.

2   Materials and Methods

The moisture diffusion coefficient was determined by the gravimetric method. For this, the sample was placed in water and the integral moisture content was determined periodically. The moisture content was determined at exposure times, one of which is twice the other. The formula is applicable for t2 > 2t1 and the Fourier criterion F > 0.2.

To determine the coefficient of moisture diffusion through coatings on a porous substrate, the method of measuring the time of moisture passage through the coating was used. In the process of humidification, the swelling of the coating is characterized by the dependence

$$\frac{M_t}{M_\infty} = \frac{2}{l}[d\tau/\pi]^{1/2} \tag{1}$$

where M is the equilibrium degree of swelling, %;
L -Semi-thickness of the coating, cm;
τ- Swelling time, s.

In coordinates $M - \sqrt{\tau}$, this dependence is depicted by a straight line. This equation is valid until moisture penetrates the substrate. Observing the straight-line relationship M-f (T)

$$D = \frac{\pi l^2}{16\tau} \tag{2}$$

where l is the thickness of the coating, cm;
τ- time of moisture penetration, s;
D- diffusion coefficient, cm^2/s

To estimate the time of moisture penetration through the coating, an express method was applied. An indicator—potassium permanganate—was applied to one of the sides of the sample, opposite to the colored one. The time of penetration of moisture through the colored sample was estimated by the time of the change in the color of the indicator and was determined by the formula

$$\tau_1 = \tau_2 - \tau_3 \tag{3}$$

where τ_3 is the time of moisture penetration through the control sample (uncolored);

τ_2 - time of moisture penetration through the painted sample;

τ_1 - time of moisture penetration through the coating.

Polyvinyl acetate PVAC, organosilicon KO-168, perchlorovinyl HV-161, water-dispersion VA-17 paints were used as paint compositions.

3   Research Results

Let us consider, as an example, the calculation of the moisture regime of a wall under nonstationary conditions of water vapour diffusion. The wall is made of expanded clay concrete with a density of 1000 kg/m^3. The relative humidity on the outside of the wall is 100%, on the inside - 60%. Let us assume that the temperature distribution in the fence is constant over time. Wall thickness 30 cm. Initial moisture content of expanded clay concrete 3 and 1.5% (as compared options). Moisture content equal to 8% was taken as the critical moisture content, which corresponds, according to the experimental data, to the maximum sorption moisture. In Fig. 1 experimental and calculated data on the kinetics of water saturation in the coating-substrate contact zone are presented.

Analysis of the experimental data shows that the resource of water-protective properties depends on the initial moisture content of the construction material. So, with an initial moisture content of expanded clay concrete of 3%, the resource of water-protective properties of PVAC coating is 27170 h, and with a moisture content of 1.5% - 24 000 h.
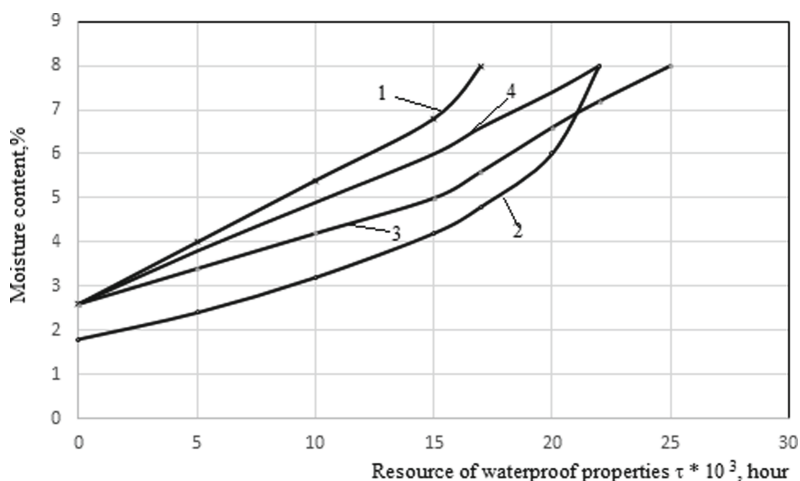

Fig. 1. Kinetics of water saturation in the "coating-to-substrate" contact zone: 1- moisture content of expanded clay concrete 35%, PVAC coating; 2- moisture content of expanded clay concrete 1.55%, PVAC coating; 3- moisture content of expanded clay concrete 3%, KO-168 coating; 4- moisture content of expanded clay concrete 3%, covered with PVAC with volumetric hydrophobization.

Volumetric hydrophobization of PVAC coating with liquid 136–41 in an amount of 0.2% of the mass of cement in the paint helps to increase the resource of waterproof properties up to 22 000 h. The more porous structure of the concrete surface contributes to the formation of a more permeable structure of the coating with a diffusion coefficient D equal to $4.04 * 10^{-7}$ cm²/s, and a resource of water-protective properties equal to 15000 h. The resource of water-protective properties of the organosilicon coating KO-168 was 25 000 h (Fig. 2).
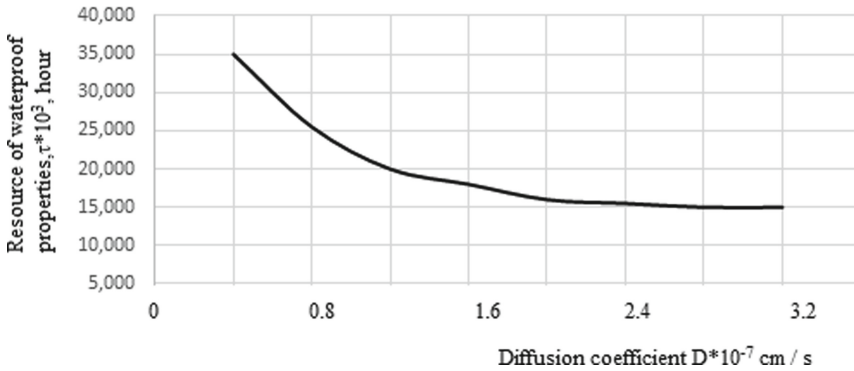

Fig. 2. Dependence of the resource of water-protective properties on the moisture diffusion coefficient.

The analysis of experimental data shows that the dependence of the resource of water-protective properties on the coefficient of moisture diffusion can be expressed by an equation of the form

$$\tau = \tau_0 \exp(-\propto D) \tag{4}$$

where D is the moisture diffusion coefficient;
τ_0, $\propto$, are constants.
$\tau = \tau_0$ at D = 0, i.e. when using an absolutely impervious coating.

The peculiarity of the destruction of cement concrete coatings is also in the increasing role of mass transfer processes in the "coating-substrate" contact zone. Calculations were made of the amount of adsorbed moisture in the contact zone for polyvinyl acetate coatings depending on the surface porosity of the substrate. The maximum moisture content at the boundary "PVAC coating-substrate" is characteristic of a substrate with a high surface porosity Pp-1.13%. After 4 h of moistening, Qt/Q for a substrate with Pp = 1.13% is 0.73, and on the substrate with P_P = 0% -0.17.

Table 1. Influence of the surface porosity of the substrate on the rate of moisture diffusion.

Type of substrate and coating	Surface porosity,%	Moisture penetration time, min		Diffusion coefficient $D * 10^7$ cm^2/s
		Across sample	Across coating	
Mortar The same, colored:	0	49	–	–
PVAC paint		131	88	2.02
Paint XB-161		201	152	1.16
Paint VA-17		121	72	3.85
The same, colored:	0.4	42	–	–
PVAC paint		107	65	2.7
Paint XB-161		180	138	1.28
Paint VA-17		101	59	4.7
The same, colored:	1.13	39	–	–
PVAC paint		83	44	4.04
Paint XB-161		142	103	1.72
Paint VA-17		75	36	7.71

The research results given in Table 1 indicate that with an increase in the surface porosity of the substrate, a decrease in the time of moisture penetration through the coating is observed, i.e. the rate of diffusion of moisture increases. Thus, the minimum time for moisture penetration through the coating is typical for mortar substrates with surface porosity Pp = 1.13%. For PVAC coating, it is 44 min, perchlorovinyl - 103 min, water dispersion - 36 min.

Moisture flow to the "coating-substrate" interfacein PVAC coatings on a substrate with a porosity of P_P begins after 2 h, and on a substrate with $P_P = 0\%$ - after 3 h (Fig. 3). At low ambient temperatures during the heating season, the role of mass transfer processes in the aging process of coatings increases, because at the same time, there is a migration of moisture (technological, sorption) from the material of the enclosing structure to the zone with a low temperature. With a low permeability of the coating in the "coating-substrate" contact zone, moisture can accumulate, which leads to the appearance of bubbles on the surface, and when moisture freezes, it can cause racking and flaking.

When introduced into PVAC, the color compositions of the liquid 136–41 increase the resistance of the coatings (Table 2). After 100 test cycles, the decrease in the adhesion strength of the coatings is 8%, while in the control it is 16%. Subsequent hydrophobization of the painted surface with 5% liquid solution 136–41 or 3% aqueous solution GKZH-11 also increases the resistance of the coatings: after 100 test cycles, the decrease in adhesive strength is 10%.

Fig. 3. Kinetics of moisture accumulation at the "coating-substrate" interface depending on the surface porosity of the substrate: 1-substrate with porosity Pp = 0%; 2 - substrate with porosity Pp = 0.4%; 3 - substrate with porosity Pp = 1.13%.

Table 2. Influence of hydrophobization on service life protective and decorative coating PVAC.

Tre atment type	Coating adhesion strength, MPa	
	Before testing	After 100 test cycles
Control PVAC	2.34	1.96
PVAC followed by hydrophobization with 5% solution 136–41	2.3	2.1
PVAC painting with GKZh-11 additive	2.4*	2.3
Painting with PVAC composition, then hydrophobization of the painted surface with a 3% solution of GKZH-11	2.3	2.05

Note. * The separation of the washer occurs in the mortar

4   Conclusion

The proposed methodological approach to assessing the water-protective properties of the coating will make it possible to more effectively select one or another paint composition, depending on the actual operation of the layered coating-enclosing structure under the given climatic conditions.

References

1. Hsu, Y.-T., Wang, W.-H., Hung, W.-H.: Architectural sustainability and efficiency of enhanced waterproof coating from utilization of waterborne poly (Siloxane-Imide-Urethane) copolymers on roof surfaces. Sustainability **12**(11), 4411 (2020)

 2. Dimmig-Osburg, A., Pietich, I., Pakusch, J.: Polymer additives and their influence on the cement microstructure in the early stages of hardening. ZKG Int. **59**(5), 72–83 (2006)
 3. Wetzel, A., Herwegh, M., Zurbriggen, R., Winnefeld, F.: Influence of shrinkage and water transport mechanisms on microstructure and crack formation of tile adhesive mortars. Cem. Concr. Res. **42**(1), 39–50 (2012)
 4. Efimov, B., Rubtsov, O., Bessonov, I., Medvedev, A.: Construction and insulation of agricultural buildings and structures. In: E3S Web of Conferences «Topical Problems of Green Architecture, Civil and Environmental Engineering» vol. 164, p. 020302019 (2020)
 5. Jenni, A., Holzer, L., Zurbriggen, R., Herwegh, M.: Influence of polymers on microstructure and adhesive strength of cementitious tile adhesive mortars. Cem. Concr. Res. **35**(1), 35–50 (2005)
 6. Wen, F., Wang, L., Huang, J.Z.: Polymer cement waterproof coating and its properties. Adv. Mater. Res. **189–193**, 252–255 (2011)
 7. Loganina, V.I.: The estimation of reliability of protective - decorative coverings. Contemp. Eng. Sci. **8**(1–4), 91–95 (2015)
 8. Loganina, V.I., Uchaeva, T.V., Monastyrev, P.V.: The method to estimate the surface appearance quality of the paint applied to the cement. J. Eng. Appl. Sci. **11**(11), 2409–2410 (2016)
 9. Loganina, V.I.: The influence of surface quality of coatings on their deformation properties. Contemp. Eng. Sci. **7**(33–36), 1935–1941 (2014)
10. Francke, B., Piekarczuk, A.: Experimental investigation of adhesion failure between waterproof coatings and terrace tiles under usage loads. Buildings **10**(3), 59 (2020)
11. Maranhão, F.L., John, V.M.: Bond strength and transversal deformation aging on cement-polymer adhesive mortar. Constr. Build. Mater. **23**(2), 1022–1027 (2009)
12. Loganina, V., Fediuk, R., Usanova, K., Timokhin, R.: Regularities of change in the properties of paint coatings on cement concretes at moistening. Lect. Not. Civ. Eng. **70**, 1–4 (2020)

Molding Properties of Alkali Silicate Compositions

O. A. Miryuk[(✉)] [iD]

Rudny Industrial Institute, Rudny, Kostanay Region, Kazakhstan
psm58@mail.ru

Abstract. The results of research on compositions based on sodium liquid glass and fillers of mineral and organic origin are presented. Materials that can affect the molding properties and thermal transformations of compositions are used as fillers. It was found that the molding properties of the compositions depend on the mineral composition and content of the filler. It is shown that the greatest increase in the viscosity of the compositions is provided by fine mineral fillers, which limit the influence of free and adsorptive water in the composition of liquid glass. The influence of the dispersion of fillers on the rheological properties of compositions is determined. It was found that an increase in the specific surface area of fillers from 350 to 550 m^2/kg can increase the structural strength of molding mixtures by 10–30%. To improve the molding properties of compositions characterized by high porosity, it is proposed to use combined fillers: glass boilerplate and organic filler; broken glass and mineral filler containing a pore-forming component (oil shale, gaize, lignite-bauxite, and refuse ore). The expediency of using fillers with a porous structure is shown. Studies of porous compositions have confirmed the advantages of using combined fillers. It is noted that the use of combined fillers contributes to the porization of liquid-glass compositions at low temperatures.

Keywords: Fillers · Liquid glass · Molding properties · Swelling · Porous structure

1 Introduction

The development of efficient light concrete technology depends on the quality of porous aggregates. Relevant research is aimed at reducing the density and increasing the strength of aggregates, reducing the energy intensity of production [1–10]. On the basis of liquid glass, cellular concretes and granulated materials of various sizes and purposes are obtained. The porization of liquid-glass compositions is carried out mainly by swelling [4, 7, 10]. For the development of effective heat-insulating liquid-glass materials, the choice of fillers is important, aimed at optimizing the technological state of the compositions.

The aim of this work is to study the influence of fillers on the molding properties of compositions based on liquid glass.

2 Materials and Methods

Sodium liquid glass with a density of 1400 kg/m^3 was used to produce the compositions. The compositions realize the multifunctionality of liquid glass: binding of the filler during the formation of the raw material, reducing the temperature of the pyroplastic state of the mass, and pore formation.

Fillers of various origins were inserted into the compositions. The broken glass – ground container and sheet silicate glass. Gaize is an overburden siliceous microporous rock, consisting mainly of amorphous silica. Oil shale is a rock that is simultaneously extracted during the development of coal deposits and contains kaolinite, hydromica, feldspar, calcite, and quartz. Lignite-bauxite is an alumina rock for the production of aluminum, represented by aluminum hydroxides and enriched with fine carbonized wood residues. Skarn-black iron ore processing wastes are formed during magnetic separation of the rock mass and include calcium silicates, aluminosilicates, pyrite, and calcite. Sawdust and wheat husks were added to the composition as fillers of plant origin. Porous fillers of compositions: ash microsphere – loose waste from fuel combustion, consisting of hollow spherical particles with a diameter of 100–350 microns; crushed gas silicate with a particle size of 0.5–1.25 mm, obtained by grinding process waste from cellular concrete production.

Mineral fillers were crushed in a high-speed Emax mill. The specific surface of the powders was measured using a FSH–6K photosedimentometer. Liquid-glass compositions were prepared by thoroughly mixing the components. The structural strength of the compositions was determined on a conical plastometer. Taking into account the structural strength indicators, a method for manufacturing samples was assigned. The dried samples were fired in a laboratory oven at a set temperature with an exposure time of 15 min. Structural transformations of materials were evaluated by density and swelling coefficient (the ratio of sample diameters before and after roasting).

3 Results and Discussion

The influence of fillers on the molding properties of liquid-glass compositions was studied, which were compared by changes in structural strength (Fig. 1). The state of the composition with 70% glass content and structure strength of 0.2 MPa (100%) was taken as the standard.

With a content of 65–75% of the filler, liquid-glass compositions acquire the required molding properties. The state of the raw material mass depends on the dispersion of the filler (Table 1). An increase in the specific surface area by 100–200 m^2/kg is comparable to an increase in the filler content by 5–12%. With the same content of fillers having equal dispersion, the influence of the mineral composition of the solid component is obvious. The greatest increase in the viscosity of the compositions is provided by gaize rock, oil shale and lignite-bauxite, which reduce the influence of adsorption water in liquid glass.
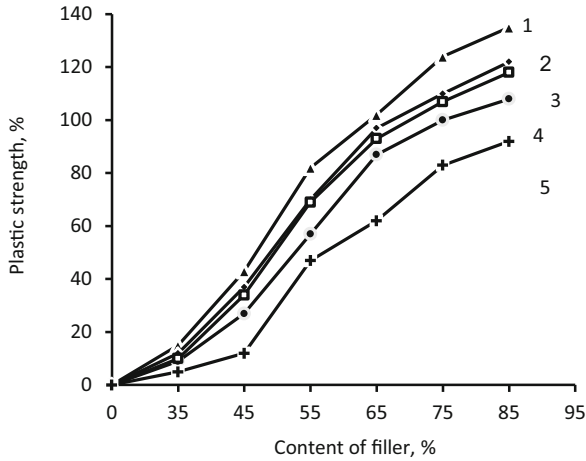
Fig. 1. Dependence of the plastic strength of liquid-glass compositions on the filler content: 1– gaize rock; 2 – oil shale; 3 – lignite-bauxite; 4 – broken glass; 5 – refuse ore.

Table 1. Impact of the specific surface area of the filler on the plastic strength of liquid-glass compositions.

Filler	Content of filler, %	Plastic strength, %, at specific surface area, m²/kg		
		350	450	550
Gaize rock	45	43	48	57
	75	124	131	140
Oil shale	45	37	42	51
	75	110	117	129
Lignite-bauxite	45	34	38	46
	75	107	110	123
Broken glass	45	27	33	41
	75	100	108	118
Refuse ore	45	12	21	38
	75	83	90	110

At a roasting temperature of 650 °C in the presence of 35–45% of fillers, the structure of the swelling samples is stable (Fig. 2). Different intensity of the swelling of such compositions is due to the chemical and mineral characteristics of the fillers. The highest coefficient of swelling is provided by fillers that exhibit thermal activity with the release of a gas phase (refuse ore, gaize) or a gel-forming effect (broken glass).
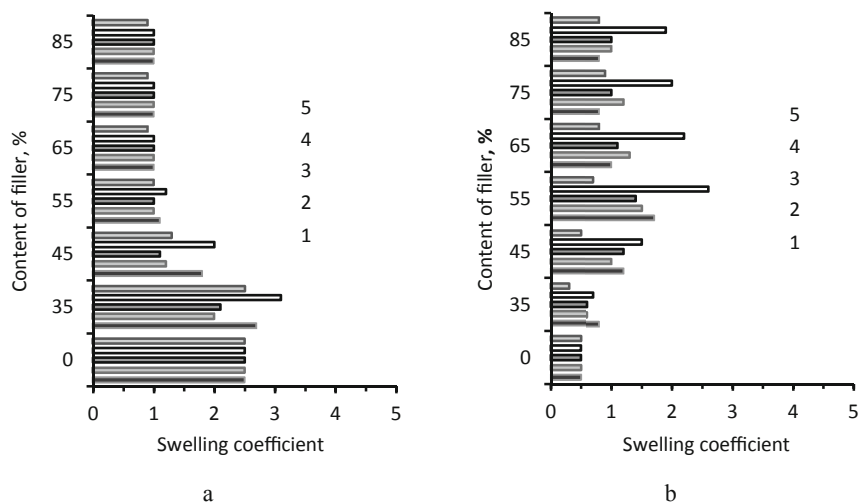
Fig. 2. Impact of the content of fillers on the swelling of liquid-glass compositions at various temperatures, °C: a – 650; b – 850; 1 – gaize rock; 2 – oil shale; 3 – lignite-bauxite; 4 – broken glass; 5 – refuse ore.

Samples containing 0 and 35% of the filler, roasted at a temperature of 850 °C, fused with shrinkage. For compositions with filler content of 45% or higher, the influence of the type and amount of filler increases (Fig. 2). Structural changes in samples with high filler content, burned at 850 °C, are due to the properties of the solid part of the compositions. At elevated temperatures, the reactivity increases, and the composition of the fired composition changes.

Liquid-glass compositions with a limited content of filler are characterized by the greatest pore forming ability. However, the molding properties of such masses are unsatisfactory (Fig. 1). To increase the viscosity of compositions with a high content of liquid glass, salt modifiers are used [3], which sharply reduce the plasticity of the composition.

To regulate the molding properties of the raw material mass, the effect of additives of plant origin was studied (Table 2). Organic fillers with a particle size of 0.1–0.3 mm were added to liquid-glass compositions based on broken glass. This contributed to a decrease in the plasticity of the raw material mass. The rational content of the vegetable additive of 5–7% allows maintaining high porosity of the composition.

The possibility of improving the properties of molding masses while maintaining the pore forming ability of liquid-glass compositions due to combined fillers is investigated. The expediency of combining broken glass that provides a high degree of swelling with materials that increase the viscosity of molding mixtures and contribute to additional porization of the composition, for example, oil shale is shown (Table 3).
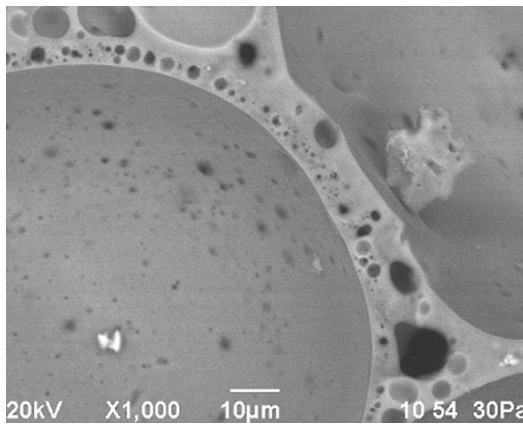
Compositions containing 45–55% of the combined filler have improved molding properties and are characterized by increased porosity. The structure of materials is characterized by thin-walled cells, the smallest cavities in the partitions between the pores (Fig. 3).

Table 2. Impact of the content of organic fillers on the plastic strength of the molding mass and the density of porous compositions.

Filler	Content of filler, %	Plastic strength, MPa	Density of porous compositions, kg/m^3
No	0	0.005	309
Sawdust	5	0.025	305
	7	0.038	350
	9	0.043	410
Wheat husk	5	0.031	300
	7	0.041	303
	9	0.052	365

Table 3. Impact of the content of fillers on the pore size and density of compositions.

Content of filler, %		Pore diameter, mm	Density, kg/m^3
broken glass	oil shale		
100	0	0.1	310
85	15	0.2	265
70	30	0.3	240
55	45	0.5	320

Fig. 3. Microstructure of a porous composition with combined filler.

Studies of compositions containing porous fillers revealed the possibility of regulating the molding properties and swelling by changing the ratio of "ash microsphere: crushed gas silicate". Compositions containing 45–50% of a porous filler with a predominance of ash microspheres are preferred (Fig. 4).
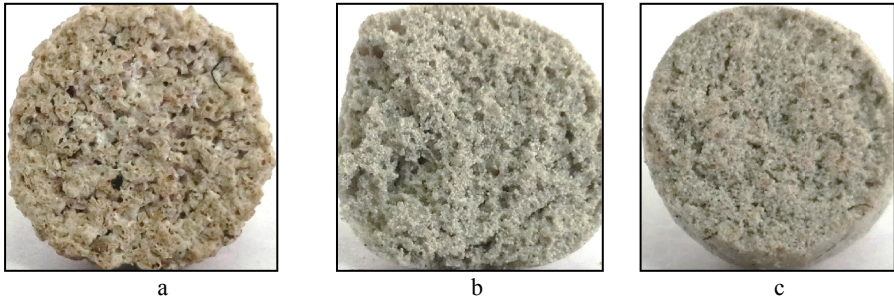
Fig. 4. Structure of compositions with porous fillers: a – crushed gas silicate; b – ash microsphere; c – crushed gas silicate and ash microsphere.

The combination of fillers ensures the implementation of various porization methods in the area of low temperatures, and helps to increase the thermal protection properties of compositions based on liquid glass.

4   Conclusion

The type of filler determines the state of the molding mass and the intensity of the processes of thermal porization of liquid-glass compositions. The expediency of using combined fillers made up of materials that directly affect the technological properties of compositions is shown. Compositions containing mineral, organic and porous fillers that provide the required molding properties of the raw material mass and increase the porosity of the roasted material are proposed.

References

1. Wang, W.C., Chen, B.T., Wang, H.Y., Chou, H.C.: A study of the engineering properties of alkali-activated waste glass material (AAWGM). Constr. Build. Mater. **1**(112), 962–969 (2016)
2. Rafael, A.R., Rivera, J.F., Gutiérrez, R.M.: Alkali-activated building materials made with recycled construction and demolition wastes. Constr. Build. Mater. **15**(149), 130–138 (2017)
3. Mizuriaev, S.A., Zhigulina, A., Solopova, G.S.: Production technology of waterproof porous aggregates based on alkali silicate and non-bloating clay for concrete of general usage. Procedia Eng. **111**, 540–544 (2015)
4. Redden, R., Neithalath, N.: Microstructure, strength, and moisture stability of alkali activated glass powder-based binders. Cement Concr. Compos. **1**(45), 46–56 (2014)
5. Radayev, S., Seleznyova, O., Ilyukhin, K., Ivanov, K., Forosevich, N.: The problem of structurization of liquid glass. Mater. Sci. Forum **871**, 90–95 (2016)

6. Yang, K.H., Lee, K.H., Song, J.K., Gong, M.H.: Properties and sustainability of alkali-activated slag foamed concrete. J. Clean. Prod. **1**(68), 226–233 (2014)
7. Miruk, O.: Development of cellular structure composites for energy efficient construction. Energy Procedia **9**(128), 469–476 (2017)
8. Kim, G.B., Jang, I.Y., Kim, S.K., Lee, K.W.: A properties of concrete using LCD waste glass subjected to sulfate attack. Key Eng. Mater. **7**(773), 233–237 (2018)
9. Jiang, X.J., Yun, Y., Hu, Z.H.: Development of non-autoclaved aerated concrete by alkali activated phosphorus slag. Adv. Mater. Res. **5**(250–253), 1147–1152 (2011)
10. Rakhimova, N.R., Rakhimov, R.Z.: Alkali-activated cements and mortars based on blast furnace slag and red clay brick waste. Mater. Des. **15**(85), 324–331 (2015)

Sulfoaluminate Cement and Low-Temperature Roasting Additive from Low Aluminate Raw Materials with a High Content of Silicon Oxide

T. Ye. Goloviznina$^{(\boxtimes)}$, V. M. Konovalov , and I. A. Morozova

Belgorod State Technological University named after V.G. Shukhov,
Belgorod, Russia
`t.goloviznina@mail.ru`

Abstract. The preparation of sulfoaluminate clinkers from low-aluminate natural and technogenic raw materials that are substandard for the production of aluminate cement due to the high content of silicon oxide is considered. Raw mixtures for the synthesis of sulfoaluminate clinkers of the most approximate chemical composition from natural raw materials and from technogenic products are calculated. The technological properties, phase compositions of clinkers obtained by sintering, and hydraulic properties of sulfoaluminate clinkers and compositions with their application are compared. The presence of a sulfate component avoids the formation of clinkers in the hydraulically inert gehlenite. The presence of alkaline and other impurity compounds in the used technogenic waste reduces the synthesis temperature of sulfoaluminate clinkers by 130 degrees; changes the phase composition and properties of cement; shifts the effect of sulfation from the aluminate phase to the silicate phase. In clinkers, mainly calcium sulfoaluminate is formed from natural raw materials, and calcium sulfosilicate is formed from technogenic products. It is established that cement stone made of clinker based on natural raw materials has high strength, including in the early stages of hardening. From the considered technogenic waste, it is possible to obtain a sulfoaluminate additive of low-temperature roasting, which increases the strength characteristics of the stone from the binding composition in the early stages of hardening.

Keywords: Sulfoaluminate clinker · Technogenic waste · Melting point · Sintering temperature · Phase composition · Strength

1 Introduction

Construction materials synthesized in the $CaO-Al_2O_3$ system have unique properties. The most popular construction and technical features of such cements are fast hardening, high strength and increased corrosion and heat resistance of products and structures made of binding compositions. A limitation for the synthesis of aluminate cement is the lack of purity of natural and technogenic raw materials. The raw materials available to manufacturers contain additional components. The most undesirable part of the raw material for aluminate cements is silicon oxide, which binds aluminum oxide to a hydraulically inert gehlenite during high-temperature synthesis until complete

saturation. Limiting the silica content in raw materials to 8% makes the production of aluminate cements expensive and uncommon.

An alternative to aluminate cements can be sulfoaluminate cements synthesized in the $CaO-Al_2O_3-SiO_2-SO_3$ system. Sulfated binders mainly retain the unique properties that are in demand [1–5]. The presence of silicon oxide in the presence of SO_3 is no longer an obstacle to the formation of hydraulically active clinker phases, as the order and priority of high-temperature synthesis reactions change [3–5].

Production of aluminate cements is based on the use of high-aluminum and low-silicate raw materials – bauxite, which are included in the list of the main types of strategic raw materials in Russia. This significantly increases the cost and limits industrial production.

Cement production is a unique high-temperature technological process in which the disposal of household and technogenic industrial waste can be carried out using waste as alternative fuels, raw materials and additives [6–10].

The paper proposes the production of sulfoaluminate clinkers from low-aluminate, high-silicate natural raw materials and technogenic waste – TPP ash and phosphogypsum.

2 Materials and Methods

For the production of sulfoaluminate cements, raw materials containing calcium oxide, aluminum oxide and sulfates are required. Limestone is used as a calcium-containing component. Aluminate-containing raw materials: natural, but atypical for the production of aluminate cements due to the high content of silicon oxide – kaolin and technogenic waste – TPP ash. Sulphate-containing: natural gypsum stone and waste from the production of mineral fertilizers - phosphogypsum. The chemical composition of the used materials is shown in Table 1.

Table 1. Chemical composition of raw materials, wt. %.

	SiO_2	Al_2O_3	Fe_2O_3	CaO	MgO	Na_2O	SO_3	p.o.i.
Limestone	2.21	0.45	0.20	54.04	0.25	0.11	0.08	42.48
Kaolin	63.98	24.68	0.60	0.00	0.00	0.00	0.08	10.20
TPP ash	45.91	25.79	7.98	12.10	4.80	2.09	0.93	0.40
Gypsum stone	0.49	0.02	0.03	32.75	0.47	0.00	46.58	19.52
Phosphogypsum	0.64	0.23	0.50	37.22	0.00	0.40	47.58	9.89

The calculation of raw mixtures for the synthesis of sulfoaluminate clinkers (SAC) was carried out according to two specified characteristics: the saturation coefficient (SC) to bicalcium silicate and the degree of saturation (DS) of aluminum and silicon with sulfate [3, 4]:

$$DS = \frac{SO_3 - 0.26Al_2O_3 - 0.116Fe_2O_3}{0.667SiO_2}, \tag{1}$$

$$SC = \frac{CaO - 0.55Al_2O_3 - 1.05Fe_2O_3 - 0.7SO_3}{1.867SiO_2}. \tag{2}$$

The values of the calculated characteristics of the two raw mixtures are as close as possible, as far as the chemical composition of the raw materials allows.

Clinker synthesis was carried out by heating compressed briquettes from raw mixtures from room temperature to the temperature of isothermal exposure - 30° below the melting point. The phase composition of the firing products was determined by x-ray phase analysis. The hydraulic properties of the synthesized materials and compositions are determined by the compressive strength of small hardened samples made of cement paste with a water-cement ratio of 0.25.

3   Results and Discussion

Material compositions of raw mixtures - № 1 from natural raw materials (limestone, kaolin, gypsum stone); № 2 – using technogenic products (limestone, TPP ash, phosphogypsum) and the specified design characteristics are shown in Table 2.

Table 2. Material composition, wt. %, and design characteristics of raw mixtures for sulfoaluminate clinkers.

Material	Mixture № 1 Natural components	Mixture № 2 Technogenic components
Limestone	48.08	50.74
Gypsum	24.60	–
Phosphogypsum	–	27.57
Kaolin	21.70	–
TPP ash	–	27.32
Design characteristics		
SC	0.85	0.9
DS	1.15	1.15

By heating compressed briquettes from raw mixtures before melting, it is established that the melting temperature of the mixture № 1 is 1400 °C, and № 2 – 1270 °C.

Traditional equipment of cement industry enterprises allows producing clinkers by sintering. For the synthesis of sulfoaluminate clinkers, temperatures of 30° below the established melting temperatures, 1370 and 1240 °C, respectively, are accepted. During the roasting process, the clinkers did not melt; the roasted briquettes retained their original shape, decreased, and compacted. There was a sintering process without the formation of a significant amount of melt. The content of free calcium oxide in the

sinters of both compositions did not exceed 1%. Therefore, the synthesis of phases of aluminate clinkers by sintering can be considered complete.

According to x-ray phase analysis (Fig. 1), the main phases of sulfoaluminate clinker from natural materials are: calcium sulfoaluminate, bicalcium silicate, and calcium sulfate.
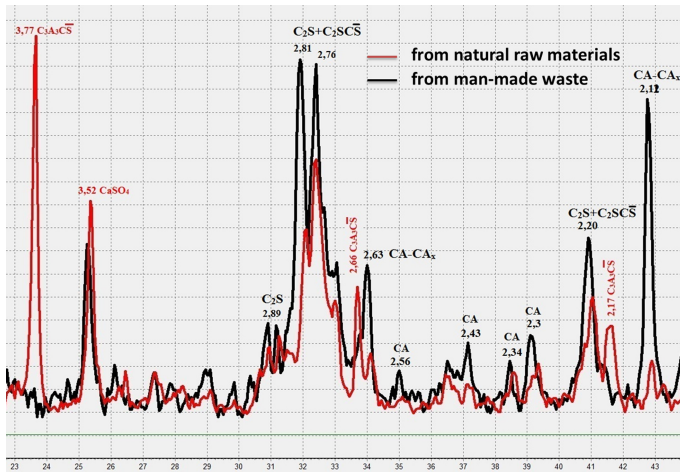

Fig. 1. Fragment of a comparative diffractogram of sulfoaluminate clinkers.

In the sulfoaluminate clinker synthesized from technogenic products, the following were identified: single-calcium aluminate and its solid solutions CA-CAx, where x is from 1 to 2; two-calcium silicate, sulfobicalcium silicate, and calcium sulfate.

According to x-ray phase analysis, when roasting a mixture of natural raw materials, the mainly aluminate phase was sulfated to form $C_3A_3C\bar{S}$. The result of roasting a raw mixture of technogenic products is the formation of bicalcium silicate sulfate– $C_2SC\bar{S}$. The diffraction maxima belonging to calcium sulfoaluminate are much less expressed in the waste clinker than in the clinker from natural raw materials. The diffraction maxima of monocalcium aluminate and calcium sulfosilicate are more intense in the waste sinter diffraction pattern (Fig. 1) The reason for the difference in melting temperatures and phase composition of sulfoaluminate clinkers is probably the presence of alkalis in the used technogenic products. Alkaline impurities intensify the synthesis reaction and reduce the formation temperature of calcium orthosilicate.

The hydraulic properties of the resulting sulfoaluminate clinkers were studied individually and as additives to Portland cement of the CEM I 42.5 N brand (Table 3).

Significant differences in the phase compositions of SAC led to a significant difference in the composition of hydration products and, accordingly, hydraulic properties.

Samples from clinker synthesized from natural raw materials – SAC № 1, actively harden with increasing strength. Samples from SAC № 2 expand to destruction by 28 days of hydration hardening.

Both synthesized clinkers in an amount of 10% were added to the Portland cement. The use of sulfoaluminate cements as an additive makes it possible to accelerate the strength gain of cement stone in the early stages of hardening up to 44% (Table 3).

Table 3. Hydraulic properties of SAC and compositions.

Binding agent	Limit of compressive strength, MPa hardening time, days		
	3	*7*	*28*
SAC № 1	66	75	101
SAC № 2	59	13	Expansion to destruction
CEM I 42.5 N+10% SAC № 1	65	74	94
CEM I 42.5 N+10% SAC № 2	61	71	89
CEM I 42.5 N	45	59	85

Despite the maximum possible similarity of the design characteristics of sulfoaluminate clinkers, the technological properties, phase composition, and, consequently, the construction and technical properties of SAC, largely depend on the presence of impurity elements, the type and properties of materials used as raw materials.

4   Conclusion

From natural raw materials - kaolin, limestone and gypsum stone, excluding expensive strategic bauxites, it is possible to produce sulfoaluminate fast-hardening cement as an independent binder and an effective additive to Portland cement to increase strength in the early (up to 7 days) hardening time.

Low-temperature synthesis of a sulfoaluminate additive to Portland cement at 1240 °C is possible from technogenic products - TPP ash, phosphogypsum, and limestone, which accelerates the strength gain in the early stages of hardening. The use of a composition based on technogenic products for the production of sulfoaluminate additives will allow recycling waste from the chemical and energy industries, control the properties of cement compositions, and replacing part of the clinker with a low-temperature roasting additive will reduce the specific fuel consumption for cement production.

References

1. Borisov, I.N., Grebeniuk, A.A., Dyukareva, V.I.: Combined cements with non-shrinking properties using sulfoferrite clinker. IOP Conf. Ser. Mater. Sci. Eng. (MSE) **451**, 56–66 (2018)
2. Borisov, I.N., Grebenyuk, A.A.: Features of hydration and strength set of sulfoferrite clinkers and special cements based on them. Cement Appl. **3**, 88–91 (2019)
3. Sycheva, L.I., Bakeev, D.V.: Investigation of the properties of a composite binder based on sulfate-containing and Portland cements. Tech. Technol. Silicates **17**(1), 2–7 (2010)
4. Sycheva, L.I., Bakeev, D.V.: Composite binder based on sulfate-containing and Portland cements. Concrete Technol. **2**, 12–15 (2013)
5. Samchenko, S.V.: Sulfated calcium aluminoferrites and cements based on them. D. Mendeleev University of Chemical Technology of Russia (2004)
6. Borisov, I.N., Mandrikova, O.S., Mishin, D.A., Goloviznina, T.E.: Impact of the use of combustible technogenic waste on physical and chemical processes of cement production and properties. Int. J. Pharmacy Technol. **8**(4), 22486–22495 (2016)
7. Miroshnikova, O.V., Borisov, I.N.: Use of automobile tires as a burn-out additive in the production of cement. Bull. BSTU Named V.G. Shukhov **2**, 131–136 (2019)
8. Klassen, V.K., Borisov, I.N., Manujlov, V.E.: Man-Made Materials in Cement Production. Belgorod State Technological University named after V.G. Shoukhov, Belgorod (2008)
9. Konovalov, V.M., Klassen, V.K., Pereskok, S.A., Novosyolov, A.G.: Peculiarities of fuel burning in dry and wet cement production kilns. IOP Conf. Ser. Earth Environ. Sci. **194**, 052016 (2018)
10. Konovalov, V.M., Pereskok, S.A., Petrova, M.A., Obrazumov, A.N.: Improving the efficiency of heat and mass transfer processes in cement production. Bull. BSTU Named V. G. Shukhov **4**, 176–181 (2016)

Transition to the Assessment of the Brickwork Quality in Terms of Compressive Strength Class

V. S. Lesovik[1] , Yu. A. Belentsov[2] , A. A. Klementyeva[3] ,
and M. Yu. Elistratkin[1(✉)]

[1] Belgorod State Technological University named after V.G. Shukhov,
Kostyukov Street, 46, Belgorod 308012, Russia
naukavs@mail.ru
[2] Petersburg State Transport University of Emperor Alexander I, Moskovsky pr.,
9, St. Petersburg 190031, Russia
[3] LLC "VNIISTROM-NV", Lyubertsy, dp. Kraskovo, st. K. Marx, 117,
Moscow Region 140079, Russia

Abstract. One of the widely used materials in the construction industry is brickwork, while it should be noted that its mechanical properties significantly lag behind other structural materials. According to the results of the analysis of emergency situations, brick structures are among the most dangerous from the point of view of accidents. The main causes of accidents are related to the violation of the construction and operation technology, but about 4% of all accidents relate to the imperfection of regulatory documents. An adequate determination of the actual strength is the key to high-quality and efficient operation of materials in the structures of buildings and structures, as reliability is laid down in the design. Based on the analysis of data obtained by various authors over the past 70 years, the search for the limiting coefficient of variation was carried out. For different groups of brickwork, its value was from 2 to 58%, so the average value of 38% was taken as the maximum allowable value for in-series tests. Taking into account the required value of the reserve coefficient, possible classes of brickwork strength were calculated. Switching to strength classes for brickwork will allow: controlling effectively the mechanical strength indicators in standard samples; simplifying the marking of brickwork and reducing the range of design resistances of brickwork.

Keywords: Brickwork · Effective masonry mortars · Assessment of strength indicators · Strength class · Coefficient of variation · Safety factor

1 Introduction

The development of the construction industry leads to the emergence of new materials and requires continuous improvement of traditional ones. One of the widely used materials is brickwork, while it should be noted that its mechanical properties significantly lag behind other structural materials. According to the results of the analysis of emergency situations, brick structures are among the most dangerous from the point of view of accidents (Fig. 1) [1].
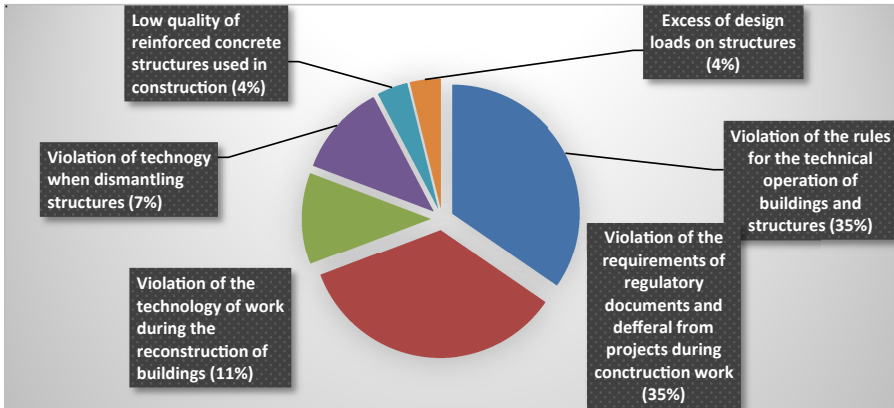
Fig. 1. Distribution of accidents that occurred in 2003 by the main reasons for their origin [1].

As it can be seen, the main causes of accidents are related to the violation of the construction and operation technology, but about 4% of all accidents relate to the imperfection of regulatory documents that define the methods for determining the actual structural properties of brickwork.
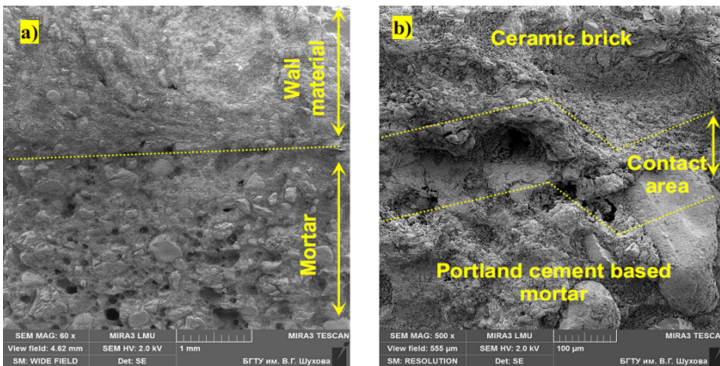

Fig. 2. Micrograph of the brick-mortar contact zone: a) modified; b) traditional.

It is necessary to note the scientific and technical features of the development of brickwork, which continues, although noticeably slower than other wall construction materials. New types of brickwork appear, with noticeably changed physical and mechanical properties, for example, with increased adhesion in the contact zone of bricks and mortar (Fig. 2) due to the use of the "theory of affinity of structures", which allows to increase the strength and other mechanical physical and mechanical properties [2, 3]. Methods of calculation and construction are being improved [4], the brickwork structure is being improved [5], and the testing and quality control methods are being improved [6–9].

Quality control of brick structures is one of the components of the reliability triad. An adequate determination of the actual strength is the key to high-quality and efficient operation of materials in the structures of buildings and constructions, as reliability is laid down during design, evaluated and provided during construction, and maintained during operation. Quality control based on imperfect methods does not always provide a high level of accuracy and reliability of measurement and control operations [10].

In this regard, this paper offers a method for correct assessment of brickwork indicators based on the use of the concept of "class".

2   Methods

To determine the limit coefficient of variation, data obtained by various authors over the past 70 years were analyzed. A statistical sample of 73 series of brickwork was evaluated. The coefficient of variation of a series of brickwork samples made of bricks M100, 150, 200 and mortar M100, 75, 50, 25, 4 was analyzed. Series of samples were made at different times, by different groups of authors, from different bricks and mortar. Using this approach allows getting objective information without reference to certain manufacturers of materials, regions and construction sites, which is necessary to establish a representative value of the coefficient of variation.

The collection of information on the performance characteristics of various types of brickwork was carried out by processing, analyzing and communicating data from open primary sources presented on the portal of the Scientific electronic library eLIBRARY. RU; collections of classic full-text journals published by Elsevier on the ScienceDirect platform; Google Scholar search engine.

3   Results and Discussion

Analysis of the data array for a series of samples revealed that in 13% of cases, the calculated strength is higher than the actual one, which means that the brickwork has a high risk of destruction. At the same time, the average coefficient of excess of the actual strength over the calculated one is 1.7 times. For standard test methods, the pattern of event probability distribution is assumed to be normal with confidence P = 0.95. The margin factor is calculated based on the required uptime probability and reliability index. The coefficient of variation for different groups is from 2 to 58%, the average value of the coefficient of variation for all non-vibrated samples was 38%, so they can take this value as the maximum allowable for in-series tests.

The maximum permissible coefficient of variation will be significantly higher than for concrete, due to the variety of types of bricks and stone, mortars, construction technology, etc. Regulatory documents assume the design of structures based on the calculated strength according to an empirical formula based on the brand of bricks and mortar for compression [17].

The concept of strength class is defined in the A.V. Rzhanitsyn's works and later [11, 12]. At the same time, the concept of class is "truncated" in comparison with the initial theoretical justification in the works on ensuring reliability using the indicator of

the probability of failure-free operation. As the literature evaluates the load-bearing capacity, when moving to a class, this concept is narrowed to the strength of the material. It is necessary to take into account the random nature of the values of the load-bearing capacity and the load effect.

The concept of strength class forms the basis of probabilistic calculation methods and allows moving on to determining the reliability of materials in structures through the relationship of indicators "design strength – class – average strength according to test results", taking into account the variability of the strength properties of the material. The main concept is that the destruction of the material occurs when the equality of the load-bearing capacity and the operating loads is achieved. This means that the actual strength of the test results should be equal to $\bar{R} = \bar{Q}$ (Fig. 3).
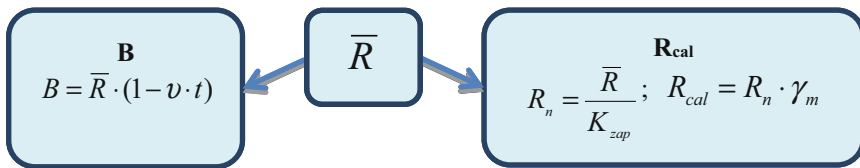

Fig. 3. Interrelation of strength indicators.

In earlier N.S. Streletsky's works, to ensure the required level of reliability, the indestructibility guarantee indicator was used, which is determined by the area of the probability distribution curves, as shown in Fig. 4. The indestructibility guarantee indicator has not found practical application, as it cannot clearly determine the probability of destruction.

$$G = 1 - \omega_1 \omega_2 \qquad (1)$$

Taking into account probabilistic characteristics of bearing capacity and load effect based on the characteristic of the probability of failure-free operation or probability of failure, which is regulated with the help of index of reliability and is controlled via the coefficient of reserve that is the relation between the failure-free operation generalized strength and the load effect.
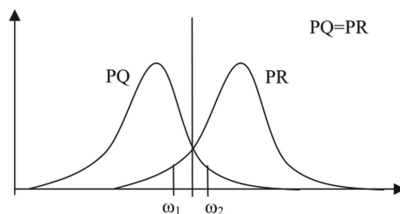

Fig. 4. Graphical representation of the indicator of the guarantee of indestructibility (G) according to N.S. Streletsky [13].

The main task of ensuring the indestructibility and reliability of structures is to provide conditions.

$$\bar{R} - \bar{Q} \geq 0 \tag{2}$$

where, $\bar{R}$ - generalized structural strength; $\bar{Q}$ - generalized load.

The security characteristic or reliability index is provided by the dependency:

$$\beta = \frac{\bar{R} - \bar{Q}}{\sqrt{S_R^2 + S_Q^2}} \tag{3}$$

where, S_R and S_Q - standard deviation of the strength properties of the material and loads. $v_R = \frac{S_R}{\bar{R}}$; $v_Q = \frac{S_Q}{\bar{Q}}$ are coefficients of variation.

Then the probability of failure:

$$P_f = \frac{1}{\sqrt{2\pi}} \frac{\beta^2 - 1}{\beta^3} \exp(\frac{-\beta^2}{2}) \tag{4}$$

The probability of failure has an inverse relationship with the variability of the strength reserve. The smaller the strength reserve, the lower the reliability index β, and the higher the probability of failure. The density of the failure probability distribution is related to both the reliability index and the coefficient of reserve.

$$\beta = \frac{K_{zap} - 1}{\sqrt{(v_Q^2 K_{zap} + v_R^2)}} \tag{5}$$

$$K_{zap} = \frac{\left(2 + \beta^2 v_R^2\right) + \sqrt{\left(2 + \beta^2 v_R^2\right)^2 - 4\left(1 - \beta^2 v_Q^2\right)}}{\sqrt{(v_Q^2 K_{zap} + v_R^2)}} \tag{6}$$

where, $R_N = \dfrac{\bar{R}}{K_{zap}}$; $R_{cal} = R_N \cdot \gamma_m$.

GOST 32047-2012 "Stonework. Compression test method" and GOST R 57290-2016/EN 1052-1: 1998 "Stonework. Method for determining compressive strength" allows determining the value of the average strength of brickwork based on the test results, but do not allow avoiding using empirical formulas. It is necessary to introduce a safety factor that provides the required level of reliability according to the indicator "probability of failure-free operation taking into account the coefficient of variation". In European norms, the coefficient of reserve is from 1.7 to 3.3 [16, 20]. As the Russian standards have lower indicators of operating conditions coefficients, it is advisable to apply this range only for structures with a reduced level of reliability for a normal level of reliability, the coefficient should be $K_{зап}$ = 3.9 [18].

When switching to the brickwork class, when calculating brick structures with the required level of reliability with a confidence of 0.95, it is necessary to take into account that the calculated strength index, without additional methods of increasing strength (such as reinforcement or vibration), can reach 3.9 MPa. The strength of brickwork with a maximum coefficient of reinforcement will reach 7.8 MPa [17], vibrated to 5.6 MPa. As it is possible to switch to the production of high-strength brickwork, so the classes of brickwork strength will be determined by the following relation.

$$R_{\text{расч}} = 3.0 \text{ MPa};$$
$$\overline{R} = R_{\text{расч}} \, K_{\text{зап}} = 3 \times 3.9 = 11.7 \text{ MPa};$$
$$B = \overline{R}(1 - vt) = 11.7(1 - 0.38 \times 1.64) = 4.4 \text{ MPa}.$$

We approximate the brickwork class to B4 (at n = ∞ and P = 0.95). Based on the above, classes of brickwork for compressive strength, taking into account the principles of standardization, can be assigned: B 0.25; 0.5; 1; 2; 3; 4; 5; 6; 7; 8; 9; 10; 12.5; 15; 20; 25. The maximum involved class value should be B10 for modern brickwork.

4   Conclusion

The introduction of the concept of brickwork class together with a new standard for its testing will significantly improve the quality of brick construction, reduce the likelihood of accidents in buildings under construction and in operation, and make more efficient use of material resources. It allows regulating the coefficient of reserve and the variability of strength properties, achieving a high probability of failure-free operation $P_f = 10^{-3}$.

  Switching to strength classes for brickwork will allow:

– controlling effectively the mechanical strength indicators in standard samples, which will increase the reliability, durability and safety of the structures being built. Control of masonry in structures using brickwork strength tests in standard samples will reduce the number of dangerous accidents due to an insufficient level of reliability due to exceeding the calculated brickwork strength over the actual one obtained experimentally;
– simplifying the marking of brickwork to reduce the range of design resistances of brickwork. At the moment according to the characteristics of the calculated strength in the standards there are more than 90 different groups of brickwork strength depending on the strength of bricks and mortar;
– simplifying the work of designers and builders when coordinating the work performed, increasing the possibility of interchangeability when creating a structure by selecting various more effective ratios of brick and mortar strength.

References

1. Accidents of buildings and structures on the territory of the Russian Federation in 2003. FTSK, Moscow (2004)
2. Elistratkin, M.Y., Lesovik, V.S., Zagorodnjuk, L.H., Pospelova, E.A., Shatalova, S.V.: New point of view on materials development. IOP Conf. Ser. Mater. Sci. Eng. 032020 (2018)
3. Volodchenko, A.N., Elistratkin, M.Yu., Zagorodnyuk, L., Kuprina, A.A., Lesovik, V.S.: Effective masonry mortars for autoclaved wall materials. Build. Mater. **12**, 22–29 (2016)
4. Pangaev, V.V.: Development of computational and experimental methods for studying the strength of masonry of stone structures: abstract of dis. doctors of technical sciences. Novosibirsk (2009)
5. Belentsov, Yu.A.: Increasing the efficiency of production and operation of composite anisotropic materials. Bull. BSTU V.G. Shukhov **3**, 6–11 (2010)
6. Kolchunov, V.I., Belov, N.N., Kopanitsa, D.G., Yugov, N.T., Ryshkov, A.V., Useinov, E.S., Arkhipov, I.N.: Study of the dynamic impact strength of brickwork. TGASU Bull. **2**, 123–131 (2017)
7. Lesovik, R.V., Klyuev, S.V., Klyuev, A.V., Tolbatov, A.A., Durachenko, A.V.: The development of textile fine-grained fiber concrete using technogenic raw materials. Res. J. Appl. Sci. **10**(10), 696–701 (2015)
8. Lesovik, R.V., Klyuyev, S.V., Klyuyev, A.V., Netrebenko, A.V., Kalashnikov, N.V.: Fiber concrete on composite knitting and industrial sand KMA for bent designs. World Appl. Sci. J. **30**(8), 964–969 (2014)
9. Klyuyev, S.V., Klyuyev, A.V., Lesovik, R.V., Netrebenko, A.V.: High strength fiber concrete for industrial and civil engineering. World Appl. Sci. J. **24**(10), 1280–1285 (2013)
10. Belentsov, Y., Smirnova, O.M.: Influence of acceptable defects on decrease of reliability level of reinforced concrete structures. Int. J. Civil Eng. Technol. **9**(11), 2999–3005 (2018)
11. Rzhanitsyn, A.R.: Theory of calculation of building structures for reliability. Stroyizdat, Moscow (1978)
12. Raizer, V.D.: The Theory of Reliability in Construction Design. ASV, Moscow (1998)
13. Streletsky, N.S.: On the study of the safety factor of structures. Metal Struc. **1** (1938)
14. GOST 32047-2012 Stone masonry. Compression test method. Standartinform, Moscow (2014)
15. GOST R 57290-2016/EN 1052-1: Stone masonry. Method for determining compressive strength. Standartinform, Moscow (2017)
16. Marchiukaitis, G.V., Yonaitis, B.B., Valivonis, Yu.S., Gnip, I.Ya.: Assessment of the strength and deformability of masonry under compression according to SNiP II-22–81 and Eurocode 6. Stroitelnye materially **11**, 48–49 (2004)
17. SP 15.13330.2012: Stone and reinforced stone structures. FAU FCS, Moscow (2012)
18. Belentsov, Y., Kharitonov, A.M.: Determination of the safety factor in assessing the quality of brick structures. Bull. Civil Eng. **4**(57), 105–110 (2016)
19. Krasnoshchekov, Y.: Probabilistic Foundations for Calculating Building Structures. Publishing and Printing Center, SibADI Omsk (2016)
20. Eurocode 6: Design of stone structures. Part 1-1. General rules for reinforced and unreinforced stone structures

Research on the Influence of Gypsum and Anhydrite Stone Impurities on the Properties of the Binder

A. F. Buryanov$^{(\boxtimes)}$, N. A. Galtseva , I. V. Morozov ,
and E. N. Buldyzhova

National Research Moscow State University of Civil Engineering,
Moscow, Russia
rga-service@mail.ru, GalcevaNA@mgsu.ru

Abstract. Gypsum ($CaSO_4$ $2H_2O$) and anhydrite ($CaSO_4$) are the most common sulfate minerals. The predominant part of gypsum and anhydrite is used as raw materials for the production of gypsum binders (construction gypsum) and additives in various types of cements, to a lesser extent–for the production of hard-burnt, high-strength, molding and medical gypsum, sulfuric acid, ammonium sulfate, and paper and for soil gypsuming. In addition, gypsum and anhydrite are used in small quantities as decorative and ornamental materials. In each deposit of natural gypsum, the distinctive features are its composition and structure, which directly affects the production conditions and construction and technical properties of gypsum binders. This paper is aimed at evaluating the influence of various impurities present in gypsum and anhydrite stones on the properties of the binder. In this work, the selected samples for each case were subjected to chemical and mineralogical analysis, passed the roasting stage, and then samples-beams are formed and tested for bending and compression on laboratory equipment. In summary, the conclusion was made about the ability of impurities to influence the indicators of setting time, strength values.

Keywords: Natural gypsum · Gypsum · Gypsum stone · Anhydrite stone · Binder · Impurities · Clay · Dolomite

1 Introduction

The proportion of produced construction binders and their consumption within the country depends on many factors, including the need for construction work and the appropriate combination of technical properties. However, the availability and volume of raw material reserves, its location and availability for further development are of paramount importance [1–3].

Gypsum is usually called not only the mineral itself, but also the rock consisting of it, as well as building material, which is obtained by partial dehydration and grinding of the mineral. Materials based on it are distinguished by their environmental friendliness. Calcium sulfate is the main component of products that exist in aqueous and non-aqueous compounds: dihydrate ($CaSO_4$ $2H2O$), semihydrate ($CaSO_4$ $0.5H_2O$) and anhydrite ($CaSO_4$). Gypsum has a neutral pH in contrast to materials made from lime

and cement. The raw material component usually has a color scheme close to white. The quantitative ratio of impurities directly affects the color of gypsum: for example, iron oxides give a yellowish-brown tone, and organic substances give a more gray color [4]. Gypsum-based binders are considered energy-saving materials, which is explained by the roasting process at significantly lower temperatures (exposure range at 135–180 °C) than when using cement and lime. Low temperature effects during roasting lead to lower fuel resource consumption, and the total amount of CO_2 emitted to the external environment in this case is insignificant. Due to fast setting and solidification, gypsum products do not require accelerated curing. They are light, have excellent ductility, exhaust gas resistance and sound insulation. However, gypsum products have low water resistance [5]. The use of chemical and mineral additives, cement or lime additives, and reinforcing elements makes it possible to achieve different properties of gypsum binders [6, 7].

In some areas, natural gypsum is considered a scarce raw material component for creating binders. In this case, an alternative option may be industrial waste. Studies on the possibility of recycling gypsum-containing industrial waste (GIW) have been initiated and are being conducted in the context of their reuse, including as raw materials for production, for example, binders [8–12].

The Russian Federation is one of the leading countries in terms of natural gypsum reserves. Natural deposits of gypsum stone and anhydrite were formed by precipitation from seawater, as well as by hydration and dehydration of calcium sulfate ($CaSO_4$) [13]. The resulting gypsum stone often contains anhydrite, and natural anhydrite - a variable amount of gypsum. In each deposit of natural gypsum, its composition and structure are distinctive features, which directly affect the production conditions and construction and technical properties of gypsum binders [14, 15].

This paper is aimed at evaluating the influence of various impurities present in gypsum and anhydrite stones on the properties of the binder. In this work, the selected samples for each case were subjected to chemical and mineralogical analysis, passed the firing stage, then samples -beams were formed and bending and compression tests were performed on laboratory equipment. In summary, the conclusion was made about the ability of impurities to influence the indicators of setting time and strength values.

2   Methods and Materials

At the first stage, chemical and mineralogical compositions were determined in order to consider the influence of gypsum stone impurities on the properties of the binder. Further, the production of gypsum binder grades G5-G7 was carried out. A sample was used as raw material, where the percentage of calcium sulfate dihydrate was 97.75%. The gypsum binder was obtained by roasting, i.e. by "cooking" in a laboratory gypsum boiler equipped with a stirrer, the capacity of which is 5 L. To do this, the gypsum stone was crushed in a jaw crusher, and then sifted through a sieve №0.315. The gypsum raw material was loaded into a preheated boiler to t = 130 °C for 5-7 min. At the end of loading, the temperature in the boiler dropped to 97–95 °C. Gypsum cooking was accompanied by a mode with temperature values of 122-126 °C, exposure was 60–65 min, then at T = 127–134 °C–exposure lasted 30–35 min, then the temperature was

raised to 138 °C for 30 min, and the total duration of cooking was 140–150 min. During the "cooking" of gypsum and after unloading from the boiler, samples were taken to determine hydrate water. The resulting gypsum binder mainly consisted of β-semihydrate of calcium sulfate. At the second stage, the above-described manufacturing sequence was repeated, only the raw material component was now supplemented with impurities represented by anhydrite stone, dolomite and clay from the Poretsky deposit. The samples were pre-dried and then crushed in a jaw crusher. The material obtained at the output was sifted through a sieve №0.315.

In the case of anhydrite stone, the chemical and mineralogical compositions were also determined. Further, the sequence of works was similar to the above. Dolomite, gypsum stone, and clay from the Poretsky deposit were taken as impurities. Previously, the impurities were dried in a drying cabinet; dolomite, gypsum stone and clay were crushed on a jaw crusher, and then the above impurities were introduced into the binder during grinding. The influence of the presence of impurities of the following rocks on the quality of the anhydrite binder was checked:

– dolomite in the amount of 10; 15; 20% by weight;
– clay rocks in the amount of 3; 5; 10% by weight;
– gypsum stone in the amount of 10; 20; 30; 50% by weight.

3 Results and Discussion

3.1 Ongoing Research on Gypsum Stone

The beginning of the work consisted in visual inspection of the selected samples of gypsum stone. In appearance, the pieces differed from each other. The first sample ("Pipe passage") was characterized by a more gray color in comparison with the second sample ("Bypass loop"), which was dominated by a uniform white color.

Using laboratory equipment, the chemical and mineralogical compositions were determined and summarized in Table 1 and 2, respectively. Stone sample №1a for the content of calcium sulfate dihydrate $CaSO_4 \cdot 2H_2O$ belongs to grade 3, and sample №2a to grade 1 according to GOST 4013-2019 "Gypsum and anhydrite stone for the production of binders".

Table 1. Chemical composition of the average sample of gypsum and anhydrite stones.

Sample	SiO_2	Al_2O_3	Fe_2O_3	CaO	MgO	SO_3	POI 500 °C	CO_2	$\sum$	Humidity, %
Gypsum stone										
1a	0.22	0.22	0.08	31.82	4.74	36.93	16.1	9.6	99.71	0.3
2a	0.18	0.14	0.06	32.53	0.3	45.52	20.44	0.59	99.76	0.33
Anhydrite stone										
1b	0.46	0.19	0.11	39.44	0.30	56.52	2.86	0.34	100.32	0.65

Table 2. Mineralogical composition of the average sample of gypsum and anhydrite stones.

№	$CaSO_4 \cdot 2H_2O$,%	$CaSO_4$,%	$CaCO_3 + MgCO_3$,%	Other oxides,%	Sum, %
Gypsum stone					
1a	77	1.9	10.07 + 9.91 = 19.98	0.52	99.4
2a	97.75	0.09	0.6 + 0.63 = 1.23	0.38	99.45
Anhydrite stone					
1b	13.66	85.47	0.3 + 0.63 = 0.66	0.73	100.52

As a result of the production of gypsum binder by roasting, a material was obtained that has a fibrous structure and has an increased level of water demand, which gives reason to attribute it to the G5, AII brand. The final data of the tested gypsum binder are summarized in Table 3.

Table 3. Preparation of gypsum binder by cooking from gypsum stone taken from different places of occurrence, used further as a reference.

№ of cooking	Location of occurrence	W/G, %	Setting time, min-sec		Values of tensile strength at bending/compression ($4 \cdot 4 \cdot 16$), kgf/cm^2, after 2 h		$CaSO_4 \cdot 2H_2O$,%	$W_{hydrate}$, %	Volumetric expansion, %
			Beginning	Ending	Bending	Compression			
1	Pipe passage	70	7–50	12–05	27.1	42.7	77.7	5.26	0.142
2	Pipe passage	68	7–35	12–00	31.7	56.4	84.95	4.83	0.137
3	Selection of white stone	75	6–30	11–10	28.2	47.0	96.16	5.83	0.14
4	Selection of gray stone	71	7–40	11–35	27.2	50.0	85.24	4.75	0.17
5	Bypass loop	80	6–20	9–50	27.5	50.0	95.6	5.1	0.141

The results show that a high amount of calcium dihydrate in the composition of gypsum stone belonging to the first grade allows getting a binding material, the grade of which is not lower than G5. A distinctive feature of this binder is its high water demand. In this case, it was in the range of 70–80%, but the bending strength of the samples still exceeded the requirements of GOST 125-2018 for this indicator for the G5 brand. Presumably, a reduction in water demand to 55–60% will lead to an increase in the grade of binder to G6 and higher.

To verify the influence of impurities on the properties of the resulting gypsum binder, the following materials were used: dolomite, anhydrite stone, and clay from the Poretsky deposit. "Cooking" of gypsum raw materials with impurities of the above-mentioned rocks was performed in a laboratory gypsum boiler. Data on the effect of these impurities on the properties of the gypsum binder are shown in Table 4 and are clearly shown in Fig. 1.

Table 4. Effect of gypsum stone impurities on the properties of the resulting binder.

№ of experiment	Impurities, %			$W_{hydrate}$ of cooking, %	W/G, %	Volumetric expansion, %	Remaining on the sieve №02, %	Volume weight, kg/cm³
	Anhydrite	Clay	Dolomite					
8	10	–	–	5.29	78	0,137 (max 0,147)	4850/8.7	1530
7	20	–	–	4.72	71	0,141 (max 0,161)	4858/8.8	1580
9	30	–	–	4.0	65	0,132	4425/8.7	1600
10	50	–	–	2.97	50	0,114 (max 0,120)	6430/5.2	1700
12	–	10	–	5.37	57	0,139	5117/8.3	1540
13	–	30	–	4.99	76	0,138	7170/4.6	1563
15	–	–	20	4.66	70	0,150 (max 0,172)	5600/6.2	1570
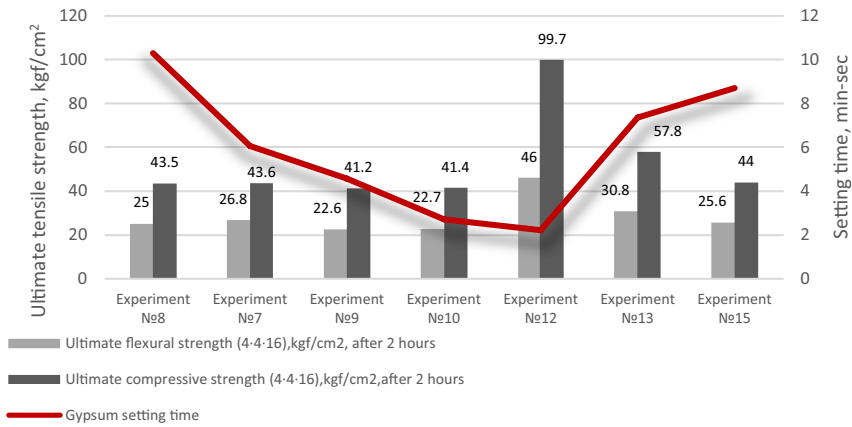
Fig. 1. Diagram of the results of the analyzed technical properties of gypsum binder in the presence of impurities.

The obtained data allow concluding that impurities of anhydrite, dolomite and clay in amounts up to 10% practically do not reduce the strength indicators of hardened samples, and in the case of clay with a noticeable decrease in the water demand of the binder, they allowed obtaining strength indicators close to the G10 grade. However, with a further increase in the content of such impurities in the composition of gypsum stone (20% or more), a decrease in the strength characteristics of the hardened stone is noted.

3.2   Ongoing Research on Anhydrite Stone

The values obtained during the mineralogical analysis for the composition of the anhydrite stone sample under study showed percentages of anhydrite and gypsum in the amount of 85.47% and 13.66%, respectively. Chemical analysis allowed determining the content of sulfur anhydrite (SO_3), according to the final values, the value

was 56.62%, which is in accordance with the regulatory and technical documentation (GOST 4013-2019) meets the requirements of grade 1 gypsum anhydrite stone.

The presence of gypsum in gypsum anhydrite stone is ambiguous. The positive factor of the presence is the increase in the solidifying process due to the formation of auxiliary crystallization centers. The negative impact of gypsum can affect the rate of hardening and strength indicators of the anhydrite binder, which requires careful additional research.

The influence of the impurities specified in paragraph 2 was evaluated based on the results of the anhydrite binder test, which resulted in relatively stable indicators for the main technical properties. Such indicators include:

– water-binding ratio;
– setting time;
– hydration capacity of the binder (degree of hydration);
– strength indicators for bending and compressing samples-beams that solidified in air after 7 and 28 days;
– linear deformations of manufactured samples in the dried state;
– stability of the volume character of the manufactured samples after 7 and 28 days.

Table 5. Effect of introducing impurities into the composition of anhydrite binder.

Activator additive						
Type	Amount, %	W/A	Linear deformations, mm/m	Bound water, %	ρ of dry samples, kg/cm^3	Volume stability
Cement (M500) K_2SO_4 FeSO$_4$	5 1 0.5	30	0,2	10.76	1757	Without changes
Dolomite	10	28		10.18	1750	
	15	28				
	20	28		9.41	1820	
Clay impurities	3	27.5		10.83	1800	
	5	27.5				
Clay impurities	10	27.5		11.2	1781	
CaSO$_4$·2H$_2$O	10	30		11.2	1700	
	20	30				
	30	30		13.9	1680	
	50	30		10.0	1630	
AlK(SO$_4$)$_2$ Clay impurities	2.5 5	28		16.56	1840	Without changes
AlK(SO$_4$)$_2$ Dolomite	2.5 15	28				↑Up to 30%
AlK(SO$_4$)$_2$ CaSO$_4$·2H$_2$O	2.5 20	28		17.89	1700	

The final values obtained during testing of significant technical properties of the anhydrite binder in the presence of impurities in the form of various types of rocks are shown in Table 5 and graphically shown in Fig. 2 (Fig. 3).
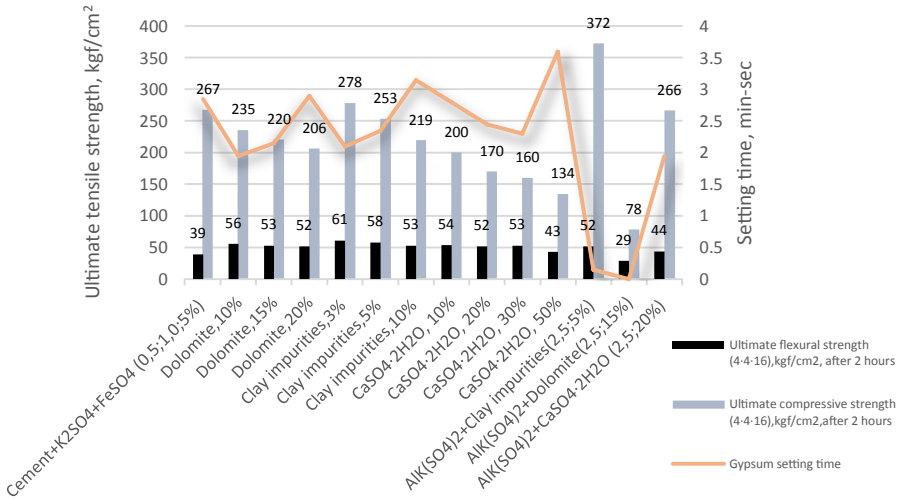

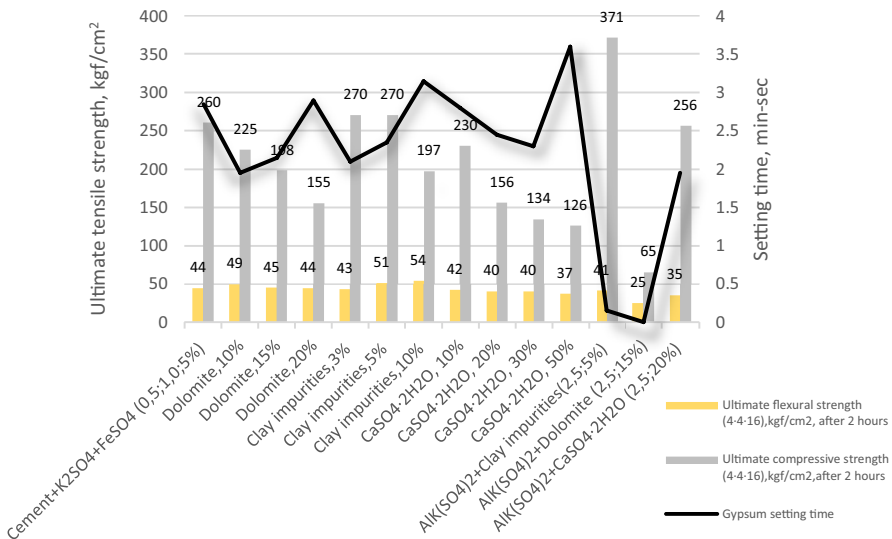**Fig. 2.** Diagram of the results of the analyzed technical properties of anhydrite binder after 7 days.

Fig. 3. Diagram of the results of the analyzed technical properties of anhydrite binder after 28 days.

The obtained test results allow drawing the following conclusions:

- the most stable indicators for the main technological properties of freshly prepared solutions and indicators of solidified solutions were obtained when using the binder as an alkaline activator – Portland cement in an amount of up to 5%, and as a sulfate activator K_2SO_4 and $FeSO_4$ at optimal concentrations of 1–1.5% and 0.2–0.5%, respectively;
- noteworthy indicators of the properties of the binder, which were obtained using aluminum-potassium alum ($AlK (SO_4)_2$) in the amount of 2.5%, but in this case there is no stability of results in the presence of impurities in the gypsum anhydrite stone, and a significant increase in the volume of solidified material when stored in water is also noted.

4   Conclusion

Studies of the influence of gypsum and anhydrite stone impurities on the properties of the binder showed the following results:

1. From gypsum stone with a high content of calcium sulfate dihydrate, which belongs to the 1st grade stone, a binder of the grade not lower than G5 can be obtained;
2. Adding anhydrite, dolomite and clay up to 10% to the gypsum binder does not affect the strength characteristics of the manufactured samples. A decrease in strength is observed only if the impurities are of 20% or higher;
3. In the case of an anhydrite binder, the addition of a strictly specified amount of alkaline and sulfate activators can lead to relatively stable indications for the main technological properties of freshly prepared solutions. Aluminum-potassium alum does not provide stable results.

References

1. Bouzit, S., Laasri, S., Taha, M., Laghzizil, A., Hajjaji, A., Merli, F., Buratti, C.: Characterization of natural gypsum materials and their composites for building applications. Appl. Sci. **9**(12), 1–15 (2019)
2. Singh, R.N., Eksi, M.: Rock characterization of gypsum and marl. Mining Sci. Technol. **6**(1), 105–112 (1987)
3. Green, H., Gleadow, A., Finch, D., Hergt, J., Ouzman, S.: Mineral deposition systems at rock art sites. J. Archaeological Sci. Rep. **14**, 340–352 (2017)
4. Tumuklu, A., Ciflikli, M., Ozgur, Z.: Determination of the trace elements effecting the color of the gypsum mineral. Int. J. Eng. Res. Manage. **3**(09), 16–19 (2016)
5. Buldyzhova, E.N., Galtseva, N.A., Buryanov, A.F., Petropavlovskaya, V.B.: Technical-economic and environmental aspects of production and application of gypsum materials and products. Actual Probl. Modern Sci. Technol. Educ. **2**(71), 197–200 (2013)
6. Galceva, N.A., Burianov, A.F., Soloviev, V.G., Tkachenko, D.I.: A modified binder on the basis of synthetic anhydrite for stowing mixtures. Construct. Mater. **7**, 74–76 (2017)

7. Gal'tseva, N.A., Bur'yanov, A.F., Buldyzhova, E.N., Solov'ev, V.G.: The use of synthetic calcium sulfate anhydrite for production of filling mixtures. Construct. Mater. **6**, 76–77 (2015)
8. Kharitonov, A., Smirnova, O., Vilenskii, M.: Principles of green architecture for the historical part of Saint-Petersburg. Urban. Architect. Construct. **10**(2), 103–112 (2019)
9. Kharitonov, A., Smirnova, O.: Optimization of repair mortar used in masonry restoration. Spatium **42**, 8–15 (2019)
10. Rashad, A.M.: Phosphogypsum as a construction material. J. Clean. Prod. **166**, 732–743 (2017)
11. Cánovas, C.R., Macías, F., Pérez-López, R., Basallote, M.D., Millán-Becerro, R.: Valorization of wastes from the fertilizer industry: current status and future trends. J. Clean. Prod. **174**, 678–690 (2018)
12. Khezhev, T.A., Pukharenko, Y.V., Khezhev, K.A., Klyuev, S.V.: Fiber gypsum concrete composites with using volcanic tuffsawing waste. ARPN J. Eng. Appl. Sci. **13**(8), 2935–2946 (2018)
13. Popov, K.N., Caddo, M.B.: Building Materials and Products. High school, Moscow (2002)
14. Alfimova, N.I., Pirieva, S.Y., Elistratkin, M.Y., Nikulin, I.S., Titenko, A.A.: Binders from gypsum-containing waste and products based on them. IOP Conf. Ser. Mater. Sci. Eng. **945**, 012057 (2020)
15. Edamenko, A.S., Matveeva, L.Y., Yastrebinskaya, A.V.: Influence of gypsum binder phase composition on operational and mechanical properties of the hydration product. Solid State Phenom. **299**, 1086–1090 (2020)

The Effect of Natural Climatic Aging on Damage Accumulation Kinetics in the Structure of Epoxy Polymers Under Tensile Loads

D. R. Nizin$^{(\boxtimes)}$, T. A. Nizina , N. S. Kanaeva ,
and A. I. Gorenkova

National Research Mordovia State University, Saransk, Russia
`nizinata@yandex.ru`

Abstract. The approach is proposed for assessing the "critical" state of polymer materials under the effect of aggressive media. Changes in kinetics of failure accumulation of three compositions of epoxy polymers based on ED-20, Etal-247 and Etal-370 epoxy resins cured by Etal-1440 in 45, 90, 180, 270 and 360 days of natural climatic exposure were analyzed. We have identified changes in the rate of damage accumulation when the total level of failures exceeds $70 \div 80\%$ of their maximum corresponding to the achievement of maximum tensile stresses. Damage accumulation kinetics was calculated based on the author's method using methods of fractal analysis of deformation curves for polymer materials samples under tension. This approach involves determining the coordinates of "critical" points of deformation curves for which the fractality index values calculated over the previous short time intervals using the least coverage method, were less than 0.5. High stability of epoxy polymer parameters based on modified Etal-247 resin under the natural climatic factors has been found. After a year of full-scale exposure, for this type of epoxy polymer the "critical" levels of tensile stresses and their corresponding relative elongation are reduced by 11% and 16%. At the same time, for polymers based on ED-20 and Etal-370 epoxy resins, these figures are 1.9 and 2.7 ($\sigma^{70}_{crit.}$) and 2.7 and 5.1 ($\varepsilon^{70}_{crit.}$) times reduced, respectively, which indicates a significant damage accumulation.

Keywords: Epoxy polymers · Deformation curves · Damage accumulation · Stress increase · Fractal analysis · Minimal coverage method

1 Introduction

One of the most effective ways to increase durability of building products and structures under the effect of aggressive factors is the use of protective and decorative coatings based on polymer binders. The use of polymer coatings for the protection of reinforced concrete structures both reliably isolates the concrete and reinforcement from the aggressive environment, and increases crack resistance and load-bearing capacity, reduces shrinkage, creep, deformability, etc. [1–4]. Polymer coatings also act

as a kind of regulator of the base material structural formation, caused by a decrease in the total volume of macro- and micro-defects on the surface and in the body of reinforced concrete structures, as well as changes in the nature of porosity due to the transfer of open pores to closed ones. In connection with the high complex of strength and adhesion characteristics, compositions based on epoxy binders [5–8] are the most widespread from a wide enough range of protective and decorative coatings of building products and structures.

As a rule, the standard mode of operation of polymer-based protective and decorative coatings implies cyclic effect of both aggressive factors and mechanical loads. It is in connection with the cyclic nature, a number of coefficients are introduced when designing them, taking into account possible multi-directional deviation of operating loads from the calculated values. As a result, the material strength limit at maximum load never corresponds to the actual value of the operating load. However, the designing polymer-based structures operated under the climatic factors practically does not take into account the decrease in performance characteristics of polymer materials due to natural aging. In addition, when calculating the maximum allowable performance characteristics of protective and decorative polymer coatings, they do not take into account the reversibility and irreversibility of the resulting changes in properties [9, 10].

The paper assessed the effect of the natural climatic aging duration on changes in kinetics of damage accumulation in the structure of polymer materials samples under tensile loads. Quantitative values are determined on the basis of the author's method, which allows determining the coordinates of critical points of deformation curves built by methods of fractal analysis [11, 12]. It was shown that the environmental exposure leads to changes both in performance characteristics and the rate of accumulation of reversible and irreversible changes in the polymer material structure.

2   Methods and Materials

The objects of study were samples of three compositions of epoxy polymers based on ED-20, Etal-247 and Etal-370 resins cured by Etal-1440 amine hardener (production of ENPC EPITAL JSC). It is designed for curing epoxy resins and compounds based on them at temperatures from +10 °C. Mixtures based on Etal-1440 hardener have a long life of 4–5 h at +20 °C, which is important in the development of compounds for protective and decorative coatings of building structures.

ED-20 epoxy resin is a liquid reactive oligomeric product based on diglicidyl ether of biphenylolpropane and corresponds to GOST R 56211-2014. Mass fraction of epoxy groups is $20 \div 22.5\%$; dynamic viscosity at 20 20 °C is $12 \div 25$ Pa · s.

Etal-247 (TU 2257-247-18826195-07) and Etal-370 (TU 2257-370-18826195-99) epoxy resins are low-viscosity modified resins with viscosity $20 \div 22$ and $4.5 \div 5.0$ times lower than that of ED-20, respectively. Mass fraction of epoxy groups for Etal-247 and Etal-370 is at least $21.4 \div 22.8$ and 21.5%, respectively.

Mechanical tensile testing of the samples of compositions under study was made using an AGS-X series tensile testing machine with TRAPEZIUM X software. Test temperature was 23 ± 2 °C and relative air humidity was $50 \pm 5\%$. The tensile testing

machine clamp movement speed was 2 mm/min. The readings were registered at 0.01 s. At least 6 samples were tested for each composition in parallel (type 2 according to GOST 11262-2017).

The samples were subjected to natural exhibition on the test stands of the environmental and meteorological monitoring laboratory, construction technologies and examinations of the Ogarev National Research Mordovia State University (Saransk). Physical and mechanical performance was determined after 45, 90, 180, 270 and 360 days of full-scale exposure.

The kinetics of damage accumulation was assessed on the basis of data obtained using the author's methodology. Its algorithm is given in [11, 12]. The proposed approach involves determining the coordinates of "critical" points of the deformation curves for which the fractality index values calculated over the previous short time intervals using the least coverage method, are less than 0.5. Typical curves of the fractality index change depending on the tensile elongation are given in [12]. This study also analyzed time intervals with a duration of 0.16 s which corresponded to the analysis of 16 previous experimental points with a displacement of the analyzed area with a step of 0.01 s.

3 Results and Discussion

In [12], the team of authors proposed to estimate the level of accumulated failures leading to the destruction of samples under tensile loads, to use a parameter defined as the ratio of the number of points with a fractality index less than 0.5 to the total number of points of deformation curves (until reaching the level of maximum voltages). It was shown that in order to obtain a reliable assessment of the polymer composite behavior under the mechanical loads, the data of the entire series under study, not individual samples, should be processed.

In this work, we studied the change in the elastic-strength performance and kinetics of failure accumulation in epoxy polymers under tensile loads in the control state and after full-scale climatic exposure for 45, 90, 180, 270, and 360 days. The results of changes in elastic-strength performance in the process of climatic aging in absolute and relative values are given in Table 1. It was found that for the control samples, the highest strength and deformation performance was registered for polymers based on ED-20 and Etal-370 epoxy resins. Tensile strength and elongation at maximum load for the ED-20 + Etal-1440 sample is 52.9 MPa and 9.8%, for Etal-370 + Etal-1440 it is 54.7 MPa and 11.1%. Epoxy polymer samples based on modified Etal-247 resin are characterized by tensile strength of 40.8 MPa and relative elongation of 8.6%, which, respectively, is 23–25% and 12–22% lower than those of other compositions.

The field test results have shown that the climatic effect within one calendar year leads to a significant decrease in the elastic-strength perf of polymers based on ED-20 and Etal-370 epoxy resins. In particular, the loss of strength and deformation characteristics of ED-20 + Etal-1440 is 34 and 49%, Etal-370 + Etal-1440-48 and 73%. At the same time, the polymer based on the modified epoxy resin Etal-247 has shown significantly greater stability both in assessing the tensile strength (8% lower than the initial value) and the relative elongation (23% lower).

Table 1. Elastic-strength performance of epoxy polymers cured by Etal-1440 during natural climatic aging.

Epoxy resin	Natural exposure duration, days					
	0	45	90	180	270	360
Ultimate tensile strength, MPa						
Relative tensile strength, rel. units						
ED-20	52.9	59.7	46.6	38.9	36.5	34.7
	1.00	1.13	0.88	0.74	0.69	0.66
Etal-247	40.8	41.4	38.7	39.4	36.9	37.3
	1.00	1.02	0.95	0.97	0.90	0.92
Etal-370	54.7	53.3	47.2	56.1	45.7	28.7
	1.00	0.97	0.86	1.03	0.84	0.52
Relative elongation at maximum load, %						
Relative tensile elongation, rel. units						
ED-20	9.8	8.9	5.9	5.0	4.1	4.9
	1.00	0.91	0.60	0.52	0.42	0.51
Etal-247	8.6	7.7	7.0	7.7	6.9	6.7
	1.00	0.90	0.81	0.90	0.80	0.77
Etal-370	11.1	7.0	6.3	8.3	5.8	2.9
	1.00	0.64	0.57	0.75	0.53	0.27

Failure accumulation curves for the samples of epoxy polymers cured by Etal-1440, depending on the level of applied tensions and relative tensile elongation are shown in Fig. 1. In this case, 100% means the maximum number of failures leading to the achievement of the maximum levels of tensile stresses. For the series of the compositions under study, this parameter, depending on the duration of full-scale exposure, varies from 4.36 to 8.19%.

The analysis of curves in Fig. 1 showed that in the process of natural climatic aging, both the elastic strength characteristics of polymer materials and the accumulation rate of reversible and irreversible changes in their structure change. Thus, if for ED-20 + Etal-1440 samples at the age of 0÷90 days, the share of accumulated failures under tensile load of 20 MPa is in the range of 25÷35% of the maximum value, then for the samples at the age of 270÷360 days, it in the range of 50÷70% Such growth of damage accumulation rate in the polymer matrix structure can be caused by high complexity of processes describing the mechanism of interaction between environment and polymer material. Hydrolysis, plasticizing effect of moisture, destruction of surface layers under the UV radiation and solar radiation, relaxation of initial structural heterogeneity, photodestruction – all this is accompanied by both reversible and irreversible changes in the macromolecular structure of the polymer materials under study.

Besides, the analysis of results showed that excess of the level of accumulated failures above 70÷80% leads to curve distortion, which indicates a change in the rate of failure accumulation associated with the transition of structural elements from a functional state to a defective one. At the same time, the level of tensile stresses and corresponding deformations at which an explicit change in the rate of damage
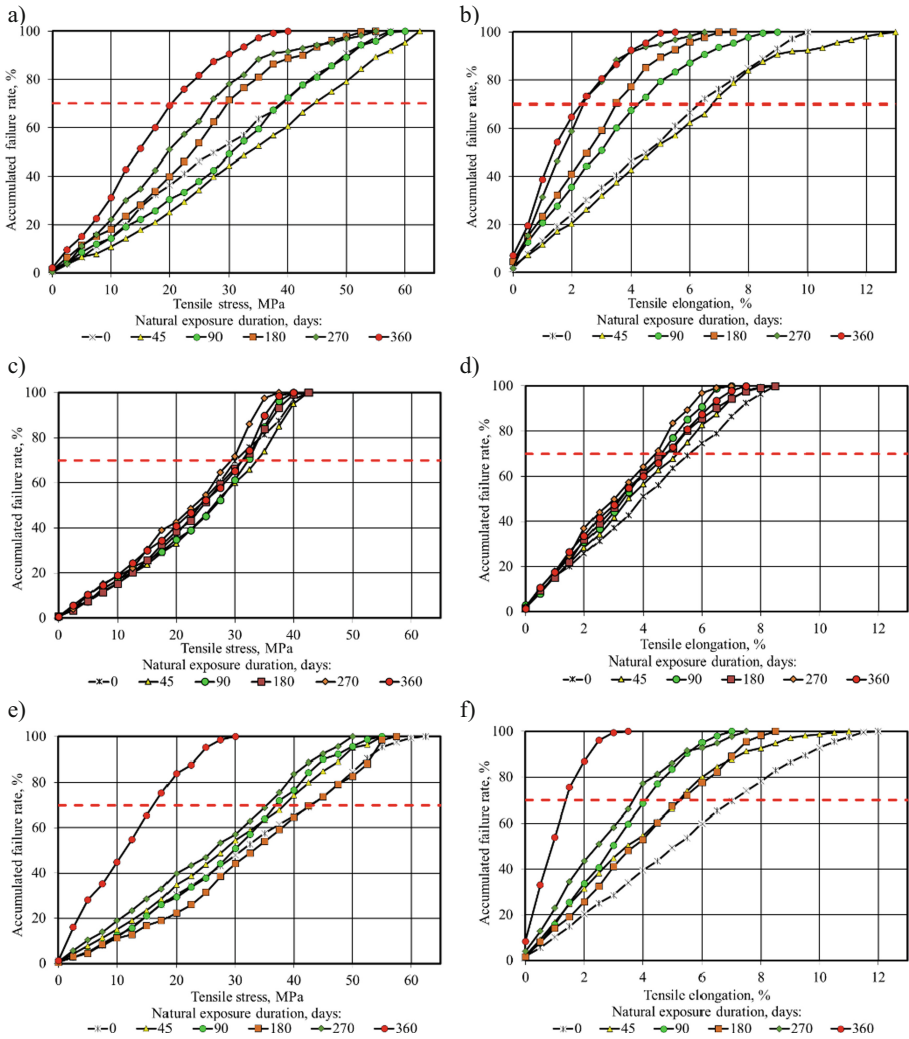
Fig. 1. Curves of failure accumulation in a series of samples of compositions based on epoxy resins: ED-20 (a), Etal-247 (b) and Etal-370 (c) cured by Etal-1440, depending on the level of applied stresses (a, c, f) and relative tensile elongations (b, d, g).

accumulation occurs can be characterized as a maximum level. Its achievement indicates formation of a significant number of defects and cracks in the polymer structure.

Based on data in Fig. 1, tensile stress levels and associated relative elongation were calculated, where the accumulated failure rate was 70% (see red dashed line in Fig. 1) – $\sigma^{70}_{crit.}$ and $\varepsilon^{70}_{crit.}$. The results grouped by the type of epoxy resin used and the duration of natural climatic impact, are shown in Fig. 2. It was found out that for polymers based on ED-20 and Etal-370 epoxy resins up to 90 and 270 days of natural exposure, respectively, it is necessary to apply higher levels of tensile stresses for transition of

composites to critical state than for epoxy polymer based on modified Etal-247 resin. At the same time, the increase in the duration of field exposure up to 360 days leads to a significant decrease in the initial critical levels – 1.9 and 2.7 ($\sigma_{crit.}^{70}$) and 2.7 and 5.1 ($\varepsilon_{crit.}^{70}$) times for polymers based on ED-20 and Etal-370 epoxy resins, which indicates a significant damage accumulation.
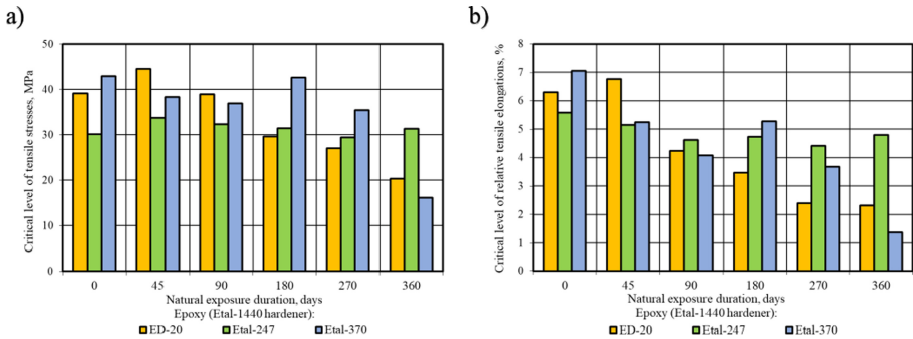
Fig. 2. The change in critical levels of tensile stresses $\sigma_{crit.}^{70}$ and corresponding relative elongation $\varepsilon_{crit.}^{70}$ of epoxy polymers cured by Etal-247 during natural climatic aging.

High stability of epoxy polymer parameters based on modified Etal-247 resin under the natural climatic factors affecting during one calendar year has been confirmed (Fig. 2). Despite lower elastic strength characteristics of control samples of this composition in comparison with the compositions based on ED-20 and Etal-370 resins, the decrease in relative elongation characterizing the embrittlement of polymers after 360 days of natural exposure is not more than 16%. Variation of the critical level of tensile stress depending on the natural exposure duration for polymer Etal-247 + Etal-1440 polymer does not exceed 11%.

In our opinion, it is the indices proposed as criteria of "critical" state, calculated according to failure accumulation curves, that allow us to provide a more representative assessment of climatic resistance of the polymers under study identifying quantitative levels of tensile stresses and relative elongation, where exceeding them is unacceptable for their subsequent normal operation. The use of fractal analysis method for deformation curves registered with a high frequency of readings, results in additional quantitative assessment of climatic resistance and durability of composite materials.

4   Conclusion

The results of the proposed fractal approach in the analysis of deformation curves of polymeric material samples under tensile loads confirmed the possibility to quantitatively analyze kinetics of damage accumulation in the structure of polymers of different compositions effected by a variety of factors (in this case, in-kind climatic effects of different durations). It has been established that the polymer based on the Etal-247

epoxy resin cured by the Etal-1440 amine hardener, has highly stable properties in conditions of exposure to in-kind climatic factors. Thus it can be recommended as a protective and decorative coating of construction products and structures exposed to in-kind climatic impact.

References

1. Selyaev, V.P., Bazhenov, Yu.M., Sokolova, Yu.A., Tsyganov, V.V., Nizina, T.A.: Polymer Coatings for Concrete and Reinforced Concrete Structures. Publishing House of SVMO, Saransk (2010)
2. Nizina, T.A.: Protective and Decorative Coatings Based on Epoxy and Acrylic Binders. Mordovia State University Press, Saransk (2007)
3. Korneev, A.D., Borkov, P.V., Klyshnikov, A.A., Papin, I.V.: Structure formation of protective polymer coatings. Bull. VolGASU. Ser. Constr. Architect. **22**, 69–72 (2011)
4. Stroganov, V.F., Kukolev, D.A., Mukhametova, A.M.: Investigation of the influence of epoxy polymer coatings on biostability and waterproofing properties of concrete surfaces. Izvestia KGASU **17**(18), 149–154 (2012)
5. Lapitsky, V.A., Kritsuk, A.A.: Physical and Mechanical Properties of Epoxy Polymers and Fiberglass. Naukova dumka, Kiev (1986)
6. Khozin, V.G.: Reinforcement of Epoxy Polymers. Publishing House of PIK "House of the Press", Kazan (2004)
7. Voronkov, A.G., Yartsev, V.P.: Optimization of the composition of polymer composites based on epoxy resins. Plastics **12**, 30–32 (2006)
8. Selyaev, V.P., Ivashchenko, Yu.G., Nizina, T.A.: Polymer Concrete: Monograph. Mordovia State University Press, Saransk (2016)
9. Startsev, V.O., Plotnikov, V.I., Antipov, Yu.V.: Reversible effects of moisture in determining the mechanical properties of PCM under climatic influences. Proc. VIAM **5**, 110–118 (2018)
10. Startsev, V.O., Molokov, M.V., Grebeneva, T.A., Tkachuk, A.I.: Dynamic mechanical and thermomechanical analysis of reversible plasticization of epoxy-diane resin-diaminodiphenylsulfon system by moisture. Poly. Sci. Ser. A **59**(5), 640–648 (2017)
11. Nizina, T.A., Nizin, D.R., Kanaeva, N.S., Kuznetsov, N.M., Artamonov, D.A.: Applying the fractal analysis methods for the study of the mechanisms of deformation and destruction of polymeric material samples affected by tensile stresses. Key Eng. Mater. **799**, 217–223 (2019)
12. Nizina, T.A., Nizin, D.R., Kanaeva, N.S.: Statistical analysis of the frequency of damage accumulation in the structure of epoxy composites under tensile loads. In: Klyuev, S., Lesovik, V., Vatin, N. (eds.) Innovations and Technologies in Construction. LNCE, vol. 95, pp. 1–8. Springer, Cham (2020)

Assessment of the Fungus Resistance of Cement Stone with a Biocide with Bacterial Cultures Used in Carbonate Biomineralization

U. N. Dukhanina , V. V. Nelyubova$^{(\boxtimes)}$, O. I. Drozdov ,
and D. A. Balitsky

Belgorod State Technological University named after V.G. Shukhov,
Belgorod, Russia
nelubova@list.ru

Abstract. The paper presents the analysis of the influence (joint and separate mutual) of bacterial cultures and an active biocidal component on the bacterio- and fungicidal properties of cement stone. The possibility of functioning of the bacterial microbiota in the conditions of biocorrosion, as well as in the presence of a biocidal additive in the composition of the cement system, was proved. The absence of a negative effect on the development of bacteria *S. Pasteurii, B. Megaterium, L. Sphaericus, B. pumilus* of 0.5% glutaraldehyde solution was experimentally proved. The fungus resistance of sample cubes modified with the active additive - glutaraldehyde, *Aspergillus niger* micromycete was determined. The greatest fungicidal effect was achieved using a solution of glutaraldehyde in the composition of a cement stone and a bacterial inoculum in an agar medium. Such a combined combination can be used to impart biostability to cement-based building materials.

Keywords: Biocorrosion · Carbonate biomineralization · Mold fungi · Glutaraldehyde

1 Introduction

The most negative impact affecting the durability of building composites is biological corrosion caused by the action of bacterial, fungal and other cultures. At the same time, micromycetes (mold fungi) are the most aggressive biodestructors, since they not only cause chemical damage to the cement matrix by waste products (acids), but also physical damage through the growth of the mycelium in the capillary-porous structure of the material to a considerable depth, damaging the integrity and leading to destruction [1–5]. The assessment of the state and changes in the properties of cement stone under conditions of biodegradation by means of field experiments is the evidence of the decrease in the operational properties of concrete products and structures [6, 7].

The use of chemical biocides is the main tool for the protection of concrete structures and buildings from biocorrosion. As a rule, the active additives are applied by coating the surface of a product. However, earlier the team of authors substantiated the possibility and efficiency of the use of biocides as a component of composite

building materials for the increase in their resistance in aggressive environment [8–13]. Another way to prolong the durability of a structure is to use components that restore naturally formed imperfections in the structure of composites. Thus, the use of bacterial cultures makes it possible to self-heal cracks in materials formed during operation due to clogging of voids as a result of carbonization [14, 15]. At the same time, it is obvious that the functioning of the bacterial microbiota, which initiates the formation of calcium carbonate crystals, in the exploited concrete materials is impossible under sterile conditions. The effectiveness of bacteria in terms of healing will depend on the composition and properties of the substrate on which they are applied: a material volumetrically or superficially modified with biocidal components can contribute to the decrease in their production capacity. In addition, the effects of the mutual influence of micromycetes and bacterial cultures are not fully studied. Insufficient development of this issue led to the need to establish the mutual influence of bacterial agents, as initiators of carbonate crystallization, and the aggressive microorganism-biodestructor *Aspergillus niger* under the conditions of a model experiment with the addition of glutaraldehyde.

2   Methods and Materials

The assessment of the combined and individual effects of the biocide and microorganisms was carried out by studying the system "bacteria - fungus - active component".

The following strains of the All-Russian collection of microorganisms of Institute of Biochemistry and Physiology of Microorganisms named after G.K. Scriabin of Russian Academy of Sciences were used: *Lysinibacillus sphaericus* (VKM B-509), *Bacillus megaterium* (VKM B-40), *Bacillus pumilus* (VKM B-23), *Sporosarcina pasteurii* (VKM B-513).

The choice was reasoned by the preliminary studies of the authors, proving their effectiveness as biological acceptors causing heterogeneous nucleation of calcium carbonate crystals [16].

As a micromycete, *Aspergillus niger* was used as one of the most aggressive species of mold fungi, the development of which on the surface of building objects causes the maximum degree of degradation effect due to its high survival rate.

The object of the study was the samples of cement stone, in which an aqueous solution of glutaraldehyde with the active substance concentration of 0.5% [13] was used as mixing water. The sample cubes with a rib size of 10 mm were molded with W/C 0.4 on the basis of CEM I 42.5 N Portland cement produced by Belgorodsky cement plant.

After molding, the cube samples were subjected to heat and moisture treatment according to the regime of 1.5 + 6 + 1.5 h at 60 °C. Then, the samples were disinfected by ultraviolet irradiation for 2 h in order to exclude the influence of other microorganisms on the experimental results. We compared them with control samples mixed with tap water.

The fungus resistance of cement stone was assessed by the growth of samples (the ability to grow and propagate on them) by mold fungi. The test was conducted according to Russian State Standard GOST 9.049–91 "Unified system of corrosion and

ageing protection. Polymer materials and their components. Methods of laboratory tests for mould resistance" (Method 3).

The evaluation of the fouling of the cement material by microscopic fungi was carried out using an AXIOSCOPEA1 biological microscope. The degree of development of fungi was evaluated on a 6-point scale, according to Russian State Standard GOST 9.048–89 (Table 1). The material has fungicidal properties if no fungi are found on its surface or the intensity of their development is estimated in less than 1 point.

Table 1. Scale of fungicidal properties.

Points	Characteristic of point
0	No spores and conidia germination was found under the microscope
1	Germinated spores and slightly developed mycelium were found under the microscope
2	Under the microscope, a developed mycelium was found, sporulation was possible
3	Mycelium or sporulation was barely visible, but it was clearly visible under a microscope
4	The development of fungi covering less than 25% of the test surface was clearly seen
5	The development of fungi was clearly visible, covering more than 25% of the test surface

To quantify the degree of growth retardation of colonies, we used the adapted Abbott equation [17]:

$$T = \frac{D_0 - D_k}{D_k} \cdot 100\% \tag{1}$$

T – inhibition (in percent) of the growth of micromycete colonies,

D_k – zone of fungicidal activity in the control sample,

D_0 – zone of fungicidal activity in the experiment.

The linear colony growth rate deceleration factor is a reliable quantitative indicator for the determination of biocidal activity of various substances. This method eliminates the "human factor" because the evaluation of fungicidal activity is mathematically calculated and visually very clear.

A dense Czapek-Dox agar medium inoculated with a bacterial culture of 10^8 CFU per 1 ml in the amount of 2 ml was used as a nutrient medium for the test culture.

The infection of the nutrient medium was carried out by spraying a solution containing the spores of the control fungus with a spray gun. After spraying, the samples of mortars were placed in the center of the Petri dishes. Then, closed Petri dishes were placed in a RI 115 thermostat with natural ventilation red LINE by Binder for 14 days at t = 30 °C, W = 90%.

The study of the morphology of microorganisms and the dynamics of biomass development was carried out by the method of light microscopy (laboratory microscope Axio Scope.A1, A-Plan 20 ×/0.45 and A-Plan 63 ×/0.1 objectives, C-mount adapter

0.63 × , camera ProgRes SpeedXTcore5) and using a stereoscopic microscope Lomo MSP-2 version 3.

3   Results and Discussion

In order to analyze the possible manifestation of the antifungal properties of bacterial cultures and assess the influence of each of the components of the system "bacterium – fungus – active component" (BFA), it was divided into subsystems: "bacterium – fungus" (BF), "bacterium – active component" (BA), "Fungi – active component" (FA). According to the obtained data (Table 2), the control composition without additives does not differ in fungal resistance: the germination of mycelium in the sample volume is clearly visible. Cement sample with the active component without bacterial cultures was characterized by fungicidal activity: a fungicidal zone was determined. At the same time, a slight infection of the sample with mold spores was found.

Table 2. Influence matrix of components in the system "bacteria - fungus - active component".

System	Bacterial culture	Evaluation of fungi growth, points	Material evaluation
Control (without additive)	–	4	Nonfungus-proof
FA	–	1	Fungicidal
BFA	S. pasteurii	0	Fungicidal
	B. pumilus	1	Fungicidal
	B. megaterium	1	Fungicidal
	L. sphaericus	0	Fungicidal
BF	S. pasteurii	1	Fungicidal
	B. pumilus	2	Fungus-proof
	B. megaterium	1	Fungicidal
	L. sphaericus	0	Fungicidal

The samples without additives contaminated with bacterial and mycelial cultures are fungicidal (Fig. 1): when using any type of bacteria, there is a slight infection of the samples with fungi. Nevertheless, the genus of bacteria *L. Sphaericus* is distinguished, in which the fungicidal zone increases from 19 to 23 mm, which is 20% more in comparison with the samples modified with biocide.

The infection with bacteria modified with glutaraldehyde of cement stone provides a persistent fungicidal effect: inhibition of fungal growth is determined, regardless of the type of bacterial culture. At the same time, the fungicidal zone varies within 23–38 mm. At the same time, spore germination and mycelium development are almost not observed.
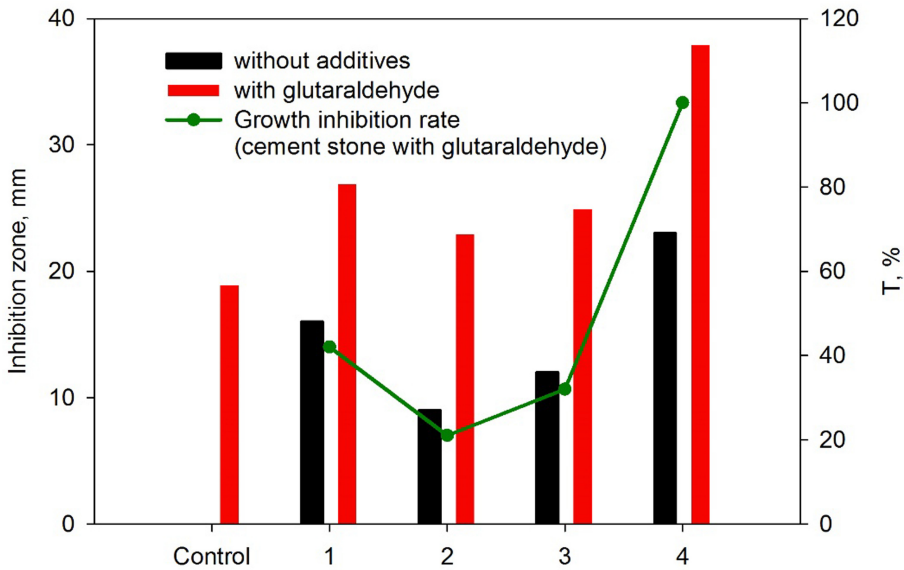
Fig. 1. Dependence of the size of the inhibition zone and the growth inhibition rate from the composition of the cement sample and the type of bacterial culture: 1 – *S. Pasteurii*; 2 – *B. Pumilus*; 3 – *B. Megaterium*; 4 – *L. sphaericus*.

It should be noted that the bacterial culture of *L. sphaericus*, used in jointly with the active component, provides complete suppression of the growth of micromycetes: the coefficient of inhibition of linear growth of the mold fungus is 100% (Fig. 1). The use of *S. Pasteurii* provides a suppression of mold by more than 40%. Cultures of *B. Pumilus* and *B. Megaterium* are characterized by less activity: the calculated coefficient of suppression of micromycete growth is 21 and 32%, respectively.

According to the research results, the absence of the bacteriostatic effect of glutaraldehyde on bacterial microorganisms used for carbonate biomineralization in a concentration of 0.5% solution in the composition of the cement matrix was determined, while maintaining the fungicidal effectiveness on *Aspergillus niger* micromycete. Moreover, in the samples with the addition of bacterial cultures, the zone of inhibition of *Aspergillus niger* growth was larger than in the samples without bacteria. A more pronounced antagonistic effect (growth inhibition) on the test culture was observed in the system of "bacterium – fungus – active component". Using the method of light microscopy, it was found that during the joint incubation of the culture broth of bacteria and micromycete spores, *Aspergillus niger* conidia did not germinate into the cement matrix.

Thus, due to the fact that molds have a high adaptive ability to changes in environmental factors and, in particular, to biocidal drugs, the combined fungicidal effect of glutaraldehyde and bacteria of the genus *Bacillus* may be promising in the fight against the fungus *Aspergillus niger* in operated concrete structures and buildings.

4   Conclusion

The authors carried out the comprehensive analysis of the joint and separate mutual influence of bacterial cultures and an active biocidal component on the bacterio- and fungicidal properties of cement stone. As a result it was found that the addition of a biocidal additive to the composition of cement samples, namely, glutaraldehyde, did not have a bactericidal effect on all tested bacterial strains. The high level of the resistance of cement materials to the type of test culture used during the application of the "bacterium - active component" system in comparison with the individual use of each component of the system allows forming the idea about the possibility of the use of carbonate biomineralization in conditions occurring in the natural environment with potential contamination of concrete with spores of *Aspergillus niger* micromycetes. Taking into account the comparative analysis of bacterial cultures according to the intensity of manifestation of fungicidal properties, they were ranked by the increase in the efficiency in the following sequence: *L. sphaericus* → *S. pasteurii* → *B. megaterium* → *B. pumilus*. The performed studies indicate the effectiveness of the complex modification of cement stone by volumetric (introduction of biocidal components) and surface (using carbonate biomineralization approaches) treatment to prolong the resistance of materials under conditions of biological corrosion.

References

1. Wei, S., Jiang, Z., Liu, H., Zhou, D., Sanchez-Silva, M.: Microbiologically induced deterioration of concrete - a review. Brazilian J. Microbiol. **44**(4), 1001–1007 (2014)
2. Estokova, A., Harbulakova, V.O., Luptakova, A., Kovalcikova, M.: Analyzing the relationship between chemical and biological-based degradation of concrete with sulfate-resisting cement. Polish J. Environ. Stud. **28**(4), 2121–2129 (2019)
3. Kip, N., van Veen, J.A.: The dual role of microbes in corrosion. ISME J. **9**(3), 542–551 (2015)
4. Strigáč, J., Martauz, P., Eštoková, A., Števulová, N., Luptáková, A.: Bio-corrosion resistance of concretes containing antimicrobial ground granulated blastfurnace slag BIOLANOVA and novel hybrid H-CEMENT. Solid State Phenom. **244**, 57–64 (2016)
5. Manzhilevskaya, S.E.: Environmental monitoring of ecological safety in areas of construction, reconstruction and operation of objects. Constr. Mater. Prod. **2**(3), 78–84 (2019)
6. Strokova, V.V., Nelubova, V.V., Rykunova, M.D., Dukhanina, U.N.: Strength and structure of cements tone exposed to domestic chicken coop. J. Phys: Conf. Ser. **1145**(1), 012015 (2019)
7. Strokova, V.V., Nelubova, V.V., Rykunova, M.D.: Resistance of cement stone in sanitation solutions. Mag. Civ. Eng. **90**(6), 72–84 (2019)
8. Do, J., Song, H., So, H., Soh, Y.: Antifungal effects of cement mortars with two types of organic antifungal agents. Cem. Concr. Res. **35**, 371–376 (2005)

9. Tokach, Y.E., Rubanov, Y.K., Vasilenko, M.I., Goncharova, E.N., Evtushenko, E.I., Kazaryan, S.A.: Design of new approaches and technological solutions of obtaining biocidal compositions to protect industrial and civil buildings and constructions against biodeterioration. Res. J. Appl. Sci. **9**(11), 774–778 (2014)
10. Otsokov, K.A.: Innovative technologies in construction and their use in organizational and technological events. Constr. Mater. Prod. **3**(1), 7–13 (2020)
11. Erofeev, V.T., Rodin, A.I., Bochkin, V.S., Jakunin, V.V., Chegodajkin, A.M., Kaznacheev, S.V.: Physico-mechanical characteristics of cement modified with mineral wool waste. Bull. BSTU named after V.G. Shukhov **10**, 10–15 (2018)
12. Denisova, Y.V.: On the use of fungicidal additives in the fight against biocorrosion of composite compounds. Bull. Sci Educ. North-West. Russia **1**, 81–87 (2015)
13. Strokova, V.V., Le Saout, G., Nelubova, V.V., Ogurtsova, Y.N.: Composition and properties of cement system with glutaraldehyde. Mag. Civ. Eng. **103**(3), 10307 (2021)
14. Strokova, V.V., Vlasov, D.Y., Frank-Kamenetskaya, O.V.: Microbial carbonate biomineralization as a tool of natural-like technologies in construction material science. Constr. Mater. **7**, 66–72 (2019)
15. Sazanova, K.V., Frank-Kamenetskaya, O.V., Vlasov, D.Y., Zelenskaya, M.S., Vlasov, A.D., Rusakov, A.V., Petrova, M.A.: Carbonate and oxalate crystallization by interaction of calcite marble with bacillus subtilis and bacillus subtilis–aspergillus niger association. Crystals **10**(9), 1–16 (2020)
16. Strokova, V.V., Duhanina, U.N., Balitsky, D.A.: Influence of medium composition on biomineralization and morphology of newgrowths. J. Phys: Conf. Ser. **1582**(1), 012083 (2020)
17. Abbott, W.S.: A method of computing the effectiveness of an insecticide. J. Econ. Entomol. **18,** 265−267 (1925)

Prospects for the Use of Neutron-Shielding Metal Hydride Materials in the Construction of NPP Power Units

R. N. Yastrebinsky[✉] , A. A. Karnauhov ,
and A. V. Yastrebinskaya

Belgorod State Technological University named after V.G. Shukhov,
Belgorod, Russia
`yrndo@mail.ru`

Abstract. A technology has been proposed for increasing the thermal stability of titanium hydride by spraying metallic copper atoms onto its spherical granules. The method of quadrupole magnetron sputtering is used, which is based on low-temperature ion sputtering of a copper target on the surface of a metal hydride substrate. The microstructure of the surface of the modified fraction of titanium hydride is investigated. It is shown that the surface has a granular structure with a grain size of 25–50 nm. In some areas of the surface, grain alignment is observed in a specific direction, indicating a uniform texture of the applied copper surface layer. The metallized copper coating fills in surface defects and creates a shell that prevents thermal diffusion of hydrogen into the environment. The thickness of the deposited metallic copper on the surface of the shot is on average 400 nm. The phase composition of the surface layer of the samples of modified and unmodified hydride fraction is estimated by the method of electron probe analysis. It is shown that as a result of modification, the thermal stability of titanium hydride increases to 700 °C.

Keywords: Titanium hydride · Modification · Deposition · Copper sheath · Structure · Thermal stability

1 Introduction

Russia is one of the countries with developed nuclear energy, which is one of the most important economic sectors and has great prospects in terms of its further development. In Russia, ten nuclear power plants operate thirty-five power units with a total installed capacity of 27900 MW. Eighteen with pressurized water-moderated thermal neutron reactors (VVER) with electric power from 440 to 1200 MW (Balakovskaya, Kalininskaya, Kola, Novovoronezh, Rostov NPP). Fifteen graffiti-water channel thermal neutron power units, including the RBMK type (Kursk, Leningrad, Smolensk NPP) and EGP-6 (Bilibino NPP). Two fast neutron power units with a capacity of 600 and 800 MW (Beloyarsk NPP) [1, 2].

One of the promising areas is the development of the «Breakthrough» project – «BREST-OD-300» lead-cooled fast nuclear reactors that implement a closed nuclear

fuel cycle (NFC) (construction starts in 2018) within the framework of the «Federal Target Program Nuclear Power Technologies of a New generation for the period 2010– 2015 and for the future until 2020» [3]. The «Breakthrough» project is considered as a module for reprocessing spent nuclear fuel (spent nuclear fuel). The design of the BREST nuclear installation was carried out by «NIKIET im. N.A. Dollezhal» [4, 5].

One of the important components of the energy strategy is «modernization, extension of the operating life of existing power units and an increase in the installed capacity utilization factor at all stages» [6].

In total, 59 power units of various types are under construction in the world, 165 power units are closed [7]. Nuclear energy provides, on average, about 17% of world energy production, with the main contribution being made by the United States, France, Japan and China [8]. The Japanese nuclear park has 42 nuclear reactors. In China, from 2005 to 2017, 27 VVER-type power units and an experimental fast breeder reactor (CEFR) were put into operation, and 20 power units are under construction. The United States is the world's largest nuclear energy producer with 99 operating nuclear power units. The IEA predicts that US nuclear power capacity will increase by 16% by 2040. France currently ranks second in the world in terms of the number of operating reactors (58) and first in terms of the share of generated nuclear energy (72.3%) [9].

Safety remains a priority in the operation and development of new NPP designs. The safety of nuclear power plant reactors is understood as a set of measures, technological and operational properties that prevent the negative impact of ionizing radiation on personnel, the public and the environment, and also ensure the established radiation exposure standards and the accident-free service life of a nuclear reactor. NPP safety must be ensured by using highly efficient structural materials, taking into account the current levels of scientific and technological development [10, 11].

In matters of NPP safety, an important role is assigned to the structures and properties of containment shells. The main requirement for materials for radiation protection of nuclear reactors of nuclear power plants is the ability to effectively attenuate neutron and gamma radiation to the established standards, to provide both the protection of maintenance personnel and the protection of electronic and technological equipment of a nuclear facility.

The physical processes of attenuation of reactor radiation by shielding materials are based on inelastic scattering of neutrons by nuclei of heavy elements (metals) and elastic scattering by nuclei of light elements (usually hydrogen). In this regard, for effective radiation protection of nuclear facilities, a combination of nuclei of heavy and light elements or the use of layer-by-layer shields with alternating light and heavy uniform shields is necessary [12]. In this direction, the most promising is the use of metal-hydrogen materials, due to their high efficiency for both neutron and gamma radiation. A special type of metal-hydrogen protection is made up of metal hydrides, in particular, lithium, zirconium and titanium hydrides. Despite their higher cost, they are the most promising materials for heat-resistant structures of metal-hydrogen shields used for ship and space nuclear power. Thus, the relaxation lengths of the neutron dose rate for hydrogenated metal plates based on titanium and zirconium hydride for the equilibrium spectrum region are, respectively, 5.5 and 7.3 cm [13–15]. The disadvantage of hydrogenated titanium and zirconium metal matrices is the complexity of

the production technology, insufficient thermal stability and low structural properties (brittleness).

This problem was partially solved by using titanium hydride shot obtained by saturation of titanium shot with hydrogen under pressure [16]. This technology allows titanium hydride to be used as a concrete filler, which provides structural protection properties. However, the possibility of cracking in hydrogenated titanium shot reduces its thermal stability to 250–300 °C due to hydrogen diffusion, which significantly limits the possibility of its use for radiation protection of nuclear reactor facilities.

In this regard, the authors considered the possibility of modifying a titanium hydride shot by applying multifunctional nanocomposite coatings in order to increase its thermal stability for effective use as a neutron-shielding material for power units operating at increased radiation and thermal loads.

2   Methods and Materials

Used titanium hydride in the form of spherical granules (shot) with a diameter of 0.6–2.5 mm. Titanium hydride is synthesized from spongy titanium grade TG-90 in accordance with GOST 17746-79 by laboratory technology developed at Federal State Unitary Enterprise "Mayak Production Association" State Enterprise "Rosatom" (Ozersk). The density of the shot is 3800 kg/m^3, the bulk density is 2640 kg/m^3, the hydrogen content is 3.6 wt%.

The deposition of multifunctional nanocomposite coatings on the titanium hydride surface was carried out by the method of quadrupole magnetron sputtering on a QUADRA 500 setup at a power of 40 kW. A copper metal plate 400 × 100 × 5 mm in size was used as a target. Before the deposition process, the surface of the shot samples was preliminarily subjected to cleaning with an ion source of an ion beam with an energy of 1–1.5 keV. The working gas is argon at a pressure of 6 • 10^{-2} Pa.

The evaluation of the surface microstructure of the titanium hydride fraction was examined on a TESCAN MIRA 3 LMU high-resolution scanning electron microscope.

The phase composition of the titanium hydride fraction before and after heat treatment was carried out by electron probe microanalysis on an X-MAX 50 Oxford Instruments energy dispersive spectrometer with an active crystal area of 50 mm^2.

3   Results and Discussion

In the course of the studies carried out on samples of titanium hydride shot, micrographs of their surface were obtained with various magnifications. Figure 1 shows micrographs of a titanium hydride shot sample without a protective metallized coating.

Analysis of micrographs shows the presence of irregularities and roughness on the surface of the titanium hydride shot, as well as microcracks, the formation of which is due to different rates of hydrogen diffusion into the surface layers during the hydrogenation of titanium metal shot. During the heat treatment of the unmodified fraction of titanium hydride, an increase in microcracks occurs, through which active hydrogen evolution occurs.
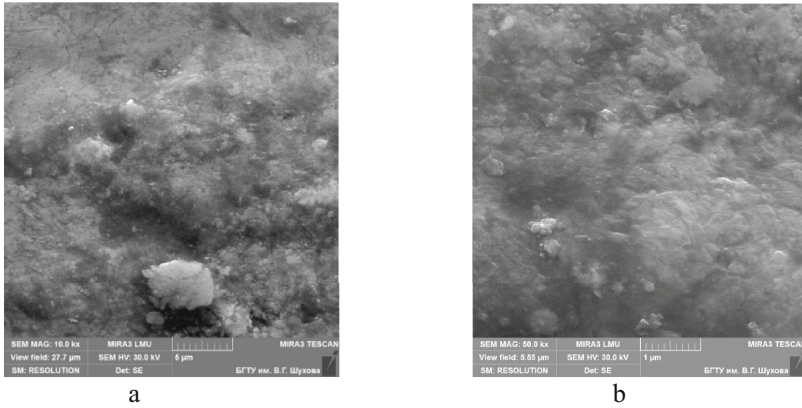
Fig. 1. Micrographs of the surface of the titanium hydride shot: magnification 10,000 times (a); 50,000 times magnification (b).

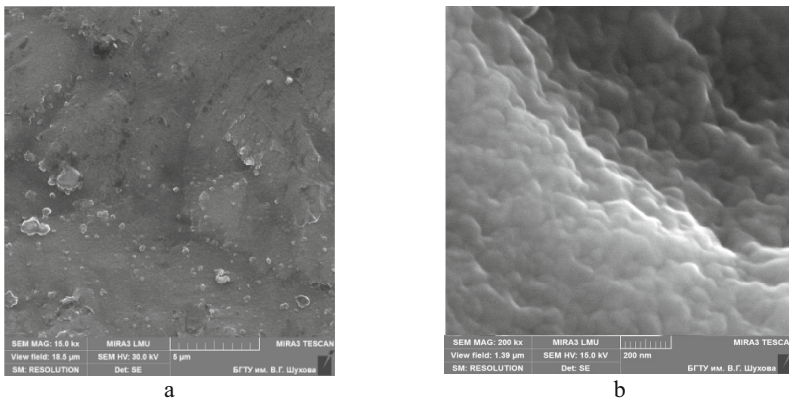Figure 2 shows micrographs of a titanium hydride shot sample with a protective metallized copper coating.

Fig. 2. Micrographs of the surface of titanium hydride shot, modified with copper coating: magnification 15000 times (a); an increase of 200,000 times (b).

Analysis of micrographs of the surface of a titanium hydride shot modified with copper metal showed that the microstructure of its surface is rougher than that of a titanium hydride shot sample without metallized spraying. The surface has a granular structure with a grain size of 25–50 nm. In some areas of the surface, grain alignment is observed in a specific direction, indicating a uniform texture of the applied copper surface layer. As on the surface of a titanium hydride shot without a metallized coating, on the surface of a titanium hydride shot with modified copper there is also an oxide film of copper, which prevents the free evolution of hydrogen.

The absence of microcracks and the smoother surface of the modified titanium hydride shot indicates that the deposited metallized copper coating fills in surface defects and creates a shell that prevents thermal diffusion of hydrogen into the environment. In this case, the surface is smoothed and the titanium hydride granules are hardened due to additional surface metallization.

To determine the thickness and structure of the deposited copper coating, the modified titanium hydride shot was cleaved. In Fig. 3 shows micrographs of a cleaved titanium hydride shot with a protective metallized coating in the form of copper. The thickness of the deposited metallic copper on the surface of the shot is on average 400 nm. The interface of the applied copper coating is clearly defined throughout the survey area. The coating has a homogeneous structure and adheres tightly to the surface of the shot.

a   b
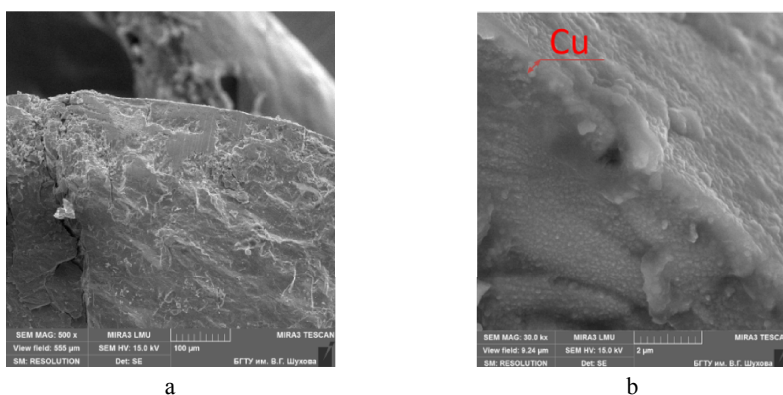
Fig. 3. Micrographs of a cleaved titanium hydride shot containing a copper coating: an increase of 500 times (a); an increase of 30,000 times (b).

Table 1 shows the data of the electron probe analysis of the phase composition of the surface layer of the samples of modified and unmodified hydride shot, heat treated at temperatures from 100 to 900 °C.

Table 1. Phase composition of surface layers of unmodified (1) and modified (2) titanium hydride fractions at different temperatures.

Phase content. masses. %	Shot processing temperature									
	100 °C		300 °C		500 °C		700 °C		900 °C	
	1	2	1	2	1	2	1	2	1	2
Ti	32.4	32.6	15.1	15.3	42.6	12.6	22.5	20.6	–	–
TiH$_n$	67.6	67.4	84.9	84.7	57.4	87.4	21.9	78.2	–	–
TiO$_2$	–	–	–	–	–	–	55.6	1.2	100	100

Analysis of the table shows that during the heat treatment of the unmodified and modified fraction of titanium hydride up to 300, approximately the same ratio between the metal and hydride phases is maintained. Starting from 500 °C, an increase in the hydride phase in the surface layer of the modified shot occurs due to the hydrogenation of metallic titanium. In this case, the presence of a protective metal shell prevents the removal of hydrogen into the surrounding space. Reverse processes occur in unmodified shot, where an increase in the phase of metallic titanium is observed due to the processes of dehydrogenation and removal of hydrogen into the environment. These processes develop up to 700 °C, where a significant formation of rutile occurs for unmodified shot. The modified shot, due to the presence of a copper shell, almost completely retains its thermal stability.

Thus, the presented data indicate the possibility of increasing the thermal stability of a titanium hydride fraction by modifying it by magnetron sputtering of metallic copper. At the same time, due to the creation of a copper shell, a diffusion barrier is created for hydrogen atoms, which prevents their removal into the environment.

4   Conclusion

1. An increase in the thermal stability of titanium hydride opens the way for its application to ensure effective radiation protection of nuclear reactors at nuclear power plants.
2. A technology has been proposed for increasing the thermal stability of titanium hydride by spraying metallic copper atoms onto its spherical granules. The method of quadrupole magnetron sputtering is used, which is based on low-temperature ion sputtering of a copper target on the surface of a metal hydride substrate.
3. Creation of a copper shell creates a diffusion barrier for hydrogen atoms, preventing their removal into the environment. As a result of modification, the thermal stability of titanium hydride increases to 700 °C.

5   Acknowledgements

References

1. Sickafus, K.E.: Radiation-induced amorphization resistance and radiation tolerance in structurally related oxides. Nat. Mater. **6**(3), 217–223 (2007)
2. Fukai, Y.: The Metal-Hydrogen System. Basic Bulk Properties, vol. 21, p. 1237. Springer, Cham (1993)
3. Cherkashina, N.I., Pavlenko, A.V.: Influence of SiO_2 crystal structure on the thermal cycle of polymer composites. Constr. Mater. Prod. **1**(4), 21–29 (2018)

4. Pavlenko, V.I., Cherkashina, N.I., Yastrebinsky, R.N.: Synthesis and radiation shielding properties of polyimide/Bi2O3 composites. Heliyon **5**, E01703 (2019)
5. Nasseri, M.M.: Comparison of HfB_2 and ZrB_2 behaviors for using in nuclear industry. Ann. Nucl. Energy **114**, 603–606 (2018)
6. Sorokin, V.V., Sharapov, O.N., Shunkin, N.M., Kiryushina, N.Y.: New polymeric composites based on epoxy resin with techogenic wastes. Bull. BSTU Named After V.G. Shukhov **6**, 8–13 (2019)
7. Pavlenko, A.V., Cherkashina, N.I., Yastrebinski, R.N.: Nanodisperse metalloorganosiloxane fillers of polymers. Nanotech. Constr. Sci. Internet J. **8**(4), 113–130 (2016)
8. Pavlenko, A.V., Cherkashina, N.I., Noskov, A.V.: Calculation of the frequency electronic transmission factors at the passage through the polymeric polyimide composite material filled by bismuth silicate. Probl. Atomic Sci. Technol. **5**, 21–26 (2017)
9. Cherkashina, N.I., Pavlenko, V.I., Yastrebinskii, R.N.: Phase transitions and electrophysical properties of tungsten(VI) oxide in a 83–673 K temperature range. Russ. Phys. J. **62**(5), 870–875 (2019)
10. Pavlenko, V.I., Edamenko, O.D., Cherkashina, N.I., Kuprieva, O.V., Noskov, A.V.: Study of the attenuation coefficients of photon and neutron beams passing through titanium hydride. J. Surf. Invest. **9**(3), 546–549 (2015)
11. Pavlenko, A.V., Cherkashina, N.I., Yastrebinski, R.N.: Nanodisperse metalloorganosiloxane fillers of polymers. Nanotech. Constr. Sci. Internet J. **8**(4), 113–130 (2016)
12. Yastrebinsky, R.N., Karnauhov, A.A., Yastrebinskaya, A.V.: Improving the radiation-thermal stability of titanium hydride. J. Phys. Conf. Ser. **1515**, 1–6 (2020)
13. Guseynov, R.M., Radzhabov, R.A., Magomedova, U.M.: The element with constant phase shift in galvanodynamic mode. Chem. Bull. **2**(2), 4–8 (2019)
14. Slyusar', O.A., Yastrebinskii, R.N., Cherkashina, N.I., Doroganov, V.A., Yastrebinskaya, A.V.: Effect of additives on dispersed system structure formation. Refract. Ind. Ceram **55**(6), 562–564 (2015)
15. Shestakov, I.Ya., Veretnova, T.A., Strekalova, T.A.: Investigation of water electrical activator with coaxial arrangement of electrodes. Chem. Bull. **4**(1), 12–18 (2018)
16. Choi, E., Ejiri, H.: Search for time-correlated fast neutrons from DD fusion at room temperature. Japanese J. Appl. Phys. A **5**(35), 2793–2796 (1996)

Experimental Research of the Process Bio-corrosion of Cement Concrete for Inspection of Building Structures

S. V. Fedosov[1] , V. Eu. Roumyantseva[2] , S. A. Loginova[2(✉)] ,
and I. N. Goglev[3]

[1] National Research Moscow State Civil Engineering University,
Moscow, Russia
[2] Ivanovo State Polytecnic University, Ivanovo, Russia
fedosov-academic53@mail.ru
[3] Joint Stock Company «Construct and Technology Bureau of Concrete
and Reinforced Concrete», Moscow, Russia

Abstract. The article presents the results of various tests of cement concretes in the research of the process of their biological corrosion, as one of the factors that reduce the durability of concrete and reinforced concrete building structures during their inspection. During the experimental research, microbiological diagnostics was performed, the results of which revealed the taxometric composition of biofilms. The results of taxometric analysis revealed that the biofilm is formed by spores and vegetative forms of bacteria Bacillus subtilis, Nitrosomonas, Lactobacterium, Desulfovibrio, as well as some forms of actiomycetes and micromycetes. The results of strength tests in the framework of experiments showed that the process of biocorrosion significantly affects the loss of strength of cement concretes. The graphs of changes in the profiles of Ca^{2+} cation concentrations in the liquid phase showed increased values compared to conventional uninfected cement concrete, which is caused by the action of waste products of fungi of the genus Aspergillus niger and bacteria of the genus Bacillus subtilis. The results of measuring the pH level of the medium of concrete samples showed that the action of fungi of the genus Aspergillus niger and bacteria of the genus Bacillus subtilis contributes to an increase in the pH value of the hydrogen index in comparison with uninfected samples.

Keywords: Corrosion · Inspection · Biocorrosion · Fungi · Bacteria · Target component · Strength · Ph · Durability

1 Introduction

In inspecting building structures of buildings and structures survey specialists rarely pay attention to the study of the component of biological corrosion of cement concretes [1, 2]. Usually, biological corrosion of cement stone is reduced to chemical corrosion (interaction of reaction products of microorganisms), which ultimately leads to its degradation and destruction [1, 2].

However, a detailed research of the process of biological corrosion is necessary when analyzing the resistance of cement stone, since it will allow us to conclude that it is durable in conditions of active activity of microorganisms [1–4].

The process of biological corrosion of concrete is associated with the course of chemical reactions of products of microorganisms (bacteria and fungi) with one of the main components (target component) of hardening concrete – free calcium hydroxide [5]. Such processes cause accelerated diffusion of the target component from the concrete pores, followed by its neutralization [5, 6]. Thus, the biological corrosion of cement concretes is described using heat and mass transfer mechanisms [2–8].

The purpose of the research is to identify patterns of influence of fungi of the genus Aspergillus niger and bacteria of the genus Bacillus subtilis on changes in the strength characteristics of cement concrete, the concentration of the target component and changes in its pH.

The aim of the research is to explain the results obtained in terms of reliability and durability of cement concretes based on the analysis of theoretical and experimental data and to explain the degree of influence of biocorrosion on the state of technical condition of building structures during the survey of buildings and structures.

2   Methods and Materials

The following equipment was used in the production of concrete samples and weighing of additive components: electric manual vibrator Zitrek Z-35-1.5, electronic scales Mucheng 0.1–500 (weighing accuracy 0.1–500g).

An electron microscope was used to study the microstructure of the surface of cement samples Meiji Techno (Japan). When studying the concentration of calcium hydroxide in pore solutions of samples, the method of complexometric titration was used. For sample solutions also using a portable certified pH meter Testo 206 PH1 (Fig. 1a) the values of pH were measured to determine their corrosion resistance.

For testing control samples in the experimental part the following devices and equipment were used: a test press Matest C055N (Fig. 1b), a digital SLR camera with the ability to quickly shoot the Canon 1200D brand.

The strength of the control samples was determined by the destructive testing method [9, 10]. Processing of the obtained numerical data and plotting were performed in the software package Microsoft Excel 2010.

As a destructive control, the method of testing the strength of concrete according to control samples was used, in accordance with GOST 10180-2012 "Concrete. Methods for determining strength from control samples". The essence of the method is the destruction of a concrete sample on a test press, which will provide data on the actual breaking load for concrete, which determines the concrete's compressive strength class [9–13].

For destructive testing, samples-cubes of $3 \times 3 \times 3$ cm in size were made from cement dough of normal density (V/C = 0.3) prepared by mixing portland cement M500D0 with distilled water. The concrete mix was compacted during mixing using a manual electric vibrator. After initial hardening, the samples were placed in a wet

Fig. 1. a) Portable certified pH meter by brand Testo 206 PH1; b) Testing press by brand Matest C055N.
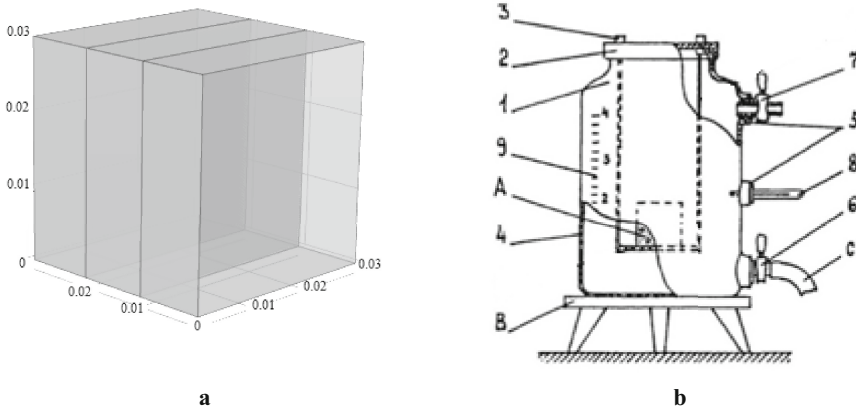

Fig. 2. a. Scheme of the corrosion test sample (dimensions are shown in meters). b. Device for studying corrosion processes of building materials: 1-vessel; 2-cover; 3-fastening element; 4-vessel wall; 5-holes; 6 and 7-shut-off devices; 8-thermometer; 9-dimensional scale; A - sample of building material; B - stand; C - drain hose.

hardening chamber at atmospheric pressure (humidity 99÷100%). After a certain period of hardening, the compressive strength of the samples was determined by breaking on a certified press.

For corrosion tests samples-cubes of $3 \times 3 \times 3$ cm in size made of portland cement of the M500D0 with a water-cement ratio V/C = 0.3. The system under study was made up of tightly fitted $1 \times 3 \times 3$ cm plates (Fig. 2a). The method of testing the corrosion resistance of concrete in aggressive environments corresponds to GOST 27677-88 "Corrosion protection in construction. Concretes. General requirements for testing" (Supplement 1).

For conducting corrosion tests, we used our own development "Device for studying the corrosion processes of building materials" (Fig. 2b) [9–14, 15].

All obtained results of strength characteristics and pH values of solutions were averaged and entered in tables.

3   Results and Discussion

Data on determining the compressive strength of concrete by destructive testing are included in Table 1.

Table 1. Results of strength tests by destructive testing of samples after exposure to various aggressive environment.

№ of sample	Sample type	Test method	Average compressive strength of cement stone during the hardening period of 28 days, MPa	Average compressive strength during 90 days in an aggressive environment, MPa
1	Samples not exposed (K-1)	Destructive testing according to GOST 10180-2012	42.02	36.17
2	Samples after exposure to water (K-2)	Destructive testing according to GOST 10180-2012	42.5	33.74
3	Samples subject to bacterial corrosion (K-3)	Destructive testing according to GOST 10180-2012	41.94	21.96
4	Samples subject to fungal corrosion (K-4)	Destructive testing according to GOST 10180-2012	43.4	19.64

Data from electron microscopy of the surface of concrete samples during corrosion tests for a period of 90 days and data from electron microscopy of the surface of concrete samples during corrosion tests for a period of 28 days are shown in Fig. 3a, b.

a   b

Fig. 3. a. Image (x60) of the cement stone surface in case of biodamage. b. Image of the cement stone surface in case of bio-damage in the period of 28 days.

Data on the dynamics of changes pH various of concrete samples are shown in Table 2.

Table 2. Change in the pH of the solution test samples.

pH	τ, days							
	0	14	28	42	56	70	84	98
	Samples is not exposed to microorganisms							
K-1, K-2	6.60	7.40	7.63	7.70	7.75	7.80	7.95	7.98
	Samples exposed to bacteria							
K-3	6.60	7.50	7.65	7.75	7.94	8.62	8.77	8.82
	Sample, exposed to the action of micromycetes							
K-4	6.60	7.66	7.82	7.91	8.6	8.84	8.96	9.02

Data on the content of calcium hydroxide in the pores of concrete samples and data on changes in the concentrations of the target component in the pore solution from coordinates are shown in Table 3.

Table 3. Changes in the concentrations of "free" calcium hydroxide in the pore solution of the sample from time to time and coordinates.

Time		Concentration, $kg_{CaO}/kg_{conc} *10^{-4}$ at the point with the coordinate		
		$x_1 = 0.005$ m	$x_2 = 0.015$ m	$x_3 = 0.025$ m
With bacterial exposure				
τ_0	0 day	2.47	2.47	2.47
τ_1	14 day	2.47	2.23	1.93
τ_2	28 day	2.38	1.98	1.76
τ_3	42 day	2.16	1.81	1.48
τ_4	56 day	1.88	1.53	1.23
τ_5	70 day	1.68	1.45	1.20

Table 3. (*continued*)

Time		Concentration, kg_{CaO}/kg_{conc} $*10^{-4}$ at the point with the coordinate		
		$x_1 = 0.005$ m	$x_2 = 0.015$ m	$x_3 = 0.025$ m
With fungal exposure				
τ_0	0 day	2.47	2.47	2.47
τ_1	14 day	2.47	2.15	1.84
τ_2	28 day	2.28	2.01	1.59
τ_3	42 day	2.12	1.69	1.24
τ_4	56 day	1.81	1.41	1.07
τ_5	70 day	1.49	1.25	1.01

Based on the numerical values of Table 3, profiles of the target component concentrations were constructed over the thickness of the cement stone sample in the water environment at various time intervals (Fig. 4 a, b). The obtained data are necessary for calculating and checking the physical and mathematical model for adequacy, which will allow determining the durability of concrete and reinforced concrete structures during their biological corrosion [9–14].
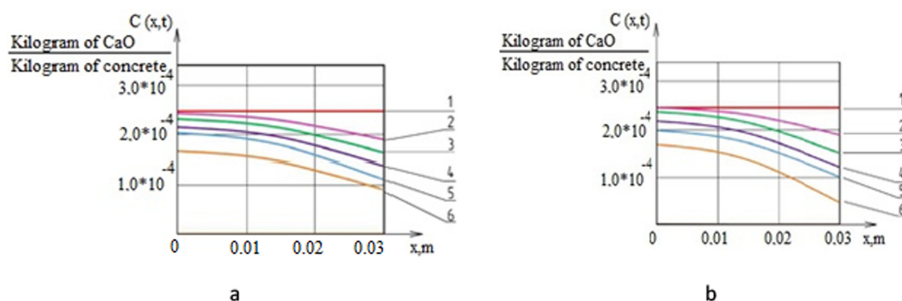
Fig. 4. Profiles of the concentrations of $Ca(OH)_2$ by the thickness of the cement stone sample in an aqueous medium at different time intervals (τ: 1 – 0 day; 2–14 day; 3–28 day; 4–42 day; 5–56 day; 6–70 day); (a) - for bacterial corrosion; (b) - for fungal corrosion.

4   Conclusions

Analyzing the results of the experiments, we can draw the following logical conclusions:

- the process of biological corrosion causes an increase in the diameter and width of the opening of the pores of the cement stone in comparison with the initial one by approximately 2–2.5 times;

- taxometric analysis of the experimental results showed that the main producers of citric, oxalic, malic, succinic and fumaric acids on the surface of cement stone are fungi of the genus Aspergillus niger;
- the process of biological corrosion in the water environment causes an increase in the content of calcium cations Ca^{2+} in the solution, which is associated with the process of neutralization of the products of microorganisms, in this case, organic acids;
- the mass transfer process that occurs during biological corrosion of cement stone causes a decrease in its strength by 27–40% compared to the impact of the water environment from the initial strength of samples aged 28 days;
- evaluation of the strength characteristics of cement stone can also serve as a criterion for its fungal resistance, which is confirmed by experimental data;
- changes in the pH of the solution have a noticeable effect on the growth of microorganisms, changing their activity and the degree of enzyme synthesis;
- biocorrosion caused by the action of Aspergillus niger and Bacillus subtilis contributes to an increase in the pH of the pore solution of cement stone, which causes alkalinization of the medium to allow the process of neutralization of the resulting organic acids.

The experimental data obtained made it possible to plot concentration profiles of $Ca(OH)_2$ by the thickness of a cement stone sample in an aqueous medium at different time intervals, which allows performing calculations in a physical and mathematical model in order to determine the durability of concrete and reinforced concrete structures during their biological corrosion. Also the obtained data will allow to determine the biostability of cement stone (including by indirect signs), which can be successfully implemented in the practice of inspection of building structures of buildings and structures and carrying out work on scientific and technical support of construction [1, 2, 6–14].

References

1. Roumyantseva, V.E., Goglev, I.N., Loginova, S.A.: The use of field and laboratory methods for the determination of carbonization, chloride and sulphate corrosion at inspection constructions of buildings and structures **15**(67), 51–58 (2019)
2. Fedosov, S.V., Roumyantseva, V.E., Konovalova, V.S., Goglev, I.N., Narmaniya, B.E.: Control of corrosion destruction processes of building materials on the basis of mass transfer laws. Bull. Civil Eng. **3**(74), 106–111 (2019)
3. Fedosov, S.V., Roumyantseva, V.E., Krasilnikov, I.V., Konovalova, V.S.: Physical and mathematical modelling of the mass transfer process in heterogeneous systems under corrosion destruction of reinforced concrete structures. In: IOP Conference Series: Materials Science and Engineering, p. 012039 (2019)
4. Roumyantseva, V.E., Loginova, S.A., Narmaniya, B.E.: Evaluation of biological resistance of cement concrete Materials of I scientific and practical forum "SMARTBUILD", the 100th anniversary of construction education in the Ivanovo region and the creation of the faculty of civil engineering Ivanovo-Voznesensky Polytechnic Institute, pp. 109–111 (2018)

5. Fedosov, S.V., Roumyantseva, V.E., Loginova, S.A., Narmaniya, B.E.: Features of mathematical modeling for bacterial corrosion of cement stone Current issues of architecture and construction. In: Proceedings of the Eighteenth International Scientific and Technical Conference: in 2 parts, pp. 348–353 (2019)
6. Chesnokova, T.V., Roumyantseva, V.E., Loginova, S.A.: Modeling the concrete bio destruction process at the textile industries News of higher educational institutions. Text. Ind. Technol. **1**(385), 206–212 (2020)
7. Loginova, S.A.: Influence of microorganisms on the phase composition of cement stone Engineering and social systems. Collection of scientific papers of the Institute of architecture, construction and transport of IVSPU, pp. 8–11 (2020)
8. Loginova, S.A.: Testing of cement stone for the ability to serve as a power source for biodegraders Engineering and social systems. Collection of scientific papers of the Institute of architecture, construction and transport of IVSPU, pp. 3–7 (2020)
9. Meza, A., Sánchez, C., Ortiz, J., Peralta, L.: Comparison between destructive and nondestructive tests in the evaluation of abrasion resistance of concrete. J. Test. Eval. **46**(3), 906–912 (2017)
10. Serebryakov, A., Chirkin, M., Mishin, V., Klimakov, V., Davydov, G., Gorlin, O., Ulitenko, A.: Electronic system of non-destructive buildings and structures condition control. In: 8th Mediterranean Conference on Embedded Computing, MECO 2019 – Proceedings (2019)
11. Fedosov, S.V., Roumyantseva, V.E., Konovalova, V.S., Goglev, I.N.: The influence of structure formation conditions of the composite on the mass transfer processes. In: Materials Science and Engineering. International Science and Technology Conference "FarEastCon 2019", pp. 42–47 (2020)
12. Fedosov, S.V., Roumyantseva, V.E., Konovalova, V.S., Goglev, I.N.: Mass transfer phenomena in the system "cement mortar-fiberglass reinforcement" at the stage of composite structure formation. Part 1. Physical representations and mathematical formulation of the problem Academia. Architecture and Construction, pp. 118–123 (2020)
13. Roumyantseva, V.E., Goglev, I.N., Loginova, S.A., Truntov, P.S., Burkov, A.A.: Development and research of properties cement concrete hardening accelerator additive based on a mixture of inorganic fluorine-containing salts. In: IOP Conference Series: Materials Science and Engineering. International Science and Technology Conference "FarEastCon 2019", p. 052026 (2020)
14. Fedosov, S.V., Roumyantseva, V.E., Konovalova, V.S., Loginova, S.A.: Mathematical modelling of diffusion processes of mass transfer of "free calcium hydroxide" during corrosion of cement concretes. Int. J. Comput. Civil Struct. Eng. **14**(3), 161–168 (2018)

Use of Chalk-Marl Rocks as a Base for Designing Pile Foundations

S. A. Gubarev[(✉)] and T. G. Kalachuk

Belgorod State Technological University named after V.G. Shukhov,
Belgorod, Russia
gubarev.sereja@yandex.ru

Abstract. This paper presents the most common physical and mechanical properties of chalk, which are necessary for calculating the foundations of buildings and structures, in particular pile foundations, by limit states and recommendations for choosing the type of foundations. Special (specific) properties of chalk as an residual soil (its fragmentation, non-uniformity, presence of large inclusions) create significant difficulties in studying its physical and mechanical properties in the process of engineering and geological surveys, as laboratory equipment available in survey organizations for determining the physical and mechanical properties of soils is of little use for determining the strength and deformative properties of chalk. This fact, unfortunately, contributes to the fact that the physical and mechanical properties of chalk rocks are calculated indirectly (by static and dynamic sounding, etc.), which invariably leads to miscalculations in the assessment of its properties. This, in the end, leads to the fact that the data available after engineering surveys on the characteristics of chalk are used to obtain results, in particular for calculating foundations and bases by limit states, which further contributes to large errors in the obtained values.

Keywords: Chalk · Foundation · Piles · Deformations · Marl · Strength

1 Introduction

In Russia and the CIS countries, there are a large number of chalk deposits, the most common of which are white writing chalk and marl. Cretaceous deposits, for the most part, are located at a shallow depth or come to the surface of the day, which implies the construction of foundations of various structures on them, and it is also very likely that they lie within the active zone of structures.

Most often, the upper layers of Cretaceous deposits are represented by white writing chalk, the tiers of the Cretaceous period of which belong to the upper Cretaceous division ($\mathcal{K}_2$), marl, unlike chalk, is extremely rare in the upper Cretaceous.

Chalk, as a rock, according to the SP section, is a representative of semi-basement soils, but there is a well-known fact that in the roof chalk is destroyed (changed) by weathering processes to a depth of 20.0 m, i.e. chalk is a residual soil and has a number of specific properties as a product of weathering of the bedrock [1].

Chalk, as the base of structures, has many physical and mechanical properties, which are invariably associated with a variety of factors (geomorphological

confinement, depth of occurrence, hydrogeological conditions, however, in the roof of chalk deposits, individual areas can be distinguished hypsometrically, within which its characteristics change to a certain depth within the limits not exceeding the specified limits according to GOST 20522-2012.

2 Materials and Methods

The question of the peculiarities of the deformation properties of chalk is also insufficiently studied, which causes certain difficulties in calculating the base for the second limit state (for deformations). The existing references in the literature practically do not allow identifying the dependence of the parameters of the deformation properties of chalk on its physical state (density, humidity, degree of preservation of structural connections) and the intensity of the load. Very serious problems arise in front of the builders (especially pressure equipment) in connection with the fracturing of the Cretaceous arrays. The water permeability of chalk through the pores is negligible (the filtration coefficient is approximately 10^{-5}–10^{-6} cm/s) and has no practical significance from the point of view of filtration capacity. It is more than 500 times lower than the values obtained by field experiments. The water content of the chalk is due only to the fracturing noted above. In the absence of cracks, chalk serves as a water-resistant horizon. The presence of open fractures can lead to significant water leaks from reservoirs and the inability to provide the required pressure horizon [8].

The classification of chalk by the number of plasticity to a variety of clay soil, followed by the use of the table method SP 24.13330.2011 to determine the depth of sinking piles and their load-bearing capacity, leads to clearly underestimated values of the load-bearing capacity of driven piles. This indicates that the flow index is not sufficiently informative for chalk and that the strength features of chalk significantly affect the bearing capacity of piles.

In some cases, the load-bearing capacity of piles is determined by the results of static soil sounding, which, however, requires justification and confirmation of the possibility of using the recommendations developed for ordinary soils for chalk [2, 3].

Completely insufficient knowledge of the features of the geotechnical properties of chalk and the lack of analogies in the scale of newly constructed structures and those built in the past lead to unjustified calculations of increased reserve coefficients (reflecting the level of ignorance of the properties of chalk), which contradicts the principles of designing structures based on limit states.

This approach cannot be considered satisfactory, especially that every year there is an increasingly urgent need to build very responsible and, often, unique structures in their parameters and purpose on the chalk, when, due to vital necessity, it is impossible to refuse construction or make compromise decisions on the construction of their foundations.

The results used in this paper were obtained experimentally using the method of static sensing at 27 points on 5 different objects.

3   Results and Discussion

For preliminary calculations of pile foundations, below there are Tables 1, 2 of chalk resistances under the lower ends of piles and soil resistances along the side surface of piles obtained as a result of static processing of static sounding results within the borders of the Belgorod region [5].

Table 1. Chalk on floodplains and I terrace above the flood-plain.

Depth of immersion of the lower end of the pile, m	1.0	2.0	3.0	4.0	5.0	6.0	7.0	8.0	9.0	10.0	11.0
Chalk resistance, t/m^2	100	110	125	140	155	170	180	190	200	220	240
Average square deviation	30	35	43	52	55	53	68	62	65	–	–
Coefficient of variation	0.3	0.33	0.34	0.35	0.35	0.31	0.37	0.32	0.32	–	–
Zones	Dispersed					Ranker					

The physical and mechanical characteristics of chalk were also obtained:

Natural moisture	0.35–0.38
Porosity coefficient	1.0–1.1
Plasticity number	0.08–0.11
Filtration coefficient, m/day	0.8–1.5
Volume weight, t/m^2	1.78–1.85
Specific adhesion, kg/m^2	0.13–0.20
Internal friction angle, deg	20–25
Modulus of deformation, kg/m^2	50–80
Weathering coefficient	0.8–1.0

Chalk as a natural foundation for building bases on the II and III terraces above the flood-plain is practically not used and rarely occurs within the core, so chalk was studied on watershed spaces and watershed slopes.

Table 2. Chalk on watershed spaces and watershed slopes.

Depth of immersion of the lower end of the pile, m	1.0	2.0	3.0	4.0	5.0	6.0	7.0	8.0	9.0	10.0	11.0
Chalk resistance, t/m^2	270	300	290	290	280	280	280	300	300	320	350
Average square deviation	68	80	45	50	65	65	55	50	68	85	90
Coefficient of variation	0.25	0.27	0.16	0.17	0.17	0.23	0.20	0.18	0.23	0.23	0.24
Zones	Dispersed					Ranker					

The physical and mechanical characteristics of chalk were also obtained:

Natural moisture	0.26–0.28
Porosity coefficient	0.8–1.2
Plasticity number	0.08–0.10
Filtration coefficient, m/day	0.6–1.5
Volume weight, t/m^2	1.7–1.8
Specific adhesion, kg/m^2	0.17–0.20
Internal friction angle, deg	20–25
Modulus of deformation, kg/m^2	80–100
Weathering coefficient	1.0

The results of this work can be used by design and survey organizations when performing surveys, designing and constructing structures for various purposes using chalk-marl rocks as the bases of these structures.

But do not forget that each case of meeting with such rocks is purely individual, as at the moment there is no classification of them.

The geological section characterizes the terrain of the site. It contains the absolute level Fig. 1.

Fig. 1. Geological section.

The Graph 1 below visually shows the dependence of the chalk resistance on different terraces on the depth of the pile sinking, as revealed above.

Graph 1. Chalk resistance depending on the depth of immersion of the lower end of the pile.

4   Conclusion

In connection with the presented results, we get the minimum recommended depth of immersion of piles in chalk, it should be at least 1.0–2.0 m from its roof. The time of "rest" of piles after driving is determined, as well as for clay soils according to the requirements of GOST [9].

The design load allowed on a pile submerged in chalk with the load-bearing capacity determined by the above tables should be calculated with a reliability coefficient equal to 1.25 [10].

References

1. Leonychev, A.V.: Problems of using chalk-marl rocks as the Foundation of structures and their solution: abstract of the doctor of technical Sciences. Moscow (1995)
2. Gubarev, S.A., Chernysh, A.S.: testing of writing chalk samples on a uniaxial compression device. Geosci. Vector **3**(3), 10–15 (2020)

3. Chernysh, A.S., Gubarev, S.A.: Determination of the compressive strength of the studied chalk sample from the time of water absorption, using a uniaxial compression device. Geosci. Vector **3**(3), 20–25 (2020)
4. Kuprina, G.A., Poltev, N.F., Sergeev, E.M.: Engineering and geological characteristics of the Cretaceous of the Voronezh region. Proceedings of Conferences on Engineering and Geological Properties of Rocks and Methods of their Study, vol. 2, pp. 90–98 (1957)
5. Akhtyrtsev, B.P., Akhtyrtsev, A.B.: Soil cover of the Central Russian Chernozem region. VSU, Voronezh (1993)
6. Sergeev, S.V., Rybalov, A.I., Sokolov, N.S.: Features of construction of pile foundations in chalk soils. Housing Constr. **4**, 33–39 (2017)
7. Sergeev, S.V., Rybalov, M.A.: Engineering and geological conditions of functioning of the Belgorod state University complex. Sci. Bull. Nat. Res. Univ. "BelSU". Nat. Sci. Ser. **3**(74), 132–136 (2010)
8. Ukhov, S.B.: Mechanics of Soils, Foundations and Foundations. Higher School, Moscow (2007)
9. Rybnikova, I.A., Rybnikov, A.M.: From the experience of Foundation construction in weak soils. Bull. Belgorod State Technol. Univ. named after V. G. Shukhov **10**, 58–63 (2017)
10. Kalachuk, T.G., Kalachuk, A.: Analysis of the causes of deformation of buildings and structures and measures to eliminate them. Bull. Belgorod State Technol. Univ. named after V. G. Shukhov **6**, 101–104 (2016)

Special-Purpose Polymer Composite Material Based on Thermoplastic Polymer and Modified Aerosil

N. V. Klyuchnikova , M. A. Klepikova$^{(\boxtimes)}$, L. V. Denisova ,
and D. S. Matvienko

Belgorod State Technological University named after V.G. Shukhov,
Belgorod, Russia
`4494.55@mail.ru`

Abstract. Every year, the humankind has been developing, improving and modifying the material qualities and properties. This is because science is not static, and each day scientists seek to learn something new and previously unknown. Polymer composite materials find their use in all areas of human life. It is not surprising that the use of such materials in outer space under conditions of high radiation and electromagnetic radiation is no exception. The development of special-purpose composite materials is a highly important engineering and technological challenge of the XXI century. The most common and effective method of improving the properties of a composition is the introduction of modifying additives into its composition, which are most often fillers. It is established that the composite polymer construction materials based on thermoplastic polymer and modified with aerosil, possess a set of properties sufficient for operation not only in nuclear plants but also in space. The introduction of modified aerosil into the polyimide matrix makes it possible to create a polymer composite material with the necessary complex of physical, mechanical and strength properties that will withstand the specified loads.

Keywords: Polymer composite material · Aerosil · Thermoplastic · Polyimide · Special-Purpose composite materials

1 Introduction

Just several decades ago, no one could imagine that soon the humankind would be able to reach the space so easily. This technological leap stimulated the science to create new unique materials that may be used in such environment [1]. This is why the global industry daily comes up with new ways of protecting polymer composite materials from radiation, electromagnetic and ultraviolet emissions [2]. Besides, the materials used in the space must possess increased resistance to aggressive environments, as well as an ability to be used in various climatic conditions. It is necessary to point out that along with the development of the nuclear power industry, there are special requirements for the construction materials used in nuclear plants.

While analysing the conditions under which these advanced materials will be used, it is possible to summarize the basic properties such materials should possess, such as

enhanced thermal resistance, enhanced material strength and physical-mechanical properties, low elasticity coefficient, minimal values of the difference of linear expansion thermal coefficient of their constituents, minor shrinkage during operation and assembling, moderate cost [3].

Now, these properties are typical for the majority of the polymer composite materials based on thermoplastic polymer modified with various fillers [4]. Based on this, it is possible to conclude that currently, this industry needs development and improvement of the finishing polymer-based materials, thus making polymer composites highly marketable and promising materials [5].

2   Methods and Materials

At the moment, no material would meet all the requirements for the use under the special conditions [6]. This fact dictates the necessity to create a modified composite material with protective properties.

A special-purpose polymer composite consists of a matrix, usually on the thermoplastic polymer basis, and a filler. This system should have stable connections between the polymer matrix and the filler; it should preserve the interphase connection at the phase boundary (in other words, it must possess technological strength); it should retain its initial properties while being used in the target environment [7].

The polymer matrix is the major composite component, the properties of which will affect the majority of the future polymer materials characteristics. The most commonly used polymer matrix for the moment is the matrix based on polyimide materials [8]. This thermoplastic material became widely used in the space industry. The most commonly used and available is the polyimide Ultem 1000. This polymer is prepared during the polycondensation of 2,2 bis-propane dianhydride [(3,4-dicarboxyphenoxy) phenyl] and m-phenylenediamine, with the addition of phthalic anhydride as a molar mass agent (Fig. 1).
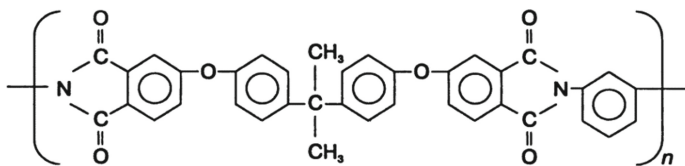
Fig. 1. Polyimide Ultem 1000 chemical structure.

Polyimide Ultem 1000 has several advantages over other polymers because it has great protective and mechanical properties, which enables to use it in aggressive environments, as well as under the conditions of increased load.

The filler introduced in the polymer matrix is no less important. This component can improve the composite properties, as well as degrade them. This is why the choice of a filler is an integral and necessary procedure during the polymer composite material creation [8].

Particulate fillers are widely used and silicon dioxide (SiO_2) is one of them. There exists a great variety of this filler's modifications that differ in their composition, shape, particle size and chemical composition. Aerosil (fumed silicone dioxide) is often used for the special-purpose composites.

Aerosil has several advantages over other synthetic fillers. The use of aerosil in the special-purpose composite material is very efficient, since it is characterized by small particles and a large specific surface area, and this allows aerosil to spread to the maximum in the polyimide matrix, thus improving its properties [9]. However it is quite expensive and it affects the cost of materials where it is used [10].

Also, while making the polymer composite material based on thermoplastic and particulate filler aerosil, there is another significant component, water-repellent agent, and in this case, dichlorodimethylsilane $(CH3)_2SiCl_2$ is used. Introduction of this component reduces the thermal conductivity of the composition and enhances its freezing resistance, as well as fungus and bacteria resistance [11].

Since the obtained composite material is going to be used under the conditions with higher radiation, electromagnetic and ultraviolet radiation, it must possess an appropriate set of physical-mechanical and performance parameters [12]. Based on this, it is necessary to run several tests, the results of which will help to conclude whether it is suitable for use in the specified conditions.

Since the obtained composite material based on thermoplastic and aerosil is supposed to be used in space, it is necessary to define the linear attenuation coefficient for γ-radiation by the material. This experiment helps test the composite for radiation resistance. The test has been run on the machine MKC-PM-1402 M. The samples of the obtained composite material without a filler and with different aerosil percentages (0.5%, 1%, 1.5%) in the form of opalescent hard plates 300–350 μm thick were placed in the machine bunker. Natural and radiation background for each sample have been measured during the experiment. Based on the measurement results, it was concluded that the composite material can be used in the specified conditions [13].

Considering that this composite material will be used in space, it must possess enhanced resistance to both high and low temperatures. This is why one of the most important things is to determine the material's thermal and cryogenic resistance.

The composite thermal resistance was determined at 200 ± 5 °C for 12 h. Composite material samples were placed in an oven with the air circulation, at least 100 mm away from the oven walls and no less than 20 mm between each other. 12 h later, the samples were taken out of the oven and cooled to 23 ± 2 °C. After this, the samples were checked for the defects by comparing them to similar samples that had not undergone the heating.

After the thermal treatment, the composite surface was studied under an atomic force microscope.

While determining the composite material cryogenic resistance, the samples were placed in liquid nitrogen 10 times for 1 min each time. Then the samples were taken out.

One of the most important tests was to determine the UV influence on the polymer composite material. This experiment was conducted with the help of the VSE-UV.c desktop unit that is specifically designed for studying the influence of the UV-radiation on the material in a vacuum and for imitation of various kinds of radiation in space.

The composite test was conducted for 3 h with the use of 12 lamps with different wavelengths (113–165 nm). Upon the completion of the experiment, the samples' surface was studied with the use of scanning electron microscope РЭМ JEOL JSM 6430F, with the magnification of ×5000 and ×1000.

The above-mentioned tests are a key condition for analysing the properties of the obtained polymer composite material based on thermoplastic and aerosil; these tests help conclude whether the derived composite can be used in space with different types of radiation [14].

3   Results and Discussion

While determining the linear attenuation coefficient for γ-radiation by the material, the characteristic curve was plotted (Fig. 2).
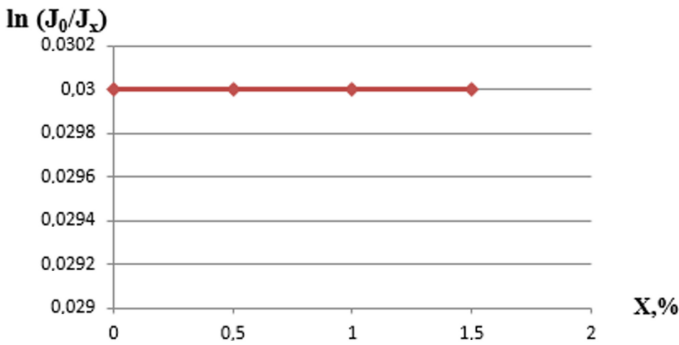
Fig. 2. γ-radiation dependency on the filler amount in the composite.

It is evident (Fig. 2) that with different filler percentage (0.5%; 1%; 1.5%), the parameters remain stable, in other words, with the increased aerosil content the material neither loses nor gains any radiation resistance.

As for the thermal and cryogenic composite resistance, the samples preserved their original form, no defects were detected on them after the tests. After the experiment, the material thickness and surface have not changed, and no cracking was observed after the exposition to both high and low temperatures. This means that the polymer composite material has the necessary thermal and cryogenic resistance [15].

After the thermal action on the material, its surface was analysed under the atomic force microscope (Fig. 3).
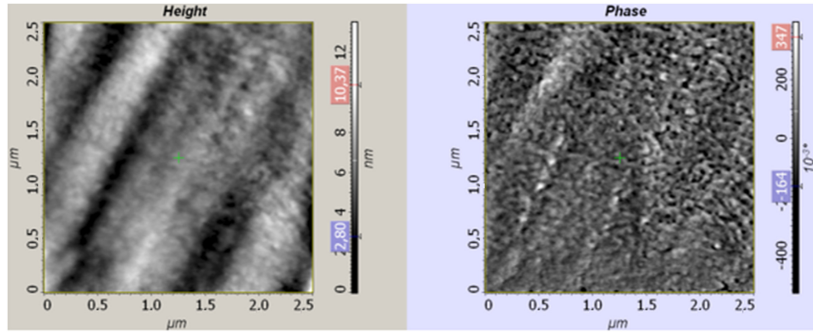
Fig. 3. The surface of the polymer composite with aerosil after the thermal action.

The analysis of structure showed that the sample surface after the thermal action remains homogeneous, which confirms this material's resistance to high temperatures [16].

After the experiment to test the UV radiation effect on the material, the tested samples were analysed under a scanning electron microscope (Fig. 4).
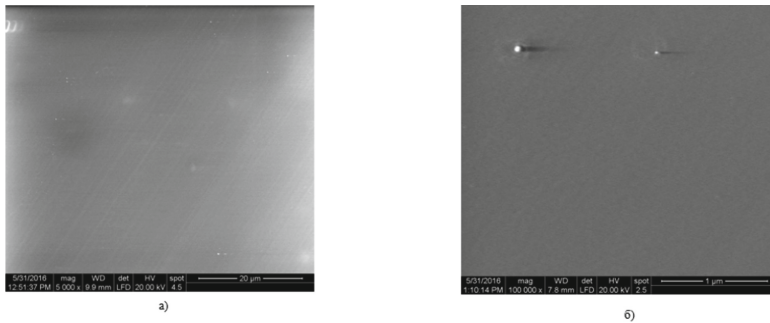
Fig. 4. The surface of the polymer composite containing aerosil after exposure to the UV radiation. a) ×500 magnification; b) ×1000 magnification.

From the figures, it is clearly seen that after the exposure to UV radiation, the material did not change and its surface remained unchanged, which confirms the resistance of this polymer composite material to photo-ageing.

After several studies conducted on the polymer composite material, we can conclude that the obtained composite based on the thermoplastic polymer with the aerosil filler possesses the necessary set of properties and can be used while being exposed to various types of radiation [17].

This material is resistant enough to high and low temperatures, UV radiation and radioactive action. All this demonstrates its potential for use in the advanced developing industries. It is necessary to consider that the material is quite expensive and may be used in niche sector-specific industries.

4   Conclusion

The use of the particulate filler aerosil in the polyimide matrix enables to make a special-purpose composite material with the set of necessary properties that can be used in the space and nuclear industry.
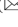
References

1. Anisimov, V.A.: Polymer Composite Materials. Chemistry, Moscow (2013)
2. Knyazeva, N.A.: Protective properties of coatings of polymer compositions filled with manganese-containing pigment. World Science: Problems and Innovations, pp. 40–44 (2017)
3. Zabegaeva, O.N., Sapotnikov, D.A., Vygodsky, Y.S.: Molecular composites based on polyimides. High-molecular Compounds. Ser. C **2**, 186–199 (2020)
4. Volgin, I.V., Larin, S.V., Lyulin, S.V.: Features of nanoparticle diffusion in polymer systems. Polymer Sci. Ser. C **1**, 122–134 (2018)
5. Xantes, M.: Functional fillers for plastics. Scientific Foundations and Technologies (2010)
6. Osipov, P.O.: Problems of utilization and processing of polymers. Pakkermash, vol. 53 (2008)
7. Karandashova, S.A.: Anticorrosive properties of coatings of polymer compositions filled with manganese-containing pigment. Bull. Kazan Technol. Univ. 23–26 (2016)
8. Khanin, M.V.: Wear and Destruction of Polymer Composite Materials. Chemistry, Moscow (2015)
9. Ezhov, A.A., Denicov, Y.I., Shandryuk, G.A.: Composites based on liquid-crystalline polymers with terminal functional groups and inorganic nanoparticles. Polymer Sci. Ser. C **1**, 102–117 (2018)
10. Khachaturov, A.A, Potapov, E.E., Fionov, A.S., Kolesov, V.V., Prut, E.V.: Functional elastomeric materials based on styrene-butadiene rubbers and magnetite. In: Materials of Reports of the Viiifrussian Conference "Rubber and Rubber 2018: Traditions and Innovations", vol. 64 (2017)
11. Solodov, V.A., Ziganshina, M.R.: Anticorrosive properties of epoxy coatings, impregnated with manga-nese-containing pigments. Int. J. Appl. Eng. Res. **10**(24), 45383–45391 (2015)
12. Klyuchnikova, N.V., Gordeev, S.A., Gordienko, M.D.: Polymer composite material based on thermoplastic polyimide. Bull. BSTU named after V. G. Shukhov **12**, 126–129 (2017)
13. Nizina, T.A., Nizin, D.R., Kanaeva, N.S., Kuznetsov, N.M., Artamonov, D.A.: Applying the fractal anaysis methods for the study of the mechanisms of deformation and destruction of polymeric material samples affected by tensile stresses. Key Eng. Mater. **799**, 217–223 (2019)
14. Solomatov, V.I.: Epoxy-urea composite for building flax structures. In: Protective Composite Materials and Technologies of the Third Millennium: II International Scientific and Practical Conference. "Composites 2001", pp. 18–20 (2001)

15. Bobrov, A.P., Kablov, W.F., Smail V.A.: Study of the abrasive activity of natural carbon-containing mineral Compound ingredients of Polymer composites. Int. Polym. Sci. Technol. **42**(9), 68–71 (2015)
16. Klyuchnikova, N.V., Sokolenko, I.V., Evtushenko, E.: Influence of metal component on caking of metal-ceramic composites research. J. Pharm. Biol. Chem. Sci. **5**(5), 1637 (2014)
17. Gomaa, A.Z.: Evaluation of the Egyptian manganese ore as a pigment and its applications in surface coatings. Anticorrosive Primers Coating the Egiptian Manganese Ore, pp. 181–183 (2015)

Effect of Mineral Filler Modification on the Intensity of Bitumen Aging

V. V. Yadykina [ID], E. V. Kuznetsova [ID], and M. S. Lebedev[(✉)] [ID]

Belgorod State Technological University named after V.G. Shukhov,
Kostyukov St., 46, Belgorod 308012, Russia
michaelLl987@yandex.ru

Abstract. Changes in the properties of bitumen under the influence of high temperatures of preparation and transportation of the asphalt mixture leads to a significant decrease in the quality of the asphalt pavement. Studies on this problem have given rather contradictory opinions about the effect of various mineral materials on the bitumen aging and on the properties of asphalt concrete. The paper presents the results of research on the effect of mineral filler hydrophobized with GF-1 specimen on the intensity of bitumen aging at the technological temperature by changing the parameters of penetration, softening point, and cohesion of asphalt binders. It was found that all the studied characteristics of samples prepared on hydrophobized mineral filler change significantly less than on the original filler. This indicates a slowdown in the aging rate of bitumen in the composite with hydrophobized mineral filler. It is shown that an increase in the resistance of bitumen to aging during preparation when using a modified mineral filler is accompanied by an improvement in the structuring of bitumen with filler. Slowing down aging can also be associated with a more uniform distribution of the binder over the surface of the hydrophobized mineral filler, an increase in the interface between them, and the formation of more bonds.

Keywords: Bitumen · Aging · Hydrophobized mineral filler · Asphalt binder · Bitumen structuring

1 Introduction

One of the main factors determining the destruction of asphalt concrete road surfaces is the aging of bitumen, which is part of asphalt concrete. It is known that aging is most intense when preparing an asphalt-concrete mixture [1, 2].

Under the influence of atmospheric factors – temperature, light, air and water–changes occur in the physical properties and chemical composition of bitumen. It is known that the aging of bitumen in asphalt concrete follows the same mechanism as in free bitumen, although there are some features associated with the presence of mineral materials.

Preparation of a bitumen and mineral mixture in practice is made by mixing bitumen with stone materials at a temperature of 150–170 °C. At these temperatures, the interaction of a thin layer of bitumen with air oxygen occurs, leading to intensive aging of the bitumen. According to studies [2, 3], the rheological characteristics of

bitumen at the technological stages of preparation, storage and transportation of mixtures change significantly more than after long-term use of asphalt concrete in the coating. The result is quite natural, as at these stages bitumen is located on the surface of mineral materials in the form of thin films with free access of oxygen to the mixer.

In the works devoted to this problem, there are quite contradictory opinions about the influence of various mineral materials on the aging of bitumen and on the properties of asphalt concrete [1, 4–7]. Some researchers believe that the use of fillers with high adsorption capacity leads to premature aging of bitumen, while others, on the contrary, claim that the speed of the bitumen oxidation process slows down.

Information on the effect of modified mineral fillers on the aging rate of bitumen is very limited. For example, the authors [8, 9] showed that the use of activated mineral filler leads to a slowdown in aging and an increase in the service life of asphalt concrete road surfaces. When studying aging, the authors [10] concluded that the increase in the viscosity of asphalt binders containing 60% of filler does not depend on its type (activated, non-activated).

2   Materials and Methods

Limestone filler manufactured by OOO Crushing and sorting plant (Kaluga region, Russia) was studied.

The "GF-1 Preparation" produced by OOO Selena (Shebekino, Russia) was used as a hydrophobizator [11]. To prepare the hydrophobized filler, the powder was pre-dried in a drying box, then the hydrophobizator was introduced into the hot powder and processed in a ball mill. Based on the results of previous studies [12], optimal parameters were established to achieve the maximum effect when obtaining a hydrophobic filler: the additive concentration is 0.4%, and the processing time is 15 min. The granulometric composition of the initial and hydrophobized fillers is shown in Table 1.

Table 1. Granulometric composition of fillers.

Filler	Passage, wt.%, through a sieve with a diameter of holes		
	2 mm	0.125 mm	0.063 mm
Limestone	100	99	90
Limestone + GF-1	100	100	92
Requirements of Russian National Standard 32761–2014	No more than 100	No more than 85	No more than 70

Bitumen of the BND 60/90 brand of OAO Novokuybyshevsk oil refinery plant (Samara region, Russia) was used in the work.

Asphalt binders for testing were prepared manually by mixing bitumen with fillers at a temperature of 150–160 °C in the following mass ratio: 60% mineral filler and 40% bitumen. Aging of asphalt binders (a mixture of bitumen with filler) was performed by

holding in a drying oven at a temperature of 160 °C for 3, 5 and 7 h. Changes in the following parameters of properties determined by the standards were studied: cohesion – DIN EN 13588–2008*; penetration – DIN EN 1426–2015; softening point by "Ring and ball" – DIN EN 1427–2007.

To study the structure-forming ability of the studied mineral fillers, the rheological parameters of asphalt binders were determined by the method of conical plastometry.

3 Results and Discussions

The applied method of temperature control at high temperature allows characterizing the aging of the binder in the production process and simulating the conditions of its transportation in hot form.

The results of studies presented in Fig. 1–3, in the form of changes in the indicators of cohesion, penetration and softening point of asphalt binders indicate that all the studied characteristics of samples prepared on hydrophobized mineral filler change to a much lesser extent than on the original filler. This indicates a slowdown in the aging rate of bitumen in the composite with hydrophobized mineral filler.
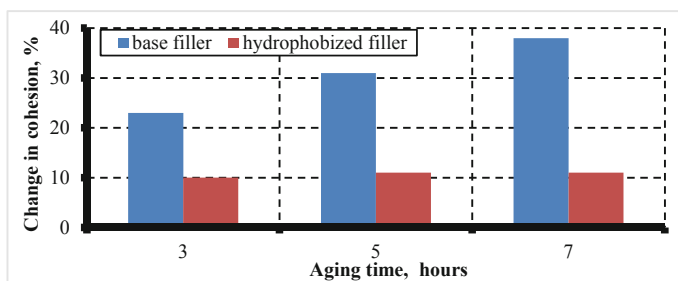
Fig. 1. Changes in the cohesion of asphalt binders after aging.
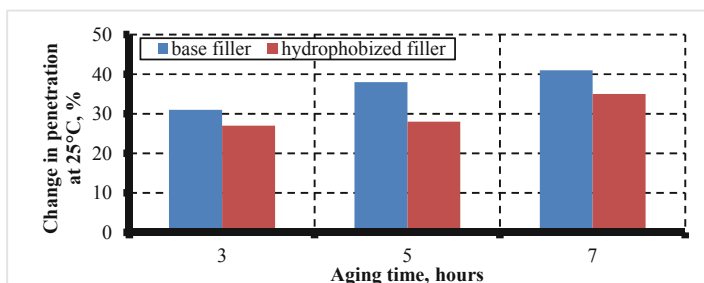
Fig. 2. Change in the penetration of asphalt binders after aging.
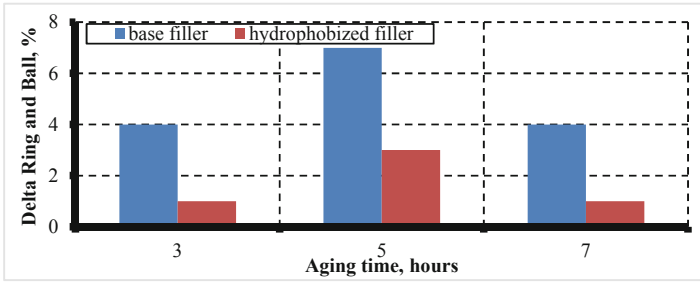
Fig. 3. Changes in the softening point of asphalt binders after aging.

For example, the cohesion of an asphalt binder containing unmodified limestone filler increased by 23, 31, and 38%, respectively, after 3, 5, and 7 h of temperature control, while the increase in this indicator when using hydrophobized filler in the asphalt binder formulation was only 10–11%. Similar results were obtained in the study of penetration (see Fig. 2) and softening point (see Fig. 3).

One of the reasons for increasing the resistance of bitumen to aging when using modified mineral filler during the preparation of the mixture may be an improvement in the structuring of bitumen with mineral filler [13]. Due to this phenomenon, bitumen is more fully converted to the film state, which, according to studies [1], slows down aging, as the binder is in the field of action of the surface forces of the mineral substrate. Adsorbed bitumen layers have one important advantage in comparison with free bitumen: bitumen molecules in structured layers have much lower mobility than in free bitumen, which, of course, reduces their reactivity [4]. This assumption is confirmed by the results of a study of the structuring ability of the studied mineral fillers (Fig. 4).

Figure 4 shows that when mineral filler is introduced into bitumen in a relatively small amount due to adsorption and increased friction, the ultimate shear stress of the system increases naturally, in accordance with the Einstein equation, and then there is a more rapid increase in the indicator.
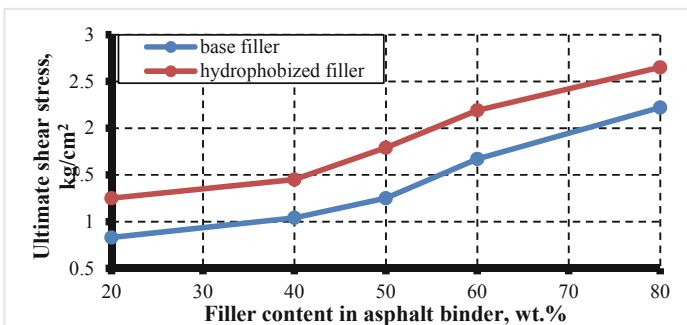
Fig. 4. Dependence of the ultimate shear stress on the content of mineral filler in the asphalt binder.

The results shown in Fig. 4 indicate that the most active mineral filler is hydrophobized with GF-1. Sharp increase in the ultimate shear stress occurs when the concentration of hydrophobic limestone in the mixture is 40%. For the base limestone, the filler concentration in the asphalt binder at which the curve is bent is 50%. When the ratio of filler to bitumen 60/40, adopted in the study, the ultimate shear stress on the hydrophobized filler was 2.19 kg/cm^2, and on the powder from the original filler – 1.67 kg/cm^2. Thus, hydrophobized mineral filler structures bitumen to a greater extent and at a concentration of 60% in bitumen, the ultimate shear stress of the binary system on hydrophobic limestone is 31% higher than on the base limestone. This had a positive effect on the rate of aging of bitumen in the asphalt binder.

In addition, when using hydrophobized filler, the conditions for wetting it with bitumen are facilitated and the binder is more evenly distributed over the surface of the mineral filler, which increases the surface of the "binder – filler" section. Due to this, more bitumen bonds are involved in interaction with the mineral substrate, which reduces its tendency to aging [4].

4   Conclusion

The results of studies on the effect of hydrophobized mineral filler on the intensity of bitumen aging at the process temperature showed that the parameters of penetration, softening point, and cohesion of asphalt binders change to a much lesser extent than on the base filler. This indicates a slowdown in the aging rate of bitumen in the composite with hydrophobized mineral filler. It is shown that an increase in the resistance of bitumen to aging during preparation when using modified filler is accompanied by an improvement in the structuring of bitumen with filler.

References

1. Rybyev, I.A.: Construction materials science. Higher school, Moscow (2003)
2. Rybalchuk, N.A.: Aging of bituminous binders. Bull. Irkutsk State Tech. Univ. **2**(997), 120–125 (2015)
3. Gezentsvey, L.B., Gorelyishev, A.M., Boguslavsky, I.V., Korolev, I.V.: Road asphalt concrete. Transport, Moscow (1985)
4. Pecheny, B.G.: Durability of bitumen and bituminous coatings. Stroyizdat, Moscow (1981)
5. Barth, E.T.: Asphalt Science and Technology. Cordon and Breach Science Publishers, New York (1968)
6. Delaporte, B., Di Benedetto, H., Chaverot, P., Gauthier, G.: Effect of ultrafine particles on linear viscoelastic of mastics and asphalt concretes. Transp. Res. Rec. **2051**, 41–48 (2008)
7. Taylor, R.: Surface interactions between bitumen and mineral fillers and their effects on the rheology of bitumen-filler mastics. Ph.D. thesis, University of Nottingham, UK (2007).

8. Sukortsev, S.V., Rapoport, P.B., Khukhryanskaya, N.A., Gazilova, E.V.: Causes of aging of bitumen-mineral mixtures. Sci. Technol. Road Indus. **3**(54), 31–32 (2010)
9. Rapoport, P.B., Sukortsev, S.V., Taskaev, O.G., Khukhryanskaya, N.A.: The aging of bitumen with activated mineral fillers. Transp. Constr. **2**, 24–25 (2011)
10. Garmanov, V.N., Gorelysheva, L.A.: Results of the study of the effect of mineral filler on the properties of asphalt binder using a shear rheometer. Roads Bridges **2**(40), 293–303 (2018)
11. Methodical recommendations for application of hydrophobisator of mineral fillers "Preparation GF". Innovative road materials OOO Selena (2020).
12. Yadykina, V.V., Kuznetsova, E.V., Lebedev, M.S.: Change in the properties of asphalt concrete when using hydrophobized mineral powder. Bull. BSTU named after V.G. Shukhov **4**, 17–23 (2020).
13. Yadykina, V.V., Gridchin, A.M., Kuznetsova, E.V., Lebedev, M.S.: Increasing the efficiency of mineral powder from technogenic raw materials due to its hydrophobization. Constr. Mater. Prod. **3**(4), 24–30 (2020)

Dependence of the Quality of the Foam Concrete Mixture on Its Mixing Modes

L. R. Mailyan[(✉)] , S. A. Stel'makh , E. M. Shcherban' ,
and K. E. Tkacheva

Don State Technical University, Rostov-on-Don, Russia
au.geen@mail.ru

Abstract. In order to make a foam concrete mixture, based on the analysis of a priori information, a single-stage technology was used. During the preparation of the mixture, a laboratory turbulent three-bladed mixer with a conical part and reflective partitions was used. A mixer was used to ensure the slurry process of particles in the mixing mass. The authors considered the features that need to be paid attention to in the process of mixing such dispersed systems as "solid phase – liquid". Such systems are characterized by high particle deposition rates. This condition can also be used for foam concrete mixtures. Experiments were conducted on the effect of the activator rotation speed on the homogeneity of mixing of the foam concrete mixture. The distributions of suspended particle concentrations over the radius and height of the mixer are considered. The dependences of the structural homogeneity of the mixture on the speed of rotation of the activator and the time component of the mixing process are analyzed. It was found that the rise of particles and increased power consumption is affected by changing the height of the agitator installation above the bottom, namely, its reduction. It is established that the efficiency of the designed mixers depends to a greater extent on the requirements for the indicator of uniformity of the concentration distribution in the foam concrete mixture. The higher the requirements for the uniformity indicator, the more power increases. An excessive reduction in the requirements for the degree of uniformity of the foam concrete mass may contribute to the deposition of some of the solid phase on the bottom of the mixer, which will lead to heterogeneity of the mixture.

Keywords: Foam concrete mixture · Solid phase · Turbulent mixer · Mixing uniformity · Rotation speed · Mixing duration

1 Introduction

The procedure for calculating the turbulent flow is a theoretically unsolved problem, based on this there are only qualitative indicators that are obtained in the course of experimental studies.

It is revealed that during the excitation of the foam concrete mixture, the activator forms a three-dimensional velocity field. This established fact allows concluding that the circumferential component significantly exceeds the radial and meridian velocity values. It is necessary to pay attention to two zones with completely different

circulation data, which ultimately affects the deterioration of the speed mode, and, consequently, the quality of mixing components.

Currently, quite a lot of modern devices with agitators have been developed [1] for the manufacture of cellular concretes, the relevance of high-quality and constant mixing is justified by great difficulties and is provided, as a rule, by conducting experiments, taking into account the specific type of mixer, composition, and volume of mixed materials.

A large number of experiments have identified a number of main mechanical factors that affect the mixing process [1–3], but it is worth noting that the formalization of the process is at an initial level. Thus, to obtain quantitative characteristics of the mixture flows using numerical methods (FEM), the not achieved computer power will be required [4].

Based on this, the result of this work is a number of parameters that significantly affect the quality of the manufactured mixture. If as an example, to increase the percent solids from 3.4 to 37.31 by mass [2], the critical velocity (speed at which the components of the solid part dispersed throughout the mixture) will increase by 27%, while the temporal component of the mixing time will increase by 70.5%. This example accurately reflects the influence of the circulating flow of the suspension. On the other hand, the circulation indicates a clear correlation between the vessel diameter and the mixing time index.

In the course of experiments [4] with the use of a two-phase water-air system, a relationship was derived between such indicators as: the pumping capacity of the agitator, which has no dimension, the gas content in the system, the time parameter of mixing components and the number of revolutions of the agitator, the amount of energy spent on the mixing process, and the aeration rate [5–7].

In order to make a foam concrete mixture, based on the analysis of abstract information, a single-stage technology was used. A special condition for using the mixer as a mixing device is to ensure that the particles are suspended in the total mixing mass. We study the distinctive features that need to be paid attention to in the process of mixing only such dispersed systems as "solid phase – liquid". Such systems are characterized by high particle deposition rates, which is also typical for foam concrete mixtures. It is known that cement-sand solutions have the property of rapid stratification from the moment of mixing completion [8–10].

2   Methods and Materials

Using a turbulent mixer D = 250 mm with a conical part $\alpha_c = 60°$ and a volume Vmix = 150 l, we studied the effect of the mixing rate on the quality of the mixture uniformity during laboratory tests. Partitions with a reflective effect with a width of $b = 0.06D$ were used. We needed four (J = 4) such partitions, which were installed on the inner side of the mixer body. A three-bladed activator was used as a mixing device. To change the speed of rotation of the activator itself from 150 to 950 rpm, the gear ratio of the V-belt drive was adjusted, using a set of pulleys with different diameters. Throughout the experiment, the speed at which the engine rotated remained stable and was equal to 1500 rpm.

To obtain foam concrete with an average density of 600 kg/m^3, we selected the following composition: cement – 60 kg; sand – 30 kg; water – 72 l.; foaming agent – 0.15 l. The density of the foam concrete mixture was determined in accordance with the method given in [9].

As part of the research, a number of parameters that have a significant impact on the quality of the resulting foam concrete mixture are proposed. A single-stage technology was used to prepare a foam concrete mixture based on the analysis of a priori information.

There is a minimum possible mixing intensity of the mixture in dispersed systems "liquid-solid phase", which is similar to slurry process. The slurry process conditions guarantee that the particles will rise from the bottom of the mixer or that they will not be lowered at all. But for cases where the particles do not have a predisposition to stick together during mixing, the examples given do not have any striking differences. The lifting of particles from the bottom of the mixer can only be carried out when the lifting force that is applied to the particle lowered to the bottom, at the time when it is influenced by the liquid flow, is much higher than the force of gravity:

$$F_{lif} \geq V_p \rho_p g \tag{1}$$

where V_p – particle volume, m^3; g – acceleration of gravity, m/s^2; ρ_p – density of the particle.

The conditions under which the lifting force appears can be either the horizontal component of the flow velocity, or turbulent pressure pulsations near the bottom of the mixer. Which of the above factors will be decisive cannot be definitively stated at the present time, even for the simplest cases of one-dimensional flow in flat channels [11]. Methods for calculating the transport of suspended particles are applied using empirical formulas. In cases with water suspensions, the Shamov formula is often used [12], which in its modified form may look like a relationship between the speed that ensures the rise of particles from the lower part of the mixer – the "self-cleansing" flow rate of v_{sc} and the speed of particle settling:

$$v_{sc} = 5.3 \omega_{sv} H^{0.22} \tag{2}$$

where ω_{sv} –settling velocity of the particles, m/s; H – depth of liquid flow, m.

3   Results and Discussion

Let us pay attention to how the uniformity of the foam concrete structure depends on the speed at which the activator rotates and the mixing time index.

The final values obtained during the experiment are shown in Fig. 1.
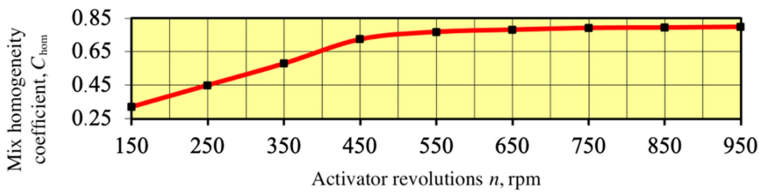
Fig. 1. Correlation of the homogeneity coefficient of the foam concrete mixture from the number of the activator revolutions.

An increase in the velocity at which the activator rotates from 150 to 550 rpm justifies an increase in the coefficient of uniformity of the C_{hom} mixture. The obtained data give grounds to assert that the intensity of propagation of the mixture particles in the radial and axial directions of the mixer increases. The subsequent increase in the velocity of the activator from 550 to 950 rpm already slightly increases the C_{hom}, but there is a rapid increase in the total density of the mixture from 800 kg/m^3 to 1100 kg/m^3, and this phenomenon is justified by the collapse of the pore structure formed during the rotation of the activator at high speeds.

The amount of involved air increases when the activator rotates at speeds from 150 to 400 rpm, but reaches the highest value at a speed of 550 rpm. Let us note that at a speed greater than 550 rpm, the processes of bubble bursting and air escaping are more active than the formation and crushing of new ones. Thus, a strong increase in the speed of the activator helps to reduce the amount of air involved, as well as increase the overall density of the mixture. It was found that with certain homogeneity of the mixture, the optimal speed of the activator during its manufacture varies in the range of 450…550 rpm.

The next step is to analyze the dependence of the homogeneity of the mixture on the time index of mixing. In order to determine how the mixing time affects the uniformity of the mixture structure, we took the activator rotation speed equal to 550 rpm. The method of conducting the experiment is identical to the method of calculating the speed at which the activator operates. The final values obtained during the experiment are shown in Fig. 2. It was found that if the preparation time of the foam concrete mixture is extended to $t = 3.5$ min, the value of the homogeneity index of the mixture will increase to $C_{hom} = 0.77$. An increase in the time indicator for the preparation of a foam concrete mixture from 3.5 to 8 min provides a slight increase in the coefficient of homogeneity of the mixture.
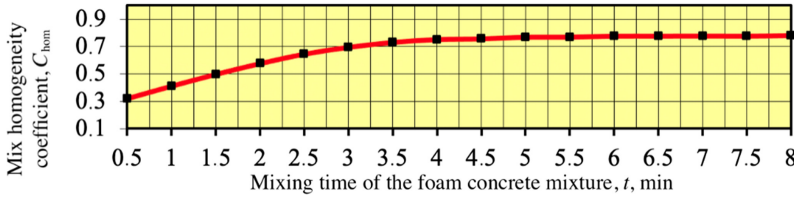
Fig. 2. Effect of the time indicator of foam concrete mix preparation on its homogeneity.

We conducted the experiments confirmed the calculated dependence (2). The data obtained are presented in Fig. 3.
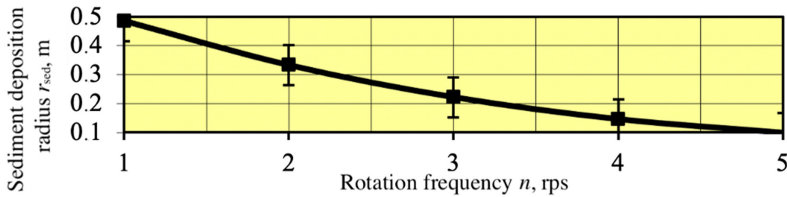
Fig. 3. The dependence of the sediment deposition radius r_{sed} on the agitator rotation frequency n (mixer diameter D = H = 1 m; three-blade agitator diameter d_m = 0.2 m; ω_{sed} = 0.018 m/s; particle diameter d_p = 10^{-4}m).

The lowest circumferential speed of the activator blades required to lift all particles from the bottom of the mixer corresponds to the condition $r_{sed} \geq R$

$$r_{sed} \geq R, \tag{3}$$

where r_{sed} – sediment radius, R – mixer radius.
Hence.

$$(\omega_0 r_0)_{sc} = \frac{5.3\omega_{sed}H^{0.22}\bar{R}}{\psi_1 + \psi_2 + 1} \tag{4}$$

where ψ_1, ψ_2 –parameters of the velocity distribution, R_{av} – the radius ratio of the activator and mixer.

Calculations based on Eq. (4), results obtained experimentally, as well as operational data [12] indicate that the power required to get rid of sediment accumulation on the lower part of the mixer, as a rule, decreases with increasing diameter of the activator. This feature is typical only up to R_{av} = 1.8…2.0 (Fig. 4).
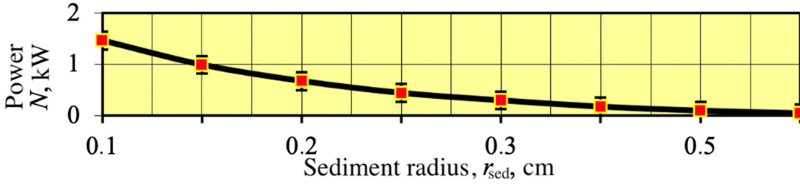
Fig. 4. Effect of the drive power on the amount of sediment formed at $R_{av} = 1.8...2.0$.

Let us note that if they continue to increase the diameter of the agitator and simultaneously reduce the angular velocity, this abundant accumulation of particles will be in the central part, provided that if the drive is on top. The results obtained allow concluding that the reduction of the agitator settings above the bottom of the mixer flies to the rise of particles. But it is worth noting that a strong change in the height of the mixer installation above the bottom of the mixer increases the amount of power required. Thus, the level of agitator installation above the lower part of the mixer is usually selected in the intervals $(0.03...0.1)$ d_m at $R_{av} \leq 1.33$, within $(0.3...0.7)$ d_m at $R_{av} \geq 1.33$ [12].

We consider the distribution of suspended particle concentrations over the radius of the mixer. Two approaches are known to calculate the distribution of suspended particles in the volume of the mixer in the production of a foam concrete mixture in dispersed systems "solid phase – liquid". One of these approaches, which is most widely used in the practical part of the study of the mixing process, is to find the critical value of the rotation frequency n_0 of a mixer of a certain type and a given size – the lowest speed of the mixture, at which a uniform dispersion of the solid phase in the mixer suspension is possible [12].

Another interpretation of this approach is considered to be the method that consists in finding the lowest power N_0 required for uniform particle dispersal. The values of the N_0 indicator are also calculated during the experiment. In the source [12], the equation was derived:

$$N_0 = C\Delta\rho g(x_{sr}\Delta\rho d_p/\rho)^{0.5} \tag{5}$$

where x_{sr} – average concentration of solid particles in the suspension mass; C – constant that depends on the type of agitator.

The movement of particles under the influence of centrifugal force relative to the liquid is calculated using the same equations as the deposition of particles under the influence of gravity. The difference is that in this case, the centripetal acceleration v^2/r takes on the role of the acceleration of free fall, and based on this, the velocity of large particles moving in the radial direction can be represented [11] as

$$\omega_c = \omega_{sed}v/\sqrt{gr} \tag{6}$$

where ω_c – point velocity of the radial motion of particles on the radius r, m/s; ω_{sed} – speed of particle deposition under the influence of gravity, m/s; v – circumferential velocity of the liquid at a radius r, m/s.

Let us analyze the dispersion of suspended particle concentrations along the mixer height. If there is a concentration of up to 20% in the suspension volume and there is no significant radial inhomogeneity, it is advisable to describe the particle transport along the axis [12] by the equation:

$$\mathrm{x}(\omega_{sed} - \omega_2) + D_2 \frac{dx}{dh} = 0 \tag{7}$$

where ω_2 – the rate of upward flow in the peripheral zone, m/s; D_2 – averaged value of the turbulent diffusion coefficient in the axis direction for the peripheral zone, m²/s.

When calculating the distribution of concentrations of particles whose density is lower than the density of the medium ($\rho_p < \rho$), the value of the deposition rate ω_{sed} is assigned a minus sign. The correlation of the level of heterogeneity of distribution of the frequency of rotation of the mixer shown in Fig. 5. The figure shows that in terms of $Pe = 0.5 - 0.25$ decrease in Peclet criterion, which is the ratio of speed of separation of particles under the influence of gravity to the speed of their movements by turbulent diffusion, determines a significant increase in the level of homogeneity of dispersion concentrations. For smaller Pe_m, the X/X_{av} values approach unity asymptotically (Fig. 5), and an infinitely high mixing intensity is required, at least theoretically, until the complete homogeneity of the suspension is reduced.
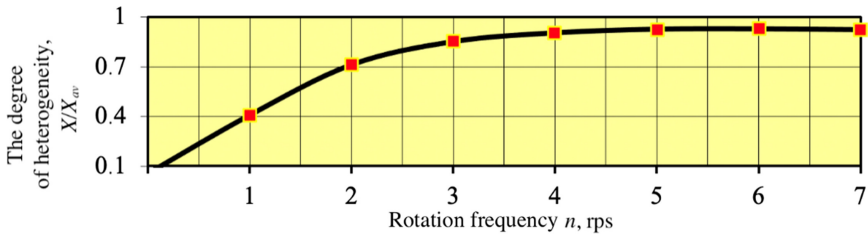
Fig. 5. Dependence of cement slurry concentrations on the speed of the activator (mixer with a diameter of 0.6 m; three-bladed agitator; $R_{av} = 2.15$; $\omega_{sed} = 0.00825$ m/s).

For most practical cases, the values of $X_{max}/X_{av} \approx 1.1...1.15$ are quite sufficient. The introduction of strict requirements for the level of uniformity has an impact on a sharp increase in power. As an example, we can consider a decrease in the value of X_{max}/X_{av} from 1.15 to 1.05 by increasing the speed of the agitator, this phenomenon is associated with a 25-fold increase in power.

4   Conclusion

The speed with which the particles settle and the scale of the mixer have a particular impact on the level of uniformity of particle dispersal within the peripheral zone. In turn, the coefficient of turbulent diffusion increases, and the speed of radial motion

decreases. This factor is associated with a decrease in the level of heterogeneity of the radial dispersion.

The cost-effectiveness of the designed mixers depends to a large extent on how high the requirements are for the level of uniformity of concentration dispersion in the mixture. The introduction of strict requirements for the level of uniformity has an impact on a sharp increase in power. An excessive reduction in the requirements for the degree of uniformity of the foam concrete mass is also undesirable, as some part of the solid phase may be deposited on the bottom of the mixer, which will lead to heterogeneity of the mixture.

References

1. Kafarov, V.V.: Basics of mass transfer. Moscow: Higher School 496 (1972).
2. Wallevik, J.E., Wallevik, O.H.: Analysis of shear rate inside a concrete truck mixer. Cem. Concr. Res. **95**, 9–17 (2017). https://doi.org/10.1016/j.cemconres.2017.02.007
3. Lerch, J.O., Bester, H.L., Van Rooyen, A.S., Combrinck, R., de Villiers, W.I., Boshoff, W. P.: The effect of mixing on the performance of macro synthetic fibre reinforced concrete. Cem. Concr. Res. **103**, 130–139 (2018). https://doi.org/10.1016/j.cemconres.2017.10.010
4. Elgindi, T.M., Zlatoš, A.: Universal mixers in all dimensions. Adv. Math. **356**, 106807 (2019). https://doi.org/10.1016/j.aim.2019.106807
5. Strenk, F.: Stirring and apparatus with stirrers. Leningrad: Chemistry 384 (1975).
6. Rumyantsev, B.M., Zudyaev, E.A., Kritarasov, D.S.: Technology and equipment for the production of foam concrete by the method of dry mineralization of foam. Build. Mater. Equipment Technol. XXI Century. **3–4**, 36–37 (1999)
7. Morgun, L.V., Morgun, V.N.: The effect of dispersed reinforcement on the aggregate stability of foam concrete mixtures. Build. Mater. **1**, 33–35 (2003)
8. Shuisky, A.I., Stelmakh, S.A., Shcherban, E.M., Torlina, E.A.: Recipe-technological aspects of improving the properties of nonautoclaved aerated concrete. In: MATEC Web of Conferences **129**, 05011 (2017). https://doi.org/10.1051/matecconf/201712905011
9. Stel'makh, S.A., Shcherban', E.M., Shuiskii, A.I., Prokopov, A.Y., Madatyan, S.M., Parinov, I.A., Cherpakov, A.V.: Effects of the geometric parameters of mixer on the mixing process of foam concrete mixture and its energy efficiency. Appl. Sci. **10**, 8055 (2020). https://doi.org/10.3390/app10228055.
10. Pavlov, A.N., Gol'tsov, Yu.I., Mailyan, L.R., Shcherban', E.M., Stel'makh, S.A.: Relaxation processes during activation of cement mixing water. In: IOP Conference Series: Materials Science and Engineering. vol. 896, pp. 012124 (2020). https://doi.org/10.1051/matecconf/201712905011.
11. Kharakhash, V.P., Tumanov, Y.: SAKHZ. **4**(3), 422–426 (1970)
12. Sadovskii, V.L., Begachev, V.I.: Chemical engineering. Moscow: NIIkhimmash, 54–64 (1980).
13. Valigi, M.C., Logozzo, S., Rinchi, M.: Wear resistance of blades in planetary concrete mixers. Part II: 3D validation of a new mixing blade design and efficiency evaluation. Tribol. Int. **103**, 37–44 (2016). https://doi.org/10.1016/j.triboint.2016.06.040.
14. Valigi, M.C., Logozzo, S., Rinchi, M.: Wear resistance of blades in planetary concrete mixers. Design of a new improved blade shape and 2D validation. Tribol. Int. **96**, 191–201 (2016). https://doi.org/10.1016/j.triboint.2015.12.020.

Lead Oxides as Fillers of Composite Materials for Protection Against Ionizing Radiation Based on Building Gypsum

V. G. Klimenko[(⊠)] , A. N. Volodchenko ,
and R. V. Sidelnikov

Belgorod State Technological University named after V.G. Shukhov,
Belgorod, Russia
klimenko34972@yandex.ru

Abstract. Based on experimental and theoretical data, the possibility of using lead oxides in the production of radiation-protective materials based on building gypsum was established. The influence of lead oxides of various compositions, such as β-PbO, β-Pb$_3$O$_4$, and α-PbO$_2$, on the physical, mechanical, and radiation-protective properties of gypsum composites was studied. It is established that the physical and mechanical characteristics of composite materials significantly depend on their structure, which in turn depends on the composition of lead oxide. The material based on BG and β-Pb$_3$O$_4$ consists of large gypsum crystals with a layered-batch structure. In contrast, the material based on BG and α-PbO$_2$ is represented by elongated thin prismatic gypsum crystals wrapped in a fine-crystalline mass of filler. No new compounds were found in the construction gypsum lead oxides system, which indicates a weak interaction between the filler and the binder. A composite finishing material for biological protection against ionizing radiation with a linear attenuation coefficient of 1.76–2.11 cm^{-1} was obtained on the basis of building gypsum and lead oxides. Composites based on BG and β-Pb$_3$O$_4$ have higher strength characteristics than those based on other lead oxides, which is due to their high dispersion and the presence of lead atoms in different degrees of oxidation. Compositions of composite materials are proposed.

Keywords: Composite materials · Building gypsum · Lead oxides of various compositions · Structure · Texture · Hydration mechanism · Radiation-protective properties of composites

1 Introduction

Radioactive radiation is successfully used in industry, energy, medicine, scientific research, production of building materials, obtaining new polymer materials, detection of defects in engineering communications, and other industries. The effectiveness of its use is not questioned by either scientists or specialists. However, the problems of protecting equipment and people from radiation exposure are always relevant and are under constant attention of scientists and the public [1].

The main part of radiation exposure (85%) the world's population receives from natural sources of radiation. Technogenic radiation sources account for about 21% of the total population exposure [2]. These include: production of electric and thermal energy at nuclear power plants and portable nuclear power plants, the nuclear fuel cycle, non-destructive testing and quality control of products in industry, sterilization and pasteurization of items and products, control of technological processes, production of radionuclides for various needs, and other processes.

For protection against radiation, lead and materials with its compounds, especially lead oxide (II), are most often used. Such materials significantly weaken photon radiation, suppress gamma radiation, and neutralize short-wave electromagnetic radiation. As binders in radiation-protective composites, both inorganic binders (Portland cement, alumina cement, magnesia cement, glycerol cement, liquid glass, etc.) are used [2–4], and organic binders (polyurethane foam, polystyrene, polyethylene, epoxy, furan and polyester resins, etc.) [5–7].

Gypsum binders, widely used for finishing works, have not found their rightful place among the binders used in the production of radiation-protective materials yet. At the same time, works on their use have recently begun to appear more often [8, 9].

Purpose of Work. To establish the possibility of obtaining materials for protection against ionizing radiation based on building gypsum and lead oxides.

2   Materials and Methods of Research

The following materials were used in the work: construction gypsum G-4 A II of JSC "Khabez gypsum plant" ($\beta-CaSO_4 \cdot 0.5H_2O$), lead oxides of the c.p specification β-PbO yellow, β-Pb_3O_4 red, α-PbO_2 brown. The initial materials and the resulting composites were studied using x-ray phase analysis on a DRON-4 diffractometer in the range $2\Theta = 4–56°$, scanning electron microscopy on a high-resolution scanning electron microscope TESCAN MIRA 3 LMU, and laser granulometry on a MicroSizer 201 device. The mass attenuation coefficient was determined using a dosimeter-radiometer DKS-96. Physical and mechanical properties of gypsum binders were studied in accordance with GOST.

3   Results and Discussion

At the initial stage of the work, laser granulometry of the initial lead oxides was performed, as the size of the filler plays a decisive role in the formation of the structure of composite materials (Table 1).

Table 1. Statistical values of the particle size of lead oxide fillers based on laser diffraction data.

Indicator	β-PbO	β-Pb$_3$O$_4$	α-PbO$_2$
Specific surface area, cm^2/cm^3	4795.0	18031.0	14246.0
Modal diameter, microns	61.51	4.73	23.98
D$_{10}$, microns	25.92	2.12	2.05
D$_{50}$, microns	55.99	4.68	8.42
D$_{90}$, microns	94.08	9.67	34.97
D$_{[4,3]}$, microns	58.20	5.40	14.30
Scope of the distribution (D$_{90}$ − D$_{10}$)/D$_{50}$	1.21	1.61	3.91

It is established that the dependence of the particle size distribution for β-PbO and β-Pb$_3$O$_4$ is monomodal, and for α-PbO$_2$ – bimodal. β-PbO has the largest particle size and, consequently, the smallest specific surface area. In contrast, β-Pb$_3$O$_4$ has the smallest particle size and the largest specific surface area. α-PbO$_2$ is an intermediate position in these indicators. The studied lead oxides can be attributed to fine fillers. They have different dispersity and should behave differently in the composition of gypsum compositions.

To study the effect of the composition and amount of lead oxides on building gypsum (BG), the following compositions were used (Table 2).

Table 2. Composition of compositions based on BG and lead oxides (BGPb).

Material	Amount of additive; %	Structure of composition; g			W/G
		BG	Lead oxide	H2O	
BG	–	70	–	38.5	0.55
BGPb-10	10	63	7	36.4	0.52
BGPb-20	20	56	14	34.3	0.49
BGPb-30	30	49	21	32.2	0.46
BGPb-40	40	42	28	30.1	0.43
BGPb-50	50	35	35	28.0	0.40
BGPb-60	60	28	42	26.0	0.37
BGPb-70	70	21	49	23.8	0.34
BGPb-80	80	14	56	21.7	0.31

W/G for G-4 A II – 0.55, for lead oxide – 0.25.

Fine fillers can both increase and decrease the water-gypsum ratio (W/G) of B G. So, fine-ground waste glass reduces W/G [10], and blast furnace slag, water removal ash, expanded clay and bricks increase W/G. All the lead oxides under study are reduced W/G of BG. When the amount of lead oxide additive is 80 wt. % this decrease is 45.5% (Table 2).

Preliminary studies showed that additives β-Pb_3O_4 and α-PbO_2 reduce the time of setting of BG, while β-PbO additives have almost no effect on them. To increase the time of setting of the BG, borax ($Na_2B_4O_7$) was selected in the amount of 0.2 wt.%. Borax additives increase the strength and time of setting of the BG.

The effect of lead oxides on the mechanical compressive strength of BG is shown in Fig. 1. From the data obtained, it follows that small amounts of lead oxide additives (up to 10 wt. %) affect the strength of the BG slightly. Moreover, β-Pb_3O_4 and α-PbO_2 increase slightly the strength of the BG. Increasing the amount of filler additive > 10 wt. % leads to a decrease in the strength of BG. Composites based on BG and β-Pb_3O_4 have higher strength indicators than those based on other lead oxides. This is the course of the Rcom dependence. The dependence on the amount of filler additive is typical for systems with little interaction between the filler and the binder [11]. Good formability of materials based on β-Pb_3O_4 and α-PbO_2 is noted, which is facilitated by the hydrophilicity of their surface and high dispersion. Composites based on BG and β-PbO are formed slightly worse, which is due to the large particle size of this filler.
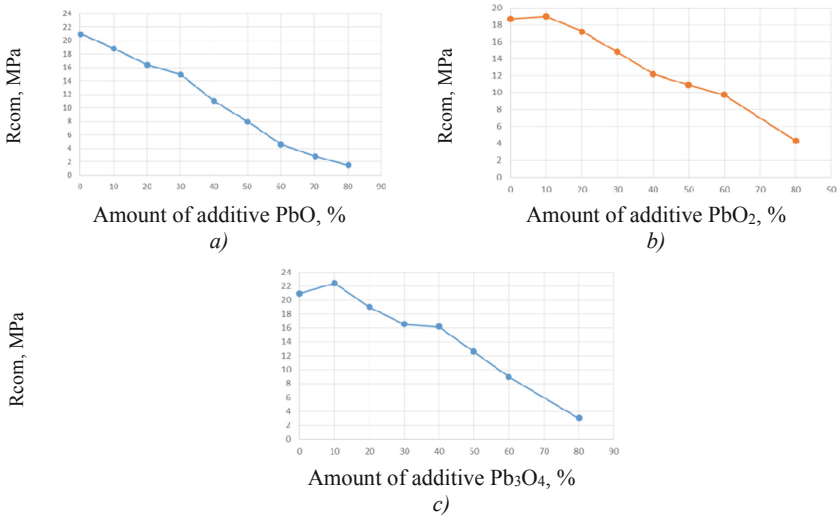
Fig. 1. Effect of lead oxide additives on the Rcom G-4 A II a – β-PbO; b – α-PbO_2; c – β-Pb_3O_4.

The density of composites based on BG and lead oxides varies from 1200 kg/m^3 (G-4) to 2000 kg/m^3 (composition with 80% filler) and practically does not depend on the nature of lead oxide.

To analyze the phase composition of the obtained composites, x-ray analysis of BGPb-50 composites was performed. It is established that the composites consist of: gypsum (reflexes at interplanar distances, Å: 7.628; 4.291; 3.801; 3.069; 2.702); α-PbO_2 (reflexes at interplanar distances, Å: 3.513; 2.801; 2.481; 1.855; 1.755); β-Pb_3O_4 (reflexes at interplanar distances, Å: 6.259; 3.389; 2.912; 2.793; 2.637); β-PbO (reflexes at interplanar distances, Å: 5.906; 3.074; 2.950; 2.747; 2.377). Non-hydrated

BG (reflexes at interplanar distances, Å: 6.046; 3.480; 3.013; 2.810) was found in insignificant amounts in materials based on α-PbO$_2$, and insoluble anhydrite (reflexes at interplanar distances, Å: 3.506; 2.858; 2.332; 2.209) in materials based on β-Pb$_3$O$_4$. At the same time, in systems based on β-Pb$_3$O$_4$, a certain distortion of the gypsum crystal lattice is observed which is expressed in an increase in the interplanar distance of the main reflexes on x-ray images and a change in their intensity. Thus, the RFA did not reveal the formation of new compounds in the BG-lead oxides system.

The structure of the obtained materials was studied using electron scanning microscopy. It is established (Fig. 2) that it depends on the nature of lead oxide. Thus, a material based on BG and α-PbO$_2$ consists of elongated prismatic thin gypsum crystals, sometimes bundles of crystals, the gaps between which are filled with a fine-grained earthy mass α-PbO$_2$ (Fig. 2 c). The structure of the composite based on BG and β-Pb$_3$O$_4$ is different and consists of larger plate-like gypsum crystals. The fine-crystalline mass is absent or present in insignificant amounts. There are more crystallization contacts in the material (Fig. 2 d).
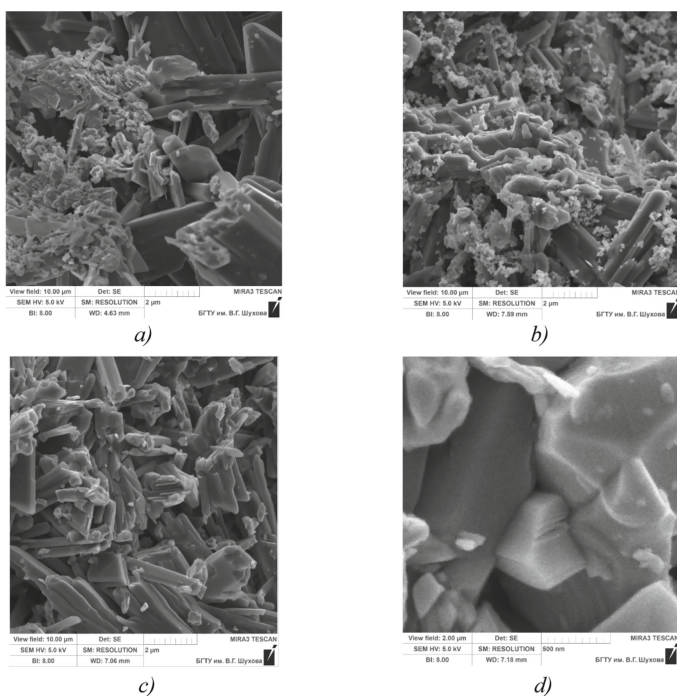
Fig. 2. Micrographs of composites based on: a – β-PbO and BG (BGPb$_1$-50); b – α-PbO$_2$ and BG (BGPb$_2$-50); c, d – β-Pb$_3$O$_4$ and BG (BGPb$_3$-50); a, b, c – magnification 10 μ; d – magnification 2.0 μ.

At the standard water-gypsum ratio, the porosity of gypsum stone is 47–55% by volume. The structure of solidified gypsum stone is characterized by high communicating porosity. These are mostly macropores. The proportion of micropores in gypsum building materials is insignificant. Modification of gypsum binders with fine-ground fillers reduces the proportion of macropores in the material and improves the structure of composite materials.

To study the radiation-protective properties of the obtained composites, pure gypsum samples and BGPb-60 compositions were taken. The results of calculations of linear (μ) and mass (μ_m) attenuation coefficients are presented in Table 3.

Table 3. Physical-mechanical and radiation-protective characteristics of composites.

Material	Rcom, MPa	ρ, kg/m^3	μ, cm^{-1}	μ_m, cm^2/g
BG	21.3	1370	1.27	0.92
BGPbO-60	4.6	1820	1.94	1.06
BGPbO$_2$–60	9.7	1810	2.11	1.16
BGPb$_3$O$_4$–60	8.9	1780	1.79	1.01

The obtained data show that the linear attenuation coefficients of composites are one and a half or more times greater than those of BG. This allows concluding that the radiation-protective properties of composites are significantly better than those of BG.

4   Conclusion

A composite finishing material for biological protection against ionizing radiation with a linear attenuation coefficient of 1.76–2.11 cm^{-1} was obtained from building gypsum and lead oxides. It is shown that the nature of lead oxide affects the strength and density of composite materials to a lesser extent than their granulometry. In the process of hydration and hardening of the composite, lead oxides do not change their texture and structure, but affect the formation and growth of gypsum crystals. The material based on BG and β-Pb$_3$O$_4$ consists of large gypsum crystals with a layered-batch structure. In contrast, the material based on BG and α-PbO$_2$ is represented by elongated thin prismatic gypsum crystals wrapped in a fine-crystalline mass of filler.

References

1. Dubrovsky, V.B.: Radiation Resistance of Building Materials. Stroyizdat, Moscow (1977)
2. Veselkin, A.P., Voskresensky, E.V., Egorov, V.: Research of protective properties of concrete of different compositions: monograph. Questions of reactor protection physics. Atomizdat, Moscow (1974)
3. Eger, T.: Concrete in the Technique of Protection from Radiation. Atomizdat, Moscow (1960)
4. Mashkovich, V.P., Kudryavtsev, A.V.: Protection from Ionizing Radiation. Energoatomizdat, Moscow (1995)
5. Li, I., Sidorov, Yu.D.: Material for protection against x-ray radiation based on a polymer composition and lead oxides. Bull. BSTU Named After V.G. Shukhov **6**, 11–16 (2016)
6. Pavlenko, V.I., Lipkansky, V.M., Yastrebinsky, R.N.: Structural defects of amorphous-crystalline phases based on lead organosiloxanes. Radiation physics of a solid body. MIEM, Moscow (2003)
7. Khakimullin, Yu.N., Abdullin, I.Sh., Galimzyanova, R.u., Ruchkin, A.V.: Polymer composition resistant to ionizing radiation. Pat. 2515558 RF 13 (2015)
8. Khezhev, T.A., Pukharenko, Y.V., Khezhev, K.A., Klyuev, S.V.: Fiber gypsum concrete composites with using volcanic tuffsawing waste. ARPN J. Eng. Appl. Sci. **13**(8), 2935–2946 (2018)
9. Klimenko, V.G., Chernyshev, A.Z., Strelnikov, A.I.: Modification of Magnesia Binder with Iron Ore Concentrate. Mater. Sci. Forum **974**, 113–118 (2019)
10. Klimenko V.G., Pavlenko V.I., Gasanov S.K.: Acid-base interactions in gypsum glass systems Bull. BSTU Named After V.G. Shukhov **5**, 77–81 (2015)
11. Klimenko, V.G.: Influence of modifying composition of gypsum binders on the structure of composite materials. J. Phys. Conf. Ser. **1118**, 012019 (2018)

Utilization of Drilling Waste in the Production of Construction Materials

Yu. E. Tokach$^{(\boxtimes)}$, Yu. K. Rubanov , O. S. Vyrodov ,
and A. N. Popova

Belgorod State Technological University named after V.G. Shukhov,
Belgorod, Russia
`tokach@bk.ru`

Abstract. A technology for the disposal of drilling waste is proposed that provides an inexpensive, environmentally friendly construction material that meets the required physical and mechanical characteristics and has protective properties against ionizing radiation. The results of research on determining the physical and mechanical properties of composite materials are presented. Studies were carried out for different contents of drilling sludge in the raw material mixture. It is shown that when the content of drilling sludge in the aggregate is 50%, the highest values of the compressive strength of samples are provided. These results correlate with data on the value of the attenuation coefficient of the ionizing radiation dose rate, which makes it possible to consider the ratio sand: drilling sludge = 50: 50 as the optimal composition of a composite material with increased mechanical strength and the ability to attenuate the ionizing radiation dose rate. The results of the study showed that the proposed compositions of composite materials are able to withstand long-term radiation exposure without significant deterioration of construction and technical properties. The proposed method of disposal of drilling waste increases environmental protection, improves the environmental situation and at the same time allows using cheap components to obtain building material for lining rooms with sources of ionizing radiation, for the construction of storage facilities for low-level radioactive waste.

Keywords: Drilling sludge · Construction materials · Environmental protection · Ionizing radiation

1 Introduction

Rational use of mineral resources, minimization of negative impacts and preservation of the productive natural environment is one of the main tasks of environmental research. Production activities of oil and gas companies inevitably lead to technogenic impact on the environment, which is expressed in the contamination of the earth's geosphere shells – the atmosphere, hydrosphere, and lithosphere [1–3]. During the construction of oil and gas wells, a significant amount of drilled rock, or drilling sludge, is extracted from the earth's crust interior from various geological formations. One of the most important tasks is to protect the natural environment from liquid and solid

drilling waste generated during the operation of drilling equipment. They consist of drilling waste water, spent drilling solution and drilling sludge, in some cases mixed in mud barns. The main factors affecting the impact of drilling waste on the surrounding elements of the biocenosis are determined by the composition and oil products and mineralized waters entering it from the bottom hole.

Drilling waste mostly consists of 30–45% of drilled rock (clay and sand particles), 30–45% – drilling fluids and 10–20% – possible technological discharges of underground water and oil: wash water, pickling solutions, waste electrolytes [4].

A promising method of utilization of drilling sludge is to use them as secondary raw materials for the manufacture of construction materials [5–7].

2   Methods and Materials

The paper considers a method for utilization of drilling sludge in an optimal way with minimization of economic costs in the production of building materials - concrete [8–11].

The object of research was drilling sludge formed during the drilling of exploration wells in the gas-bearing reservoir of the Yamburg oil and gas condensate field (YAOGCF) from a depth of 3400–3800 m.

Figure 1 shows an x-ray image of drilling sludge waste.
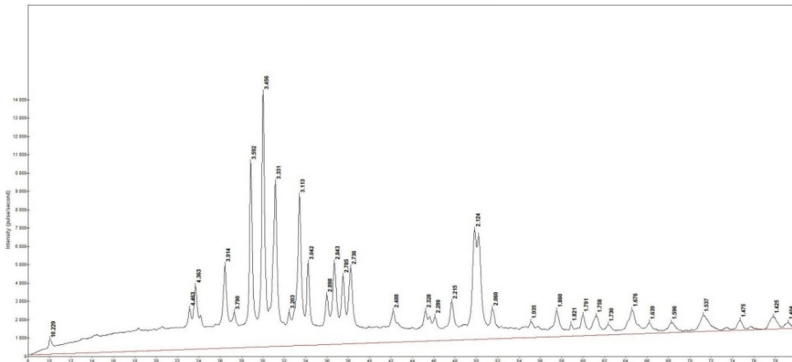
Fig. 1.   Radiograph of drilling sludge.

The x-ray phase composition is represented by the following phases: Kaolinite $Al_2[Si_2O_5](OH)_4$, Muscovite $KAl_2[AlSi_3O_{10}] (OH)_2$, Barite $BaSO_4$, Quartz SiO_2.

Table 1 shows the chemical composition of drilling sludge.

Table 1.   Chemical composition of drilling sludge (wt.%).

BaO	SO_3	SiO_2	CaO	Al_2O_3	Fe_2O_3	MgO	Na_2O
40.930	21.500	18.130	5.76	4.21	2.810	2.26	1.800

Chemical analysis of drilling sludge samples showed the presence of barium compounds. Analysis of the data presented in the literature [12–14] allows concluding that concretes based on barite aggregates have a fairly good radiation resistance. These concretes are able to withstand long-term radiation exposure without significant deterioration of their construction and technical properties.

Table 2. Granulometric composition.

Size of fractions, mm	1–0.25	0.25–0.05	0.05–0.01	0.01–0.005	0.005–0.001
Content, %	25.81	25.59	23.12	4.72	6.62
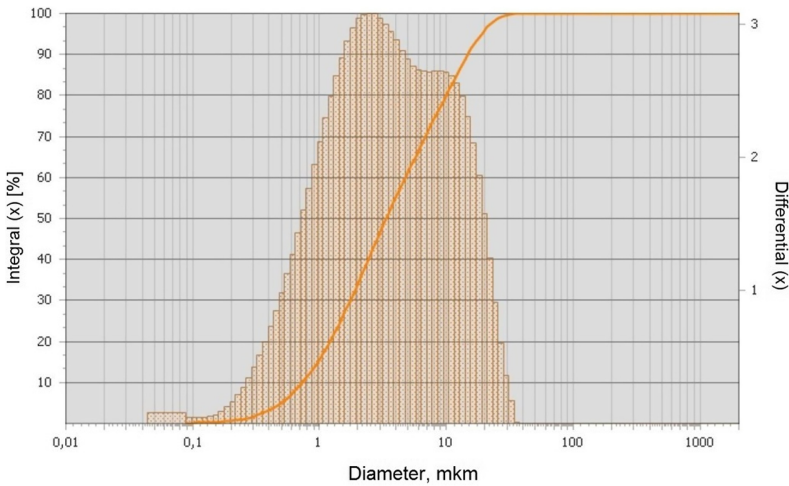
Fig. 2. Particle size distribution.

Table 2 and Fig. 2 show the granulometric composition of drilling sludge.

The study of the particle size distribution using an optical microscope and laser radiation scattering showed that most of the studied samples of drilling sludge are characterized by a bidisperse composition, expressed in one way or another.

3   Results and Discussion

Raw mixture for manufacture of building materials samples were prepared by mixing Portland cement grade 400 and filler in the form of drilling sludge and quartz sand with grain size of 1.5–3 mm, at various mixing ratios with added water, based on the conditions necessary plasticity of the mixture and depending on the moisture content of drilling sludge.

The results of studies with different content of drilling sludge in the raw material mixture are shown in Fig. 3, 4, 5 and 6.

When the content of drilling sludge in the aggregate is 50% in terms of dry matter, the highest values of the compressive strength of the samples are provided (Fig. 3). These results correlate with data on the value of the coefficient of half attenuation of the ionizing radiation dose rate, which makes it possible to consider the ratio sand: drilling sludge = 50: 50 as the optimal composition of a composite material with increased mechanical strength and the ability to attenuate the ionizing radiation dose rate (Fig. 6).

The increase in sample density with an increase in the content of drilling sludge in the mixture is due to the high density of drilling sludge (2800 kg/m^3).
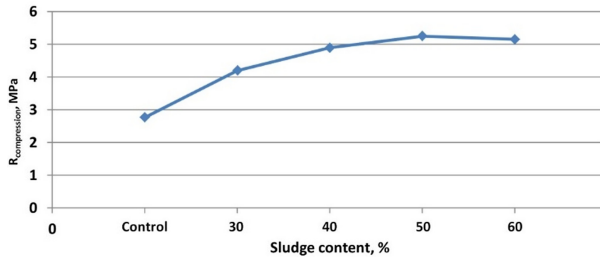
Fig. 3. Dependence of the compressive strength of samples on the mass fraction of drilling sludge in the composite.

The lowest water absorption is observed in samples with the ratio sand: drilling sludge = 50: 50.
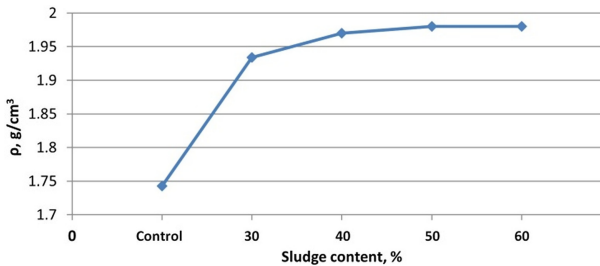
Fig. 4. Dependence of sample density on the mass fraction of drilling sludge in the composite.

The presence of sulfuric acid barite BaSO$_4$ in the drilling sludge allowed making an assumption about the possibility of using composite materials based on drilling sludge as materials for protection against ionizing radiation.
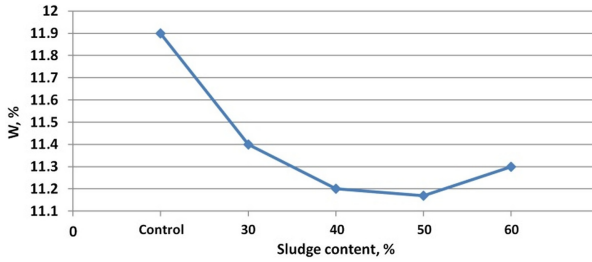
Fig. 5. Dependence of water absorption of samples on the mass fraction of drilling sludge in the composite.

Using a dosimeter-radiometer DKS-96, the thickness of the attenuation layer of the equivalent dose of ionizing radiation and the mass attenuation coefficient were determined. The dependence of the ionizing radiation attenuation coefficient on the mass fraction of drilling sludge in the filler and the thickness of the samples is shown in Fig. 6.

The data presented in Fig. 6 allow concluding that when the content of drilling sludge in the filler is 50–60%, the maximum value of the ionizing radiation attenuation coefficient is provided for a sample thickness of 0.4–0.8 cm.
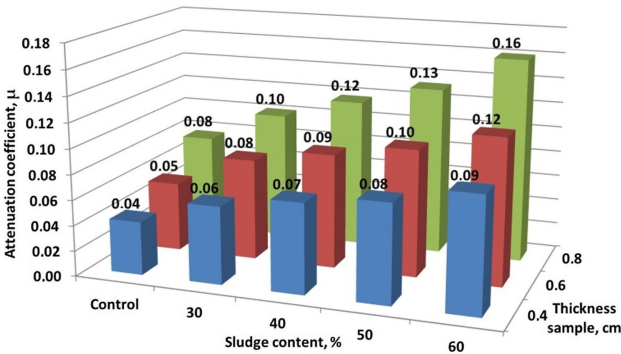
Fig. 6. Dependence of the attenuation coefficient on the mass fraction of drilling sludge in the composite.

4   Conclusion

The proposed method of disposal of drilling waste increases environmental protection, improves the environmental situation and at the same time allows using cheap components to obtain building material for lining rooms with sources of ionizing radiation, for the construction of storage facilities for low-level radioactive waste.
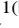
References

1. Bulatov, A.I.: Ecology in the Construction of Oil and Gas Wells. "Prosveschenie-Yug", Krasnodar (2011)
2. Pichugin, E.A.: Assessment of the impact of drilling sludge on the environment. Young Sci. **9**(56), 122–123 (2013)
3. Kujawska, J., Pawlowska M.: Earthworms as bio-indicators of chemical pollution in soils with drilling waste. In: 9th Conference on Interdisciplinary Problems in Environmental Protection and Engineering EKO-DOK 2017, Boguszow Gorce, Poland (2017)
4. Klyuchnikova, N.V., Genov, I., Kudina, A.E.: Polymeric surfactant for the oil industry. Bull. BSTU named after V.G. Shukhov **3**(11), 99–104 (2018)
5. Gorbunova, O.I., Kanitskaya, L.V.: Enviromental management in Russian oil and gas companies: environmental responsibility rating. Bull. Baikal State Univ. **27**(3), 366–371 (2017)
6. Ayati, B., Molineux, C., Newport, D., Cheeseman, C.: Manufacture and performance of lightweight aggregate from waste drill cuttings. J. Cleaner Prod. **208**, 252–260 (2019)
7. Wang, C.Q., Lin, X.Y., Mei, X.D., Luo, X.G.: Performance of non-fired bricks containing oil-based drilling cuttings pyrolysis residues of shale gas. J. Cleaner Prod. **206**, 282–296 (2019)
8. Batalin, B.S., Nechaeva, A.E.: Utilization of drilling sludge by processing into construction materials. Master's J. **2**, 148–152 (2013)
9. Pat. 2426708 Russian Federation, IPC, C04B33/06, B09B3/00. Building material. In: Utkina N.N., Akhmedsafin S.K., Arabsky A.K., Andreev O.P., Petrov G.F., Chesnov I.P.; patent holder of LLC "Research and production enterprise "Soyuzgaztechnology", LLC "Gazpromdobycha Yamburg". №2010127162/03; declared 05.07.2010; published 20.08.2011, Byul. 23. 14 p
10. Yagafarova, G.G., Barakhnina, V.B.: Utilization of environmentally hazardous drilling waste. Oil Gas Bus. **2**, 48–61 (2006)
11. Pat. 2389564 Russian Federation, IPC B09B3/00, C04B33/132, C04B33/32. Method for neutralization of drilling sludge to obtain construction material from it. In: Gorin V.M., Kabanova M.K., Kazmaly I.K., Kartashov A.A., Tokareva S.A., Uksyuzov V.L.: patent holder Closed joint stock company "SRIkeramzit". №2009122101/03; declared 10.06.2009; published 20.05.2010, Byul. 14
12. Korolev, E.V., Samoshin, A.P., Smironov, V.A., Koroleva, O.V., Grishina, A.P.: Methodology and Algorithm for the Synthesis of New Generation Radiation Protection Materials. PSUAC, Penza (2009)
13. Poroshin, A.P., Korolev, E.V., Demyanova, V.S., Komokhov, P.G.: Construction Solutions and Concretes for Protection from Radiation. PSUAC, Penza (2005)
14. Timoshenko, T.I., Zalogina, A.V., Khudasov, V.I.: Influence of ZnO and BaSO$_4$ additives on construction and technical properties of low-base white cements. Constr. Mater. Prod. **1**(3), 17–24 (2018)

The Role and Significance of Electric and Surface Properties of Mineral Filler in Increasing the Frost Resistance of Powder Concretes

Sh. M. Rakhimbayev[1] , N. M. Tolypina[1] , A. A. Kosinova[2] ,
and E. N. Khakhaleva[1(✉)]

[1] Belgorod State Technological University named after V.G. Shukhov,
Belgorod, Russia
hahaleva7@mail.ru
[2] Joint Stock Company "Plant of Reinforced Concrete Structures No. 1",
Belgorod, Russia

Abstract. The influence of mineral fillers with positively and negatively charged electric and surface properties on the frost resistance of powder concretes is studied. The authors put forward a hypothesis that in the processes of hydration and corrosion, where water molecules always participate, an important role is played by the electric and surface properties of the solid phase, which make up the binding system. Concretes where the charge on the surface of the pores and capillaries is strongly shifted to the negative area will be subject to a deeper saturation of the material with water and, consequently, will have less frost resistance. Tests for frost resistance were carried out according to GOST 10060-2012 (clause 5.1), according to the first basic method. It was found that the lowest frost resistance is found in samples of powdered concrete with 30% ground quartz sand, compared with powdered concrete with 30% ground marble and fine-grained concrete C:S = 1:3. The results confirmed hypothesis contained in this work. This is evidenced by the results of changes in the mass of samples during tests for frost resistance. It is proposed to use the obtained data as a theoretical basis for selecting rational compositions of high-frost-resistant concretes, both fine-grained and powdered.

Keywords: Electric and surface properties · Powder concrete · Mineral filler · Frost resistance

1 Introduction

It is known that electric and surface phenomena play a significant role in the processes of hardening and corrosion of building materials based on binders, including Portland cement [1–3]. In most cement concretes, materials with active centers of different charge signs and numerical values are used as mineral additives, small and large aggregates. Materials with a negative zeta potential sign include quartz sand, granite, quartzite sandstone, calcium hydrosilicates, etc., and positively charged active centers

are located on the surface of portlandite particles, calcium and magnesium hydroxides, calcium hydroaluminates, and iron oxides [4–10]. As for calcium carbonates, the charge sign of their active centers depends on the synthesis conditions, the composition of the external environment, and other factors [11, 12].

Water molecules have a weakly expressed positive effective charge, which is concentrated on two hydrogen ions that are part of them [13]. The hypothesis follows from the above, which is that in the processes of hydration and corrosion, where water molecules are always involved, an important role is played by the electric and surface properties of the solid phase, which make up the binding system. In particular, in the case of magnesia aggression, which is carried by positively charged magnesium ions, filler and aggregate particles, which usually carry a negative charge sign, will stimulate the advance of the corrosion front deep into building products and structures. This can also be facilitated by the pore walls of cement stone, which is dominated by negatively charged calcium hydrosilicates. If positively charged materials, such as limestone, dolomite, marble, iron oxides, etc., are used as mineral additives, as well as small and large aggregates in concrete, the intensity of corrosion processes will decrease. During freeze-thaw corrosion, which plays a particularly important role in the harsh climate conditions typical for most of the Russian Federation, as well as countries such as Canada and Norway, the most important processes are the migration of water molecules through the pores of the material.

This leads to the conclusion that under conditions of freeze-thaw corrosion when using fine mineral additives, as well as fine and coarse aggregates, materials with a positive zeta potential sign, the intensity of destructive processes will decrease, and when using quartz sand, granite and other rocks – increase.

In sulfate corrosion, the main aggressive agent is the sulfate ion, which has a negative charge sign. In this regard, it can be assumed that the use of materials with a negative zeta potential as mineral components in this type of corrosion is more preferable than those with a positive charge.

To test these hypotheses, studies were performed, the results of which are described below.

2   Methods and Materials

Two types of aggregates (fillers) were used for research: marble with a predominantly positive electric and surface charge and quartz sand with a predominantly electronegative surface charge.

The electrokinetic potential was determined using the Zetasizer Nano ZS equipment using the M3-PALS method. The prevailing surface charge of quartz sand corresponds to -31.6 mV, marble $+19.3$ mV. In small quantities there are active centers of the opposite sign: quartz sand has $+3.13$ mV (7.9%), marble -85.6 mV (5.1%). But in general, the surface of quartz filler is dominated by a negative charge, while marble has a positive charge.

As a binder, we used CEM I 42.5 N of JSC "Belgorodcement", mineral fillers – powders of marble and quartz sand crushed to a specific surface of Ssp = 330 m^2/kg. The amount of fillers in the powder concrete compositions was 30%. The mobility of

the mixture (Pq) was determined according to GOST 5802-86 (clause 2). For the production of samples, forms with a size of $70.7 \times 70.7 \times 70.7$ mm were used. Storage of control samples and determination of strength was performed in accordance with the requirements of GOST 10180. The properties of the studied compounds are shown in Table 1.

Table 1. Technical properties of the studied compounds.

Parameter	Compound №1	Compound №2	Compound №3 control
	PC: ground marble = 70:30 (%)	PC: ground quartz sand = 70:30 (%)	PC: ground quartz = 1:3 (%)
Working composition of the mixture for a batch of 1 l, g: CEM I 42.5 N	1260	1260	500
Ground marble	540	–	–
Ground quartz sand	–	540	–
Quartz sand	–	–	1500
Water	556	617	359
W/C	0.44	0.49	0.72
Characteristics of the mixture: P_q, cm	12,1	11,4	10,7
Mixture density, kg/m^3	2016	2030	2176
Mixture yield coefficient	0.86	0.84	0.92
Properties of concrete that hardened 28 days in n. c.: Density, kg/m^3	1973	1841	2128
Compressive strength, MPa	48.0	90.2	20.2

3   Results and Discussions

Tests for frost resistance were carried out according to GOST 10060-2012 (clause 5.1), according to the first basic method: saturation medium – water; medium and freezing temperature – air (-18 ± 2 °C); medium and thawing temperature – water (20 ± 2 ° C). After every 5 cycles of alternate freezing and thawing, the samples were weighed and examined for defects (cracks, chips). The tests were stopped when the limit values were reached: a decrease in the sample mass of more than 2%; the crack opening width of more than 0.1 mm. When the sample reached one of the specified limit values, the sample was tested for compressive strength. Tests were carried out until 100 cycles of alternating freezing and thawing was reached.

Samples of powdered concrete with 30% ground quartz sand have the lowest frost resistance, compared to powdered concrete with 30% ground marble and fine-grained concrete C:S = 1:3.

The destruction of samples of compound №2 began much earlier than that of the other two compounds. Half of the samples withstood 26 cycles, and the rest – 78 freeze-thaw cycles. Defects appeared in the form of cracks: at the initial stage, hairline, then with different opening widths (Fig. 1).

Fig. 1. Sample of compound №2 after frost resistance tests.

During the last cycles of freezing and thawing, flaking in the form of plates was observed. It should be emphasized that there were no mass losses during testing of samples of compound № 2, but on the contrary, there was an increase in mass by an average of 0.7–1.2%. Samples with a size of 7. 07 × 7. 07 × 7.07 cm, destroyed after 26 and 78 cycles, added about 5 g in mass, i.e. the mass increased by 0.7–1.2%, while other compositions were characterized by mass loss (Table 2).

Table 2. Results of frost resistance tests.

Compound № 1	Compound № 2	Compound № 3
The average loss of mass in a series of core samples – 0.33% The average loss in strength in a series of core samples – 21.8%	The increase in mass in a series of core samples – 0.7–1.2%. Loss of strength in a series of basic samples after a different number of freezing and thawing cycles 21–84%.	The average loss of mass in a series of core samples – 0.13% The average loss in strength in a series of core samples – 7%

The destruction of the sample-cube during the compression test was carried out in bursting layers without crumbling, perpendicular to the loading plane. The strength loss during the test is significant, ranging from 21 to 84% of the strength of the control samples that were not subjected to freezing.

Compounds №1 and №3 withstood 100 freeze-thaw cycles (Fig. 2).

The use of an additive of ground marble (30%) as a micro-filler has a positive effect on the frost resistance of powdered concrete in comparison with the addition of the same amount of ground quartz sand. This is explained as follows. The addition of ground marble shifts the electrokinetic potential of the surface of cement stone
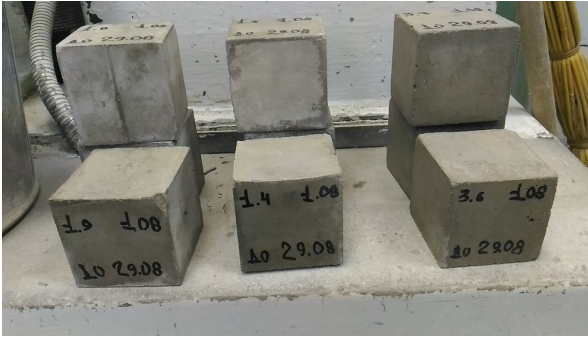
Fig. 2. Samples of compositions №1 and №3 after 100 freeze-thaw cycles.

capillaries to the positive side, which makes it difficult for water molecules to migrate in the capillary-porous system during periodic freezing-thawing, as the positive charge prevails in water dipoles. Ground quartz sand with electronegative surface properties shifts the charge of the surface of pores and capillaries to the negative area, which contributes to more intensive migration of water molecules and deeper saturation of the material with water. This is evidenced by the results of changes in the mass of samples during tests for frost resistance.

From our working hypothesis stated in this paper, it follows that concretes in which the negative electric charge is strongly shifted to the negative area should have an increased affinity for water and a tendency to water saturation. This forecast is fully confirmed by the example of composition №2, in which ground quartz sand is added. It is obvious that fine-grained concretes with a high content of quartz sand have the same properties. It follows from this that the method of determining frost resistance according to GOST 10060-2012 by determining mass loss can give unreliable results, as the mass loss as a result of painting the corners and edges of samples can be more or less compensated by water accumulation. In this regard, this method requires adjustment.

From the above data, it follows that the working hypothesis put forward by the authors, set out in the introduction of this work, was fully confirmed.

4   Conclusion

The most interesting result obtained in experimental studies is the fact that powdered concrete with the addition of ground quartz sand turned out to be less frost-resistant than standard fine-grained concrete of the composition C:S = 1:3, although the latter is characterized by significant porosity in the area of medium pore size, as well as lower mechanical strength. This result is due to the fact that the zeta potential of the surface of pores and capillaries in powder concrete with a filler of ground quartz sand is more strongly shifted to the negative area than in concretes with quartz sand of the compound 1:3. These data are the theoretical basis for the selection of a rational composition of both fine-grained and powder concrete with increased frost resistance.

References

1. Solomatov, V.I.: On interaction forces in a dispersed cement system. Izv. vuzov. Constr. Archit. **3**, 49–52 (1996)
2. Rakhimbaev, Sh.M., Tolypina, N.M., Khakhaleva, E.N.: Influence of fine aggregate on efficiency of liquidizing agents. Vestn. SibADI **3**(49), 74–79 (2016)
3. Rakhimbaev, Sh.M., Tolypina, N.M., Karpacheva, E.N.: The role of films adsorbed on the surface of natural quartz sand particles in the processes of plasticization of concrete mixtures. Ind. Civil Constr. **8**, 15–18 (2014)
4. Alves, J.A., Baldo, J.B.: The behavior of zeta potential of silica suspensions. New J. Glass Ceram. **4**, 29–37 (2014)
5. Plugin, A.N.: Electropitanie interaction during curing of the cement binder. Avtoreferat thesis. Ph.d. Kharkiv 282 (1989)
6. Ersoy, B., Dikmen, S., Uygunoğlu, T., Icduygu, M.G., Kavas, T., Olgun, A.: Effect of mixing water types on the time-dependent zeta potential of Portland cement paste. Sci. Eng. Compos. Mater. **20**(3), 285–292 (2013)
7. Lesovik, V.S., Shukhov, V.G., Tolstoy, A.D., Glagolev, E.S., Novikov, K.Y., Valerievna, S.V.: Powdered concretes on composition binders with application of technogene raw materials. Int. J. Pharm. Technol. **8**(4), 24726–24732 (2016)
8. Vovk, A.I.: Superplasticizers in concrete: analysis of the chemistry of processes. Technol. Concr. **3**, 12–14 (2007)
9. Moulin, P., Roques, H.: Zeta potential measurement of calcium carbonate. J. Colloid Interface Sci. **261**, 115–126 (2003)
10. Minakov, S.V.: Influence of complex organo-mineral additives on the properties of cement stone. Technology, organization, mechanization and geodetic support of construction. In: Conference Proceedings on Bulletin Of The DonNACEA vol. 3, no. 83, pp. 43–45 (2010)
11. Rusanov, A.I.: Thermodynamics of Surface Phenomena. Leningrad University, Leningrad (1960)
12. Tolstoy, A.D., Kovaleva, I.A., Novikov, K.Yu.: Improving the composition and properties of powder concrete with technogenic raw materials. Bull. BSTU named after V.G. Shukhov **2**, 19–24 (2016)
13. Minakov, S.V.: Influence of mineral additives on the effectiveness of plasticizers of cement systems. In: Theory and Practice of Improving the Efficiency of Building Materials. Proceedings of the all-Russian Conference of Young Scientists, Penza, PGUAS, pp. 124–127 (2008)

Strengthening of the Adhesive Joint in the Production of Glued Beams

S. I. Ovsyannikov[1(✉)] , A. A. Suska[2] , D. A. Levkin[2] ,
and O. L. Rudenko[1]

[1] Belgorod State Technological University named after V.G. Shukhov,
Belgorod, Russia
ovsrg@mail.ru
[2] Kharkov National Technical University of Agriculture named after Petro
Vasilenko, Kharkiv, Ukraine

Abstract. Wood is widely used in construction for the production of walls, partitions, floor structures and roofs. Since wood is an anisotropic material, its physical and mechanical properties depend on many factors, including the presence of defects in the form of knots and cracks. To ensure the stability of the properties of the structure, they are made by layer-by-layer gluing of wooden blanks with removed defects. Based on the conducted research, it was found that the strength of the adhesive joint is limited by the strength of the wood to cleave along the fibers, especially for spruce species. To strengthen the deeper layers of wood, it is proposed to prick the glued surfaces. Through the holes, the glue gets into deeper layers and spreads over the tracheal cells, making them more durable. The experiments showed that the strength of the joint with impaled wood is 27% higher compared to wood without impaling.

Keywords: Wood structure · Glued laminated timber (Glulam) · Adhesives · Shear stress

1 Introduction

Wood is a unique building material. It has a number of advantages in comparison with other building materials [1–5]: sufficiently high compressive and Flexural strength; it is an environmentally friendly finishing and construction material; it has low thermal conductivity; it is easily connected using adhesives, nagels and threaded connections. In construction, in most cases, wood structures are made in the form of panel [6–9] and beam [10–13] products.

Wood belongs to anisotropic materials [14, 15], has defects that reduce its strength properties and durability of products and structures [16–18]. To reduce the influence of anisotropic properties of wood on the quality of products and structures, areas with defects and defects are removed. The resulting defect-free parts are joined with glue on a smooth milled surface or on a toothed spike [2, 19]. The quality and strength of the adhesive joint depends on many factors [20, 21]: the type of glue used, the technological modes of bonding, the structure of wood and the direction of fibers on the surfaces to be bonded, and the operating conditions of the products.

Destruction of the adhesive joint can be divided into peeling along the adhesive seam [21] and destruction of wood along the adhesive seam. The reasons for the destruction of the adhesive seam can be various factors. For example, the destruction of the adhesive seam under the influence of solar ultraviolet light for PUR-glue or high humidity for PVA-glue, insufficient amount of glue, the so-called "starvation bonding", insufficient depth of penetration of the glue into the wood, and other reasons.

The practice of production of glued wood shows that gluing technologies can achieve the strength of the adhesive seam above the strength of wood [21]. The destruction of wood occurs along the layers of early wood adjacent to the adhesive seam (Fig. 1). most often, the destruction of wood along the adhesive seam occurs when the humidity of wood changes. The resulting stresses from changes in wood moisture exceed the strength properties, which leads to the destruction of wood along the adhesive seam. In most cases, destruction occurs in layers of early wood. As noted in the works, when gluing on a smooth puffer [2, 4, 7, 24], the depth of penetration of the glue is about 1 mm, which is not enough to saturate the pores of the wood and strengthen the deeper layers.

Thus, it can be concluded that the strength of the adhesive joint is limited not so much by the strength of the adhesive layer, but by the strength of the adjacent layers of wood for chipping.

It is proposed to increase the strength properties of wood, and therefore the adhesive compound, by strengthening the walls of wood vessels with an adhesive composition. For deeper penetration of the adhesive composition into the vessels of the annual layers of wood, it is proposed to prick the surfaces to be glued. This ensures that the glue penetrates through the holes into the deeper layers and further spreads through the tracheal vessels.

The purpose of this study is to investigate the process of strengthening the adhesive joint of wood in the production of glued beams by increasing the depth of penetration of the adhesive composition into the pores of wood by pricking the glued surfaces. The purpose of the study is to determine the optimal density and depth of the pinned holes.

The test program provides a comparison of the strength of the adhesive joint and the process of destruction of wood without impaling (control samples) and with impaling of different densities.

The method of impaling wood is widely used when saturating wood with protective solutions [20–24].

2   Methods and Materials

2.1   Wood

As samples, we used sawn timber from common or European spruce (Picea abies or Picea exselsa), which grows in the Vladimir region of the Russian Federation. The quality of sawn timber samples corresponded to grade 2 according to the state standard of the Russian Federation GOST 8486. The humidity of the samples was $12 \pm 2\%$, and the average density was 446 kg/m^3.

Blanks were selected from the same batch of blanks to ensure uniformity of wood properties of different stands. The blanks were conditioned in a room with an air humidity of 65 ± 5% and a temperature of 22 ± 2 ° C. for experiments, blanks 1000 mm long, 150 mm wide and 25 mm thick were cut out of lumber.

2.2   Glue

For wood bonding, a 2-component dispersion glue based on an emulsion of polymer isocyanate – EPI-glue Kleiberit 304.4. when Adding KLEIBERIT 808.0 hardener in an amount of up to 5%, the moisture resistance increases to the D4+ level. This type of glue is used in wooden housing construction for the production of products with increased load when used outdoors.

The viscosity is 10.0 MPa/s, the open exposure time is 8–12 min, and the pressing time is 45 min. The glue consumption varied between 120–200 g/m^2 according to the manufacturer's recommendations.

2.3   Experimental Methods

The experimental program included manufacturing and testing the strength of wood-wood adhesive joints when chipping along the fibers of the adhesive joint. Samples of glued wood were tested according to the method of assessing the strength of adhesive joints described in the state standard of the Russian Federation GOST 33120-2014. The parameters of cleavage strength along the fibers of the adhesive layer, the percentage of adhesive failures, as well as the form of wood destruction were compared.

For the purity of the experiment, the glued lamellas were divided into three equal parts. One part was filled with holes with a density of 15 pcs/cm^2, the second part with a density of 8 pcs/cm^2, and the third part was the control part (Fig. 1). the test Program is presented in Table 1.
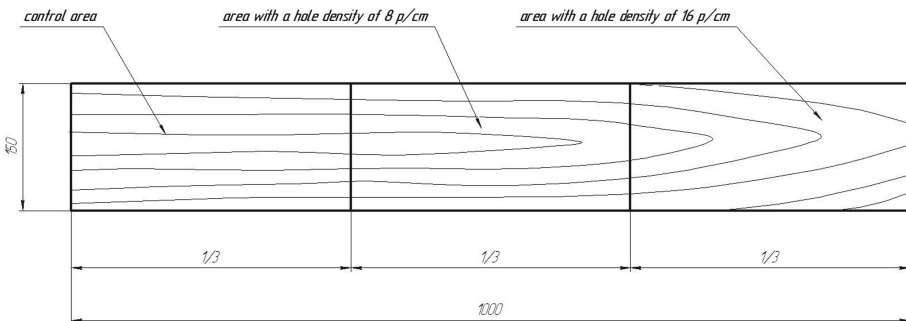
Fig. 1. Areas of the workpiece before gluing.

Table 1. The parameters of the test program.

Parameters	Dimension	Min	Max
Density of punched holes	pcs/cm^2	8	15
The depth of penetration of the needles	mm	1.5	2,5
Pressing pressure	MPa	0.7	0.9
Needle diameter	mm	0.8	0.8

The wood surface was impaled by rollers with needles on the surface with a diameter of 0.8 mm (Fig. 2). the density of holes was 8 and 15 pcs/cm^2, provided by one or two rolling of the workpiece. The depth of impaling was regulated by the degree of pressing the roller to the surface of the workpiece through a pressure spring. The pressure of pressing when gluing spruce wood was 0.7–0.9 MPa.

18 samples were cut out of glued beams from each zone for strength tests. The size and shape of the samples corresponded to the recommendations in the state standard of the Russian Federation GOST 33120-2014.

The cleavage strength along the adhesive seam was determined using a PGM-50 hydraulic press.
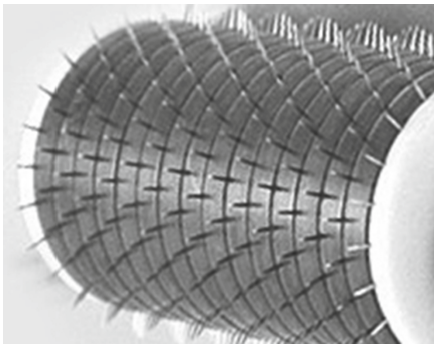
Fig. 2. General view of the roller with needles.

Fig. 3. Glue spreading through the pin hole.

3   Results and Discussions

As a result of tests, it was found that the adhesive composition penetrates the entire depth of the impaled hole and spreads over the tracheids (Fig. 3). In the course of the research strength of the adhesive bond established that the destruction of a specimen occurs at the bonded wood (64%), on a glutinous seam (8%) and mixed (28%) (Fig. 4).

The strength of the connection of workpieces with the sprayed-on surfaces increased 7.69 MPa at density of holes 8 PCs/cm^2 and of 8.46 MPa at density of holes 15 pcs/cm^2 (Fig. 5).

With an increase in the depth of the pinned holes from 1.5 mm to 2.5 mm, the joint strength increased by 11%.
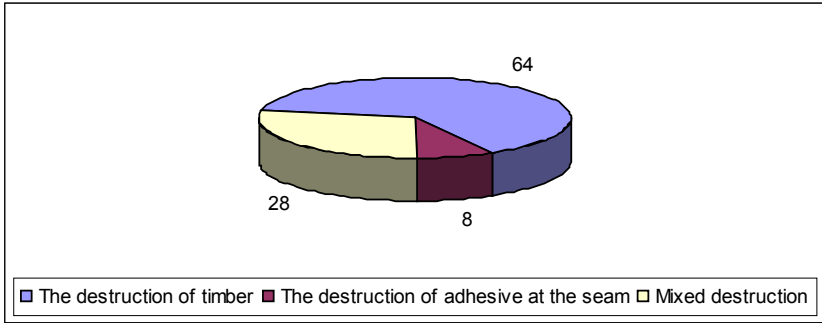
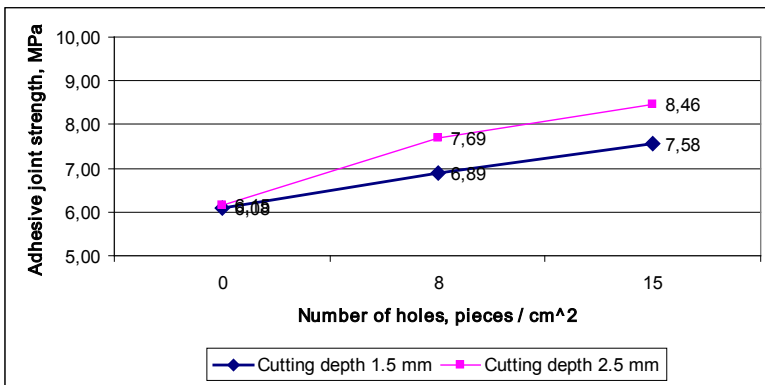**Fig. 4.** Structure of destruction of samples with a density of pin holes 8 pcs/cm^2, %.

Fig. 5. Strength of the adhesive joint depending on the density and depth of impaling.

4   Conclusion

Modern adhesive compositions provide the normalized strength of the adhesive seam when longitudinal gluing of lamellas into a bar. Destruction occurs along the wood along the adhesive seam. This effect is especially evident in soft wood species such as spruce or fir. These breeds are widely used in the production of glued beams for construction. To strengthen the wood layers adjacent to the adhesive seam, it is proposed to impregnate the vessel walls of deeper layers with an adhesive composition through holes obtained by piercing the surfaces to be glued.

As a result of the conducted experiments, it was found that at a pricking density of 15 PCs/cm^2 and a depth of 2.5 mm, the strength of the adhesive joint increases to 27% compared to samples without pricking. With an increase in the piercing depth from 1.5 mm to 2.5 mm, the joint strength increases by 11%.

References

1. Negrão, J.H.J.D.O., et al.: Glued composite timber-concrete beams. I interlayer connection specimen tests. J. Struct. Eng. **136**(10), 1236–1245 (2010)
2. Ramage, M.H., et al.: The wood from the trees: the use of timber in construction. Renew. Sust. Energy Rev. **68**, 333–359 (2017)
3. Ovsyannikov, S.I., Dyachenko, V.Y.: Wooden nano-composite materials and prospects of their application in wooden housing construction. Mater. Sci. Forum **931**, 583–588 (2018)
4. Kuzman, M.K., Oblak, L., Vratuša, S.: Glued laminated timber in architecture. Drvna Industrija **61**(3), 197–204 (2010)
5. Ovsyannikov, S.I., Suska, A.A., Shevchenko, S.A.: The formation of the heat-insulating protecting structures of dome buildings to the Far North. Constr. Mater. Prod. **4**(2), 21–26 (2019)
6. Jayalath, A., et al.: Life cycle performance of cross laminated timber mid-rise residential buildings in Australia. Energy Build. **223**, p. 110091 (2020)
7. Gamerro, J., Bocquet, J.F., Weinand, Y.: Experimental investigations on the load-carrying capacity of digitally produced wood-wood connections. Eng. Struct. **213**, 110576 (2020)
8. Boggian, F, Andreolli, M, Tomasi, R.: Cross Laminated Timber (CLT) beams loaded in plane: testing stiffness and shear strength. Front. Built Environ. **5**, p. 58 (2019)
9. Shahnewaz, M., Popovski, M., Tannert, T.: Deflection of crosslaminated timber shear walls for platform-type construction. Eng. Struct. **221**, 111091 (2020)
10. Muttashar, M., Manalo, A., Karunasena, W., Lokuge, W.: Flexural behaviour of multi-celled GFRP composite beams with concrete infill: experiment and theoretical analysis. Compos. Struct. **159**, 21–33 (2017)
11. Rajczyk, M., Jonczyk, D.: Behavior of glulam beams strengthened with BFRP bars. Mater. Sci. Eng. **603**, p. 042004 (2019)
12. Fu, Q., et al.: Interfacial bond behavior between wood chip concrete and engineered timber glued by various adhesives. Construct. Build. Mater. **238**, p. 117743 (2020)
13. Vahedian, A., Shrestha, R., Crews, K.: Experimental and analytical investigation on CFRP strengthened glulam laminated timber beams: Full-scale experiments. Compos. Part B. Eng. **164**, 377–389 (2019)
14. Trtik, P., et al.: 3D imaging of microstructure of spruce wood. J. Struct. Biol. **159**(1), 46–55 (2007)
15. Kahle, E., Woodhouse, J.: The influence of cell geometry on the elasticity of softwood. J. Mater. Sci. **29**, 1250–1259 (1994)
16. Ponomarev, V.S., Kashevarova, G.G.: PNRPU. Mechanics. Bulletin **2**, 112–122 (2020)
17. Benvenuti, E., Orlando, N., Gebhardt, C., Kaliske, M.: An orthotropic multi-surface damage-plasticity FE-formulation for wood: Part I – Constitutive model. Computers & Structures 240 (2020)
18. Lukacevic, M., et al.: A microstructure-based multisurface failure criterion for the description of brittle and ductile failure mechanisms of clearwood. Eng. Fract. Mech. **176**, 83–99 (2017)
19. Estrella, X., et al.: Efficient nonlinear modeling of strong wood frame shear walls for mid-rise buildings. Eng. Struct. **215**, 110670 (2020)

20. Betti, M., et al.: Comparison of newly proposed test methods to evaluate the bonding quality of cross-laminated timber (CLT) panels by means of experimental data and finite element (FE) analysis. Constr. Build. Mater. 952–963 (2016)
21. Calil Neto, C.: Madeira Laminada Colada (MLC): Controle de Qualidade em Combinações Espécie-Adesivo-Tratamento Preservativo 118 (2011)
22. Baraks, A.M., Nikiforov, Yu. N.: Deep impregnation of wood by applying pricks. Forest industry publishing house 176 (1969)
23. Sharapov, E., Brischke, C., Militz, H.: Assessment of preservative-treated wooden poles using drilling-resistance measurements. Forests **11**(1), p. 20 (2020)
24. Henrik, D., Erik, S.: Cross laminated timber at in-plane beam loading – prediction of shear stresses in crossing areas. Eng. Struct. **171**, 921–927 (2018)

Composite Binders and Dry Building Mixes for 3D Additive Technologies

E. S. Glagolev , V. S. Lesovik , L. H. Zagorodnyuk$^{(\boxtimes)}$,
and D. S. Podgornyi

Belgorod State Technological University named after V.G. Shukhov,
Belgorod, Russia
`lhz47@mail.ru`

Abstract. Currently, there are many revolutionary technologies in construction, among which a significant place is occupied by construction 3D printing. It attracts an increasing number of researchers and entrepreneurs. However, the creation of effective compositions for this technology is still an urgent issue, as these mixtures must have a number of required characteristics: high plasticity during extrusion and low fluidity after laying the mixture, as well as a high setting speed. The results of research on the preparation of composite binders based on Portland cement using a superplasticizer and a hardening accelerator are presented. To reduce the energy intensity and cost of production, wet magnetic separation dropouts of metallurgical production were added to the compositions. Optimal dosages of the accelerator additive and superplasticizer when used together were established. A comprehensive study of the samples was performed using x-ray phase analysis and electron microscopy. A two-factor mathematical model of the obtained composite binders is proposed using regression equations and the optimal composition is selected for construction 3D printing. Energy-efficient, cost-effective compositions were obtained that have the required characteristics for workability in 3D printing, as well as a high speed of setting and hardening with guaranteed strength characteristics. A technological solution for the introduction of hardening accelerators directly during extrusion is proposed.

Keywords: Composite binders · Dry building mixes · 3D additive technologies · Composition · Microstructure

1 Introduction

As a result of global urbanization and significant demographic changes, modern construction methods will not be able to solve the tasks assigned to them, as a result, the construction industry will undergo significant changes in the coming years. One of the main directions of development of construction technologies will be construction 3D printing. The main feature of this technology is the layer-by-layer construction (printing) of buildings and structures implemented using computer modeling.

However, traditional compositions of building mixes [1] cannot provide the required rheological and strength properties when constructing structures using this

technology [2–4]. In 3D technologies, it is advisable to use dry building mixes (DBM) with the necessary parameters. To ensure high quality of the DBM, it is necessary to select raw materials rationally, ensure optimal granulometric composition, homogeneity and high-quality mixing of the components of the raw mixture [4–8].

In this paper, composite binders (CB) have been developed that provide the required properties for construction 3D printing.

2   Materials and Methods

The following raw materials were used in the development: Portland cement of the 500 Brand without mineral additives produced by JSC Oskolcement, waste from wet magnetic separation (WMS) of ferruginous quartzite was used as mineral filler, and a plasticizing additive SP-3 and a hardening accelerator sodium carbonate (Na_2CO_3) were used to modify the mixtures.

CB preparation was carried out in a vibrating mill. The microstructure of samples of hydrated CB at the age of 28 days was studied using a high-resolution scanning electron microscope TESCAN MIRA3 LMU. X-ray phase analysis was performed on an ARL 9900 WorkStation series x-ray fluorescence spectrometer with a built-in diffraction system. Physical and mechanical properties of CB were determined in accordance with regulatory requirements.

3   Results and Discussions

CB creating for construction 3D printing requires the selection of a composition with the required rheological properties and the speed of setting and hardening [8–10]. To achieve maximum energy efficiency and reduce the cost of binders, it is advisable to insert mineral fillers into the compositions. We used wet magnetic separation waste [10–13].

The insertion of additives-accelerators allows not only to speed up the setting and hardening time (by 25% or more at normal temperature), but also to increase the strength in the early stages of hardening (up to 20% at the age of 1 day), as well as to reduce the consumption of cement [12].

In addition to creating the required rheological properties of the mixture, the plasticizing additive also reduces cement consumption by 15% [1].

The SP-3 superplasticizer was used as a plasticizing additive. It was found that the optimal dosage of the plasticizer is 0.5%. At this dose the required standard of flow of minicons is achieved.

Selection of the optimal amount of the hardening accelerator additive (sodium carbonate) was carried out by inserting from 0 to 1% into the cement paste. It was found that the required setting start time, which provides accelerated setting and hardening times, is observed at dosages from 0.2 to 0.4%.

A matrix of experiment planning was made, and two variables were taken as the following: the WMS waste dosage from 0 to 50% and the amount of accelerator

additive (Na_2CO_3) from 0.2 to 0.4% with a constant content of plasticizing additive SP-3 – 0.5% (Table 1).

Table 1. Conditions for an experiment planning.

Factor		Variation levels			Range of variation
Natural form	Encoded form	−1	0	1	
Amount of accelerator additive (Na_2CO_3), %	x_1	0	0.2	0.4	0.2
Share of WMS in the binder	x_2	0.5	0.25	0	0.25

The planning matrix includes 9 compositions. For each planned part of fluidity was determined using minicons, the samples were formed and tested within the established deadlines.
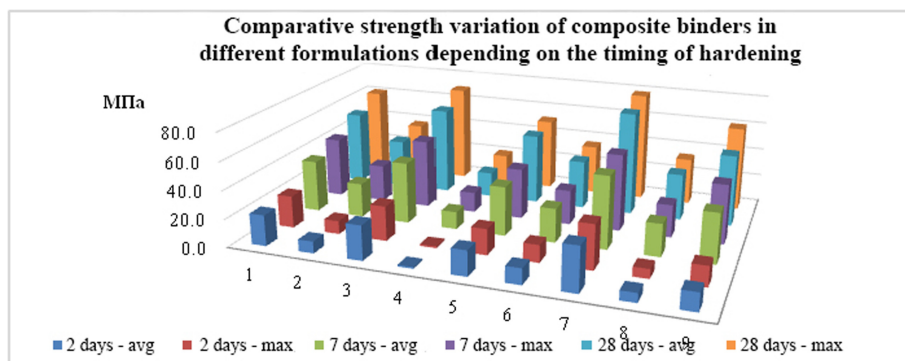
Fig. 1. Changes in the strength of composite binders of various compositions depending on the time of hardening.

Analyzing the results (Fig. 1), an increase in the hardening time with an increase in strength is observed in all compositions. In compositions with 100% cement content (compositions 1, 3 and 7), the insertion of sodium carbonate (0.4%, composition 1) reduces the strength of the cement stone from 70.00 MPa to 61.29 MPa (12.5%), which is due to the decompression of the internal structure with the inserted additive. The insertion of the accelerator in the composition 7 (0.2%) provided an increase in compressive strength by 11.2%, while the miniconus flow decreased to 40 mm (20 min after mixing), these facts indicate a rational content of Na_2CO_3 additives in the composition.

Composition 2 with 50% WMS and 0.4% Na_2CO_3 showed a 35 mm miniconus flow after 20 min, but the strength at the age of 28 days was 37.71 MPa. The decrease in strength is due to an excess of WMS. When the WMS dosage is reduced (up to 25%) without changing the accelerator dosage (0.4%) strength was 51.71 MPa, which

indicates a rational dosage of WMS waste. Fine WMS particles fill the volume of the composite, reducing porosity, while saving expensive energy-intensive Portland cement.

The obtained results indicate that the most effective combination of indicators is composition 5 (Portland cement - 75%, WMS - 25%, Na_2CO_3 - 0.4%, SP-3 - 0.5%). Compositions 1 and 7 also meet the requirements, but have a higher cost due to the higher consumption of Portland cement.

As a result of processing the experimental results, mathematical models of strength indicators of CB compositions were obtained. The compression strength regression equations are shown below:

$R_2 = 15.93 + 1.85x_1 + 10.35x_2 — 2.75x_1^2 + 1.65x_2^{2-2}.475x_1 \cdot x_2$

$R_7 = 36.69 + 2.63x_1 + 12.067x_2 — 7.43x_1^2 + 0.367x_2^2 - 4.675x_1 \cdot x_2$

$R_{28} = 52.41 + 3.76x_1 + 17.238x_2 — 10.62x_1^2 + 0.524x_2^2 - 6.679x_1 \cdot x_2$

The obtained regression equations allow determining the influence of factors x_1 and x_2 on the strength characteristics of the compositions.

To obtain a comprehensive view of the effect on the strength of two variable components of the mixture, nomograms are compiled (Fig. 2), which allow optimizing the process of obtaining the required composition with an optimal ratio of components.
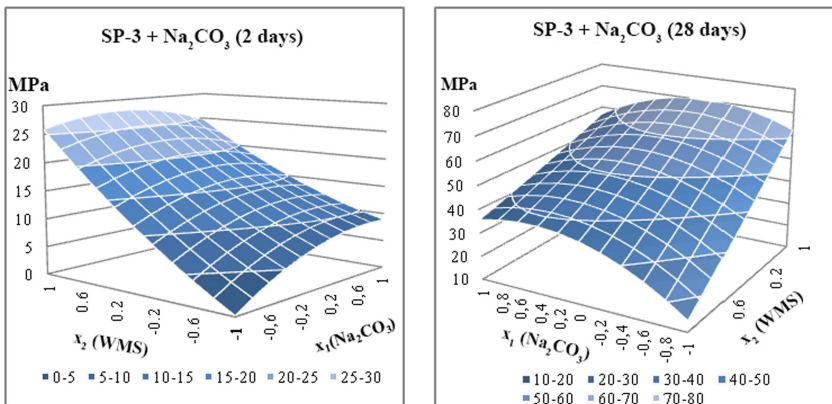
Fig. 2. Nomograms of compressive strength of composite binders at the age of 2 and 28 days.

A comparative x-ray-phase analysis of all the studied CB compositions was carried out, which showed that all compositions undergo the classic processes of hydration of clinker minerals (Fig. 4), which are typical for Portland cement, providing a given guaranteed strength to the created composites.
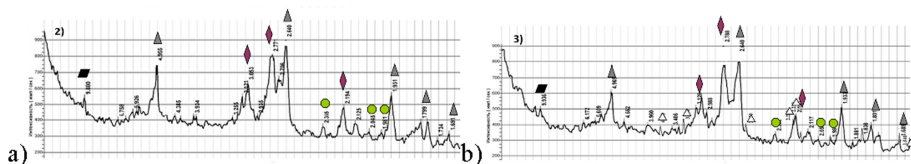
Fig. 3. Fragments of x-ray diffractograms: a) PC 100%; b) PC 75%, WMS 25%, Na_2CO_3- 0.4%.

The diffractogram of the control composition (Fig. 3, a) showed a high content of calcium hydrosilicates and a smaller amount of portlandite.

In the hydrated CB of the composition 5 made of Portland cement and WMS (25%) (Fig. 3, b), along with the hydrated clinker minerals inherent in Portland cement stone, the presence of a small amount of SiO_2, which was inserted by the mineral additive, is noted. It should be noted that a detailed study of the quartz of WMS waste revealed the presence of several generations randomly distributed over the entire mass of waste. Optimization of the processes of CB structure formation occurs due to the consistent growth of new formations during the hardening of the system "clinker minerals – quartz of different genesis – water – superplasticizer", due to the different intensity and time of interaction of polygenetic quartz and slag particles with hydration products. Chalcedon-shaped, metamorphosed, and partially dynamic-metamorphic varieties of quartz and WMS ferruginous quartzite intensively bind calcium hydroxide to small-crystal insoluble calcium hydrosilicates, and the contact-metamorphic variety and larger slag particles act as substrates and centers of crystallization, which generally helps to reduce the number of defects, reduce the crystallization pressure, and optimize the structure of the material, which is confirmed by the results of physical and mechanical tests.

To obtain additional information about the developed compositions, studies were performed on a Tescan MIRA 3 LMU scanning electron microscope.

The microstructures of hydrated CB obtained by various preparation options using mineral filler - WMS waste have a uniformly granular structure, the grains of mineral filler - WMS waste are evenly distributed in the total volume of cement stone and are densely "overgrown" with fine-crystalline new formations (Fig. 4,b).
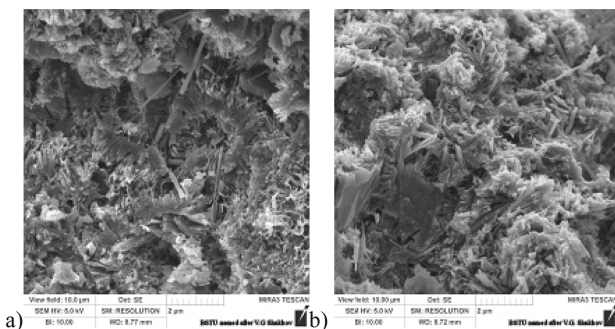

Fig. 4. Microstructure of composite binders in 10mkm magnification: a) PC - 100%, Na_2CO_3 - 0%; b) PC - 75%, WMS - 25%, Na_2CO_3 - 0.2%.

The entire array of cement composite is composed of blocks-aggregates formed by parallel oriented layers of scaly polycrystals. Such areas form a visual representation of the shapeless mass, but a detailed examination reveals their layering. A characteristic feature of cement stone is that quartz particles of dynamic-metamorphosed and contact-metamorphosed WMS waste act as filler, compacting the composite structure and simultaneously serve as dampers to reduce internal stresses. All particles of the dispersed mineral filler are covered with a submicrocrystalline structure in the form of a fringe. The presence of such structures indicates the possibility of a hydration process on the surface of the mineral filler grains with the formation of additional submicrocrystalline hydrate phases that compact the structure of the cement stone and additionally bind individual grains of the composite, which is adequately consistent with the sufficiently high compressive strength of the cement stone.

4 Conclusions

In this way, we have developed CB compositions whose properties are primarily formed by rational selection of a combination of the active component and mineral additives, as well as their production modes. Due to chemical modifiers: plasticizers and hardening accelerators, "fine setting" of the system is implemented, which determines the fulfillment of the required technological and physical-mechanical indicators in the new innovative construction technology.

The use of the developed CB will allow creating effective compositions for innovative technologies in construction.

References

1. Elistratkin, MYu., Minakov, S.V., Shatalova, S.V.: Composite binding mineral additive influence on the plasticizer efficiency. Constr. Mater. Prod. **2**(2), 10–16 (2019)
2. Nadiv, R., Peled, A., Mechtcherine, V., Hempel, S., Nicke, D., Schroefl, C.: Improved bonding of carbon fiber reinforced cement composites by mineral particle coating. In: Strain-Hardening Cement-Based Composites, SHCC 2017. RILEM Bookseries 15. Springer, Dordrecht (2018)
3. Panda, Biranchi., Paul, S.C., Tan, M.J.: Anisotropic mechanical performance of 3D printed fiber reinforced sustainable construction material. Mater. Lett. **209**(15), 146–149 (2017)
4. Klyuev, S.V., Khezhev, T.A., Pukharenko, Y.V., Klyuev, A.V.: Experimental study of fiber-reinforced concrete structures. Mater. Sci. Forum **945**, 115–119 (2018)
5. Lesovik, V.S., Popov, DYu., Glagolev, E.S.: Textile-concrete - an effective reinforced composite of the future. Constr. Mater. **3**, 81–84 (2017)
6. Lesovik, R.V., Klyuev, S.V., Klyuev, A.V., Tolbatov, A.A., Durachenko, A.V.: The development of textile fine-grained fiber concrete using technogenic raw materials. Res. J. Appl. Sci. **10**(10), 696–701 (2015)
7. Lesovik, R.V., Klyuyev, S.V., Klyuyev, A.V., Netrebenko, A.V., Yerofeyev, V.T., Durachenko, A.V.: Fine-grain concrete reinforced by polypropylene fiber. Res. J. Appl. Sci. **10**(10), 624–628 (2018)

8. Klyuyev, S.V., Klyuyev, A.V., Lesovik, R.V., Netrebenko, A.V.: High strength fiber concrete for industrial and civil engineering. World Appl. Sci. J. **24**(10), 1280–1285 (2013)
9. Compton, B.G., Lewis, J.A.: 3D printing of lightweight cellular composites. Adva. Mater. **26** (34), 5930–5935 (2014)
10. Secrieru, E., Fataei, S., Schröfl, C., Mechtcherine, V.: Study on concrete pumpability combining different laboratory tools and linkage to rheology. Constr. Build. Mater. **144**, 451–461 (2017)
11. Elistratkin, M.Y., Kozhukhova, M.I.: Analysis of the factorsof increasing the strength of the non-autoclave aerated concrete. Constr. Mater. Prod. **1**(1), 59–68 (2018)
12. Zagorodnyuk, L.H., Lesovik, V.S., Glagolev, E.S., Elistratkin, M.Yu., Lashina, I.V., Masanin, O.O.: Objective prerequisites for the transition to composite binders. In: Science-intensive technologies and innovations. Collection of reports of the International scientific and practical conference, pp. 110–116. BSTU, Belgorod (2016)
13. Lesovik, V.S., Absimetov, M.V., Elistratkin, MYu., Pospelova, M.A., Shatalova, S.V.: For the study of peculiarities of structure formation of composite binders fornonautoclavedaerated concrete. Constr. Mater. Prod. **2**(3), 41–47 (2019)

Effective Road-Impregnating Materials

E. A. Lukash[1(✉)] , E. A. Vlasova[1] , E. V. Kharlamov[2] ,
and A. V. Kurlykina[1]

[1] Belgorod State Technological University named after V.G. Shukhov,
Belgorod, Russia
svh8@yandex.ru
[2] Moscow State University of Civil Engineering, Moscow, Russia

Abstract. The country's transport infrastructure is an important factor in its economic development. However, often roads do not meet the operational requirements, there is: peeling, painting with loss of thickness of the coating layer, the formation of a grid of cracks, ruts. In this regard, research in the field of preventive measures to maintain and preserve asphalt concrete pavements in working condition is relevant. In the presented research, the author's methodology for evaluating the effectiveness of road-impregnating compounds as preventive measures to preserve the operational condition of road surfaces is proposed. Based on the proposed method, samples of developed impregnating materials based on polar (water) and non-polar (nephras) solvents are tested. It is established that road-impregnating materials based on non-polar solvents with high penetrating power contribute to the destruction of the upper layer of asphalt concrete pavement by weakening the cohesive-adhesive bonds at the division "bituminous binder – stone material". While the impregnating material, based on a polar solvent, forms an elastic protective layer of bituminous binder, reinforced with a complex of rheological additives. The paper experimentally confirmed the effectiveness of the use of road-impregnating materials. A method for evaluating their effectiveness and cooking technology is proposed.

Keywords: Road-impregnating materials · Protection of the asphalt concrete · Technology of preparation

1 Introduction

The country's transport infrastructure is an important factor in its economic development. However, often roads do not meet the operational requirements, there is: peeling, painting with loss of thickness of the coating layer, the formation of a grid of cracks, ruts [1]. At the same time, the costs of road construction and repair are constantly increasing, and the pace of new construction does not meet the needs of the industry. Roads age faster than they can be repaired. In this regard, research in the field of preventive measures to maintain and preserve asphalt concrete pavements in working condition is relevant. One of these areas is the development and application of road-impregnating materials (RIM) [2].

The current world level of technology demonstrates the results of restoring layers of asphalt concrete coatings, through the use of RIM, protective-regenerating compounds

(PRC) and reunivators [3–10]. However, there are no scientific studies on road-impregnating materials that allow assessing fully their effectiveness. Moreover, there is no data in the scientific literature on the effect of the solvent (base) used for the preparation of RIM. Modern research in the field of road-impregnating materials does not have a comprehensive approach, and some facts of the effectiveness of the use of impregnating compounds do not allow evaluating the effectiveness of the RIM.

2 Methods and Materials

The aim of the study is to develop the composition and technology of preparation of impregnating materials, as well as methods for evaluating their effectiveness.

The research was based on the following methods: ODM 218.3.073-2016 "Recommendations for the use of impregnating compounds to increase the durability of asphalt concrete coatings" (ODM); GOST 19007-73 (ISO 1517-73) "Paint-and-lacquer materials. Method for determining the time and degree of drying"; GOST R 52487-2005 (ISO 3251: 2003 "Paint-and-lacquer materials. Determination of the mass fraction of non-volatile solids"; GOST 12730.5-2018 (ISO 3166: 2018 "Concretes. Methods for determining water resistance".

Sample preparation was performed to analyze the efficiency coefficient of RIM (K_{effect}) using the ODM method. For this purpose, asphalt concrete samples of type B were made on a gyrator; they were sawn to exclude heterogeneity of the samples. The dried samples were covered with RIM in accordance with the manufacturer's recommendations. For each series of impregnation, 9 samples were prepared. The processed samples were stored in a climate chamber at a temperature of 20 °C with air blowing for 72 h. Prepared samples in accordance with the ODM procedure were tested for water saturation to assess the effectiveness of treatment.

As research objects to analyze the effectiveness of existing techniques RIM was studied: Chem-Crete, Brit, Silcoat, GEKOS (GKS). They vary in composition: Chem-Crete and Brit on the basis of bitumen-polymer emulsion and Silcoat and GKS – on the basis on solvent. All impregnations contain mineral material.

BND 70/100 bitumen, polar and non-polar solvents were used to prepare the impregnation compositions.

3 Results and Discussion

3.1 Development of a Methodology for Evaluating the Effectiveness of the RIM

According to theoretical assumptions, the use of road-impregnating materials should lead to a certain slowdown in the destruction of the road surface. The effect of RIM is that after application, it penetrates deep into the coating, forming a thin film on the surface. In general, the effect of using impregnating materials should be to reduce the impact on the coating of adverse climatic factors, increase corrosion resistance, increase abrasion resistance and improve the low-temperature properties of asphalt concrete.

However, in practice, there are cases of peeling the surface of the coating after applying impregnations, weakening and coloring the crushed stone grains of the upper asphalt layer, etc.

The resulting effects are logical. It is difficult to get a high technical result in the absence of a tool that allows evaluating the effects of the use of RIM, as the evaluation methods set out in the ODM do not reflect the real picture of the behavior of materials in natural conditions on the road. Therefore, the need to include in the standard methods based on simulating the actual working conditions of the RIM is obvious. In this regard, a method was proposed based on the assessment of a set of negative factors that have a consistent impact on the road surface [1].

The study used prepared samples-washers with a surface layer of impregnations, which were subjected to a complex of effects. In accordance with the research program, natural factors were included in the list of tested effects. Each point of the experiment simulates certain operating conditions:

1) Water permeability. The experiment revealed that not all cases of the RIM formed on the coating durable and waterproof layer, the test samples were filled to volume with water.
2) Thermostating. For 96 h, the test samples were subjected to temperature control at a temperature of 60 °C to a constant mass.
3) Freezing/thawing. The study showed that the transition through 0 °C is the most unfavorable and destructive period for RIM.

After that, the K_{effect} of impregnation before and after exposure to the modeled factors was determined, Fig. 1. It should be noted that the proposed sequence and numerical indicators of impacts in the method are valid for the conditions of the Central Federal district.
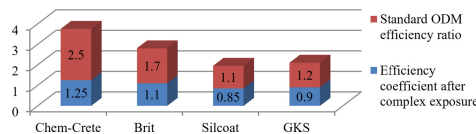

Fig. 1. Study of the effectiveness of impregnations using the ODM method and under the influence of a combination of natural factors modeled in the laboratory.

The figure shows that cracks appeared on the surface of the impregnated samples (two samples on the right) after the test cycle. It is obvious that with more severe and prolonged freezing/thawing cycles, the intensity of crack formation on the coating surface will increase.

Also, after the cycles of the described effects, K_{effect} significantly decreased, Fig. 2. It was found that the water saturation of a number of samples covered with impregnations increased significantly relative to the control series, which calls into question the effectiveness of impregnations under the influence of natural factors.

The validity of questions on the effectiveness of a number of RIM is clearly illustrated by data on the change in the tensile strength of samples coated with RIM to split at a temperature of 20 °C after exposure cycles, Table 1.

Table 1. Study of the strength of asphalt concrete at 20 °C on the crack.

Indicator	Name of RIM			
	Chem-Crete	Brit	Silcoat	GKS
Ultimate strength of samples for cracking, MPa	0.98	0.97	0.54	0.65
R'_k	1.22			
R_k	0.98			

As it can be seen from the table, samples that are not impregnated and have been exposed to water and temperature changes (R'_k) are characterized by the highest strength compared to the samples of the control series (R_k). Thus, despite the fact that all RIM meet the requirements of the ODM for their properties, not all impregnating compounds are effective.

A comprehensive analysis of the data showed that emulsion-based RIM are more effective, they preserve the strength characteristics of asphalt concrete, while solvent-based RIM reduce them.

Thus, it was of scientific and practical interest to study the influence of the RIM basis on the characteristics of asphalt concrete. The developed method, tested on well-known commercial compositions of impregnating material, was later used to evaluate the effectiveness of the developed compositions.

3.2 Development of Effective Compositions of Road-Impregnating Materials

At the next stage of research, two series of RIM were developed:

on the basis of the polar solvent (emulsified in water);
on the basis of a non-polar solvent (nefras).

Possible variations in the compositions of the developed road-impregnating material are shown in Table 2.

Table 2. Compositions of developed RIM based on non-polar solvent (nefras) and polar solvent (in water).

№ of composition	Ratio of components in RIM,% non-polar solvent (nefras)				
	Solvent	Bitumen	Rheological additives complex (organic clay)	Petroleum polymer resin	Silica flour
1	37	45	4	3.5	10.5
2	35.5	45	4.5	3.5	11.5
3	30.5	45	4.5	3.5	16.5
4	35	45	5	3.5	11.5
5	30	45	5	3.5	16.5
6	29.5	45	5.5	3.5	16.5
7	29	45	6	3.5	16.5
№	Polar solvent (water/emulsifier)				
1	21.2/0.8	60	3	3.5	15
2	20.7/0.8	60	3.5	3.5	15
3	20.2/0.8	60	4	3.5	15
4	19.2/0.8	60	5	3.5	15
5	18.7/0.8	60	5.5	3.5	15

The prepared compositions were tested for compliance with the ODM, Table 3.

Table 3. Characteristics of RIM based on polar and non-polar solvents.

№ of compositions	Indicators non-polar solvent (RIM-P)			
	Appearance	Conditional viscosity according to a VUB-1 type viscometer with a hole diameter of 5 mm at 20 °C, sec	Adhesion, point	Drying time, h
1	Non-homogeneous	110	3	1.05
2	Non-homogeneous	98	3	1.2
3	Non-homogeneous	120	4	1.0
4	Non-homogeneous	100	5	1.1
5	Homogeneous	95	5	1.25
6	Homogeneous	104	5	1.1
7	Homogeneous	100	5	1.15
№	Polar solvent (RIM-B)			
1	Non-homogeneous	20	3	1.25
2	Homogeneous	14	5	1.45
3	Homogeneous	13	5	1.50
4	Homogeneous	9	5	1.75
5	Homogeneous	9	5	2.10

Analysis of the developed impregnation compositions shows that the most effective compositions are: based on solvents RIM-P №5; based on an emulsion-RIM-B №3. The selected RIM were tested for compliance with the requirements of the ODM. To compare the properties, the Brit impregnation material was tested.

It was found that the best drying rate is shown by solvent-based impregnations. The indicator of the drying time of the RIM is one of the most important factors, as the movement on the treated asphalt pavement can only be opened after the impregnation compound has completely dried. Premature opening of movement of vehicles increases the risk of accidents.

The impregnating compounds, RIM-B (№3) and RIM-P (№5), were further subjected to comparative tests according to the standard and developed methods for the efficiency coefficient, Table 4.

Table 4. Changes in the efficiency coefficient of the developed formulations under the influence of natural factors modeled in the laboratory.

Indicator	Name of RIM			
	RIM-B	RIM-P	Brit-P	Brit-B
Standard K_{effect} according to ODM	2.1	1.7	1.8	2.1
K_{effect} after a complex impact	1.3	1.1	1.15	1.5

The impregnation composition based on a non-polar solvent, showing high results in drying speed and technological viscosity indicators, is less effective, as, having a high penetrating power; it obviously initiates the destruction of asphalt concrete layers. RIM based on polar solvent, forming a strong elastic film of bituminous binder, prevents moisture from entering the asphalt concrete.

3.3   Technology of Making of Impregnating Compositions

The process of making road impregnation was carried out in the following sequence. Bitumen from the preheating module was fed to a mechanical stirrer with a heating unit. Solvent, filler and rheological additives were fed from the corresponding modules, followed by mixing until the mixture was completely ready. Figure 2 shows the device diagram for obtaining road impregnations.
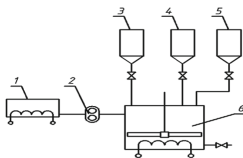
1 – bitumen preheating module;
2 – pump; 3 – solvent module;
4 – fillers module;
5 - rheological additives module;
6 - mechanical stirrer

Fig. 2. Device diagram for obtaining road impregnations.

4   Conclusions

The effectiveness of RIM as a preventive measure to preserve the durability of asphalt concrete coatings by forming a strong elastic film of bituminous binder, reinforced with a complex of rheological additives and dispersed filler, which prevents moisture from entering the structure of asphalt concrete by means of colmatation of surface defects, is experimentally proved. The technology of their making is offered.

It is established that RIM based on non-polar solvents, having a high penetrating power, initiate destruction of asphalt concrete layers by weakening the cohesive-adhesive bonds at the interface "bituminous binder – stone material".

References

1. Vysotskaya, M.A., Vlasova, E.A., Kuznetsov, D.A., Kurlykina, A.V., Shekhovtsova, S.Yu.: Review of the state of the segment of impregnating materials for road coatings. Bull. BSTU named after V.G. Shukhov **8**, 6–12 (2018)
2. Vysotskaya, M.A., Kuznetsov, D.A., Kurlykina, A.V., Vlasova, E.A.: Impact of impregnating materials with different bases on asphalt concrete. Bull. BSTU named after V.G. Shukhov **2**, 8–13 (2019)
3. Lee, J., Li, S., Kim, Y., Lee, J.: Efficiency of asphalt rejuvenator. J. Test. Eval. **41**(3), 433–440 (2013)
4. Estakhri, C.K., Agarwal, H.: Effectiveness of fog seals and rejuvenators for bituminous pavement surfaces. Texas Transportation Institute. Texas A&M University, Texas (1991)
5. Ubas'kina, Y., Chigorin, E.A., Razinov, A.L., Ryabenko, V.S., Kovtun, I.D.: Optimal formulations of some asphalt concrete roadway protective impregnation compositions. Orient. J. Chem. **32**(1), 305–311 (2016)
6. Ryabenko, V.S., Chigorina, E.A., Razinov, A.L., Ubas'kina, Y., Kovtun, I.D.: The preparation of the quick-drying bitumen emulsion for the protection of the road surface asphalt concrete layer. Orient. J. Chem. **32**(6), 129–134 (2016)
7. Priorov, G., Bessarabov, A., Glushko, A.: Development of industrial production of impregnating compositions for road coatings based on the concept of CALS. Chem. Eng. Trans. **76**, 457–462 (2019)
8. Shekhovtsova, S., Korolev, E.V.: Review of the modern experience of using reunifiers for reversing asphalt concrete pavements. Build. Mater. Prod. Reg. Archit. Constr. **3**, 5–16 (2018)
9. Vysotskaya, M.A., Vlasova, E.A., Mohamadu, A.: Technologically, simple, efficient. World Roads **104**, 62–64 (2017)
10. Trautvain, A.I., Akimov, A.E., Chernogil, V.B., Lukashuk, A.G., Yakovlev, E.A.: Influence of impregnation "dorluk" on the physical and mechanical characteristics of asphalt concrete pavements of highways. Bull. Belgorod State Technol. Univ. V.G. Shukhov **11**, 11–17 (2017)

Stability of a Multistoried Building on a Ground Base Described by a Bilinear Model

A. I. Oleynik[(✉)] , K. M. Akhmedov , and V. V. Shamov

Rudny Industrial Institute, Rudny, Kazakhstan
`aoleinik@mail.ru`

Abstract. The paper uses computer programs based on the finite element method to study the problems of loss of stability and collapse of multistoried buildings located on weak soils with elastic-plastic properties. Such properties, in particular, can be shown by clay rocks, which are often found on construction sites and in conditions of overload and excessive moisture behave as perfectly plastic materials. A characteristic feature of these soils is the loss of bearing capacity, which is accompanied by a sharp decrease in the modulus of deformation. The problem is solved in a non-linear formulation using a bilinear model of the ground base that best corresponds to the analyzed computational situation. From the point of view of construction mechanics, the critical state of the "ground base – structure" system is considered as an indifferent state. In this situation, with small external forces, an unlimited growth of deformations is observed. From this point of view, the use of numerical research methods is very effective. To solve this problem, the perturbation theory is used in combination with the method of successive loadings. A multistoried building on a slab foundation is considered. A weak wind effect is used as a disturbance. Stepwise increase in the vertical load allows determining the critical reactive pressure in the base. Based on the results obtained, a variant of strengthening the foundation is proposed.

Keywords: Stability of ground bases · Numerical methods · Progressive collapse of multi-storied buildings · Nonlinear systems · Bilinear model · Perturbation method · Sequential loading

1 Introduction

Experimental and theoretical study of deformations of multistoried buildings and structures located on weak soils with unstable characteristics is one of the promising areas in the field of construction, the relevance of which is even more important due to the current tendency to increase the number of floors of buildings under construction [1, 2]. Research in this area combines a complex of closely related issues, among which we can distinguish: the mutual influence of foundations, bases and structures of buildings under construction; issues of stability, progressive collapse, as well as methods for strengthening bases and foundations [3]; refinement of kinematic and mathematical models of stability loss, taking into account their non-linearity under

various loads [4, 5]. At the same time, the use of numerical research methods is very effective [6–8].

Emergency manifestations of instability of the foundations can occur unexpectedly even if there are no obvious features such as downhills of slopes and workings near the construction site, which is confirmed by numerous practical cases. The most famous example of this [9] is an accident in Canada at an elevator in North Transcone (1913) when the silo was evenly loaded with grain. At the same time, there was an emergency roll of the structure at 27° with a draft of one of the sides at 8.8 m and a rise from the level of the layout of the other side at 1.5 m. Such deformations were associated with a decrease in the thickness of the compressible clay layer under one side of the foundation plate due to the presence of boulders in this place and insufficient strength of the water-saturated clay soil.

In China, on 29.06.2009 (Shanghai), a monolithic 13-storey building under construction collapsed (Fig. 1, *a*), which was under finishing work [10]. The collapse occurred as a result of the construction of an underground garage and the influence of heavy rains, which moistened and significantly reduced the modulus of deformation of the base.

A similar collapse of a multistoried building occurred in the residential complex "Besoba" in Karaganda (04.2012) [11] (Fig. 1, *b*), where the fall and complete destruction of the building was preceded by a rapid increase in the roll due to a decrease in the elastic modulus of the base.

Let us note that the problem is not the quality of building materials used in construction, or errors in the construction technology, as it is often presented in expert opinions, but the loss of stability of the base that interacts with the supported structure of the building. This is especially evident in Fig. 1, *a*, where the collapsed monolithic building has completely preserved its integrity.

a)   *b)*

Fig. 1. Examples of building collapses due to loss of stability; (a) the fall of a multistoried building in China (Shanghai 06.2009); (b) collapse of a new building in Karaganda (04.2012).

The aim of this work is to study the conditions of loss of stability of multistoried buildings erected on soils that are structurally unstable rocks, which in the extremely loaded state come to an unconsolidated state and behave like perfectly plastic materials.

2   Methods and Materials

Various approaches can be used to assess the stability of foundations. In particular, kinematic methods of fracture mechanics often used in practical calculations based on the application of the theory of limiting equilibrium [4] or the mechanics of motion of dispersed media, which take into account the mechanisms of extrusion [5] or displacement of significant areas of soil (prisms) along sliding surfaces. It should be noted that when overloaded and significantly moistened, clay rocks can behave as perfectly plastic materials. The main effect of overloading the base affects the reduction of the modulus of elasticity of the soil.
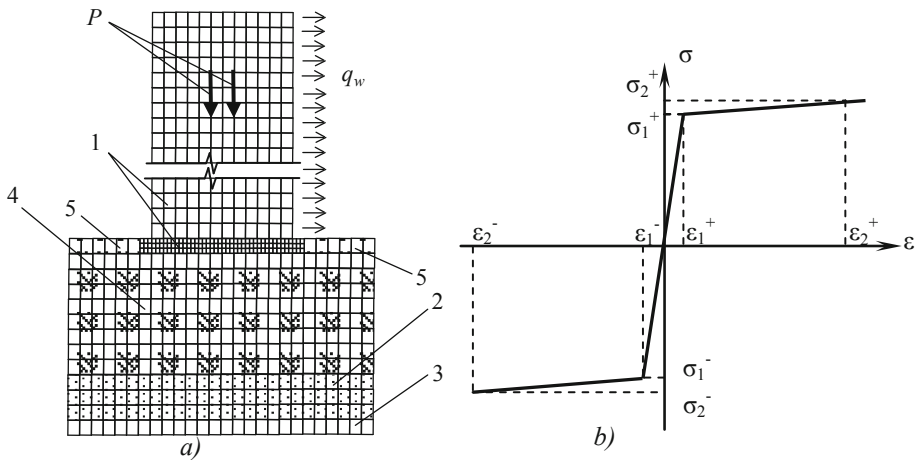
Fig. 2. Computational model: a − the base and the building is divided into finite elements ($P = 2000$ kN, $q_w = 3$ kN/m); b − bilinear model of an elastic base ($\varepsilon_1^- = -0.01$; $\varepsilon_2^- = -0.1$; $\sigma_1^- = -200$ kPa; $\sigma_2^- = -210$ kPa; $\varepsilon_1^+ = 0.01$; $\varepsilon_2^+ = 0.1$; $\sigma_1^+ = 200$ kPa; $\sigma_2^+ = 210$ kPa;).

In this case, it is advisable to use models of elastic-plastic medium [4], which are used in the calculation of bases containing both areas of the limit and pre-limit stress state of the soil. To account for nonlinear soil deformation in elastic-plastic models, the generalized Hooke's law introduces variable characteristics of the elastic modulus E and the Poisson's ratio v, which depend on the level of the achieved stress state [4, 5]. When using the finite element method (FEM) [6], the formation of plastic and quasi-plastic areas is realized within the framework of the bilinear model used in this study.

In this case, we will focus on a multistoried monolithic building with a foundation plate at the base, located on an elastic half-space with a bilinear change in the elastic modulus (Fig. 4). Special case of the considered soil model is an elastic-plastic soil model that obeys the Prandl hypothesis [12]. We consider a rectangular multistoried building with a width of 12 m, the length of which is much longer than its width, and the rigidity of the building structures is much higher than the rigidity of the base. The building is based on a foundation plate, 1 m thick with a 1 m offset from the exterior walls of the building. Taking into account the extended dimensions of the building, we will consider the problem in a flat setting, considering the cross-section of the building. In order to simplify the design scheme, the weight of the load-bearing structures of a monolithic building is approximately taken into account using two symmetrically located forces P, the value of which varies. To solve this problem, the perturbation method is used. For this purpose, a horizontal load is applied on the right side of the design scheme (simulating wind or seismic effects) with a constant q_w intensity, which plays the role of a trigger for loss of stability and also varies. The problem is solved in the program Lira-SAPR, using the criteria of loss of stability of the second kind, corresponding to changes in the physical properties of the soil base.

Figure 2, a shows the analysis model of a building divided into finite elements: meshing of buildings and main layers of the foundation soil close to a square with sides of 1 m, and for the foundation plate – 0.33 m. A reinforced concrete foundation plate and the structures of a monolithic reinforced concrete building are described by an isotropic linear elastic medium 1 with an elastic modulus E_1. At the base of the plate there is a physically nonlinear layer 4, the elastic modulus of which depends on the external load and obeys a bilinear law (Fig. 2, b) with an almost horizontal second section corresponding to the development of plastic deformations in the ground caused by deconsolidation phenomena. Layers 2, 3 (below the physically nonlinear soil 4) and the surface layer 5 obey the linear-elastic model of Hooke's law. Layer 3, located below layer 2, has stiffness comparable to that of model 1 and corresponds to that of rock.

The stability calculation method is based on classical approaches of structural mechanics [12], which take into account the occurrence of an indifferent state, in which any asymmetric perturbation or asymmetry of the physical properties of the base can trigger an uncontrolled growth of deformations. With small disturbances, a structure that is in a critical indifferent state allows the development of excessive deformations. Preliminary calculations allowed determining the values of the critical load P and the parameters of the bilinear model of the calculated layer 4, shown in Fig. 3. As a trigger for loss of stability, a horizontal disturbance evenly distributed over the height of the building is taken ($q_w = 3$ kN/m).

3   Results and Discussion

In accordance with the method of successive step loads, the vertical load on the foundation increases (which is equivalent, for example, to an increase in the number of stores of a building) and the resulting horizontal deformations are recorded at the level of the upper floor of the building. When the maximum load is reached (the appearance of an indifferent state), the level of deformations increases indefinitely.
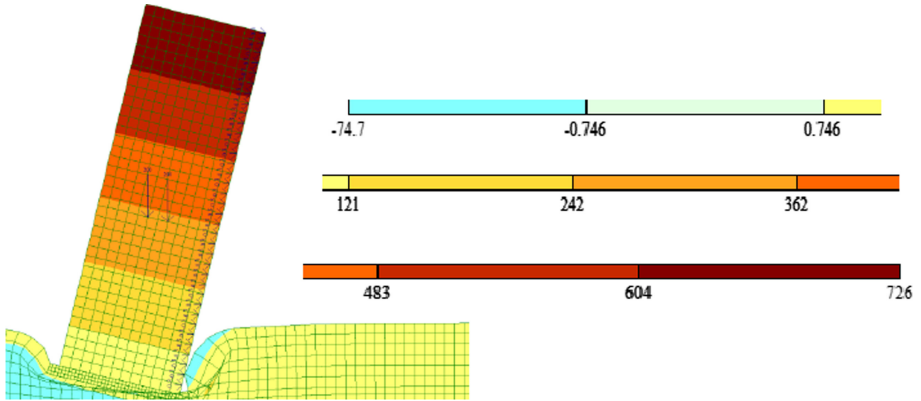
Fig. 3. Isofield of horizontal movements of the model (Fig. 3, *a*) with the base plate offset by 1 m from the building boundaries.

The analysis of isofields of deformations in Fig. 3 shows that at the maximum load in the level of the top of the building, there are exorbitant horizontal displacements of 72.6 cm $(72, 6/4000 = 1/55 \gg 1/200)$; that is, at critical loading parameters, the displacements grow indefinitely and become commensurate with 1 m, which at a building height of 40 m exceeds the standard values several times and is a prerequisite for destruction.

We will outline ways to increase the stability of the base.

An obvious way to improve the situation is to expand the size of the foundation plate. In the case of a foundation plate with a cantilever projection of 3 m relative to the external walls of the building, the maximum displacement of $X_{max} = 98.9$ mm is obtained. In this case, the maximum movements decreased by more than 7 times compared to the data in Fig. 3.

The disadvantage of this type of reinforcement is the need to provide a rigid connection of the existing foundation plate with the reinforcement, which is often difficult to implement due to problems with the coupling of working reinforcement.

Figure 4 shows the isofields of deformations and stresses in the case of expanding the size of the foundation plate by installing a single row of bored piles with a diameter of 0.33 m with a step of 1 m and a grillage with a width of 2 m, in the case when the coupling of the main part of the plate and the reinforcement is weakened. The decrease in the coupling stiffness is taken into account by introducing additional elastic finite elements 6 in the coupling node, which have a reduced elastic modulus $E_6 = 700$ kN/m^2. Spatial nature of pile installation (installation step 1 m in the transverse direction) also taken into account by reducing the elastic modulus of the final elements of piles by half). It is assumed that the piles are not brought to hard rocks and are hanging.
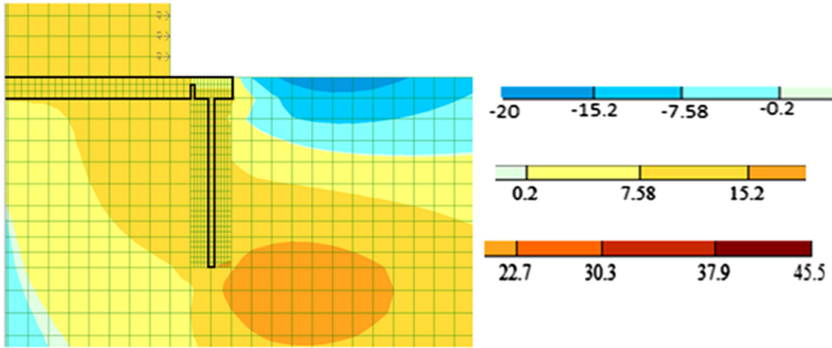
Fig. 4. Isofield of horizontal movements when using a foundation plate with an additional extension of 2 m and one row of piles.

It is assumed that the piles are not brought to hard rocks and are hanging. A significant reduction in the level of deformations was obtained (X_{max} = 45.5 mm). In addition, isofields of forces and deformations were obtained for the option of extending the plate by 3 m and using two rows of piles, which allowed to increase the efficiency of reinforcement by an additional 16%.

Table 1 shows the maximum horizontal displacements and stresses for the studied models. The stresses in the foundations do not exceed the maximum permissible standards.

Table 1. Maximum displacements in the building and stresses in the foundation elements at P = 200 t q_w = 3 kN/m.

Cantilever projection of the foundation plate	X_{max} (mm)	Z_{max} (mm)	$N_{x,max}$ (MPa)	$N_{x,min}$ (MPa)	$N_{z,min}$ (MPa)	$T_{xz,max}$ (MPa)	$T_{xz,min}$ (MPa)
Without piles plate projection 1 m	726	577	3,130	3,690	2,000	1,360	−0,960
Without piles plate projection 3 m	98,9	170	5,850	6,790	2,480	1,470	1,080
Grillage 2 m and 1 pile row	45,5	109	7,810	7,960	5,600	3,630	−3,050
Grillage 3 m and two pile rows	38,1	110	7,870	9,740	3,730	2,120	−3,730

4   Conclusion

1. The obtained results confirm the correctness of using the bilinear model of the ground base in combination with the iterative method of calculating stability and allow not only to prevent the collapse of buildings, but also to develop effective measures to ensure a stable state.

2. Sufficient for practical purposes is the use of extending the foundation plate along the perimeter by 2 m with reinforcement by one row of piles installed in 1 m increments.
3. The installation of piles also prevents the extrusion of plastic soil masses from the congested area under the building and forms a kind of encased pile border.

References

1. Ter-Martirosyan, A.Z., Ter-Martirosyan, Z.G.: Research of soil bases of multistoried buildings. Found. Bases Soil Mech. **5**, 2–12 (2009)
2. Mangushev, R.A.: Plate-pile foundation for multistoried buildings. Found. Bases Soil Mech. (1), 15–19 (2008)
3. Romanov, N.V., Rasine, Zh.: Review of modern methods for strengthening and stabilizing weak bases. Bull. MSCU **4**(115), 499–513 (2018)
4. Bugrov, A.K.: Soil Mechanics, p. 287. Polytechnic University Press, Saint Petersburg (2011)
5. Borozenets, L.M.: Geotechnics of Foundation Construction and Soil Stability Monograph: Monograph, p. 285. TSU Publishing House, Tolyatti (2015)
6. Fadeev, A.B.: Finite Element Method in Geomechanics, p. 221. Nedra, Moscow (1987)
7. Oleynik, A.I., Rakhimov, Z.R.: Determination of stable parameters of loaded clay slopes. Bull. Natl. Eng. Acad. Repub. Kazakhstan **2**(52), 57–66 (2014). Publishing House of NIA RK, Almaty
8. Oleynik, A.I., Akhmedov, K.M., Rakhimov, Z.R.: On assessing the stability of the "Construction-foundation" system. Collection of reports of the MNC Innovations in Science, Education and Production of Kazakhstan, 18–19 November 2015, pp. 212–218. ETU, Almaty (2015)
9. Kosterin, E.V.: Bases and foundations, p. 375. Higher School, Moscow (1978)
10. http://softoroom.net/topic58457.html
11. http://piter.tv/event/Zhiloj_dom_ruhnul_na_glaz/
12. Rzhanitsyn, A.R.: Construction mechanics, p. 400. Higher School, Moscow (1982)

Compounding Features of Special Molding Mixes for 3D Printing Technology

E. S. Glagolev , N. V. Chernysheva(✉) , V. S. Lesovik ,
and E. N. Lesnichenko

Belgorod State Technological University named after V.G. Shukhov,
Belgorod, Russia
chernysheva56@rambler.ru

Abstract. World experience shows that to ensure the speed of building construction and minimize labor costs, the technology of layer-by-layer synthesis (3D printing or three-dimensional extrusion) will develop rapidly in the next decade. In modern Russian conditions, 3D printing is ideal for mass and individual construction of low-rise houses and cottages. The main idea of construction printing is to create a finished product or structure with a single device. For a stable technological process of construction of low-rise buildings by layer-by-layer synthesis, special fast-hardening molding mixes are offered, including clinker minerals, gypsum binders, mineral and organic additives, as well as fine aggregate. The joint insertion of gypsum binders of α - and β - modification (G-5BII and GVVS-16) into the composition of CGB contributes to the early structure formation of stone on CGB. The insertion of modifying additives into its composition - the hyperplasticizer MARP SU 84, the thickener MARF (Forbocrete 9010) and the hydrophobic rheological additive MAPF №T 10 can significantly reduce the water demand of the binder by 28…56%) and improve plasticity, while the compressive strength increases by 2 times in 2 h, by 1.7 times in 1 day, and by 1.5 times in 7 days. Developed for 3D additive technologies, molding mixtures based on CGB and quartz sand quickly harden and gain strength, providing concrete compressive strength class B3.5 in the early stages of hardening (1 day), and at the age of 7 days – B7.5.

Keywords: Construction 3D printing · Molding mixes · Composite gypsum binder

1 Introduction

In recent years, Russia has paid special attention to such a direction of the construction industry as low-rise construction. This rapidly developing area requires the development and implementation of new construction technologies and building materials. One of the most advanced trends in the development of construction technologies is construction printing. According to a large number of publications [1–9], its advantage is an increase in the pace of construction, the ability to create structures of a wide variety of configurations.

Multi-component molding mixes with various mineral and organic modifying additives are used for low-rise construction using 3D printing. The use of traditional hydraulic binders due to their slow hardening, and air binders-gypsum, due to low water resistance, is not rational. In this regard, in our opinion, building systems of layer-by-layer molding from a special fine-grained molding mixture based on effective fast-hardening binders [10, 11] with a low content of clinker–composite gypsum binders (CGB) – can be promising for these purposes in monolithic low-rise construction.

In terms of physical and mechanical properties and durability, forming mixtures on CGB are similar to concrete mixtures on Portland cement, but they have significant advantages in the ability to control their setting time and hardening speed within a wide range. In addition, the low energy consumption and simplicity of their production are extremely important in the technology of layer-by-layer synthesis (the consumption of conventional fuel for the production of gypsum is 3…5 times less than that of Portland cement). In Belgorod region there are unlimited supplies of raw materials of technogenic origin (dropouts of crushing quartz sand stone – QSS, waste of wet magnetic separation of ferruginous quartzite– WMS waste, etc.) whose use as mineral admixtures and fine aggregate can significantly reduce the cost and materials intensity of monolithic low-rise construction with the help of 3D technology.

Thus, the development of 3D printing with special fast-hardening fine-grained molding mixtures based on CGB will make the technology attractive for small and medium-sized businesses, as well as open up new opportunities for its use.

This area requires additional targeted research.

The solidified molding mix on CGB is a very complex multiphase system. The use of chemical modifiers and active mineral additives, various fillers and aggregates allows regulating directly the water demand and the processes of structure formation of the hardening composite. Workability, plasticity and setting time of the special molding mix are especially important that allows maintaining the dimensional stability of the layers of the structure in the 3D printing process and rapid curing in the early stages of hardening, which contributes to quick lock structure, finding design load capacity and further hardening.

In this regard, the main task of the study was to study the effect of various modifying additives on the properties of hardened special molding mixtures based on CGB, the need for experimental selection of their dosage to a specific binder and fine aggregate due to the lack of a developed knowledge base on compatibility [12–16].

2   Methods and Materials

Experimental research was carried out at the Department of Construction Materials Science, Products and Structures, in the test center "BelGTAS-sertitis" in BSTU named after V.G. Shukhov.

To obtain special molding mixtures, a modified CGB composition was developed, consisting of:

– 58% of gypsum binders (70% G-5BII and 30% GVVS-16(G-16);
– 20% of Portland cement CEMI 42.5 N (PC);
– binary active mineral additive (20% fine ground to a specific surface area of 500 m^2/kg of WMS waste and 0.5%; metacaolin);
– dispersed chalk (1.5%) with a $CaCO_3$ content of at least 96%.

To regulate the mobility of the molding concrete mix and the speed of strength gain, surface-active additives were used (in dry form):

– polycarboxylatehyperplasticizer (HP) MAPP SU 84. For molding mixtures based on CGB, the recommended dosage of HP is 0.1–0.3%;
– CP Kelko - Kelco-Crete dutane gum is a MARF (Forbocrete 9010) thickener with a high response to shear removal. It has little effect on hydration, which allows selecting more accurately the rcompounding. The recommended dosage for molding mixtures based on CGB is 0.07% of the total mass of water;
– rheological additive MAPF №T 10 based on modified bentonite clays, provides the creation of weakly expressed hydrophobic properties (0.1–0.3% of the mass of CGB);
– citric acid is a retarder of the setting time (0.2% by weight of CGB);
– CMC–carboxymethylcellulose (2% by weight of CGB)

Due to the fact that the components of the molding mix originally mixed in concrete mixer and then the resulting mixture is fed into the hopper and the extruder of molding device, we need to comply with the time interval between the start (not earlier than 15 min) and the end of setting (not later than 40 min) of the molding mixture. This is necessary to reduce the number of stops during 3D-layer printing for cleaning the forming head of the extruder, as well as to form and set the necessary initial strength of the hardening mixture before the next layer is laid.

Quartz sand was used as a fine aggregate in the ratio of CGB: sand-1:2, respectively.

During the experiments, the existing basic research methods were used.

3   Results and Discussions

The composition of the modified CGB was developed using a separate technology, according to which WMS waste was initially ground to a specific surface area of 500 m^2/kg, and then mixed together with Portland cement, gypsum binders of β-and α-modifications, with metacaolin and chalk in a laboratory ball mill, combined with short-term re-crushing (for 5 min).

Indicators of the properties of the developed CGB compositions are presented in Table 1.

The values of the compressive strength of the hardened samples after 2 h were 2.8 …14.4 MPa, after 1 day of hardening – 3.9 …19.8 MPa, and at 7 days of age – 8.2 … 34 MPa.

The use of various modifiers affects the water demand and the setting time of the hardening CGB.

Table 1. Indicators of CGB properties.

№	HP	TH	RA	W/B$_{in}$	Spread, m	Setting time, min,-s		R$_{comp}$, MPa,in terms		
						Beginning	Ending	2 h	1day	7 day
1	–	–	–	0.46	0.110	5-00	7-00	4.4	6.5	8.4
2	–	–	–	0.53	0.120	10-30	11-30	3.3	5.8	9.6
3	–	–	–	0.6	0.200	12-40	15-00	2.8	3.9	8.2
4	0.1	–	–	0.46	0.200	11-00	13-20	3.8	6.0	10.8
5	0.1	–	–	0.38	0.110	7-30	9-00	4.5	6.7	11.3
6	0.3	–	–	0.30	0.260	14-00	16-30	6.2	9.2	17.9
7	0.3	–	–	0.26	0.230	12-30	14-00	6.7	9.8	22.2
8	0.3	–	–	0.23	0.120	10-30	12-00	13.3	19.1	28.4
9	0.3	0.07	–	0.26	0.120	10-00	11-00	14.0	16.4	32.2
10	0.3	0.07	0.1	0.26	0.120	9-30	10-30	14.4	19.8	34.0
11	0.3	0.07	0.1	0.27	0.170	12-00	13-00	8.1	11.3	23.7
12	0.3	0.07	0.2	0.26	0.120	9-20	10-20	10.0	11.8	24.6
13	0.3	0.07	0.3	0.26	0.120	9-10	10-10	8.2	11.2	23.6

Note. Composition of CGB – gypsum binder 58% (G-5-40%, G-16-18%,);
PC-20%, fine ground WMS waste-20%, metacaolin-0.5%, chalk-1.5%.
HP – hyperplasticizer MAPPSU84, TH – thickener MAPF (Forbocrete 9010),
RA - rheological additive of the MAPF brand № T 10.

The dosage of HP (0.1–0.3% of the weight of CGB), allows for 28…56%, respectively, to reduce the W/B$_{in}$ ratio almost without reducing the strength (compositions 2, 5, 8).

There is some delayed dilution of the molding mixture over time, which is the result of competitive adsorption, due to which the GP MAPP SU 84 begins to work after binding more strongly charged particles of the binder components.

The MARF thickener (Forbocrete 9010) at a low dosage (0.07% by water) allows stabilizing highly mobile systems (compositions 7, 9) and getting a higher early strength. The binding mixture becomes more plastic, while the compressive strength increases by 2 times in 2 h, by 1.67 times in 1 day, and by 1.5 times in 7 days.

Rheological additive of the MAPF brand №T 10 at a rational dosage of 0.1% of the mass of CGB due to the lamellar structure of bentonite clays in their composition acts as a lubricant, as well as an associative thickener (compositions 9, 10).

The X-ray phase analysis results confirm the stability of the formed structures of the solidified binder at the age of 7 days (Fig. 1).
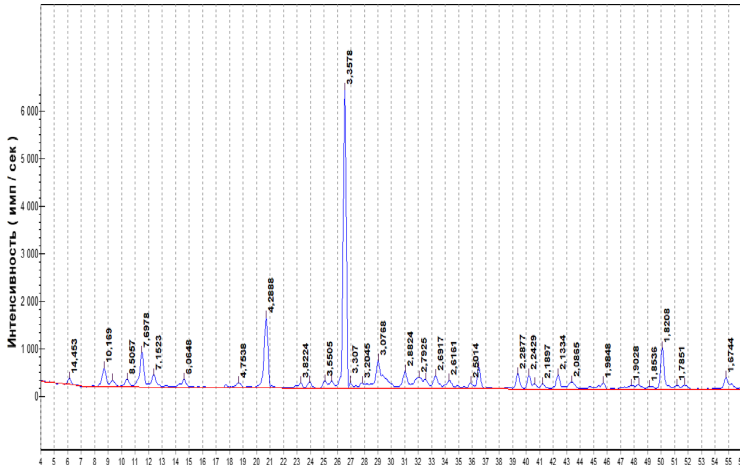
Fig. 1. X-ray phase analysisof solidified CGB (7 days).

In the studied sample, calcium dihydrate(d = 7.69; 4.29; 3.82; 3.076; 2.882…Å) is mainly present as hydration products of CGB; quartz (d = 3.35; 2.54; 2.46; 2.22; 2.28; 2.133; 2.08; 1.54…Å); calcium carbonate (d = 2.086; 1.902 … Å). The radiograph shows traces of portlandite $Ca(OH)_2$ (d = 4.93; 2.61; 1.78…Å). The absence of ettrintite (d = 9.7; 5.6; 4.92…Å) indicates the creation of conditions for the interaction of the amorphous SiO_2 phase in the WMS waste, as well as metacaolin with $Ca(OH)_2$ to form CSN (B), a partially crystallized tobermorite-like calcium hydrosilicate (d = 3.07; 2.88; 2.13; 1.82…Å). And chalk particles act as additional centers of crystallization for various hydroaluminate new formations, which contributes to the rapid strength gain of the composite in the early stages of hardening.

In further studies in the laboratory, layer-by-layer synthesis of model structures was carried out on an experimental laboratory 3D printer, taking into account its features with a fine-grained molding mixture [12].

For tests on an experimental laboratory device for 3D construction printing, the preparation of a special molding mixture on the CGB was carried out as follows. Initially, citric acid (0.2% by weight of CGB) was inserted into the required amount of water to increase the time interval between the beginning and ending of setting of the molding mixture. Then, with constant stirring (at least 3 min), a pre-prepared dry mixture was added, including CGB with modifying additives and quartz sand (in a ratio of 1:2, by weight, respectively) and 2% of the mass of the binding carboxymethyl cellulose (CMC) to give the molding mixture the required viscosity and plasticity.

During the extrusion process, the mobility of the molding mixture, its setting time, shape stability, uniformity and strength set of the molded layers of the structure were recorded. Experimental verification of the strength characteristics of solidified molding mixtures in the initial hardening period (at the age of 2 h, 1 day and 7 days) was carried out when testing samples-cubes with a size of 7.07 × 7.07 × 7.07 cm.

Composition and results of physical and mechanical tests of a special molding mixture on CGB (composition 10, Table 1) and the solidified composite are shown in Table 2.

Table 2. Composition and properties of the hardened molding compounds on CGB.

Ratio of CGB:TH	Citric acid, %	CMC, %	W/B$_{in}$	Spread, m	Setting time, min,-s		R$_{comp}$, MPain terms		
					Beginning	Ending	2 h	1 day	7 day
1:2	0.2	2	0.47	0.120	36-00	40-00	3.2	5.6	9.4

The laboratory experimental device for 3D construction printing consists of a moving platform, a mixer, a hopper, a vertical and horizontal forming head with replaceable nozzles, a vibrator and a control panel (Fig. 2).
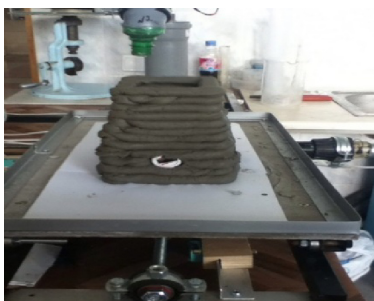
Fig. 2. Experimental laboratory device for 3D construction printing.

The device is managed manually. The speed controller for extrusion of the molding mixture by the extruder is located on the control panel. Together with the mixer, a vibrator is turned on, which does not allow the mixture to set.

4   Conclusion

Based on the conducted research, the following was found. The joint insertion of gypsum binders of α - and β-modification (G-5BII and GVVS-16) into the composition of CGB contributes to the early structure formation of stone on CGB.

Optimization of the CGB structure formation process with the insertion of modifying additives-the hyperplasticizer MAPP SU 84, the thickener MARF (Forbocrete 9010) and the hydrophobic rheological additive MAPF № T 10 can significantly reduce the water demand of the mixture by 28…56%) and improve its plasticity, while the compressive strength increases by 2 times in 2 h, by 1.7 times in 1 day, and by 1.5 times in 7 days.

Developed for 3D additive technologies, molding mixtures based on CGB and quartz sand quickly harden and gain strength, providing a concrete compressive strength class of B3.5 in the early stages of hardening (1 day), and B7.5 at the age of 7 days.

References

1. Lesovik, V.S., Glagolev, E.S., Volodchenko, A.N., Drebezgova, M.Yu.: Effective composites for 3D additive technologies in construction. Bull. Cent. Territorial Dept. Russ. Acad. Archit. Constr. Sci. Voronezh **15**, 149–156 (2016)
2. Bazhenov, Y.M., Zagorodnjuk, L.H., Lesovik, V.S., Yerofeyeva, I.V., Chernysheva, N.V., Sumskoy, D.A.: Concerning the role of mineral additives in composite binder content. Int. J. Pharm. Technol. **8**(4), 22649–22661 (2016)
3. Permyakov, M.B., Permyakov, A.F., Davydova, A.M.: Additive technologies in construction. Eur. Res. **1**(24), 14–18 (2017)
4. Vatin, N.I., Chumadova, L.I., Goncharov, I.S., Zykova, V.V., Karpenya, A.N., Kim, A.A., Finashenkov, E.A.: 3D printing in construction. Constr. Unique Build. Struct. **1**(52), 27–46 (2017)
5. Tay, Y.W.D., Panda, B., Paul, S.C., Noor Mohamed, N.A., Tan, M.J., Leong, K.F.: 3D printing trends in building and construction industry: a review. Virtualand Phys. Prototyping **12**(3), 261–276 (2017)
6. Luneva, D.A., Kozhevnikova, E.O., Kaloshina, S.V.: Application of 3D printing in construction and prospects for its development. Bull. Perm Natl. Res. Polytech. Univ. Constr. Archit. **8**(1), 90–101 (2017)
7. Drebezgova, M.Yu.: Modern additive technologies in low-rise construction. Bull. BSTU named after V.G. Shukhov **6**, 66–69 (2017)
8. Pustovgar, A.P., Adamtsevich, A.O., Volkov, A.A.: Technology and organization of additive construction. Ind. Civ. Constr. **9**, 12–20 (2018)
9. Inozemtsev, A.S., Korolev, E.V., Zuong, T.K.: Analysis of existing technological solutions for 3D printing in construction. Bull. MSCU **13**(7)(118), 863–876 (2018)
10. Chernysheva, N.V., Lesovik, V.S., Drebezgova, M.Yu., Shatalova, S.V., Alaskhanov A.H.: Composite gypsum binders with silica-containing additives. In: IOP Conference Series: Materials Science and Engineering, vol. 327, p. 032015 (2018)
11. Chernysheva, N.V., Shatalova, S.V., Evsyukova, A.S.: Fischer, Hantz-Bertram: features of selection of rational composition of composite gypsum binder. Constr. Mater. Prod. **1**(2), 45–52 (2018)
12. Klyuev, S.V., Klyuev, A.V., Shorstova, E.S.: Fiber concrete for 3-D additive technologies. Mater. Sci. Forum **974**, 367–372 (2019)
13. Elistratkin, MYu., Minakov, S.V., Shatalova, S.V.: Influence of mineral additives in the composition of a composite binder on the effectiveness of the plasticizer. Constr. Mater. Prod. **2**(2), 10–16 (2019)

14. Klyuev, S.V., Khezhev, T.A., Pukharenko, Y.V., Klyuev, A.V.: To the question of fiber reinforcement of concrete. Mater. Sci. Forum **945**, 25–29 (2018)
15. Klyuev, S.V., Khezhev, T.A., Pukharenko, Y.V., Klyuev, A.V.: Experimental study of fiber-reinforced concrete structures. Mater. Sci. Forum **945**, 115–119 (2018)
16. Markin, V., Nerella, V.N., Schröfl, C., Guseynova, G., Mechtcherine, V.: Material design and performance evaluation of foam concrete for digital fabrication. Materials **12**, 2433 (2019)

Research of Chernozemic Soil Roads' Dusting Surfaces Fixation Method

L. M. Smolenskaya[✉] ⓘ, E. A. Pendyurin ⓘ, S. Yu. Rybina ⓘ, and M. M. Latypova ⓘ

Belgorod State Technological University named after V. G. Shukhov, 46 Kostyukova St., Belgorod 308012, Russia
Smolenskaylarisa@yandex.ru

Abstract. Dust is presented with a mixture of organic and mineral impurities, contained in the outdoor air and varying in chemical composition. Its high content reduces road visibility, thus increasing the accident risk and slowing down the traffic speed. Accumulation of explosive or combustible materials' dust in the air can cause explosions or fires. In this research we have used the chemical agent «Bespylin», which appears as a sticky biopolymer emulsion, for dusting surfaces fixation. To study the dust loss an experimental plant was designed and assembled, which consisted of a wind tunnel, with wind speed varying in the range 4–10 m/s, a return pump and an electric motor. The dust loss was evaluated after one day, one week and one month. The dust loss was determined by calculation, i.e. by the difference in weight of the material under study. It has been determined that after applying the agent on the dusting surface, a stable crust is formed, which prevents the dust loss. The agent can be used in amount of 250–300 ml/m^2 at the minimum concentration 1:3. It has been also determined that this method of dusting surface fixation has no adverse effects on the condition of green cover.

Keywords: Soil roads · Dust · «Bespylin» · Dusting surface · Dust loss · Dust suppression

1 Introduction

One of the vital components of the environment is the atmospheric air, which is a natural mixture of gases, formed in the course of the Earth's evolution, contained in the ground layer of the atmosphere outside residential, industrial or other buildings. Dust is a finely-dispersed system, which consists of solid particles, suspended in the air. Dust particles, containing the admixtures of various organic and inorganic compounds, predetermine its toxic effect. Dust pollution of the atmosphere impedes the global water, carbon-dioxide and oxygen circulation. Dust can cause failures and breakdowns of various types of equipment, deteriorate the product quality, minimize the room illumination, as well as cause various respiratory diseases or allergic reactions, eye and skin damage, acute or chronic intoxications. So, dust control is an important health-care, social and economic task.

Dust reduces the road visibility, increasing the accident risk and slowing down the traffic speed. Accumulation of explosive or combustible materials' dust in the air brings about the risk of explosions or fires. The increased amount of dust has an adverse effect on the state of technological equipment. Apart from the mechanical wear (due to abrasive particles getting into the friction parts), the increased amount of dust can result in malfunctions of car control systems, as dust gets inside the electronic control units. The service life of engines, working in conditions of dust pollution, is reduced by 2–3 times. Dust increases the intensity of corrosion process; the technological equipment begins to require more complicated and lengthy repairs and maintenance works [1].

The dust, generated by the motor traffic on roads, is classified among the air pollution sources; the dust from soil roads and various road surfaces is very fine and barely visible, consisting of particles 1–100 μm or larger. The maximum permissible content of dust in the atmospheric air is no more than 5 mg/m^3. But in fact, near motor roads its content reaches 100 mg/m^3, or even more. Soil roads are located on the natural soil, so, there is no hard road surface on them. Dust from soil roads, depending on the thickness of dust layer and the amount of fine particles in it, saturates the surrounding air to a considerable extent. In summer the length of a dust cloud at soil roads makes up from 50 to 150 m. The capacity of roads with accumulated dust is reduced by 4 times. On new roads with the enhanced surfacing the dust is generated mostly from the surrounding soil, from earth shoulders and the adjoining soil roads. On gravel and crushed-rock surfaces the dust is generated from the carriageways' material wear [2, 3].

Fixation of dusting surfaces is a set of means and methods to prevent dust pollution of the air by reducing dust release and its sedimentation.

Dust control and dust suppression on road surfaces is a complex and rather costly procedure. For dust control various methods and types of equipment are used – from complicated stationary exhaust ventilation systems, cyclone separators and electrostatic dust collectors to irrigation machines, hydromonitors and fog cannons, which spray water, chemicals or foam [4–6].

Roads with the enhanced surfacing are cleared with power sweepers and sprayed with water. For roads with the intermediate or simple surfacing the most efficient way of dust control is treating them with materials, which bind the dust particles – liquid bitumens and tars, petroleum, petroleum residue, some industrial production waste products, for example, sulfate-alcohol stillage. A less durable effect is achieved at using hygroscopic salts – chlorides, which, absorbing the moisture from the air, dedust a road for 2–4 weeks. From soil roads dust is raked off with drags or graders, which instantly produces the appreciable effect [7–9].

2 Materials and Methods

In this research an attempt to fix a potentially dusting surface with a biopolymer material named «Bespylin» was performed. Unlike most materials, intended for dust control, «Bespylin» absorbs moisture from the air and keeps it for a long time in the

road surface. Due to such property as hygroscopicity (high capacity of absorbing moisture even from relatively dry air), «Bespylin» provides the maximum dampness of the road surface. It prevents dust from rising and staying suspended in the air. This moisture-absorbing effect provides better result than dust suppression by spraying it with water. Besides, «Bespylin» lengthens the working lifespan of a roadbed, stabilizing the soil.

To study dust loss an experimental plant (Fig. 1) was designed and assembled, which consisted of a wind tunnel, in which the wind speed varied in the range 4–10 m/s, a return pump and an electric motor. Wind speed was determined with a measuring instrument – a vane anemometer.
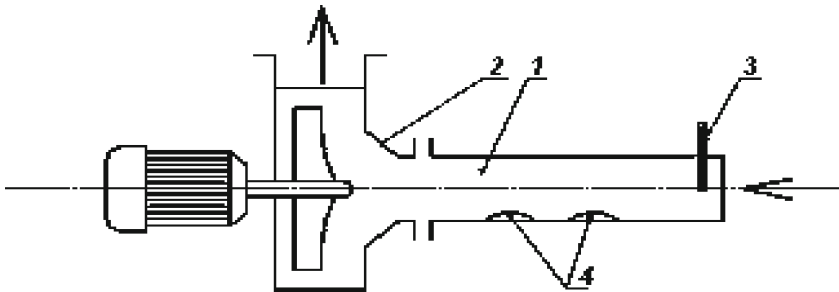
Fig. 1. Laboratory-scale plant: *1* – wind tunnel, *2* – fan; *3* – shutter; *4* – analyzed samples.

The dust loss was evaluated after one day, one week and one month. It was determined by calculation, i.e. by difference in the weight of the material under study. It should be mentioned that the applied biopolymer agent appeared as a dark sticky mass with a sweet scent. The experimental research was carried out with the original substance, and the substance diluted with water in the ratio 1:1, 1:2, 1:3. The substance keeps its «stickness» at dilution 1:1 and 1:2. The ratio 1:3 changes the texture of the agent.

3   Results and Discussion

The previously prepared samples of clay-textured chernozemic soils of various fractions from 0.08 to 0.5 mm were treated with the biopolymer agent «Bespylin» in different concentrations and placed into the experimental plant, where various wind speed from 4 to 10 m per second was emulated. The findings of the experimental research are presented in Tables 1, 2 and 3.

Table 1. The influence of «Bespylin» solution concentration on the dust loss process at wind speed 4 m/s.

№	Ratio of «Bespylin» solution and water	Dust loss after applying the biopolymer, %		
		1 day	7 days	30 days
Soil fraction 0.5 mm, dust loss 2.2%				
1	1	0	0	0
2	1:1	0	0	0
3	1:2	0	0	0
4	1:3	0	0.03	0.06
Soil fraction 0.25 mm, dust loss 4.1%				
1	1	0	0	0
2	1:1	0	0	0
3	1:2	0	0	0
4	1:3	0	0.05	0.07
Soil fraction 0.14 mm, dust loss 5.6%				
1	1	0	0	0
2	1:1	0	0	0
3	1:2	0	0	0
4	1:3	0	0.04	0.05
Soil fraction 0.08 mm, dust loss 6.2%				
1	1	0	0	0
2	1:1	0	0	0
3	1:2	0	0	0
4	1:3	0	0.18	0.20

Table 2. The influence of «Bespylin» solution concentration on the dust loss process at wind speed 6 m/s.

№	Ratio of «Bespylin» solution and water	Dust loss after applying the biopolymer, %		
		1 day	7 days	30 days
Soil fraction 0.5 mm, dust loss 2.3%				
1	1	0	0	0
2	1:1	0	0	0
3	1:2	0	0	0
4	1:3	0	0.05	0.06
Soil fraction 0.25 mm, dust loss 5.1%				
1	1	0	0	0
2	1:1	0	0	0
3	1:2	0	0	0
4	1:3	0	0.08	0.09

(*continued*)

Table 2. (*continued*)

№	Ratio of «Bespylin» solution and water	Dust loss after applying the biopolymer, %		
		1 day	7 days	30 days
Soil fraction 0.14 mm, dust loss 7.9%				
1	1	0	0	0
2	1:1	0	0	0
3	1:2	0	0	0
4	1:3	0	0.09	0.09
Soil fraction 0.08 mm, dust loss 10.8%				
1	1	0	0	0
2	1:1	0	0	0
3	1:2	0	0	0
4	1:3	0	0.11	0.15

Table 3. The influence of «Bespylin» solution concentration on the dust loss process at wind speed 10 m/s.

№	Ratio of «Bespylin» solution and water	Dust loss after applying the biopolymer, %		
		1day	7days	30days
Fraction 0.5 mm, dust loss 8.7%				
1	1	0	0	0
2	1:1	0	0	0
3	1:2	0	0	0
4	1:3	0	0.15	0.17
Fraction 0.25 mm, dust loss 10.7%				
1	1	0	0	0
2	1:1	0	0	0
3	1:2	0	0	0
4	1:3	0	0.17	0.20
Fraction 0.14 mm, dust loss 11.7%				
1	1	0	0	0
2	1:1	0	0	0
3	1:2	0	0	0
4	1:3	0	0.20	0.22
Fraction 0.08 mm, dust loss 21.3%				
1	1	0	0	0
2	1:1	0	0	0
3	1:2	0	0	0
4	1:3	0	0.22	0.25

As we can see from the presented data, the biopolymer agent «Bespylin» effectively fixes the dusting surface, which contains a clay fraction, – the dust loss is reduced from 2.2–6.2% to 0.03–0.20% (by 30–70 times). So, the biopolymer demonstrated its high efficiency at wind speed 4 m/s.

According to the data in Table 2, the biopolymer agent «Bespylin» also effectively fixes the dusting surface at wind speed 6 m/s – the dust loss is reduced from 2.3–10.8% to 0.05–0.15%. The application of the agent decreases the dust loss by nearly 100 times.

The obtained data in Table 3 indicate that the increase of wind speed up to 10 m/s results in the increase of dusting process from 8.7–21.3%, at which the dust loss also increases from 0.15 to 0.25% (dust suppression alters within the range 58–96%).

Consumption of the agent and its solutions remained approximately the same and amounted to 290–300 ml/m^2. In 24 h after its application the dust loss was not observed, which indicated the process of coalescence of soil particles under the influence of «Bespylin».

After spraying the agent on the dusting surface and its drying, a crust is formed, that has the external stability and prevents dust loss (Fig. 2).

fraction 0.5 mm   fraction 0.08 mm

Fig. 2. Soil surface after the application of «Bespylin».

It should be noted that the fixing ability of «Bespylin» stayed for a month. But a mechanical impact can cause damage to the fixed surface (Fig. 3).

Fig. 3. The fixed surface, damaged with a mechanical impact.

To study the effect of «Bespylin» on condition of the plant cover along the dust-suppressed roads, the experimental research of the agent's influence on growth and development of aerial parts of the plants was carried out.

The lawn grass at the experimental plot was sprayed, using a spray bottle, with the biopolymer agent in various concentrations. The action of the agent on the grass was monitored daily. According to the observation data, the agent had no tangible adverse effects on the vegetation straight after the treatment, or in the interval from the first to the seventh day. The color of the grass didn't change; the grass wasn't drying or turning yellow. No bare spots were found in the grass at the treated plot. After the atmospheric precipitation the biopolymer agent «Bespylin» partially stayed on the aerial parts of plants. Even after completion of the experiment no negative action of the agent on the plants was observed. The grass continued to grow in the same way as before the treatment.

4   Conclusions

The biopolymer agent «Bespylin» demonstrated the positive dynamics of dust suppression process on clay-textured chernozemic soil roads. In comparison with dust suppression by spraying a dusting surface with water – which can't be called high-efficient, as it requires high water consumption and after drying the dust loss is resumed – «Bespylin» can be used for fixing the dusting surfaces in amount 250–300 ml/m^2 at the minimum concentration 1:3. After the treatment the substance forms a stable crust that has the external stability and prevents dust loss. The crust can be damaged by mechanical impacts. It has been determined that this method of application has no influence on the condition of green cover.

References

1. Komonov, S.V., Komonova, E.N.: Wind Erosion and Dust Suppression. SFU Publishing House, Krasnoyarsk (2008)
2. Vysotskaya, M.A., Lashin, M.V., Kurlykina, A.V.: The usage of shelly ground in transport construction. Bulletin BSTU named after V.G. Shukhov **5**(3), 8–15 (2020)
3. Logachev, I.N., Logachev, K.I.: Characteristics of dust emissions at transloading loose materials and their prevention. Bulletin BSTU named after V.G. Shukhov **3**, 163–167 (2009)
4. Dust control on roads» [Electronic source]. https://studopedia.su/10_77856_borba-s-pilyu-na-dorogah.html. Accessed 02 Sept 2020
5. Lychagin, E.V., Sinitsina, V.V.: Improving methods of dusting surfaces fixation. Seminar **8**, 136–140 (2007)

6. Pendyurin, E.A., Starostina, I.V., Smolenskaya, L.M., Rubanov, Yu.K.: Biological method of dust suppression at spoil heaps of Lebedinsky MPP. Ecol. Ind. Russia **6**, 46–48 (2010)
7. Gurin, A.A., Lyashenko, V.I., Domnichev, N.V.: Dust emission control at operating tailing dumps of mining and processing plants. News of Higher Educational Institutions. Mining J. **5**, 13–22 (2012)
8. Saranchuk, V.I., Zhuravlev, V.P.: Chemicals for dust control. Naukova Dumka, Kiev (1987)
9. Katola, V.M., Komogortseva, V.E. Dust: sources of generation, general characteristics, dust diseases. Bulletin **67**, 111–116 (2018)
10. Grafkina, M.V., Azarov, A.V., Tikhonova, M.M.: Analysis of the adverse effect on ecosystem's elements from dust raising, caused by motor traffic on road surfaces of various types. Adv. Mod. Sci. **8**(12), 142–147 (2016)

Composite Material Based on Polyvinyl Chloride and Methylcellulose Fibers with Improved Performance and Environmental Characteristics

L. N. Naumova[1]($\boxtimes$) , N. A. Kristalova[1] , E. V. Burmakina[1] ,
and A. N. Ryzhkova[2]

[1] Belgorod State Technological University. V. G. Shukhov, Belgorod, Russia
`naymova_ln@mail.ru`
[2] SBEE "Belgorod Engineering Youth Lyceum Boarding", Belgorod, Russia

Abstract. The article presents data on obtaining a polymer composite material based on polyvinyl chloride and methylcellulose fibers, testing it for Flexural strength and impact strength, and evaluating the Toxicological properties of this material for the survival of Daphnia moina due to the presence of a toxic stabilizer in the material. The samples were obtained by mixing the components in a mixer and then hot pressing. The samples were obtained considering the mass and volume fraction of the components. The optimal matrix-filler ratio was determined based on the obtained experimental characteristics. It was 10% of the volume of methylcellulose from the content of polyvinyl chloride. It is shown that the resulting polymer composite material has increased strength characteristics, such as Flexural strength and impact strength, and does not exhibit toxic properties in certain ratios of methylcellulose and polyvinyl chloride. Electron microscopic analysis of the surface state of the samples was performed, which confirms the above conclusion.

Keywords: Polymer composite material · Methyl cellulose fibers · Polyvinyl chloride · Optimal composition · Environmental safety

1 Introduction

The 21st century is the century of composite materials. The greatest demand for the construction industry is polymer composite materials using natural fibers as a filler.

Wood-polymer composite (WPC) combines the practical properties of plastic and the advantages of wood. This is a modern, improved material, which has found wide application [1]. Polyvinyl chloride (PVC) was chosen as the polymer matrix. This polymer is chemically resistant to alkalis, mineral oils, fats, alcohols, many acids and solvents. It doesn't burn in air, but is prone to decomposition with evolution of hydrogen chloride at temperatures above 110–120 °C. To prevent this, stabilizers are added to the composites. PVC is a rather heavy material, its density is 1320–1340 kg/m^3, and the melting temperature is 150–220 °C. The flexural modulus of PVC can reach 4 GPa. The disadvantages of PVC include low heat resistance (operating

temperature range from –30 to 70 °C) and high fragility [2]. Tribasic lead sulfate (TOCS) was used as the thermostabilized of PVC. Lead stabilizers are cheap and common among other PVC thermal stabilizers. The use of wood fibrous materials and cellulose fibers is promising [3]. High reactivity and low molecular weight of cellulose allow its chemical modification at small liquid modules, more efficiently using reagents for a shorter time and under milder conditions. Methyl cellulose (MC) is one of the products of this modification. This work presents data on the optimal composition of the matrix-filler, establishes the strength characteristics of the composite and its environmental component.

2   Experimental Section

Determining the optimal composition of PCM is a labor-intensive process, since it includes many factors affecting the production parameters and the quality of the finished product.

The moisture content is one of the important parameters for the processes of obtaining and processing PCM, since the presence of excess free moisture can contribute to the appearance of many scrap products.

The determination of moisture content is carried out through the determination of the dry matter content.

An important indicator for determining combustibility is the ash content. The determination of the ash content of materials is related to the quality content of the studied sample of organic and mineral substances. As a rule, the lower the content of organic substances, the higher the ash content [4].

In the manufacture of PCMs, chemically bound water plays an important role in the filler structure, which can manifest its properties under various temperature characteristics and affect the physicochemical interaction between the components. For high molecular weight substances, the swelling property is the most characteristic, namely, in comparison with low molecular weight compounds. In many cases, swelling occurs almost without changing the shape of the sample. The interaction of polymers with solvents is of great importance in their application, processing, in biological processes, etc.

To determine the degree of swelling of the material, the samples were weighed, and then placed on a rod in a 17.5% sodium hydroxide solution, leaving to swell for 5 min. At the end of the set time, the cellulose rod was set on fire, leaving to burn for another 5 min. Then, the alkali solution was removed from the rod with filter paper and the remaining material was weighed. The resulting value indicates acceptable regulatory indicators that are used to adjust the process.

3   Results and Discussion

The preparation of a composite based on polyvinyl chloride with methyl cellulose filler and its environmental component were the main goal of the work.

The components were mixed in a laboratory stirrer. First, PVC and TOSS were mixed to evenly distribute the stabilizer in the composite, then MCwas added in small portions. Stirring was carried out at 500 rpm. To obtain samples, the following component contents were taken (Table 1). Samples were formed on a hydraulic press 100-400-2E.

Table 1. The composition of the samples of the duodenum.

Sample No.	The content of MC in the composite, % of PVC	Mass MC, g	PVC weight, g	Mass of TOSS, g
1	5	2.5	50	1.5
2	10	5		
3	15	7.5		
4	20	10		

The material was laid out on a mold, measuring 150 * 100 * 2 mm, evenly distributed over it. The sample was kept for 5 min at a temperature of 170 °C [5]. After removing the samples from the molds, a discoloration of the finished product was observed due to the temperature effect on the cellulose fibers. Samples for further experiments were cut into strips 150 * 25 * 2 mm in size.

The calculation of the content of the components was carried out considering volume and mass percent. Initially, WPC samples were made considering only mass percent. In this calculation and preparation of the mixture, there was no uniform distribution of methyl cellulose fibers in it, since this did not correspond to the bulk density of this fiber. Based on the foregoing, the obtained samples with compositions of 25 mass. % MC, 50 wt. % MC, 75 wt. % MC from the mass of the composite did not correspond to a uniform distribution in the composite. Qualitative samples were obtained with a content of MC in the range of 5–15 mass. % by weight of PVC. To determine the toughness, a pendulum driver was used. The measurement results are listed in Table 2 (Fig. 1):

Table 2. The results of the determination of toughness.

Sample No.	The content of MC, % of PVC	Arithmetic mean applied energy, An, J	Impact strength, kJ / m^2
1	5	1.49	37.82
2	10	1.66	37.58
3	15	1.89	37.41
4	20	1.94	37.32

From the test results it follows that the most durable is a composite with a content of MC 20% by weight of PVC.
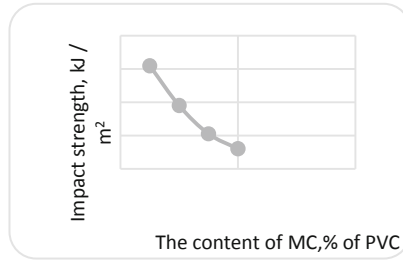
Fig. 1. Graph of impact strength versus MC content.

Tests for static bending were carried out according to GOST 4648-71.The results of measurements and calculations are presented in Table 3 (Fig. 2).

Table 3. The results of determining the bending strength.

Sample No.	The content of MC,% of PVC	Width of a sample, mm	Sample Thickness, mm	Distance between supports, mm	Load, kN	Bending stress, GPa
1	5	25	2	10	29.7	4.46
2	10				36.2	5.43
3	15				21.4	3.21
4	20				15.6	2.34

Based on the results, we can conclude that the optimal content for the composite MC is 10% by weight of PVC.
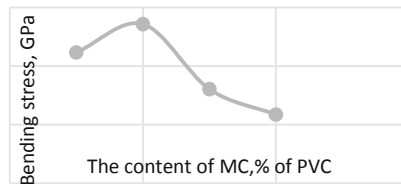
Fig. 2. Graph of bending stress on the content of MC.

3.1 Assessment of the Toxicological Properties of the Composite

Assessment of the toxicity of the studied samples using the test organisms Daphnia magna Straus and Ceriodaphnia affinis was carried out by biotesting in accordance with PND F T 14.1: 2: 3: 4.3-99 and PND F T 14.1: 2: 3: 4.4-99, PND F T 14.1: 2: 3: 4:16 – 2000 [6]. For this, test organisms (10 daphnia's in 8 glasses) were placed on a sample of samples.

The first one was an express analysis, immersing in each container a strip of each sample. The high mortality of test organisms was in the vessel with the sample, in which the content of MC was 20% of PVC.

Then a full analysis was carried out, leaving the samples in a beaker and daphnia for 10 days, tracking the population of organisms every day. Within 4 days, the number of daphnia in glasses with a content of MC of 5% and 20% of PVC came to zero, within 6 days in a glass with a content of MC 10% of PVC and within 8–9 days in a glass with a content of MC 15% of PVC (Table 4). Thus, the least toxic sample is a composite with an MP content of 15% of the amount of PVC.

Table 4. Toxicology test results.

Sample No	The content of MC, % of PVC	The number of days after which the number of test organisms was reduced to zero
1	5	4
2	10	6
3	15	8–9
4	20	4

Based on the data obtained, the best performance is possessed by a sample with a content of MC of 10% by weight of PVC. When using more MCs, the samples exhibit worse bending properties, and when using a smaller amount, the impact strength drops sharply, while the bending strength does not change.

3.2   Analysis of the State of the Structure of the Obtained Polymer Composite Material

Electron microscopic studies of filled materials were performed using an electron microscope. High resolution brand TESCAN MIRA 3 LMU. Samples were used with the compositions shown in Table 1.

PCM strength is determined mainly by the strength of the polymer matrix. Thermoplastic polymers used as matrix materials for PCMs are densely reticulated, spatially cross-linked biphasic substances consisting of globules or micelles with a high density and an amorphous phase with structureless and loose packing of macromolecules with a low density. During bending and stretching, densely reticulated polymers are destroyed with small plastic deformations [7, 8].The introduction of hard dispersed filler particles into such polymers mainly leads to a decrease in the breaking stresses during bending and tension, an increase in the elastic modulus, an increase in the yield strength and compressive and shear strength.

The increase in strength mainly depends on the contact of the filler particles with the polymer matrix [4, 9, 10]. When the composite is formed, the boundary layers of the polymer and the filler have a different energy surface, which leads to an uneven distribution of particles, but helps to compensate for the energy excess. Due to this effect, filler particles begin to group in such a way that the polymer in the space between them passes into a hardened boundary state. The transition of the polymer

from the bulk state to the boundary layer is considered as a first-order phase transition and as applied to the filler, is important when studying their properties [10].

Fig. 4. Electron microscopic images containing 10 wt.% MC.

Fig. 5. Electron microscopic images containing 15 masses. % MC.
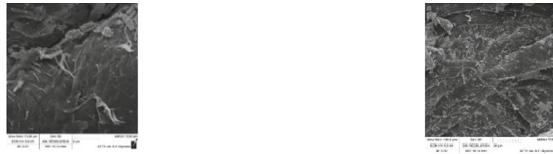
Fig. 6. Electron microscopic images containing 20 masses. % MC.

The special properties of polymer composites are primarily due to the adhesive interaction of the polymer with a dispersed filler; therefore, the regulation of adhesion is one of the main problems associated with the creation of composites [11, 12].The electron microscopy images (Figs. 4, 5 and 6) of a polymer composite with various filling with methylcellulose fibers confirm the above mechanism.

4   Conclusion

The obtained polymer composite material based on a polymer matrix of polyvinyl chloride and methyl cellulose fibers as a filler. The method of experimental experiment selected the optimal content of the components. Impact strength and static bending resistance are high. Survival tests of Daphnia moina showed the environmental safety of the resulting material. Electron microscopic images of the state of the surface of the composite with different content of methylcellulose fibers confirm the relationship of physical and mechanical characteristics from the distribution of the filler in the polymer matrix.

References

 1. Klesov, A.A.: Wood-Polymer Composites. Scientific Foundations and Technologies, St. Petersburg (2014)
 2. Wilkie, C.: PVC (Polyvinyl chloride). TsOP "Profession", St. Petersburg (2012)
 3. Markusova, V.A.: Wood-polymer composites - green innovations. https://www.waste.ru/modules/section/item.php?Itemid=278. Accessed 20 Oct 2020
 4. Sidorova, M.: Market review of wood-polymer composites. https://www.waste.ru/modules/section/item.php?itemid=279. Accessed 20 Oct 2020
 5. Bogdanov, A.: Prospects for the development of the KDP market. https://www.waste.ru/modules/section/item.php?itemid=278. Accessed 20 Oct 2020
 6. Terentyev, E.P., Udovenko, N.K., Pavlova, E.A.: Chemistry of wood, cellulose and synthetic polymers. Part 1, Study Guide. SPbGTURP, SPb (2014)
 7. Aleksandrova, V.V.: Application of the bioassay method in the analysis of toxicity of natural and wastewater. On the example of the Nizhnevartovsk district of the Tyumen region (2009)
 8. Klyuev, S.V., Khezhev, T.A., Pukharenko, Y.V., Klyuev, A.V.: Experimental study of fiber-reinforced concrete structures. Mater. Sci. Forum **945**, 115–119 (2018)
 9. Takahama, H., Geil, P.H.: Structur inhomogeneities of curred epoxy resins. Macromol Chem. Rapid Commun. **3**, 389–394 (1982)
10. Lesovik, R.V., Klyuev, S.V., Klyuev, A.V., Tolbatov, A.A., Durachenko, A.V.: The development of textile fine-grained fiber concrete using technogenic raw materials. Res. J. Appl. Sci. **10**(10), 696–701 (2015)
11. Lesovik, R.V., Klyuyev, S.V., Klyuyev, A.V., Netrebenko, A.V., Kalashnikov, N.V.: Fiber concrete on composite knitting and industrial sand KMA for bent designs. World Appl. Sci. J. **30**(8), 964–969 (2014)
12. Tuzhilin, S.P., Lopatin, U.A., Sviridova, A.S.: Prozessing of polymer materalis by method of free casting in vacuum. Bulletin BSTU named after V.G. Shukhov **7**, 93–100 (2020)

Purification of Model Waters from the CONGO Red Dye with Organomineral Sorption Material Based on Sludge Waste

Zh. A. Sapronova[✉] , I. V. Starostina , and I. V. Bomba

Belgorod State Technological University named after V.G. Shuchov,
Belgorod, Russia
sapronova.2016@yandex.ru

Abstract. The food industry generates a lot of large-capacity sludge waste that requires recycling. The paper presents the results of a study on sorption treatment of model waters containing the Congo red dye using sorption materials based on diatomite-containing sludge formed in the brewing industry and carbonate sludge formed in the sugar industry. It was found that when using sorbents separately, the most effective is heat-treated at 450 °C diatomite-containing sludge (DS450), the optimal time of interaction of the sorbent with the solution is 20 min. The sorption material based on thermally modified carbonate sludge (TCS) showed the lowest cleaning efficiency under the conditions of this experiment. It is shown that combining TCS to DS450 in a ratio of 1:9 significantly increases the cleaning efficiency. When the TCS content in the mixture increases, the efficiency decreases. At the same time, using DS450 and TCS separately gives a lower cleaning effect, 93% and 41%, respectively, while a mixture containing 10% TCS allows achieving 98% efficiency. The identified effect requires further study.

Keywords: Waste water treatment · Dyes · Diatomite waste · Carbonate sludge

1 Introduction

Industrial wastewater contains various compounds, most of which are dangerous to the environment and the inhabitants of water reservoirs. Dyes end up in the drains of the textile, paper, food, pharmaceutical, and other industries [1, 2]. Natural dyes are rarely used, as they are usually not very stable, and their production is quite expensive. Therefore, most of the used coloring substances are of artificial origin. To date, more than 10,000 of them have been synthesized. These substances are classified in various ways: by chemical structure (e.g. azo, nthraquinone, sulphur, acridine, metal complex, anthraquinone, indigoid, phthalocyanine etc.), according to the method of staining (acid, basic, mordant, reactive, direct, disperse etc.). In addition, they can be divided into anionic, nonionic and cationic dyes [3–5].

Despite the fact that dyes are not usually associated with highly toxic substances in society, and therefore cause less concern and discussion than heavy metals and petroleum products, these compounds, which are alien to natural ecosystems and artificially created for active interaction with the fibers of fabrics and other colored materials, cause significant harm to the environment.

When they enter water objects, they reduce light transmission and air exchange in the surface layer, which affects directly the processes of photosynthesis and the life cycles of plankton, destabilizing the ecosystem at all levels. Depending on their nature and individual chemical characteristics, dyes cause allergic reactions and irritation of the skin, mucous membranes, have a toxic effect, carcinogenic and mutagenic. In the soil layer, dyes affect negatively microbial communities, which can lead to a decrease in the bio-productivity of terrestrial ecosystems. Many dyes are very stable, accumulate in precipitation and bioaccumulate in living organisms [1, 4, 5].

One of the ways to clean colored effluents is to use adsorbents [6]. Sorption materials are classified into organic, mineral and organomineral, natural and artificial, obtained from natural raw materials and industrial waste [7]. The latter group of sorption materials is the most attractive from an economic and environmental point of view [8]. Their cost is usually low, and their use in wastewater treatment allows not only to remove pollutants from the water, but also to solve the problem of waste accumulation.

The food industry generates a lot of large-capacity sludge waste. In this work, studies were conducted on the sorption treatment of model waters containing the Congo red dye using thermally modified sludge: diatomite sludge formed in the brewing industry and carbonate sludge of the sugar industry.

Diatomaceous ground is a natural sorption material that has long been used for filtration in the brewing industry. Beer is the fifth most popular drink in the world, so even taking into account the fact that some brewing technologies use other methods of cleaning the product, the amount of diatomite used worldwide is huge, and the disposal of sludge is a significant problem [9, 10].

Natural diatomite is a sedimentary rock formed as a result of the life activity of microscopic diatoms. From the chemical point of view, it consists of SiO_2 with admixtures of a small amount of other oxides Al_2O_3, Fe_2O_3, CaO, etc. [11–13]. Spent diatomite (sludge) contains organic substances that were deposited during beer filtration: insoluble substances of barley malt, beer yeast residues, proteins, glucose polymers, etc. [14].

Carbonate sludge of sugar production is formed at enterprises that receive sugar from sugar beet. It consists of fine $CaCO_3$ particles and organic substances adsorbed on its surface, extracted from beet juice [15].

Storage of such organomineral sludge is associated with problems of formation of unpleasant odors, the threat of rain runoff entering nearby water reservoirs, bacteriogenic threat, excessive reproduction of insects, etc. Therefore, the issue of their processing and disposal is very relevant.

2   Methods and Materials

The thermal treatment of the sludge test samples has been carried out in the muffle furnace LOIP LF-7/13 in the presence of oxygen.

For the preparation of model solutions the dye "Congo red" was used chemical formula $C_{32}H_{22}N_6Na_2O_6S_2$, 4-aminonaphthalene-1-sulphonic acid) classified as a benzidine-based anionic diazo dye [16].

The concentration of dye was measured photocolorimetric at a wavelength of 590 nm (spectrophotometer device "KFK-3", Russia). The cleaning efficiency was determined by the formula:

$$E = (Ci - Cf) * 100\%/Ci;$$

where Ci – initial concentration of the substance in solution, mg/l; Cf – final concentration of the substance in solution, mg/l (Fig. 1).
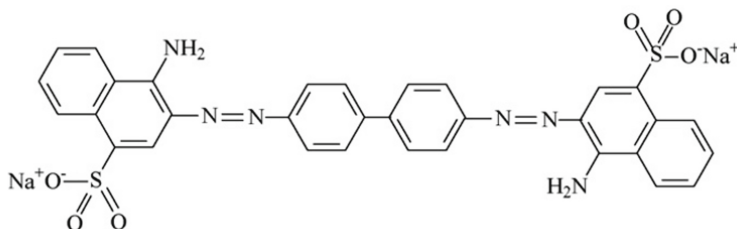
Fig. 1. The Congo Red dye molecule structure.

3   Results and Discussion

As organic substances adsorbed on the surface of diatomite and calcium carbonate in the corresponding sludge waste they can be partially desorbed into the solution, which poses a threat of additional contamination of the water environment, instead of cleaning it, the materials were subjected to heat treatment at various temperatures. In previous studies [17, 18], an effective sorption material TCS was obtained from the carbonate sludge by roasting at a temperature of 600 °C for 20 min, so in further work, the carbonate sludge was roasted only at this temperature.

Diatomite sludge was roasted at various temperatures: 250, 350, 450, 550, 650 °C for 20 min. The resulting fine powder was used in the purification of model waters.

The initial concentration of the Congo red dye solution was 12.5 mg/dm^3. 1 g of sorption material was added to 100 cm^3 of the solution, after which the liquid was mixed for 20 min, filtered through a paper filter, and the residual dye concentration was measured. In addition, TCS in the same ratio was used at the ratio liquid: sorbent. Figure 2 shows a diagram of the dependence of the efficiency of cleaning the model solution on the roasting temperature of diatomite sludge in the brewing industry.
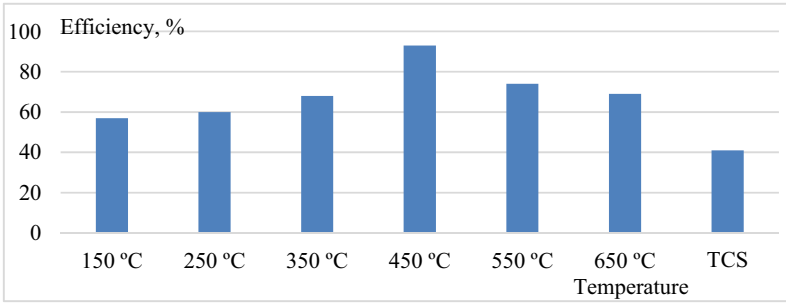
Fig. 2. Dependence of the efficiency of cleaning the model solution on the roasting temperature of diatomite sludge in comparison with TCS.

From the obtained results, it is clear that the most effective sorption material among the tested ones is heat-treated at 450 °C, with an increase in the roasting temperature, the efficiency begins to decrease. The TCS sorption material showed the lowest cleaning efficiency under the conditions of this experiment.

We studied the dependence of the efficiency of cleaning model solutions on the time of interaction of the sorbent with the solution. The DS450 sorption material was used to purify the model waters, as the most effective according to the results of the previous experiment.

It is established (Fig. 3) that the optimal interaction time is 20 min. As the contact time increases, the efficiency changes within 1%.
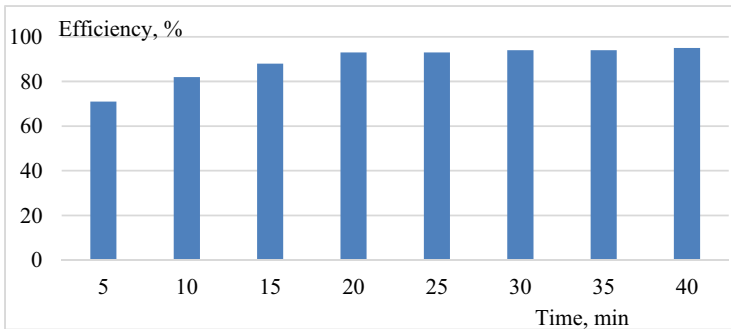
Fig. 3. Dependence of the cleaning efficiency of the model solution on the time of interaction of the sorbent with the solution.

Then a combined sorption material was prepared by mixing DS450 and TCS in various proportions. The model dye solution was purified using a method similar to the one described above. Table 1 shows the composition of the sorption material and the results of purification.

Table 1. Efficiency of purification of model solutions with the sorption material of different composition.

№	Sorption material, quantity in the mixture		Efficiency, %
	TCS, g	DS450, g	
1	0.1	0.9	98
2	0.2	0.8	97
3	0.3	0.7	93
4	0.4	0.6	91
5	0.5	0.5	87
6	0.6	0.4	82
7	0.7	0.3	80
8	0.8	0.2	78
9	0.9	0.1	57

Research results have shown that adding TCS to DS450 in a 1:9 ratio significantly improves cleaning efficiency. When the TCS content in the mixture increases, the efficiency decreases.

Previous experience has shown that the efficiency of cleaning using DS450 and TCS separately gives a lower cleaning effect, 93% and 41%, respectively, while a mixture containing 10% TCS allows achieving 98% efficiency. The identified synergistic effect requires further study. It is probably caused by electrokinetic interactions in the system, however, the mechanism has not been established yet.

4   Conclusion

The research made it possible to obtain a sorption material based on diatomite sludge, which effectively extracts the Congo red dye from the model solution. Heat treatment of carbonate sludge at 450 °C results in a sorbent with the best cleaning efficiency, up to 93%. The sorbent obtained on the basis of carbonate sludge from sugar production was ineffective under experimental conditions – only 41%. Combining DS450 and TCS in different proportions showed a synergistic effect with the ratio of these sorbents in the ratio of 1: 9. The revealed effect requires further study to determine the mechanism of electrokinetic interactions in the system.

References

1. Zheng, X., Liu, J.: Dyeing and printing wastewater treatment using a membrane bioreactor with a gravity drain. Desalination **190**, 277–286 (2006)
2. Sivakumar, K.K., Balamurugan, C., Ramakrishnan, D., Bhai, L.H.: Assessment studies on wastewater pollution by textile dyeing and bleaching industries at Karur. Tamil Nadu. Rasayan J. Chem. **4**(2), 264–269 (2011)
3. Yaseen, D.A., Scholz, M.: Textile dye wastewater characteristics and constituents of synthetic efuents: a critical review. Int. J. Environ. Sci. Technol. (2018)
4. Hassaan, M.A., El Nemr, A.: Health and environmental impacts of dyes: mini review. Am. J. Environ. Sci. Eng. **1**(3), 64–67 (2017)
5. Saini, R.D.: Textile organic dyes: polluting effects and elimination methods from textile waste water. Int. J. Chem. Eng. Res. **9**(1), 121–136 (2017)
6. Sivakumar, P., Palanisamy, P.N.: Low-cost non-conventional activated carbon for the removal of reactive red 4: kinetic and isotherm studies. Rasayan J. Chem. **1**(4), 871–883 (2008)
7. Galblaub, O.A., Shaykhiev, I.G., Stepanova, S.V., Timirbaeva, G.R.: Oil spill cleanup of water surface by plant-based sorbents: Russian practices. Process Saf. Environ. Prot. **101**, 88–92 (2016)
8. Ghazy, S.E., Khedr, A.E.S., Youssef, H.M.M.: Biosorptive-flotation of copper(II) from environmental water samples using sugar beet pulp as sorbent and oleic acid as surfactant. Chem. Speciat. Bioavailab. **21**(3), 131–140 (2009)
9. Fillaudeau, L., Blanpain-Avet, P., Daufin, G.: Water, wastewater and waste management in brewing industries. J. Cleaner Prod. **14**, 463–471 (2006)
10. Poreda, A., Zdaniewicz, M., Sterczyńska, M., Jakubowski, M., Puchalski, C.: Effects of wort clarifying by using carrageenan on diatomaceous earth dosage for beer filtration. Czech J. Food Sci. **33**(4), 392–397 (2015)
11. Lin, K.L., Lan, J.Y.: Porous ceramic characteristics sintered from waste diatomite and sodium silicate sand. Int. J. Mater. Mech. Manuf. **1**(3), 240–244 (2013)
12. Tsai, W.T., Hsien, K.J., Chang, Y.M., Lo, C.C.: Removal of herbicide paraquat from an aqueous solution by adsorption onto spent and treated diatomaceous earth. Bioresour. Technol. **96**, 657–663 (2005)
13. Ubaskina, Y.A., Korosteleva, Y.A.: Adsorption of cations and anions of organic compounds on the surface of diatomite. Bull. BSTU named after V.G. Shukhov **10**, 172–178 (2016)
14. Rudenko, E.Y., Bakharev, V.V., Mukovnina, G.S.: The possibility of using spent diatomaceous earth for wastewater treatment from copper. Proc. Samara Sci. Center Russ. Acad. Sci. **5–1**, 24–28 (2016)
15. Sapronova, Z.A., Sverguzova, S.V., Svyatchenko, A.V.: About a possibility of usage of sugar beet industrial carbonate containing byproducts in dry construction mixtures and oil paints manufacturing. Solid State Phenom. **284**, 899–904 (2018)
16. Khaniabadi, Y.O., Mohammadi, M.J., Shegerd, M., et al.: Removal of Congo red dye from aqueous solutions by a low-cost adsorbent: activated carbon prepared from Aloe vera leaves shell. Environ. Health Eng. Manage. J. **4**(1), 29–35 (2017)
17. Sapronova, Z.A., Svergusova, S.V., Fomina, E.V.: Nanocomposite carbon-bearing sorption material. Adv. Eng. Res. **133**, 728–733 (2017)
18. Sverguzova, S.V., Sapronov, F.A., Voronina, Y., Mel'nikov, S.N.: Purification of starch-containing wastewater. Chem. Bull. **2**(1), 14–20 (2019)

Impact of Technological Parameters of Vibration on the Integral Characteristics of Vibrocentrifugal Concrete

L. R. Mailyan , S. A. Stel'makh , E. M. Shcherban'$^{(\boxtimes)}$,
and A. K. Sysoev

Don State Technical University, Rostov-on-Don, Russia
`au.geen@mail.ru`

Abstract. For the best compaction of the concrete mix, it is appropriate to use the method of centrifugation together with vibration. This mode is appropriately called vibrocentrifugal. In the process of vibrocentrifugation, vibration can also be considered as a method for diluting the concrete mixture at the stages of its dispersal under the influence of centrifugal forces. Under the proposed experimental setup to generate vibrocentrifugal items with variational structure and method of their production was allocated to the process parameters that have the most significant influence on the characteristics of vibrocentrifugal concrete and constructions. In the experiments, the following technological factors varied: the height and length of the technological projections of the clamps, the step between them, and the vibration mode. The problem of evaluating the influence of these factors on the integral (general, cross-section averaged) characteristics of concrete was investigated. The results of experimental studies of the integral characteristics of vibrocentrifugated concrete are analyzed. The most effective will be the use of clamps with a height of technological projections of 5 mm, a length of 20 mm and a step between them of 30 mm, the vibration mode is alternating. At combinations of technological parameters of vibrating vibrocentrifugal concretes have better values of integral characteristics.

Keywords: Vibrocentrifugated concrete · Integral characteristics · Technological parameters of vibration · Reinforced concrete products · Vibration · Strength · Density

1 Introduction

Classification of methods for manufacturing reinforced concrete products and structures depends on the method used in the process of compacting the concrete mixture at the molding stage. This factor also affects the design of the basic equipment required for the production process of products.

The main methods of manufacturing reinforced concrete products are: vibrating; combined with vibrating methods, as well as centrifugation. Absolutely all of these methods have their positive and negative sides, but it is worth noting that these methods also have rational areas of application [1].

It is advisable to use the vibrating method when the form is in a vertical or horizontal position. With this in mind, for compacting the concrete mix, they can use vibration exciters mounted on the form, a fixed or mobile vibration heart (vibropuanson), a vibration platform, or a combination of them. Devices based on this principle are in demand in Russia, Germany, Denmark, and other countries [2].

The method of manufacturing reinforced concrete products by centrifugation is widely used. The essence of the method consists in rotating a horizontally positioned mold filled with a concrete mixture with a sufficiently high frequency and a circumferential speed equal to 15 … 20 m/s. Concrete mixture under the action of centrifugal forces moves closer to the inner surface of the mold, and is evenly distributed over it [3, 4].

The centrifugation process can be divided into two stages: at the first stage, the concrete mixture is evenly distributed over the shape of the product, and at the second stage, the formed product is compacted. The initial period of distribution of the concrete mix is characterized by the fact that it is observed to break off and fall from the upper zones of the form. After a certain period of time, the concrete mixture gets its initial compaction. This stage of compaction is explained by the fact that under the action of radially directed pressing centrifugal tension; the heavier components of the concrete mix move to the outer surface of the molded product, respectively, the lighter components and water are pressed to the inner surface of the product [5–7].

In his research, I.N. Akhverdov adopts the law of pressure distribution over the wall thickness of the formed product as for hydrostatic pressure according to the law of the triangle: the liquid squeezed out during centrifugation moves from the outer layers of the product to the inner layers of the product along radially directed filtration channels of a cone-shaped section [1].

The uneven distribution of the components of the concrete mix for the wall thickness of annular section of the product causes the concrete at the outer surface of the wall of the product has higher strength than the concrete inner wall surface. This phenomenon is called variatropy, i.e. different layers of concrete of the same product have different structural characteristics and density [8–11].

To increase the density and ensure a more uniform distribution of the components of the concrete mixture over the wall thickness of the product of the annular section, it is proposed to combine centrifugation with vibration and call this mode vibrocentrifugation. Vibration will be provided by the use of clamps that are put on the shafts of the device.

2 Methods and Materials

To create vibrocentrifugated products with a variatropic structure, an experimental laboratory centrifuge with a DC electric motor and thyristor power supplies was used. This provided smooth speed switching by changing the speed of the motor shaft. The shape vibrations were created using clamps placed on the installation shafts (two for each shaft) with technological projections of various lengths, heights and steps between them [12].

The purpose of the tests was to study the general, cross-section averaged characteristics of concrete. In total, 9 basic vibrocentrifugated samples of annular cross-section were manufactured and tested in the following dimensions: external diameter D = 450 mm; internal diameter of the hole d = 150 mm; total height H = 1200 mm.

All samples were made of concrete of the same composition, the material consumption per 1 m^3 was: C = 1203 kg, R = 696 kg, S = 416 kg, W = 181 l. From the general annular section of one basic sample, 3 conditional quadrants were selected from which the following samples were cut: 4 cubes with an edge of 150 mm for axial compression tests; 5 prisms with dimensions of 150 × 150 × 600 mm for axial compression tests, flexural tension tests, and axial tension tests.

Prisms and cubes for axial compression were tested on the IPS-10 press, and prisms for axial tension were tested on a special installation in the R-10 test press. Measurements of concrete deformation of prisms were made by a chain of load cells with a base of 50 mm and hour-type indicators with a division price of 0.001 mm [13, 14].

Under the proposed experimental device to generate vibrocentrifugal annular section samples with variational structure and method of their production technological parameters of vibration have been selected that have the most significant impact on the vibrocentrifugal concrete performance. These technological parameters include: height of technological projections of clamps; step between technological projections of clamps; length of technological projections of clamps; vibration mode.

3   Results and Discussion

In the experiments, we varied the selected technological factors and studied the problem of evaluating their influence on the integral characteristics of concrete: density; cubic and prismatic compressive strength; bending tensile strength; axial tensile strength; limit deformations under axial compression and axial tension; elastic modulus.

The results of experimental studies of the effect of technological parameters of vibration on the integral characteristics of concrete are presented in Tables 1, 2 and 3 and Figs. 1, 2, 3, 4, 5, 6, 7 and 8.

Table 1. Results of experimental studies of the effect of the height of technological projections of clamps and the step between them on the integral characteristics of concrete.

Concrete characteristics	Height of technological projections of clamps, mm								
	2.5			5			10		
	Step between technological projections of clamps, mm								
	15	30	45	15	30	45	15	30	45
Density, kg/m^3	2328	2338	2313	2390	2412	2418	2375	2381	2391
Compression Strength, MPa:									
a) cube	49.9	50.9	48.9	55.1	56.8	56.8	54.4	54.7	55.2
b) prismatic	41.1	41.8	40.5	44.1	46.2	46.5	43.8	43.8	44.3
Tensile Strength, MPa:									
a) at bending	4.4	4.5	4.3	4.7	4.8	4.8	4.6	4.6	4.7
b) axial	4.1	4.2	4.1	4.4	4.5	4.5	4.3	4.3	4.4
Limit deformations under axial compression, mm/m*10^{-3}	2.01	2.03	2.10	1.89	1.65	1.61	1.97	1.96	1.88
Limit deformations under axial tension, mm/m*10^{-4}	1.17	1.17	1.20	1.14	1.13	1.15	1.16	1.15	1.14
Elastic modulus, MPa	26.8	26.5	25.5	29.2	29.8	29.8	28.8	29.1	29.3

Table 2. Results of experimental studies of the influence of the height of technological projections of clamps and their length on the integral characteristics of concrete.

Concrete characteristics	Height of technological projections of clamps, mm								
	2.5			5			10		
	Length of technological projections of clamps, mm								
	15	20	30	15	20	30	15	20	30
Density, kg/m^3	2328	2338	2311	2391	2412	2397	2365	2381	2363
Compression Strength, MPa:									
a) cube	49.9	50.9	48.9	52.2	56.8	55.7	52.9	54.7	52.6
b) prismatic	41.1	41.8	40.2	44.3	46.2	44.4	41.7	43.8	42.2
Tensile Strength, MPa:									
a) at bending	4.4	4.5	4.4	4.7	4.8	4.7	4.6	4.6	4.6
b) axial	4.1	4.2	4.1	4.4	4.5	4.5	4.2	4.3	4.2
Limit deformations under axial compression, mm/m*10^{-3}	2.12	2.03	2.11	1.88	1.65	1.81	1.97	1.96	1.96
Limit deformations under axial tension, mm/m*10^{-4}	1.17	1.17	1.22	1.14	1.13	1.14	1.16	1.16	1.15
Elastic modulus, MPa	26.8	26.5	25.4	29.3	29.7	29.4	28.3	29.1	28.7

Table 3. Results of experimental studies of the influence of the height of technological projections of clamps and the vibration mode on the integral characteristics of concrete.

Concrete characteristics	Height of technological projections of clamps, mm								
	2.5			5			10		
	Vibration mode								
	Synchronous	Alternating	Asynchronous	Synchronous	Alternating	Asynchronous	Synchronous	Alternating	Asynchronous
Density, kg/m^3	2314	2338	2300	2390	2412	2381	2368	2381	2360
Compression Strength, MPa:									
a) cube	48.9	50.9	48.8	55.1	56.8	54.7	52.9	54.7	52.5
b) prismatic	40.7	41.8	40.0	44.1	46.2	43.8	42.1	43.8	41.3
Tensile Strength, MPa:									
a) at bending	4.4	4.5	4.4	4.7	4.8	4.6	4.6	4.6	4.6
b) axial	4.1	4.2	4.1	4.4	4.5	4.4	4.3	4.3	4.2
Limit deformations under axial compression, mm/m*10^{-3}	2.11	2.03	2.12	1.89	1.65	1.96	1.97	1.96	2.01
Limit deformations under axial tension, mm/m*10^{-4}	1.21	1.17	1.22	1.14	1.13	1.16	1.15	1.16	1.17
Elastic modulus, MPa	25.6	26.5	25.1	29.2	29.7	29.1	28.7	29.1	28.2
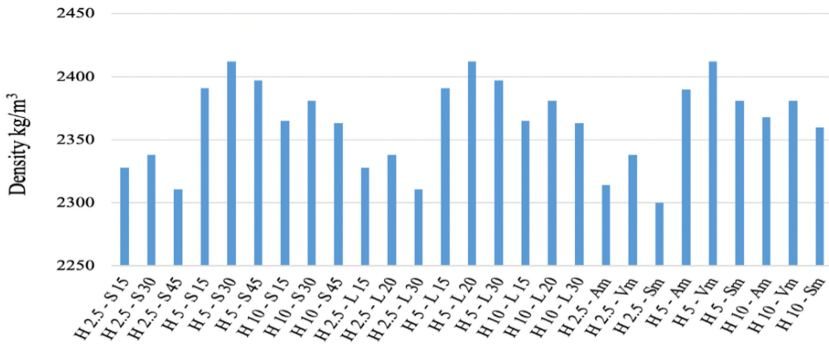
Fig. 1. Dependence of vibrocentrifugal concrete density on the technological parameters of vibration.
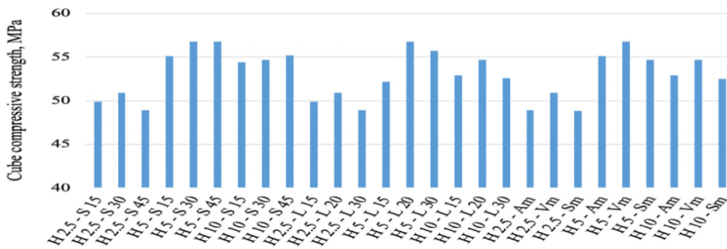
Fig. 2. Dependence of the cube compressive strength of vibrocentrifugal concrete on the technological parameters of vibration.
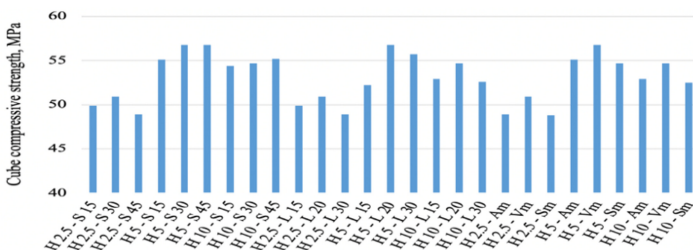
Fig. 3. Dependence of the prismatic axial compressive strength of vibrocentrifugated concrete on the technological parameters of vibration.
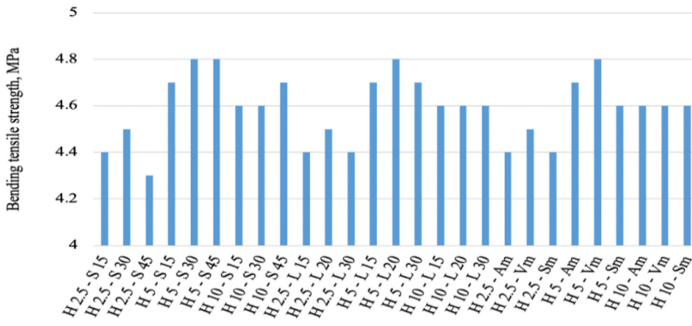
Fig. 4. Dependence of the bending tensile strength of vibrocentrifugal concrete on the technological parameters of vibration.
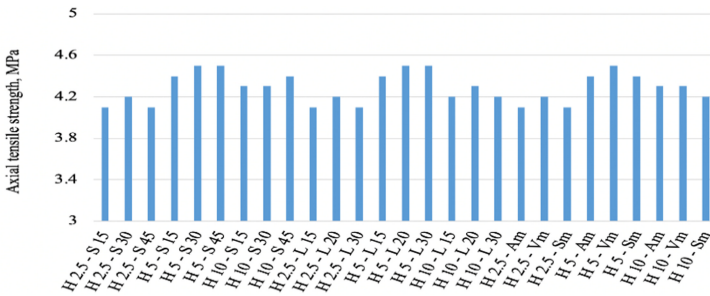
Fig. 5. Dependence of the axial tensile strength of vibrocentrifugated concrete on the technological parameters of vibration.
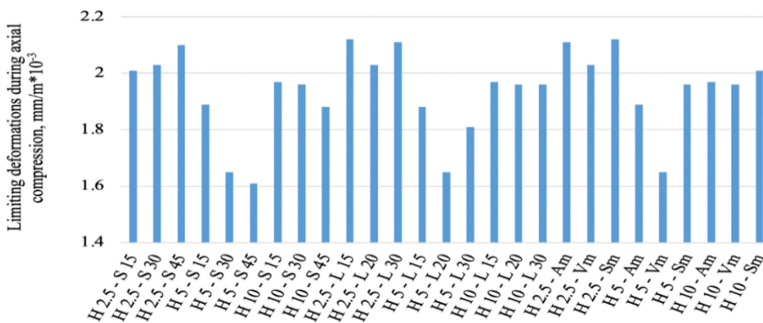
Fig. 6. Dependence of the limiting deformations under axial compression of vibrocentrifugal concrete on the technological parameters of vibration.
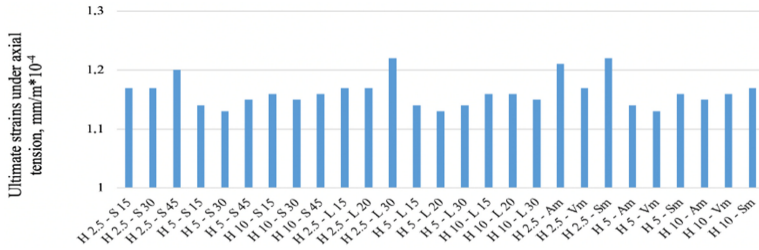
Fig. 7. Dependence of ultimate strains at axial tension of vibrocentrifugated concrete on technological parameters of vibration.
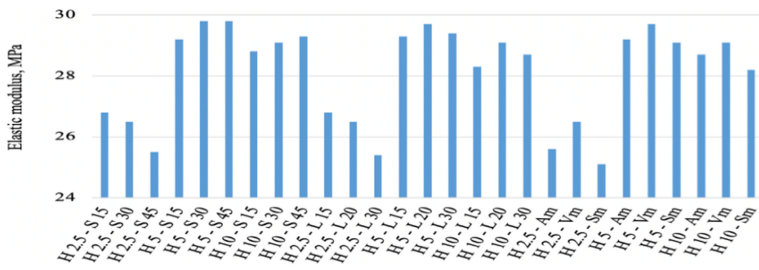
Fig. 8. Dependence of limiting deformations at axial tension of vibrocentrifugated concrete on technological parameters of vibration.

In all figures: H – height of technological projections of clamps, mm; S – step between technological projections of clamps, mm; L – length of technological projections of clamps, mm; Am – asynchronous vibration mode; Vm – alternating vibration mode; Sm – synchronous vibration mode.

As it can be seen in Fig. 1 the maximum density values of vibrocentrifugated concrete are achieved in three cases: 1) clamps with a height of 5 mm and a step between them of 30 mm were used; 2) clamps with a height of 5 mm and a length of 20 mm were used. 3) when using clamps with a height of 5 mm projections and alternating vibration mode.

In Fig. 2, the cubic compressive strength reaches its maximum values in four cases: 1) clamps with projections 5 mm high and 30 mm wide were used; 2) the height remained the same, the step between the projections was 45 mm; 3) when using clamps with projections 5 mm high and 20 mm long; 4) clamps with projections 5 mm high were used, and the vibration mode was alternating.

Figure 3 shows that the maximum values of prismatic compressive strength are achieved in three cases: 1) clamps with a projection height of 5 mm and a step of 45 mm were used; 2) clamps with a projection height of 5 mm and a length of 20 mm were used; 3) clamps with a projection height of 5 mm were used in alternating vibration mode.

Analysis of Fig. 4 showed that the maximum values of the bending tensile strength are fixed in four cases: the combination of technological parameters of vibration is similar to that described in Fig. 2.

Figure 5 shows that maximum values of strength in axial tension is observed in five cases: the first and second cases, the height of the projections of the clamps is 5 mm, the step between projections in the first case is 30 mm, the second is 45 mm; the third and fourth cases – the height of the projections is 5 mm, the length of the projections in the first case is 15 mm and the second 30 mm; the fifth case is the height of the projections is 5 mm, and the mode of vibration is alternating.

Figure 6 shows that the highest values of limit deformations under axial compression are observed in three cases. In the first case, clamps with a height of 2.5 mm and a step of 45 mm were used. In the second case, projections with a height of 2.5 mm and a length of 30 mm were used. In the third case we used the height of the projections 2.5 mm and synchronous mode of vibration.

The highest values of the maximum deformations under axial tension (Fig. 7) were also recorded in three cases: in the first case, clamps with a height of 2.5 mm and a step of 45 mm were used, in the second case, projections with a height of 2.5 mm and a length of 30 mm were used, and in the third case, clamps with projections with a height of 2.5 mm

In Fig. 8 the maximum value of the modulus of elasticity was recorded in four cases: the first and second cases, the height of projections of the clamps is 5 mm, the step between projections in the first case is 30 mm, the second is 45 mm; the third case is the height of the projections is 5 mm and length 20 mm; a fourth case – the height of the projections is 5 mm, and the mode of vibration is alternating.

4   Conclusion

The most effective will be the use of clamps with a height of technological projections 5 mm, a length of 20 mm, and a step between them of 30 mm, as well as alternating vibration mode. When these technological parameters of vibration are combined, vibrocentrifugated concretes have the best values of integral characteristics.

References

1. Akhverdov, I.N.: Reinforced concrete centrifuged pressure pipes. Moscow, Stroyizdat, 164 (1969)
2. Ovsyankin, V.I.: Reinforced concrete pipes for pressure water conduits (3rd edition). Moscow, Stroyizdat, 320 (1971)
3. Volkov, L.A.: Design, research and determination of the parameters of equipment for the manufacture of reinforced concrete pipes by centrifugation. Dissertation of the candidate of technical sciences. Moscow, 173 (1999)
4. Dubinina, V.G.: Development of optimal parameters for centrifugation of reinforced concrete gravity pipes. Dissertation of the candidate of technical sciences. Nizhny Tagil, 150 (2002)

5. Geiker, M.R., Michel, A., Stang, H., Lepech, M.D.: Limit states for sustainable reinforced concrete structures. Cement Concr. Res. **122**, 189–195 (2019)
6. Li, K., Li, L.: Crack-altered durability properties and performance of structural concretes. Cement Concr. Res. **124**, 105811 (2019). https://doi.org/10.1016/j.cemconres.2019.105811
7. Ferrotto, M.F., Fischer, O., Cavaleri, L.: Analysis-oriented stress–strain model of CRFP-confined circular concrete columns with applied preload. Mater. Struct. **51**, 44 (2018). https://doi.org/10.1617/s11527-018-1169-0
8. Bourchy, A., Barnes, L., Bessette, L., Chalencon, F., Joron, A., Torrenti, J.M.: Optimization of concrete mix design to account for strength and hydration heat in massive concrete structures. Cement Concr. Compos. **103**, 233–241 (2019)
9. Lu, W.-Y., Chu, C.-H.: Tests of high-strength concrete deep beams. Mag. Concr. Res. **71**(4), 184–194 (2019)
10. Alani, A.H., Bunnori, N.M., Noaman, A.T., Majid, T.A.: Durability performance of a novel ultra-high-performance PET green concrete (UHPPGC). Constr. Build. Mater. **209**, 395–405 (2019)
11. Mailyan, L., Yaziev, S., Sabitov, L., Konoplev, Y., Radaykin, O.: Stress-strain state of the "combined tower-reinforced concrete foundation-foundation soil" system for high-rise structures. In: E3S Web of Conferences, vol. 164, p. 02035 (2020). https://doi.org/10.1051/e3sconf/202016402035
12. Stel'makh, S.A., Shcherban', E.M., Kholodnyak, M.G.: Analysis of concrete deformation diagram, received by different ways of formation, and their separate layers. In: IOP Conference Series Materials Science and Engineering, vol. 687, p. 022008 (2019). https://doi.org/10.1088/1757-899X/687/2/022008
13. Stel'makh, S.A., Shcherban, E.M., Sysoev, A.K.: Influence of type of filler and dispersive reinforcement on the nature of structured formation and deformative properties of vibrocentrifuged concrete. In: IOP Conference Series Materials Science and Engineering, vol. 753, p. 022014 (2020). https://doi.org/10.1088/1757-899X/753/2/022014
14. Shcherban', E.M., Stel'makh, S.A., Prokopov, A.Y.: Features of change in strength and modulus of elasticity of various layers of vibrocentrifuged fiber-reinforced concrete columns of annular section. In: IOP Conference Series Materials Science and Engineering, vol. 687, p. 022009 (2019). https://doi.org/10.1088/1757-899X/687/2/022009

Analysis of the Methods of the Connection Calculation

O. S. Chernyavskiy[(✉)] and D. E. Pashkov

Belgorod State Technological University, Belgorod, Russia
`olegik-go@ya.ru`

Abstract. In the present research work the compression analysis of the method of calculating joint connections made of roll-welded profiles, specified in the "Guide on structural steel design (for Construction Standards and Regulations II-23-81*)" (hereafter - SNiP), was performed. According to item 15.16. of the guide [1], two types of joints, F and F_r, were chosen as the study object. During the research several combinations of the construction of such joint types were accepted and modelled with the help of the software solution IDEA StatiCa which does calculations based on the component-based finite element method (hereafter - CBFEM). The obtained results from the software solution were checked against the results calculated by the procedure described in the guide. It was established that during the compression calculation of the connections, the load-carrying capacity of the joint is reduced by the receiving gusset, which is disregarded in SNiP. The research was conducted with the help of the CBFEM used by the software solution IDEA StatiCa.

Keywords: Building · Construction · IDEA StatiCa · BIM · Modern technologies · Snip calculation procedure specification

1 Introduction

According to the calculation procedure described in the "Guide on structural steel design (for SNiP II-23-81*)", the joint connections made of roll-welded profiles are tested for:

a) the strength and stability of the joint elements and of the profile area adjacent to the joint;

б) the strength of the welded connections.

For the chosen joint types (F and F_r) regarded as study objects, the load-carrying capacity for compression is calculated by formula 104:

$$\frac{N}{A_{fc}} + \frac{N_{e1}}{W_{fc}} = R_{yd}$$

A different calculation method was adopted by the component based on the component-based finite element method (hereinafter CBFEM). CBFEM is aimed at the most accurate approximation of the model to reality, and its advantage is the calculation of internal forces and stresses in the elements of the node. The finite element meshes generated by the program are not related to each other in any way; they are created separately for each element of the model. Equivalent stresses and plastic deformations are calculated
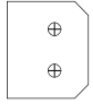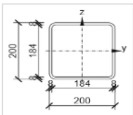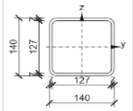
in each plate. Upon reaching the yield point, the plates are checked for equivalent plastic deformation. This unique design model provides accurate member stress results.

In the course of the study, it was found that the calculation method specified in the manual for SNiP does not take into account the rigidity of the receiving rib of the connection, which in turn significantly reduces the bearing capacity of the unit as a whole.

2   Methods and Materials

The study object in the present work is several types of joint connections made of roll-welded profiles for the compression strength. Conditionally, the research can be divided in 3 stages during which the joint was gradually strengthened and the applied

Table 1. Elements specification.

Name	Total dimensions [mm]	Form	Stage No.	Note
PL1	8.0 x 180.0 - 120.0 (S255)		1,2,3	Receiving gusset of the joint.
PL2	8.0 x 160.0 - 160.0 (S255)		1,2,3	Connection flange
PL3	8.0 x 120.0 - 140.0 (S255)		1,2,3	Connection gusset
PL4 (2 pcs)	8.0 x 160.0 - 120.0 (S255)		3	Strengthening plates of the receiving gusset
PL5	10.0 x 120.0 - 62.0 (S255)		2, 3	Strengthening rib of the connection gusset
PL6	8.0 x 120.0 - 70.0 (S255)		3	Strengthening rib of the receiving gusset
K	RWP 200 x 8 (S255)		1, 2, 3	Support element
B	RWP 140 x 6.5 (S255)		1, 2, 3	Connection bar

loads were increased as well. The steel grade, the electrode material and the weld legs were unified and are S255, E50 and 7 mm respectively. The bolts are 16 mm, grade 8.8. The bolt and weld checks are to be considered successful. Table 1 presents the elements specification. The elements of the constructions were calculated by the procedure described in the guide [1]. The obtained results were checked against the results received in the software solution IDEA StatiCa. These studies are presented in Tables 2, 3 and 4.

3   Results and Discussion

Table 2. Results.

Calculation method	Applied load N, kN	Obtained results at the joint elements, kN	
		PL$_1$	PL$_3$
IDEA	40	23.91	23.95
SNiP	40	25	–
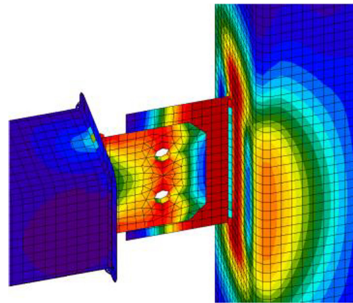
Fig. 1. Equivalent stresses.

At the first stage, the joint connection without the strengthening elements was examined. The compression strength of 40 kN was applied to the joint, the results of the calculations are summarized in Table 2. As follows from the results, the connection gusset (hereafter - PL1) calculated by SNiP has an insufficient load-carrying capacity which leads to the spread of plastic deformations and to the loss of stability. The results of the CBFEM (Fig. 1) show that the element PL1 experiences the identical stresses but within the norm. The receiving rib (hereafter - PL2) is exposed to even higher stresses in the area of its junction with the support element and eventually experiences plastic deformations. Such joint will lose its stability due to PL2. To increase the load-carrying capacity, the SNiP guide recommends to add the stiffness rib PL5 onto the PL1

element. According to the calculations, it must increase the load-carrying capacity of the joint multi-fold (Fig. 2).

Table 3. Results.

Calculation method	Applied load N, kN	Obtained results at the joint elements, kN	
		PL$_1$	PL$_3$
IDEA	40	17.96	24,03
	110	24.89	27.23
SNiP	40	7.93	–
	110	23.79	–

Several tests with different compression strengths were performed. In Fig. 3 the stiffness rib PL5 was added.
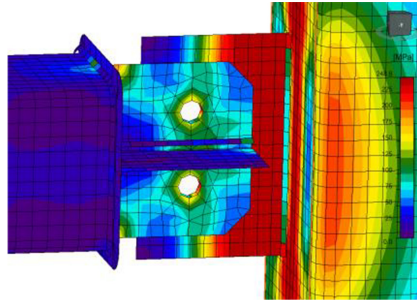
Fig. 2. Equivalent stresses at N = 40 kN.
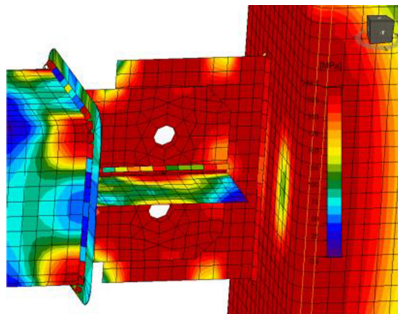
Fig. 3. Equivalent stresses at N = 110 kN.

According to the SNiP calculations, this joint carries the load of 40 kN. The maximum load which the joint carries by the SNiP calculation is 110 kN. If the load of 110 kN is applied (see Fig. 4), the joint loses its stability and experiences large plastic deformations.

Table 4. Results.

Calculation method	Applied load N, kN	Obtained results at the joint elements, kN	
		P_1	P_3
IDEA	40	16.35	13.19
	110	24.09	24
SNiP	40	7.93	–
	110	23.79	–

To compensate the plastic deformations, the receiving joint is strengthened in the next stage while the load remains similar to that in stage 2, i.e. 110 kN (Fig. 5).
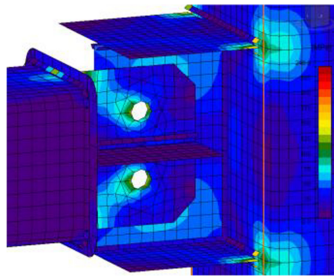
Fig. 4. Equivalent stresses at N = 40 kN.
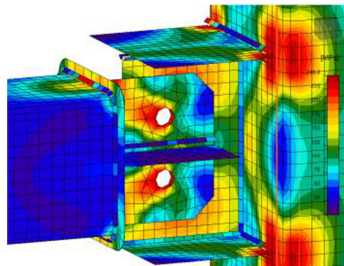
Fig. 5. Equivalent stresses at N = 110 kN.

The receiving rib was strengthened, two strengthening plates PL4 were added on the top and on the bottom, the complementary stiffness rib PL6 was added as well. At 40 kN the joint does not experience large stresses, at 110 kN the plastic deformations and the loss of stability of the receiving rib do not appear.

4   Conclusion

Based on the above-mentioned experiments, it is possible to make the following conclusions:

1. The receiving rib of the joint considerably reduces the load-carrying capacity of the joint, as it has lower stiffness.
2. The connection strengthening rib (PL5) increases the load-carrying capacity of the joint only if the receiving rib stiffness is higher than or equal to that of the connection gusset. Therefore, it is possible to obtain the strength gain of 275%.
3. If the joint strength of any connection construction is insufficient, it makes no sense to strengthen this connection without the preliminary increase of the receiving rib stiffness.
4. Along with the calculation by the guide, it is also necessary to do the strength and stability calculations for the receiving rib of the joint connection.

References

1. Le, T.T., Austin, S.A., Lim, S., Buswell, R.A., Law, R., Gibb, A.G.F., Thorpe, T.: Hardened properties of high-performance printing concrete. Cement Concr. Res. **42**(3), 558–566 (2012)
2. Belov, V.A.: Modeling and calculation of metal structures of buildings and structures. MGSU, 160 (2012)
3. Haginski, G.M.: Deformation and long-term strength of metals/scientific world, 136 (2008)
4. Tumanov, A.V.: Reinforced concrete and metal structures. Infa-engineering, Vologda, 141 (2016)
5. Semenov, A.A.: Metal structures. Calculation of elements and connections using SCAD Office. ACB, Moscow, 338 (2012)
6. Moskalev, N.S.: Metal structures. ACB, Moscow, 344 (2010)
7. Karpanina, E.N.: Metal structure. Rusines, Moscow, 160 (2017)
8. Wald, F., Sabatka, L., Jehlicka, B.P., Kabelac, J., Kozich, M., Kutikova, M., Vild, M.: Component-based finite element design of steel connections/CTU, 245 (2014)
9. Wald, F.: Journal Heron 1/2: component method for steel column bases/Heron, 3–19 (2008)
10. Grudev, I.D.: Bearing capacity of compressed members of bar structures/MGSU, 387 (2012)
11. Lebed, E.V.: Computer technologies in design of spatial metal frames of builings/MGSU, 141 (2017)
12. Jaspart, J.P., Wald, F.: Steel column base classification/Heron. J. Heron **1**(2), 69–86 (2008)

Research of Fiberglass Polymer Concrete Switch Bars on Endurance Under Cyclic Loading

B. A. Bondarev[1] , A. A. Kosta[2(✉)] , and A. Y. Sychev[1]

[1] Lipetsk State Technical University, Lipetsk, Russia
[2] Moscow State University of Civil Engineering (National Research University),
Moscow, Russia
`KostaAA@mgsu.ru`

Abstract. The purpose of this work is to identify to assess comprehensively the strength and endurance of fiberglass polymer concrete (FPC) elements at bending. To research the degree of influence of the reinforcement coefficient and controlled loading on the value of the destructive bending moment of fiberglass polymer concrete, the method of planning an experiment with the construction of an orthogonal central composite plan of the second order was used. It is proved that the percentage of reinforcement of prestressed beams and the degree of controlled stress significantly affect the load-bearing capacity of bars, the second factor is the most significant. The change in deformations along the height of the cross-section of beams confirms the acceptability of the flat cross-section hypothesis for fiberglass polymer concrete bending elements. It was found that the neutral axis gradually rises with increasing reinforcement coefficient and the degree of controlled stress, reducing the value of the relative compressed zone of polymer concrete. The nature of the destruction is basically the same, the destruction occurred in the compressed zone of polymer concrete in the area of pure bending. The values of the ultimate endurance for fiberglass polymer concrete elements are obtained for the cycle asymmetry coefficient $\rho = 0.3$ and for different degrees of pre-stress of fiberglass reinforcement. A theoretical analysis of the resistance of fiberglass polymer concrete elements to cyclic loads using a structural diagram is presented. The results of experiments and obtained theoretical dependences are compared.

Keywords: Fiberglass reinforcement · Fiberglass polymer concrete · Furfural-acetone monomer · Polymer composite material · Ultimate endurance · Pre-stress

1 Introduction

Along with conducting experiments to increase the service life of reinforced concrete elements, research is being conducted on more durable and cost-effective materials that can replace reinforced concrete in the structures of switch bars [1]. One of these materials is polymer concrete reinforced with fiberglass reinforcement (hereinafter referred to as FR) [2].

In this regard, the purpose of the research is to identify and assess comprehensively the strength and endurance of fiberglass polymer concrete (FPC) elements at bending.

2   Methods and Materials

It was made 18 beams for tests with repeatedly applied load, differing in the degree of pre-stress, reinforced with two FR rods with a diameter of 6 mm with μ = 1.77%.For the G series, the value of the controlled voltage was 413.4 MPa. The loading level varied from 8.5 kN to 5.8 kN. The largest number of cycles before failure was passed by the BN 3–6 beam – 2.21 * 106 cycles, and the smallest is the BN-3–1 beam – 158600 cycles. The results of the experiment are shown in Table 1. The equation of the empirical endurance line is "Eq. (1)":

$$M_N = 3.094 - 0.351 lgN. \tag{1}$$

Based on 2 * 106 cycles MN = 0.88 kN * m or MN = 0.43 MP. The growth of beam deflections was directly dependent on the number of load application cycles, and for the BN-3–6 beam, the elastic deflection value was:

at N = 2.0 * 105 cycles – f = 5.1 mm;

at N = 1 * 106 cycles – f = 5.2 mm;

at N = 2 * 106 cycles – f = 5.7 mm.

At 2 * 106 cycles, the process of deflection growth stabilized and by the end of the tests on the basis of 2.2 * 106 cycles was 5.8 mm. The destruction of this series of beams occurred due to fatigue of polymer concrete in the compressed zone. The results of processing the experiment are shown in Table 1:

Table 1. Results of processing experimental data on the research of the endurance of FR-reinforced beams, with μ = 1.77%, P = 413.4 MPa, ρ = 0.3.

№ of beam	Breaking~bending moment M_{br} (kN * m)	Deviation from the average value M_p	Square deviation	Number of cycles to failure N	lgN	Deviation from the average value	Square deviation	Product of the deviations
BN-3-1	1.24	0.235	0.0552	158600	5.200	−0.749	0.561	−0.176
BN-3-3	1.14	0.135	0.0182	491740	5.691	−0.258	0.0665	−0.0348
BN-3-4	1.00	−0.005	2.5 * 10−4	920630	5.964	+0.015	0.000225	−0.000075
BN-3-5	0.95	−0.055	0.003025	1620700	6.209	+0.260	0.0676	−0.0143
BN-3-2	0.85	0.155	0.0240	1950510	6.290	+0.341	0.1163	−0.0529
BN-3-6	0.85	−0.155	0.0240	2217101	6.345	+0.396	0.1568	−0.0614
	M_{br}^{av} = 1.005		Σ = 0.125		lg_p^{av} = 5.949		Σ = 0.968	Σ = −0.339

The second group of beams (series D) differed in the degree of pre-stress and was 551.2 MPa. Six beams were tested. The largest number of cycles before the failure passed the beam BN-3–12 2.8 * 106 cycles, and the smallest is the beam BN-3–7 – 80100 cycles. The results of the experiment were processed according to the above

method. Correlation coefficient r = −0.96. The equation of the empirical endurance line is "Eq. (2)":

$$M_N = 3.052 - 0.322 lgN. \tag{2}$$

Based on 2 * 106 cycles MN = 1.023 kN * m or 0.50 M_p. The growth of the deflection value for beams of this series can be traced using the example of the BN-3–12 beam:

at N = 2.0 * 105 cycles – f = 5.6 mm;
at N = 106 cycles – f = 5.7 mm;
at N = 1.5 * 106 cycles – f = 5.8 mm;
at N = 2 * 106 cycles – f = 5.2 mm.

The destruction of the beam occurred due to the destruction of the compressed zone of polymer concrete. The results of the experiment are shown in Table 2.

Table 2. Results of processing experimental data on the research of the endurance of FR-reinforced beams with μ = 1.77%, P = 551.2 MPa, ρ = 0,3.

№ of beam	Breaking~bending moment M_{br} (kN * m)	Deviation from the average value M_p	Square deviation	Number of cycles to failure N	lgN	Deviation from the average value	Square deviation	Product of the deviations
BN-3-7	1.45	0.284	0.0806	80100	4.903	−0.938	0.879	−0.266
BN-3-8	1.3	0.134	0.0179	300120	5.477	−0.364	0.132	−0.0487
BN-3-9	1.2	0.034	0.00116	850810	5.929	0.088	0.0077	−0.00299
BN-3-10	1.1	−0.066	0.00436	920900	5.964	0.123	0.0151	−0.00811
BN-3-11	1.0	−0.166	0.0276	2120400	6.326	0.485	0.235	−0.0805
BN-3-12	0.95	−0.216	0.0466	2800120	6.447	0.606	0.367	−0.1308
	M_{br}^{av} = 1.166		Σ = 0.1782		lg_p^{av} = 5.841		Σ = 1.636	Σ = −0.537

For the "E" series beams, the degree of pre-stress was 0.5 RS or 689 MPa. Six beams were tested. The largest number of load cycles sustained BN-3-18 beam 2.45 * 106 cycles, and the least passed before the destruction of the BN-3–13 beam 125900 cycles (see Table 3 for experimental results). Equation of the empirical endurance line for beams is the "Eq. (3)":

$$M_N = 3.266 - 0.351 \, lgN. \tag{3}$$

Based on 2 * 106 cycles MN = 1.05 kN * m or 0.52 Mp. The elastic deflection value for the BN-3–18 beam was changed as follows:

at N = 2.0 * 105 cycles – f = 5.2 mm;
at N = 106 cycles – f = 5.6 mm;
at N = 2 * 106 cycles – f = 5.8 mm.

Table 3. Results of processing experimental data on the research of the endurance of FR-reinforced beams with $\mu = 1.77\%$, P = 689.0 MPa, $\rho = 0.3$.

№ of beam	Breaking~bending moment M_{br} (kN * m)	Deviation from the average value M_p	Square deviation	Number of cycles to failure N	lgN	Deviation from the average value	Square deviation	Product of the deviations
BN-3-13	1.65	0.366	0.134	125900	5.100	−0.709	0.503	−2.259
BN-3-14	1.45	0.167	0.0279	280690	5.448	−0.361	0.130	−0.0603
BN-3-15	1.30	−0.017	0.000289	431610	5.635	−0.174	0.0302	−0.00298
BN-3-16	1.20	−0.083	0.006890	920500	5.964	0.155	0.0240	−0.01290
BN-3-17	1.10	−0.183	0.0335	2101100	6.322	0.513	0.263	−0.0938
BN-3-18	1.0	−0.283	0.0801	2450500	6.389	0.58	0.3364	−0.164
	M_{br}^{av} = 1.283		Σ = 0.283		lg_p^{av} = 5809		Σ = 1.287	Σ = −0.593

3   Results and Discussion

The structural diagram of polymer concrete is shown in Fig. 1a. The structural diagram of fiberglass polymer concrete is shown in Fig. 1b.
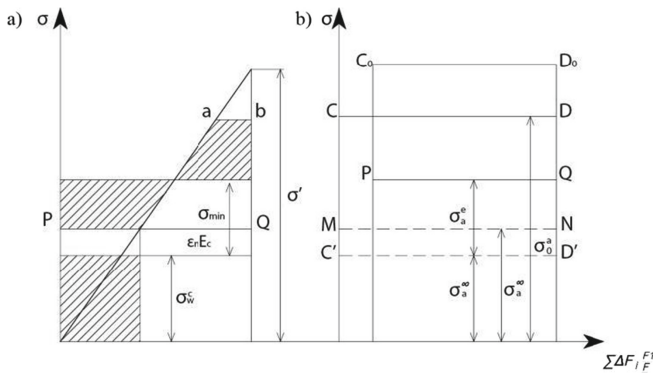
Fig. 1. Structural diagrams: polymer concrete (a); fiberglass reinforcement (b).

N.K. Artyukhovsky [3] proposed an equation for determining the final values of stresses in pre-stressed fiberglass polymer concrete elements "Eq. (4)":

$$\sigma_a^\infty = \frac{-\sigma'(1-m)[1+\mu n(1-m)] + \sigma_0^a(1-m)}{(1+\mu n)\sqrt{n^2\sigma'^2\left(1+\mu n(1-m) - \frac{2\sigma'\sigma_0^a(n+\mu n^2(1-m)-1)}{1+\mu n}\right)}},$$

where σ' – coefficient that characterizes the structural diagram of polymer concrete;
m – percentage of the viscous phase in the total cross-section of the reinforcement;
$\mu = \frac{F_a}{F_c}$ – coefficient of polymer concrete reinforcement;
$n = \frac{F_a}{F_c}$ – coefficient of reduction of FR to polymer concrete;
σ_0^a – the initial stress in the reinforcement.

To simplify formula 4, we assume that $\mu n = \alpha(1 - m) = \beta$, then "Eqs. (5), (6)" will have the form:

$$\sigma_a^\infty = -\sigma'\beta[1 + \alpha\beta] + \sigma_0^a\alpha\beta\sqrt{n^2\sigma'^2\left(1 + \alpha\beta - \frac{2\sigma'\sigma_0^a(n + \alpha n(\beta - 1))}{1 + \alpha}\right)}. \quad (5)$$

The value of pre-stress losses in the reinforcement is:

$$\sigma_a = \sigma_0^a - \sigma'n\beta[1 + \alpha\beta] - \sigma_0^a(1 - \alpha) - \beta\sqrt{n^2\sigma'^2(1 + \alpha\beta) - \frac{2\sigma'\sigma_0^a(n + \alpha n(\beta - 1))}{1 + \alpha}}. \quad (6)$$

Formulas 5 and 6 are valid for $\sigma_c^e \leq \sigma_R^c$ and $\sigma_a^e < \sigma_{DC}^a$, where σ_c^e is the stress in the elastic frame of polymer concrete; σ_R^c is the ultimate strength of polymer concrete; σ_a^e is the limit of long-term resistance of reinforcement; σ_{DC}^a is the stress in the elastic frame of reinforcement.

The value of the material endurance limit depends on the cycle characteristic (ρ) and therefore, if the pulsating load changes from 0 to P_{max}, the stress in the material will also change from 0 to σ_{max}. In the presence of pre-stress, the limits of stress change in the material will already be different, namely from σ_a^∞ to some new value σ'_{max}, and the coefficient of cycle asymmetry will be equal to ("Eq. (7)"):

$$\rho = \frac{\sigma_a^\infty}{\sigma'_{max}}. \quad (7)$$

Under the action of a pulsating load at time (t), the stresses in the polymer concrete and FR will form ("Eq. (8)"):

$$\{\sigma_c(t) = \sigma_{min} - \varepsilon_n E_c; \sigma_a(t) = \sigma_a^\infty - \varepsilon_n E_a, \quad (8)$$

which corresponds to the lines PQ and MN in Fig. 1, and ε_n is the relative shortening of the element associated with deformations of elastic frames. However, this process may not continue indefinitely, but only until the stresses in polymer concrete and FR exceed the endurance limits in polymer concrete and FR, respectively ("Eq. (9)"), i.e.

$$\sigma_c(t) \leq \sigma_w^c \text{ и } \sigma_a(t) \leq \sigma_w^a, \quad (9)$$

where σ_w^c and σ_w^a – maximum stresses corresponding to the endurance limits of polymer concrete and FR.

Then the Eq. (8) can be rewritten as follows ("Eq. (10)"):

$$\{\sigma_w^c \leq \sigma_{min} - \varepsilon_n E_c; \sigma_w^a \leq \sigma_a^\infty - \varepsilon_n E_a, \quad (10)$$

where "Eq. (11)" comes

$$\varepsilon_n = \frac{\sigma_{min} - \sigma_w^c}{E_c} = \frac{\sigma_w^a - \sigma_a^\infty}{E_a}. \tag{11}$$

When redistributing forces from polymer concrete to reinforcement

$$\sigma_c(t)F_c = \sigma(t)F_a \ \ \text{or} \ \ \sigma_c(t) = \sigma(t)\mu$$

but taking into account (9), "Eq. (12)" will have the form

$$\sigma_w^c = \sigma_w^a \mu. \tag{12}$$

Equation (12) is a condition for safe operation of the structure; substituting (12) in (11), we get "Eq. (13)":

$$\frac{\sigma_w^a - \sigma_a^\infty}{E_a} = \frac{\sigma_{min} - \sigma_w^c \mu}{E_c}; \tag{13}$$

from (13) we find the "Eq. (14)":

$$\sigma_w^a = \frac{\sigma_{min} E_a + \sigma_a^\infty E_c}{(E_c + E_a)\mu}. \tag{14}$$

But σ_{min} in Eq. (14) is nothing more than the greatest possible stress in polymer concrete, when the amplitude ("Eq. (15)"):

$$\sigma_a = \sigma_{max} - \sigma_{min}. \tag{15}$$

The value σ_{min} is found from the equation ("Eq. (16)"):

$$\sigma_{min} = \frac{1}{2\sigma_R} \left[\frac{\sigma_R}{2} + \sqrt{\frac{\sigma_R^2}{4} - \sigma_R \sigma_a} \right], \tag{16}$$

where σ_R – compressive strength of polymer concrete; σ_a – the amplitude of the stresses.

Substituting (15) in (16), we get the equation of the Goodman diagram as applied to plastics ("Eq. (17)"):

$$\sigma_{max} = \sqrt{2\sigma_R \sigma_{min}} - \sigma_{min}; \tag{17}$$

replacing the equation σ_{min} with $\sigma_{min} = \sigma_{max}\rho$ we finally have ("Eq. (18)"):

$$\sigma_{max} = \frac{2\sigma_R \rho}{(1 + \rho)^2}; \tag{18}$$

substituting σ_{min} in (14) and remembering that $\sigma_{min} = \sigma_{max}\rho$, we get the "Eq. (19)":

$$\sigma_w^a = \frac{2\sigma_R\rho^2 E_a + \sigma_a^\infty (1+\rho)^2 E_c}{(E_c + E_a)(1+\rho)^2}, \tag{19}$$

but $\sigma_w^c = \sigma_w^a \mu$, then the "Eq. (20)" is:

$$\sigma_w^c = \frac{2\sigma_R\rho^2 E_a + \sigma_a^\infty (1+\rho)^2 E_c}{\mu(E_c + E_a)(1+\rho)^2}; \tag{20}$$

for fiberglass polymer concrete of the accepted composition, the Eq. (20) is written as follows ("Eq. (21)"):

$$\sigma_w^c = \frac{1,63\sigma_R\rho^2 E_a + \sigma_a^\infty (1+\rho)^2 E_c}{\mu(E_c + E_a)(1+\rho)^2}. \tag{21}$$

The results of the experiment and the values of the endurance limits of fiberglass polymer concrete obtained by formulas (19) and (21) coincide satisfactorily.

4   Conclusion

The values of the ultimate endurance for fiberglass polymer-concrete elements are obtained for the cycle asymmetry coefficient $\rho = 0.3$ and for different degrees of pre-stress of fiberglass reinforcement.

It is proved that the percentage of reinforcement of pre-stressed beams and the degree of controlled stress significantly affect the load-bearing capacity of beams, the second factor is the most significant.

A theoretical analysis of the resistance of FPC elements to cyclic loads using a structural diagram is presented. The experimental results and the obtained theoretical dependences correspond satisfactorily.
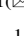
References

1. Borkov, P.V., Komarov, P.V., Bondarev, A.B., Bondarev, B.A.: Accelerated method for predicting the durability of polymer composite materials. Sci. Bull. VSTU. Constr. Archit. **3** (31), 46 (2013)
2. Bondarev, B.A., Bondarev, A.B., Saprykin, R., Korvyakov, F.I., Kharchevnikov, V.I.: Forecasting the cyclic durability of reinforced concrete bars made of wood-fiberglass composite materials. Constr. Mater. **7**(715), 78–81 (2014)
3. Artyukhovsky, N.K.: Accounting for pre-stress losses in the core fiberglass reinforcement of polymer concrete FAM from creep of materials. Reinforced polymer concrete in building structures: proceedings of VISI. Voronezh **17**(6), 73–78 (1971).

4. Bondarev, B.A., Borkov, P.V., Bondarev, A.B.: An outlook on the application of glass-reinforced plast and polymer concrete in bridge construction. In: 2nd International Conference on Industrial Engineering, ICIE 2016, Chelyabinsk, pp. 1617–1622 (2016)
5. Klyuev, S.V., Khezhev, T.A., Pukharenko, Y.V., Klyuev, A.V.: Experimental study of fiber-reinforced concrete structures. Mater. Sci. Forum **945**, 115–119 (2018)
6. Klyuev, S.V., Khezhev, T.A., Pukharenko, Y.V., Klyuev, A.V.: To the question of fiber reinforcement of concrete. Mater. Sci. Forum **945**, 25–29 (2018)
7. Khezhev, T.A., Pukharenko, Y.V., Khezhev, K.A., Klyuev, S.V.: Fiber gypsum concrete composites with using volcanic tuffsawing waste. ARPN J. Eng. Appl. Sci. **13**(8), 2935–2946 (2018)
8. Klyuev, S.V., Khezhev, T.A., Pukharenko, Y.V., Klyuev, A.V.: The fiber-reinforced concrete constructions experimental research. Mater. Sci. Forum **931**, 598–602 (2018)
9. Bondarev, B.A., Borkov, P.V., Bondarev, A.B.: An outlook on the application of glass-reinforced plastic and polymer concrete components in bridge. Procedia Eng. 1617–1622 (2016).

Tensile Deformations of "Mild" Reinforcing Steels for Reinforced Concrete Structures

O. M. Donchenko[1] , L. A. Suleymanova[1(✉)] , V. I. Rimshin[2] ,
and I. S. Ryabchevskiy[1]

[1] Belgorod State Technological University named after V.G. Shukhov,
Belgorod, Russia
`ludmilasuleimanova@yandex.ru`
[2] National Research Moscow State University of Civil Engineering,
Moscow, Russia

Abstract. Reinforced concrete structures are widely used in all areas of modern construction, which is explained by their durability, the possibility of using local building materials, low consumption of steel, and a variety of forms. The increasing requirements for ensuring the reliability of reinforced concrete structures makes it necessary to improve the calculation of bent elements. The main difficulty of the calculation is that "mild" steels, like all real structural materials, are deformed under force loading non-equilibrium and non-linear, while the desired physical relationship "stress – deformation" is usually reflected by analytical dependencies of high degrees (5 and higher). The authors consider the nature of the "stress – deformation" curves taking into account the heterogeneity of the physical properties of various steel components, the elastic limits on the tensile curve, the nature of steel deformation, the transition sections of the experimental tensile curves of reinforcing bars from the elastic limits and proportionality to the yield point determined by the results of experimental data from various devices, and the expression of the secant modulus of deformation of mild" steels is developed, which allows not only to calculate accurately reinforced concrete bending elements, but it also allows getting the elastic coefficients of individual sections of reinforcing steel when they are stretched.

Keywords: Reinforced concrete · Strength · Deformation · Steel · Constructions

1 Introduction

The most widely used group of hot-rolled reinforcing steels of low and medium strength is usually called mild, which display yield strength when stretched, in the manufacture of reinforced concrete structures. According to Russian standards [1], this group includes steel classes: A240, 400, 500, 600, 800 and 1000 with a relative elongation at break ε_{sten} from 6 to 25%. It should be noted that class A600 steel, considered "mild", has almost no obvious yield point and belongs to this group only due to the relatively high value of the relative deformation $\varepsilon_{sten} = 6.0\%$ at break, and class A800 and 1000 steels do not have a yield point at all.

Such a variety of decorative properties of these steels significantly complicates the development of a non-labor-intensive analytical deformation-tension relationship, i.e., $\varepsilon_s = \varphi(\sigma_s)$, which is common for all steels of this group. The complexity of solving this problem is explained by the fact that "mild" steels, like all real structural materials, deform under force loading non-equilibrium and non-linear. Their non-equilibrium is manifested in the fact that in addition to elastic-instantaneous deformations, inelastic deformations develop under loading, and the nonlinearity of deformation is explained by the absence of a proportional relationship between the tension σ_s and the deformations ε_s. All this leads them to the curvilinearity of deformation, reflected by the phenomenological equations of the mechanical state of materials.

As it is evidenced by the results of attempts by a number of researchers [2–7], the desired physical relationship is usually reflected by analytical dependencies of high degrees (5 and higher).

In the absence of such a physically valid analytical relationship, many researchers and standards [1] use the approximate linear dependence of $\varepsilon_s = \sigma_s/E_s$ to determine ε_s. This has been the case for a long time, until the non-linear deformation model was adopted as the main one in the standard methodology for calculating bent reinforced concrete elements. A two-line diagram of the state of a stretched armature also uses the above linear relationship, thereby allowing serious errors in the accuracy of the results obtained.

This is especially important for the calculation of bending elements on the strength of the normal sections, establishing the distribution of relative deformation of concrete ε_b and the ε_s reinforcement of the sections according to a linear law of plane cross-section hypothesis, because an incorrect value for the tensile reinforcement strain ε_s with its stress σ_s can lead to completely erroneous values of the deformations of compressed zone of concrete ε_b and the marginal computational effort M.

It is natural that for calculations based on a nonlinear deformation model, the presence of a correct analytical relation of $\varepsilon_s = \varphi(\sigma_s)$ is an urgent and very necessary task. To develop such an unconventional and fairly correct dependence, it is advisable to identify its main physical significant factors.

2 Methods and Materials

A deep analysis of the behavior of the "$\sigma_s - \varepsilon_s$" extension curve reveals a number of common features [2–4, 8–11]. From the consideration of this diagram of mild reinforcing steels, we can add the following:

1. The initial section of the curve diagram can be considered straight only at the required tension to the limit of proportionality $\sigma_{n.u}$ or $\sigma_{s.ol}$ from the conditions of deviation of more than 0.1%. This allows the approximation to take the entire initial section as a curve that asymptotically approaches the *arctg* E_s line, while maintaining the requirement that an arbitrary one at the initial point equals the standard modulus of deformation E_s.

2. The length of the yield point gradually decreases as the steel strength increases. Along with the horizontal position of the yield point, its gradual rise to 4…5% of the yield point σ_m is often observed, which is explained by an increase in its stress σ_s due to a decrease in the cross-section area of the neck.
3. If the yield strength is sufficient, the inclined straight line E_s immediately passes into the horizontal section of the yield site, that is, it leads to a break in the continuity of the analytical function, and is a conditional approximation. From a physical point of view, this is due to the polycrystalline structure of the wall, in which the simultaneous beginning of sliding in all crystals does not occur.

3   Results and Discussion

From the physical point of view, this is a consequence of the heterogeneity of the physical properties of various components of the polycrystal, as well as the anisotropy of mechanical properties within individual grains that make up the metal [12].

The anisotropy of single crystals is explained by the fact that the number of particles in the crystal lattice is different, falling on the same length, but different in direction segments (Fig. 1), i.e. the density of the particles of the crystal lattice in different directions are not identical, which leads to the difference of the crystal properties along these directions. In polycrystals, anisotropy is observed only for individual small crystals, but their different orientation leads to the fact that the properties of the polycrystal in all directions are on average the same.
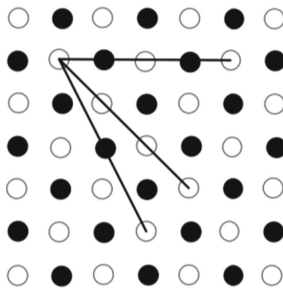
Fig. 1. Difference of particles that fall on the same length, but different in direction segments.

Even for a single crystal, it is impossible to talk about the simultaneous transition to the plastic state of all blocks and the entire volume of each block, although the degree of uniformity in a single crystal is much higher than in a polycrystal. This difference is primarily reflected in the nature of the mono – and polycrystal stretching curves shown in Fig. 2.
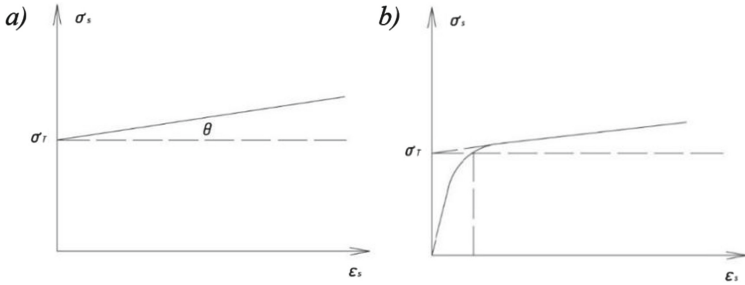
Fig. 2. Character of the tension – deformation curves of a single crystal (a) and a polycrystal (b).

Thus, the elastic limit is more clearly revealed on the curve that characterizes the deformation of a single crystal, while on the stretching curve of a polycrystalline structure, there is no clearly defined elastic limit, and the initial section becomes more and more curved with increasing load.

Figure 2 shows the transition sections of the experimental tension curves of reinforcing bars of classes: A240 (Fig. 2a) and A400 (Fig. 2b) from the limits of elasticity and proportionality to the yield point, determined by the results of experimental data from various devices. In the first case, the measurement results were set by one device with a large base (200 mm); in the second – by the results of devices with a base of 20 mm, installed in a chain along the length of the future yield site. As a result, the fact of gradual entry into the fluidity of individual measurements of steel sections was established (Fig. 3).
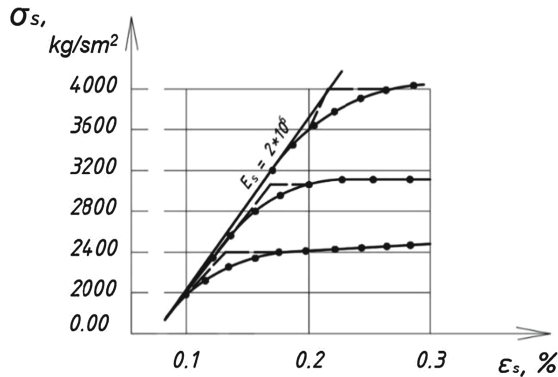
Fig. 3. Transition areas of mild steel yield: ▬ ▬ – according to the device with a large base (200 mm); ●━━━ – the same applies to several devices with a small base.

A review of the steel deformation graphs of Figs. 1 and 2 shows that their yield strength can simultaneously be estimated by a significant value of the relative deformation ε_{st}, corresponding to the beginning of the yield point.

According to the results of research, the beginning of yield strength of A240 steel is determined by deformation not $\frac{R_t}{E_s} = \frac{240}{2*10^5} = 0.0012$, but by a value of 0.00136, i.e. by 13.3% more, and steel class A400 is not 0.002, but 0.0025, i.e. by 25% more.

Of course, that attempts to describe with one of the analytical dependence $\sigma_s = (\varepsilon_s)$ all straight and curved sections of the curve of these steels lead to the creation of numerous high-degree equations that make it difficult to conduct scientific and engineering calculations.

It is possible to simplify the calculation by using in the calculations of such elements the concept of the secant modulus of deformations of reinforcing steel E'_s, which, depending on the stress level σ_s, will give the current value of the actual modulus of deformations as the relative value of the well-known elastic modulus of steel $E_s = 2 \cdot 10^5$ MPa.

Based on the results of experimental studies [6–11], the authors developed an exact expression of the desired secant modulus of mild steel deformations:

$$E'_s = E_s \left[1 - 0,25 \left(\frac{\sigma_s}{500} \right) \left(\frac{\sigma_s}{R_s} \right)^3 \right], \tag{1}$$

where σ_s – corresponding value of the tensile reinforcement; R_s – yield strength; E_s – the initial modulus of elasticity of steel, equal to $2 \cdot 10^5$ MPa.

Figure 4 shows the actual deformation curves of mild steels, which real deformations, starting from their stress level of 0.55…0.60 R_s, deviate up to 5% from the straightness of the initial elastic modulus E_s and, approaching their yield strength R_t, reach the values of relative deformations that are equal to the values obtained from the above dependence and are more accurate than those obtained by the standard method [1].
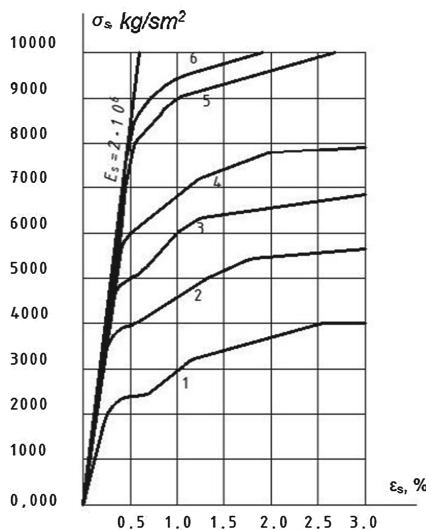
Fig. 4. Valid tensile diagrams of mild reinforcing steels A240 (1), A400 (2), A500 (3), A600 (4), A800 (5), A1000 (6).

All these values of relative tensile deformations of reinforcing steels are obtained as a result of using well-known expressions in the resistance of materials:

$$\sigma_s = \varepsilon_s * E'_s \tag{2}$$

$$\varepsilon_s = \sigma_s / E_s \tag{3}$$

4 Conclusion

The resulting solution allows solving actual problems not only of calculation of reinforced concrete bending elements in normal sections, but also other difficult problems in the theory of resistance and methods of calculation of reinforced concrete structures, as the developed solution in a simple and easy form as the secant modulus of deformation E'_s allows extracting manually the coefficients of elasticity of individual sections of reinforcing steel at tension.

References

1. SP 63.13330.2012. Concrete and reinforced concrete structures. Main provisions/Updated version of SNiP 52-01-2003. Ministry of Regional Development of Russia (2012)
2. Lee, J.Y., Kim, U.Y.: Effect of longitudinal tensile reinforcement ratio and shear span-depth ratio on minimum shear reinforcement in beams. ACI Struct. J. **105**(2), 134 (2008)
3. Obernihin, D.V.: Numerical study of strength, fracture toughness and deformativnosti of steel reinforced concrete elements of trapezoidal cross-section. Bull. Belgorod State Technol. Univ. Named V G Shukhov **2**(5), 24–29 (2017)
4. Eryshev, V.: Deformation method for calculating the strength of reinforced concrete bending elements using deforming diagrams for elastoplastic materials. Syst. Methods Technol. 79–84, (2018)
5. Nikulin, A.I., Qasim, A.-K.A.F.: Improving the methodology for calculating the bearing capacity of eccentrically compressed reinforced concrete elements based on the use of the refined curvilinear deformation diagrams of concrete and reinforcement. Mater. Sci. Forum **974**, 570–576 (2019)
6. Cadoni, E., Forni, D.: Strain rate effects on reinforcing steels in tension. EPJ Web Conf. **94**, 01004 (2015)
7. Poloz, M.A., Sami, Y.G., Shevchenko, A.V.: Application of stepwise and iterative method in the calculation of bending prestressed precast and monolithic elements taking into account the physical nonline-arity. Constr. Mater. Prod. **2**(3), 12–27 (2019). https://doi.org/10.34031/2618-7183-2019-2-3-12-27
8. Kochkarev, D., Galinska, T.: Calculation Methodology of Reinforced Concrete Elements Based on Calculated Resistance of Reinforced Concrete. In: MATEC Web of Conferences, vol. 116, p. 02020 (2017)
9. Shatri, V., Shefkiu, B., Shatri, B.: Design to serviceability limit states of concrete elements subject to pure bending. In: 3rd Annual International Conference on Architecture and Civil Engineering (ACE 2015) (2015)

10. Soren, S.: Effect of deformation on the structure and properties of interstitial free steels. Mater. Today Proc. **4**(8), 9029–9038 (2017)
11. Taiwo, A.M., Olarewaju, K.O.: Structural Strengths of Concrete Beams Reinforced with Various Types of Steel Reinforcements. J. Architect. Environ. Struct. Eng. Res. **2**(1), (2019)
12. Suleymanova, L.: High-quality energy-saving and competitive building materials, products and constructions. Bull. Belgorod State Technol. Univ. Named V G Shukhov **2**(1), 9–16 (2016)

Research on Properties of Pressed Silicate Materials of Non-autoclave Hardening with the Addition of Synthetic Tobermorite-Like Calcium Hydrosilicates

A. A. Volodchenko$^{(\boxtimes)}$

Belgorod State Technological University named after V.G. Shukhov, Belgorod, Russia
Alex-0904@mail.ru

Abstract. At the present stage of development of construction materials science, the tasks of producing high-performance construction composites of a new generation, including those using natural and technogenic raw materials, are of particular relevance. To a greater extent, these requirements are met by wall silicate materials. Currently, the raw material base for the production of silicate materials is not expanding, and the use of quartz sand in the technology determines the high energy intensity of the synthesis of new formations in the $CaO\text{-}SiO_2\text{-}H_2O$ s
ystem, as well as the production process as a whole. In the production of wall silicate materials using non-autoclave technology, instead of quartz sand, it is possible to use clay rocks of an incomplete stage as the main component. The question of study of influence of synthetic tobermorite-like calcium hydrosilicates (STCH) on synthesis system $CaO–Al_2O_3–SiO_2–H2O$ and properties of extruded silicate materials of non-autoclave hardening using clay rocks of unfinished stage of formation is relevant. In the course of research, the nature of the influence of synthetic tobermorite-like calcium hydrosilicates (STCH) on the physical and mechanical properties of non-autoclaved silicate composites based on unconventional aluminosilicate raw materials represented by clay rocks of the incomplete stage of mineral formation was established. The rational content of the STCH additive is 1 wt.%, and with an increase in the percentage, the strength characteristics of finished products decrease.

Keywords: Non-autoclave silicate materials · Synthetic calcium hydrosilicates · Clay rocks · Wall materials

1 Introduction

At the present stage of development of construction materials science, the tasks of producing high-performance construction composites of a new generation that contribute to the optimization of the "man-material-environment" system, the production of which is based on resource-saving nature-like technologies, are of particular relevance [1–5].

Currently, the construction materials industry provides consumers with a limited range of products, and in many regions of the Russian Federation there is a shortage of them. In this regard, the issues of obtaining new-generation construction composites, including those using natural and technogenic raw materials [6–11], and combining high structural, decorative and operational qualities with a relatively low cost, are very relevant and require detailed study. To a greater extent, these requirements are met by wall silicate materials. Currently, the raw material base for the production of silicate materials is not expanding, and the use of quartz sand in the technology determines the high energy intensity of the synthesis of new formations in the $CaO-SiO_2-H2O$ system, as well as the production process as a whole [12–14].

Enterprises producing silicate materials have very good prospects for expanding the range of produced products, as well as reducing the energy intensity of production. Thus, in the production of wall silicate materials using non-autoclave technology, instead of quartz sand, it is possible to use clay rocks of an incomplete stage of mineral formation as the main component [6], characterized by the presence of mixed-layer formations such as hydromica, montmorillonite, x-ray amorphous phase, fine quartz, feldspar, mica.

An interesting question is to study the effect of synthetic tobermorite-like calcium hydrosilicates (STCH) on the synthesis of the $CaO–AI_2O_3–SiO_2–H2O$ system, represented by lime and clay rocks of the incomplete stage of mineral formation, and the properties of pressed silicate materials of non-autoclave hardening.

2   Methods and Materials

As a raw material component for obtaining laboratory samples of non-autoclaved silicate composites, coarse-dispersed clay rocks saturated with fine quartz of the incomplete stage of mineral formation of the weathering crust of the diagenesis zone, in particular, sandy loam (plasticity number – Ip = 6) of the aeolian-eluvial-deluvial genetic type were used. The rocks were selected in the area of the iron ore basin of the Kursk magnetic anomaly (Russia, Belgorod region).

Lump quicklime was used as an astringent component. The content of active CaO + MgO in terms of dry matter was 90% by weight, the lime quenching temperature was 98.5 °C, and the lime quenching time was 4 min 20 s.

The studied clay rocks were pre-dried in a drying cabinet at a temperature of 105 °C to a constant weight and, if necessary, crushed in a laboratory vibrating mill to a specific surface of 80 kg/m^3. Lump lime was crushed to a specific surface of 400 m^2/kg.

The synthesis of tobermorite-like calcium hydrosilicates was carried out under autoclave conditions from a mixture of $Ca(OH)_2$ and SiO_2. The parameters of hydrothermal synthesis were as follows: P = 1 MPa, T = 175 °C. A synthetic product, aerosil, was used as SiO_2.

Samples for research were made by mixing the initial raw components in a laboratory mixer in the specified ratios. Then the mixture was moistened with the necessary amount of water, and kept in a sealed container, in order to convert completely CaO to $Ca(OH)_2$ in the raw mixture. Samples cylinders with a diameter and height of 88 mm were obtained from the obtained raw material mixture by semi dry pressing. The pressing pressure was

20 MPa. The obtained samples were processed in saturated water vapor at a temperature of 95 °C for 9 h. For the obtained samples the indicator of the limit of compressive strength, average density, water resistance was determined.

The research was performed using a MIRA 3 LM electron microscope (Czech Republic), an ARL 9900 WorkStation x-ray fluorescence spectrometer with an integrated diffraction system (USA), and a Q-derivatograph of the F. Paulik, J. Paulik, and L. Erdey systems.

3   Results and Discussion

The specific features of clay rocks of incomplete stage of mineral formation used for research are the presence of thermodynamically unstable layered aluminosilicates, such as imperfect structure of hydromica, mixed-layer minerals, x-ray amorphous substance, and finely dispersed weakly rolled quartz (see Fig. 1).
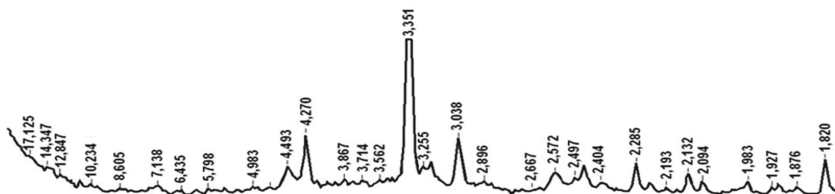
Fig. 1. Roentgenogram of the used clay raw material.

Synthetic calcium hydrosilicates in these studies were obtained from a mixture of CaO:SiO$_2$ at a ratio of 1:1. Based on the data of x-ray phase (reflexes 11.4, 3.084, 2.9, 2.8, 2.4, 2.1 2.0–2.2 Å) and differential thermal analysis (intense exoeffect on the DTA curves at 836 °C, corresponding to the crystallization of wollastonite) shows the presence of low-base calcium hydrosilicates (see Fig. 2), mainly of the toberomorite type (characteristic reflex on the roentgenogram 11.4 Å).
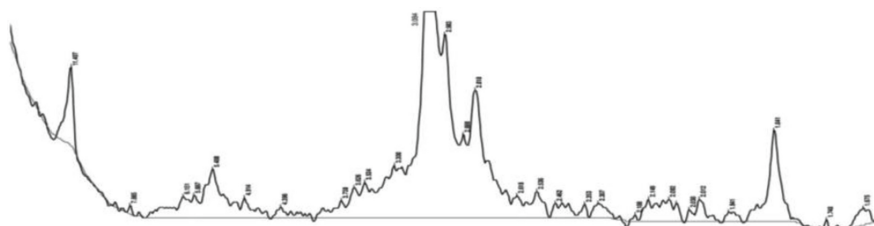
Fig. 2. Roentgenogram of the obtained calcium hydrosilicates.

When studying the microstructure of the obtained tobermorite-like calcium hydrosilicates, it was found that the total mass is composed of curved scales and flat fibers, among which there are thin leaf-like plates with a surface size of about 650 nm and a rib thickness of about 20 nm (see Fig. 3).

×10000   ×50000
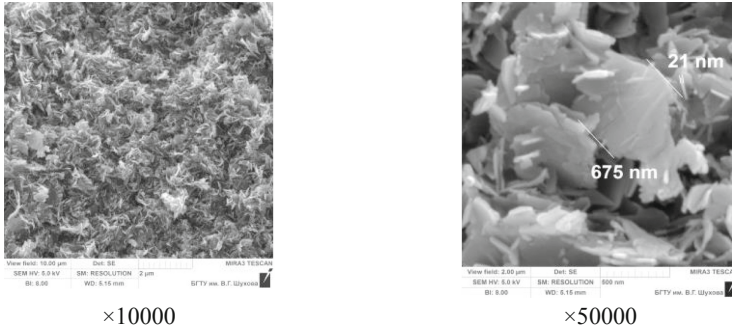
Fig. 3. Derivatogram of received calcium hydrosilicates.

In real conditions of construction production, it is difficult to obtain homogeneous synthetic calcium hydrosilicates, due to possible fluctuations in the properties of the raw material and synthesis conditions. In this regard, studies were conducted using calcium hydrosilicates of heterogeneous composition, which will be more close to the conditions of real production, including for small and medium-sized businesses.

The amount of quicklime in the raw mixture was 6, 8 and 10 wt.%. The content of synthetic tobermorite-like calcium hydrosilicates was 1, 3, 6 wt.%. The humidity of the raw mixture, depending on the composition of the raw mixture, was 10–12 wt. %.

Based on the analysis of the properties of the obtained samples, it was found that the optimal content of synthetic tobermorite-like calcium hydrosilicates, which provides maximum strength characteristics (compressive strength – 21 MPa), is 1 wt. %, which is 11% higher compared to the control samples (see Fig. 4).
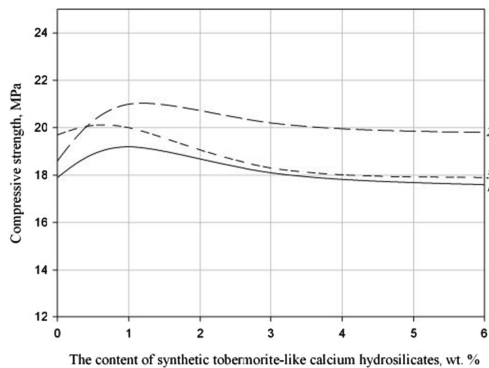
Fig. 4. Effect of synthetic tobermorite-like calcium hydrosilicates on the properties of the obtained samples: 1 – CaO 6 wt. %; 2 – content of CaO 8 wt. %; 3 – content of CaO 10 wt. %.

Further increase in the content of synthetic toberomorite-like calcium hydrosilicates to 6 wt. % reduces the strength characteristics to 19.8 MPa with a CaO content of 8 wt.%. The optimal content of quicklime is 8 wt.%.

The average density of samples (see Table 1) decreases by 2–3% with an increase in the content of synthetic tobermorite-like calcium hydrosilicates, and an increase in the CaO share in the raw material mixture additionally reduces this indicator by 3–5%.

Table 1. Properties of the obtained samples.

Properties of samples	Content of STCH, wt. %			
	0	1	3	6
Content of CaO 6 wt. %				
Average density, kg/m^3	1960	1960	1935	1900
Softening coefficient	0.65	0.69	0.78	0.68
Content of CaO 8 wt. %				
Average density, kg/m^3	1950	1930	1910	1905
Softening coefficient	0.7	0.8	0.77	0.74
Content of CaO 10 wt. %				
Average density, kg/m^3	1890	1870	1840	1835
Softening coefficient	0.71	0.71	0.76	0.74

The introduction of the STCH additive to the raw material mixture increases the softening coefficient of samples from 0.7 to 0.8 (CaO content of 8 wt.%).

The increase in the operational properties of samples is determined by changes in the microstructure of composites (see Fig. 5).
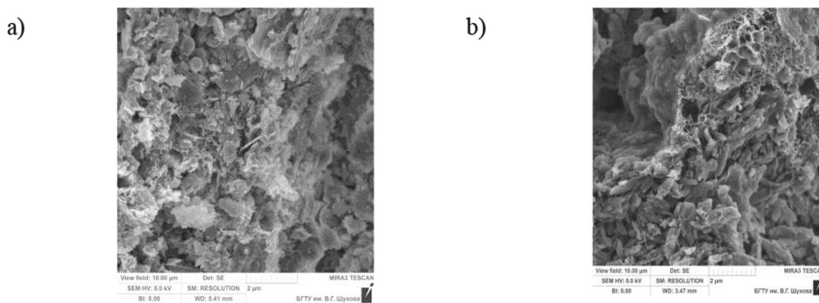
Fig. 5. Effect of STCH on the microstructure of non-autoclave composites: a – control composition; b – with the addition of STCH.

The results of studies of samples using scanning electron microscopy of samples show an increase in the total mass of the crystalline substance compared to samples without the addition of STCH (see Fig. 5), which is also confirmed by x-ray phase analysis (see Fig. 6).

a)

b)
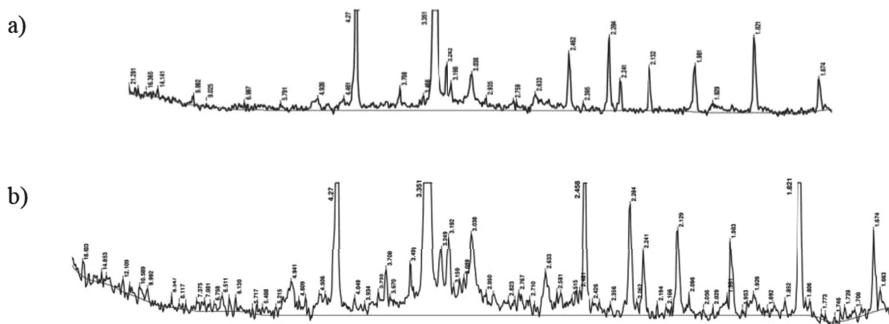
Fig. 6. Roentgenograms of the obtained samples: a – control composition; b – with STCH additive.

Based on the results of x-ray phase analysis (see Fig. 6) it was found that the addition of synthetic tobermorite-like calcium hydrosilicates increases the number of crystallized new formations in the $CaO–SiO_2(Al_2O_3)–H2O$ system, compared with samples without additives (see Fig. 6a), which determines the increase in the physical and mechanical properties of the samples.

4   Conclusion

Thus, based on the obtained data, the nature of the influence of synthetic tobermorite-like calcium hydrosilicates on the physical and mechanical properties of non-autoclaved silicate composites based on non-traditional aluminosilicate raw materials represented by clay rocks of the incomplete stage of mineral formation is established. The rational content of the STCH additive is 1 wt.%, and with an increase in the percentage, the strength characteristics of finished products decrease.

References

1. Bazhenov, Y.M., Zagorodnjuk, L.H., Lesovik, V.S., Chernysheva, N.V., Sumskoy, D.A.: Concerning the role of mineral additives in composite binder content. Int. J. of Pharm. Technol. **8**(4), 22649–22661 (2016)
2. Kuprina, A.A., Lesovik, V.S., Zagorodnyk, L.H., Elistratkin, M.Y.: Anisotropy of materials properties of natural and man-triggered origin. Res. J. Appl. Sci. **9**(11), 816–819 (2014)
3. Loganina, V., Zhegera, C., Fediuk, R., Timokhin, R., Zayakhanov, M., Liseitsev, Y.: Amorphous Aluminosilicates as a Structure-Forming Additive in Cementitious Systems. J. Mater. Civ. Eng. **32**, 06020004 (2020)

4. Urkhanova, L., Khardaev, P., Lkhasaranov, S.: Composite binders based on natural raw materials and waste products of the baikal region. ARPN J. Eng. Appl. Sci. **13**(17), 4751–4756 (2018)
5. Fedyuk, R., Amran, Y.H.M., Mosaberpanah, M.A., Klyuev, S.V., Vatin, N.: A critical review on the properties and applications of sulfur-based concrete. Materials **13**(21), 1–23 (2020). 4712
6. Volodchenko, A.A., Lesovik, V.S., Volodchenko, A.N., Zagorodnjuk, L.H., Pukharenko, Y.V.: Composite performance improvement based on non-conventional natural and technogenic raw materials. Int. J. Pharm. Technol. **8**(3), 18856–18867 (2016)
7. Tolstoy, A.D.: Fine-grained high-strength concrete. Constr. Mater. Prod. **3**(1), 39–43 (2020)
8. Nelyubova, V.V., Babayev, V.B., Alfimova, N.I., Usikov, S.A., Masanin, O.O.: Improving the efficiency of fibre concrete production. Constr. Mater. Prod. **2**(2), 4–9 (2019)
9. Lesovik, R.V., Klyuyev, S.V., Klyuyev, A.V., Netrebenko, A.V., Kalashnikov, N.V.: Fiber concrete on composite knitting and industrial sand KMA for bent designs. World Appl. Sci. J. **30**(8), 964–969 (2014)
10. Lesovik, R.V., Klyuyev, S.V., Klyuyev, A.V., Netrebenko, A.V., Kalashnikov, N.V.: Fiber concrete on composite knitting and industrialsand KMA for bent designs. World Appl. Sci. J. **30**(8), 964–969 (2014)
11. Klyuev, S.V., Khezhev, T.A., Pukharenko, Y.V., Klyuev, A.V.: Experimental study of fiber-reinforced concrete structures. Mater. Sci. Forum **945**, 115–119 (2018)
12. Volodchenko, A.N., Strokova, V.V.: Development of scientific bases for production of silicate autoclave materials using clay raw materials. Constr. Mater. **9**, 25–31 (2018)
13. Klimesch, D., Ray, A.: Evaluation of phases in a hydrothermally treated $CaO\text{-}SiO_2\text{-}H_2O$ system. J. Therm. Anal. Calorim. **70**(3), 995–1003 (2002)
14. Nourredine, A., Chelghoum, N., Jauberthie, R., Molez, L.: Formation of C-S-H in calcium hydroxide–blast furnace slag– quartz–water system in autoclaving conditions. Adv. Cem. Res. **27**(3), 153–162 (2015)

Effect of Cubic and Orthorhombic Crystal Systems of Tricalcium Aluminate to Form Ettringite in the Presence of Dihydrate Calcium Sulfate

A. O. Erygina[(✉)] and D. A. Mishin

Belgorod State Technological University named after V.G. Shukhov,
Belgorod, Russia
erygalyona@yandex.ru

Abstract. Hydration of clinker minerals plays an important role in the formation of a strong cement stone. Depending on the composition, quantity, shape, size, and structural defects of the formed crystallohydrates, the physical and technical properties of the hardened cement stone are determined. The most chemically active mineral in Portland cement clinker is tricalcium aluminate ($3CaO \cdot Al_2O_3$), which also reacts easily and forms solid solutions with R_2O. In turn, alkaline solid solutions affect the solubility of tricalcium aluminate in water and the further formation of crystallohydrates. The effect of alkaline solid solutions of tricalcium aluminate on the formation of ettringite ($3CaO \cdot Al_2O_3 \cdot 3CaSO_4 \cdot 32H_2O$) during hydration was studied. It is established that the rates of hydration of cubic and orthorhombic crystal systems of tricalcium aluminate are different, and when they interact with dihydrate calcium sulfate, different hydration products are formed. Thus, the orthorhombic crystal system $3CaO \cdot Al_2O_3$ (C_3A) with $CaSO_4 \cdot 2H_2O$ in water promotes the formation of calcium aluminate sulfate hydrate ($3CaO \cdot Al_2O_3 \cdot CaSO_4 \cdot 12H_2O$), which then formed calcium aluminate trisulfate hydrate ($3CaO \cdot Al_2O_3 \cdot 3CaSO_4 \cdot 32H_2O$). A cubic system of C_3A with $CaSO_4 \cdot 2H_2O$ in water, on the contrary, first forms a calcium aluminate trisulfate hydrate, which is eventually converted to calcium aluminate sulfate hydrate.

Keywords: Portland cement clinker minerals · Tricalcium aluminate · Hydration of clinker minerals · Tricalcium aluminate of cubic system · Tricalcium aluminate of orthorhombic system · Ettringite · Calcium aluminate sulfate hydrate · Calcium aluminate trisulfate hydrate · Dihydrate calcium sulfate · Solid solutions of Na_2O

1 Introduction

The strength of Portland cement stone depends on many factors, such as the Blaine specific surface of cement, the type of dihydrate calcium sulfate ($CaSO_4 \cdot 2H_2O$), the cement-water ratio, etc. One of the main factors affecting the properties of cement stone is the chemical activity of clinker minerals. Tricalcium aluminate (C_3A) is the most chemically active mineral in Portland cement clinker. When it interacts with dihydrate

calcium sulfate, which occurs in the first minutes of hydration, acicular crystals of ettringite are formed [1, 2]. They form the initial framework of the cement stone, which largely determines the final strength characteristics of the cement stone.

When hydrating tricalcium aluminate and dihydrate calcium sulfate, the degree of supersaturation of the solution with reacting phases should be taken into account. Previously, Ressler and Stark in [3] found that the degree of supersaturation of solutions affects the morphological characteristics of ettringite. Thus, when the saturation coefficient is equal to 10, ettringite crystals are formed with a length-to-width ratio of ≈ 6.5, and when the reacting phases are supersaturated, the transverse growth of crystals increases [3]. It should be remembered that the reactions that occur during cement hydration occur due to the processes of dissolution and precipitation when clinker minerals come into contact with water [3, 4]. The rate of interaction of the aluminate phase of Portland cement clinker depends on the defect of its structure and the formation of solid solutions. Tricalcium aluminate reacts easily and forms solid solutions with R_2O [5–7], which is likely to affect the solubility of tricalcium aluminate in water and the further formation of crystallohydrates.

The aim of the study was to study the effect of alkaline solid solutions of tricalcium aluminate on the formation of ettringite during hydration.

2 Methods and Materials

For the study, C_3A and a solid solution of Na_2O in tricalcium aluminate were synthesized. The solid solution of C_3A contained 3.7 wt % Na_2O. For the synthesis, chemical reagents were used: $CaCO_3$, Al_2O_3 and Na_2O with the purity category: "cp" according to GOST 13867–68. The conditions for the synthesis of tricalcium aluminate and a solid solution of C_3A (C_3A + 3.7% Na_2O) are presented in Table 1.

Table 1. Conditions for the synthesis of initial components.

Source component	Firing temperature,°C	Number of roasting	Isothermal exposure, min
C_3A	1400	2	60
C_3A + 3.7 wt. % Na_2O	1400	2	20

In studies [8, 9], chemical interactions between tricalcium aluminate, Portland cement clinker minerals, and Na_2O in various combinations were considered at firing temperatures of 1100–1300 °C. The interaction of minerals containing Al_2O_3 with sodium oxide was accompanied by the formation of $Na_2O\cdot Al_2O_3$.

The completeness of the synthesis was controlled by x-ray phase analysis of the composition of the burned samples (Fig. 1, 2). No phases similar to those detected were identified in [8, 9]. The tricalcium aluminate and its solid solution with sodium oxide (C_3A + 3.7% Na_2O) can be considered as synthesized compounds [10].

When studying the processes of hydration of tricalcium aluminate and a solid solution of C_3A with sodium oxide ($C_3A + 3.7\%$ Na_2O) with dihydrate calcium sulfate, a chemical reagent $CaSO_4 \cdot 2H_2O$ of the purity category: "p" according to GOST 13867–68 was used (Fig. 3).

The ratio in the studied mixtures between C_3A and $CaSO_4 \cdot 2H_2O$, $C_3A + 3.7\%$ Na_2O and $CaSO_4 \cdot 2H_2O$ corresponds to the average calculated content of tricalcium aluminate and dihydrate calcium sulfate in ordinary cements (Table 2).
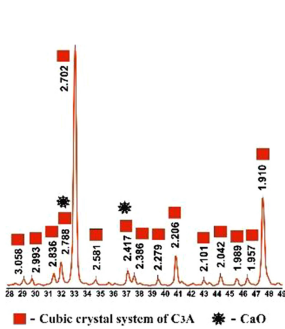
Fig. 1. Section of the x-ray spectrum C_3A.
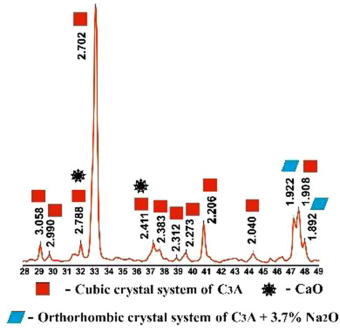
Fig. 2. Section of the x-ray spectrum of a solid solution of C_3A ($C_3A + 3.7\%$ Na_2O).
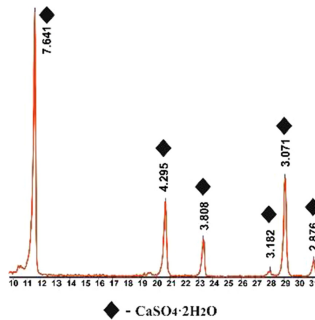
Fig. 3. Section of the x-ray spectrum $CaSO_4 \cdot 2H_2O$.

Table 2. Ratio of initial components in the studied mixtures.

$C_3A + CaSO_4 \cdot 2H_2O$		Solid solution of C_3A ($C_3A + 3.7\%$ Na_2O)[*] $+ CaSO_4 \cdot 2H_2O$	
Quantity of C_3A, wt. Parts	Quantity of $CaSO_4 \cdot 2H_2O$, wt. Parts	Quantity of ($C_3A + 3.7\%$ Na_2O), wt. Parts	Quantity of $CaSO_4 \cdot 2H_2O$, wt. Parts
8	5	8	5

[*]The content of free CaO in the solid solution of C_3A ($C_3A + 3.7\%$ Na_2O) is equal to 2%

3   Results and Discussion

Tricalcium aluminate when interacting with dihydrate calcium sulfate, depending on the ratio between them, can form two forms of calcium hydrosulfoaluminate: calcium aluminate sulfate hydrate and calcium aluminate trisulfate hydrate. For Portland cement stone, the calcium aluminate trisulfate hydrate is important, which crystallizes in the form of acicular crystals or elongated prisms. When the ratio of the initial components corresponds to the average content of C_3A and dihydrate calcium sulfate in ordinary cements (8% C_3A and 5% $CaSO_4 \cdot 2H_2O$), the amount of $CaSO_4 \cdot 2H_2O$ is not enough to form a calcium aluminate trisulfate hydrate. The molar ratio between C_3A and $CaSO_4 \cdot 2H_2O$, a solid solution of C_3A (C_3A + 3.7% Na_2O) and $CaSO_4 \cdot 2H_2O$ is ≈1:1 in both studied mixtures. With this molar ratio, a calcium aluminate sulfate hydrate is formed according to the equation:

$$3CaO \cdot Al_2O_3 + CaSO_4 \cdot 2H_2O + 10H_2O \rightarrow 3CaO \cdot Al_2O_3 \cdot CaSO_4 \cdot 12H_2O \quad (1)$$
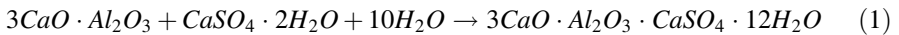
The reaction products will depend on the chemical activity of the initial components, which is determined by the formation of solid solutions based on Na_2O. If the hydration of tricalcium aluminate (C_3A) proceeds faster than the dissolution processes of dihydrate calcium sulfate, then the calcium aluminate sulfate hydrate ($3CaO \cdot Al_2O_3 \cdot CaSO_4 \cdot 12H_2O$), or calcium hydroaluminates (C_xAH_y), or a mixture of them will be formed as hydration products. Conversely, if the dissolution rate of dihydrate calcium sulfate is high at a given C_3A hydration rate, then the calcium aluminate trisulfate hydrate will be used as the hydration products of the initial components ($3CaO \cdot Al_2O_3 \cdot 3CaSO_4 \cdot 32H_2O$).

The growth of colorless acicular crystals is recorded after 15 min of hydration in a mixture of C_3A + 3.7% Na_2O and dihydrate calcium sulfate (Fig. 4b). At the same time, in a mixture with pure C_3A and $CaSO_4 \cdot 2H_2O$, only the beginning of the interaction of tricalcium aluminate with dihydrate calcium sulfate in solution is observed with the formation of an aluminate hydrated film on the grain surface (Fig. 4a).

The low rate of dissolution of $CaSO_4 \cdot 2H_2O$, compared with the rate of dissolution and hydration of a solid solution of C_3A orthorhombic crystal system (C_3A + 3.7% Na_2O), contributes to the formation of plates of the calcium aluminate sulfate hydrate (Fig. 4d) by 16 h of hydration according to Eq. (1). By this time (16 h of hydration), only an increase in the external hydration product on the grain surface was recorded between pure C_3A (cubic crystal system) and dihydrate calcium sulfate (Fig. 4c).

By 20 h of hydration of a solid solution of C_3A orthorhombic crystal system (C_3A + 3.7% Na_2O) and a dihydrate calcium sulfate, acicular crystals of ettringite are massively crystallized (Fig. 4f). This situation persists even when the shutter speed is 25 h (Fig. 4h).

By 20 h of hydration in a solution with tricalcium aluminate of cubic crystal system and dihydrate calcium sulfate, the appearance and further growth of thin filamentous ettringite crystals on the grain surface and in the intergranular space are noticeable (Fig. 4e). By 25 h, the calcium aluminate trisulfate hydrate recrystallizes into spherulites (Fig. 4) of the calcium aluminate sulfate hydrate.
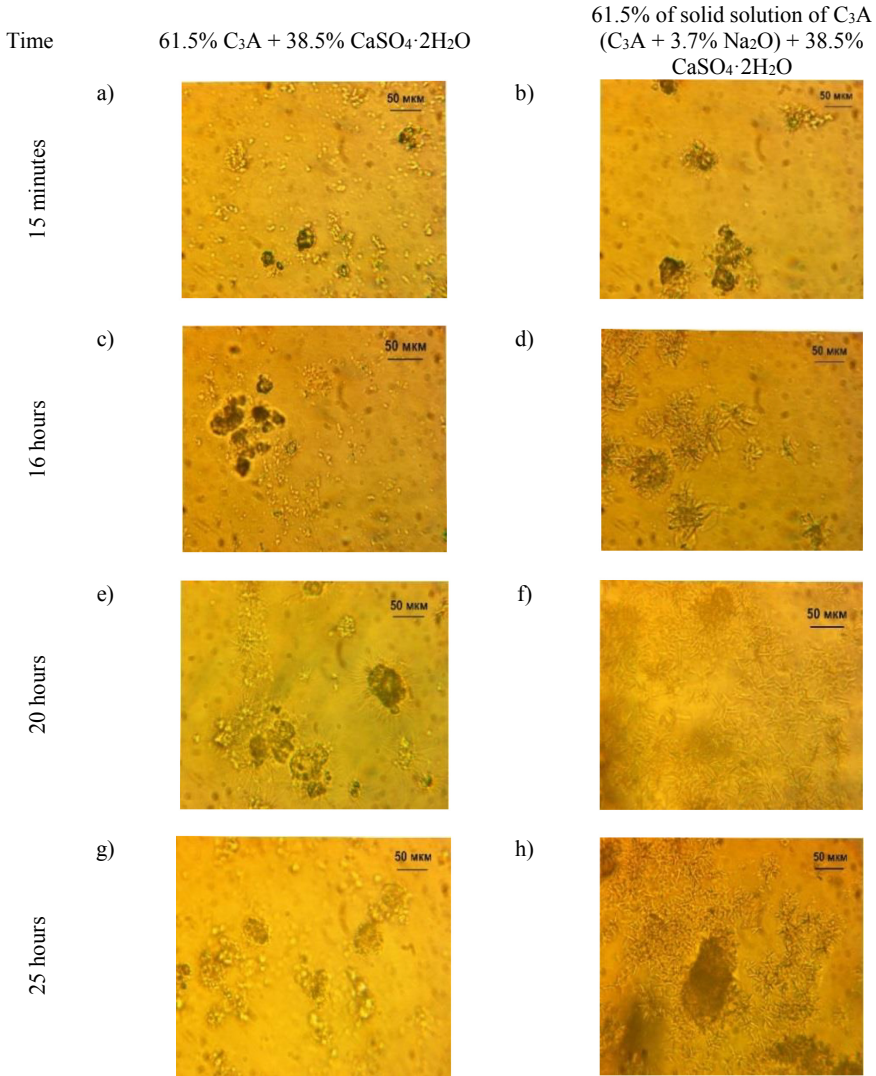
| Time | 61.5% C$_3$A + 38.5% CaSO$_4$·2H$_2$O | 61.5% of solid solution of C$_3$A (C$_3$A + 3.7% Na$_2$O) + 38.5% CaSO$_4$·2H$_2$O |

Fig. 4. Features of C$_3$A (C$_3$A + 3.7% Na$_2$O) solid solution hydration in the presence of CaSO$_4$·2H$_2$O.

4   Conclusion

As a result of the data obtained, we can state:

1. The processes of hydration of tricalcium aluminate of cubic and orthorhombic crystal systems proceed at different speeds, contributing to the formation of various hydration products with dihydrate calcium sulfate. The reaction was studied at the

ratio between C_3A and dihydrate calcium sulfate corresponding to their concentration in cement.

2. Fast hydrating C_3A (orthorhombic crystal system) are mixed with dihydrate calcium sulfate promotes formation of the calcium aluminate sulfate hydrate, which is then the calcium aluminate trisulfate hydrate. Crystals of the calcium aluminate trisulfate hydrate are formed massively in the entire volume.

3. Relatively slowly hydrating C_3A (cubic crystal system) in a mixture with dihydrate calcium sulfate contributes to the formation of a the calcium aluminate trisulfate hydrate, which is then recrystallized into a the calcium aluminate sulfate hydrate. Crystals of the calcium aluminate trisulfate hydrate are formed in a small amount on the surface of tricalcium aluminate particles.

References

1. Taylor, H.: Cement Chemistry; translation from English. Mir, Moscow (1996)
2. Luginina, I.G.: Chemistry and Chemical Technology of Inorganic Binders 2(2). BSTU, Belgorod (2004)
3. Stark, J., Wicht, B.: Zement und Kalk: Der Baustoff als Werkstoff. Basel, Birkhäuser (2000)
4. Glasser, F.P.: The pore fluid in Portland cement: its composition and role. In: Proceedings of the 11th International Conference on the Chemistry of Cement, pp. 19–30. Durban (2003)
5. Klassen, V.K.: Roasting Cement Clinker. Stroyizdat, Krasnoyarsk (1994)
6. Klassen, V.K., Dolgova, E.P.: Alkali Metal Chlorides in Cement Production: Monograph. BGTU, Belgorod (2015)
7. Luginina, I.G.: Chemistry and Chemical Technology of Inorganic Binders 2(1). BSTU, Belgorod (2004)
8. Erygina, A.O., Mishin, D.A.: Interaction of calcium alumoferrite with Na_2CO_3 and Na_2SO_4. In: High Technologies and Innovations: International Scientific-Practical Conference, vol. 12, No. 1, pp. 125–130. BSTU, Belgorod (2016)
9. Erygina, A.O., Mishin, D.A., Klassen, V.K.: The sequence of Na_2O interactions with clinker mineral in their various combinations. Bull. BSTU Named V.G. Shukhov **12**(12), 98–104 (2018)
10. Gorshkov, V.S., Timashev, V.V.: Methods of Physico-Chemical Analysis of Binders. Higher School, Moscow (1963)

Prospects for Construction of Monolithic Cement-Concrete Transport Infrastructure Facilities in the Siberian Region

I. G. Endzhievskaya$^{(\boxtimes)}$, A. A. Yakshina , R. T. Emelyanov ,
and M. L. Berseneva

Siberian Federal University, Svobodny Avenue 79, Krasnoyarsk 660041, Russia
{IEndzhievskaya,AYakshina}@sfu-kras.ru

Abstract. Today, one of the priority tasks of road construction in the Russian Federation is to improve road safety and increase the quality and service life of road surfaces. The climate of the Siberian Federal district, selected as a construction area, is characterized as sharply continental, with hot summers, harsh winters, and a sharp drop in daily temperatures. Therefore, improving the quality of road surfaces and their durability is an urgent problem both in the short and long term. In this paper, we analyzed the effectiveness of testing the technology of laying monolithic transport infrastructure objects using a concrete paver and their operation in the city of Krasnoyarsk. As the object of research, we selected road drainage trays made in 2015 using the Power Curber 5700-C concrete paver, located at a transport interchange near the village of Badalyk in the Krasnoyarsk territory. The results of the survey showed that the identified defects do not affect the operational suitability of the elements. However, when studying the possibilities of using cement concrete coatings in the city of Krasnoyarsk, it turned out that the issues of manufacturing technology and selection of concrete mix compositions taking into account local conditions were not sufficiently developed.

Keywords: Cement concrete pavement · Road surface · Concrete paver · Drainage trays · Inspection · Krasnoyarsk

1 Introduction

To date, one of the priority tasks of road construction in the Russian Federation is to improve road safety and increase the quality and service life of road surfaces [1, 2]. A feature of road construction in the Russian Federation is the high cost of covering, caused by a variety of climatic conditions within the country, low temperatures in winter, a large depth of soil freezing, a significant amount of precipitation, and a large length of roads [3]. Another important factor of high cost is the large territory of the country and the resulting remoteness of the site of road works from the objects of mining or production of construction materials, as well as the associated labor costs.

In connection with these features, the issue of cost is one of the key issues in the road industry of the Russian Federation.

The development of construction of roads with cement-concrete pavement, transport infrastructure facilities using concrete pavers, which involves complete mechanization

and automation of the main processes for laying and compacting concrete mixtures, is one of the possible solutions to the above problems [4, 5]. The comparative characteristics of roads with cement-concrete and asphalt-concrete surfaces are shown in Table 1.

Table 1. Advantages and disadvantages of roads with a cement concrete surface.

Cement concrete surface		Asphalt concrete surface	
Advantages	Disadvantages	Advantages	Disadvantages
Wear resistance (30–50 years does not require repair)	Lack of experience in construction of roads with cement concrete surfaces in the Russian Federation	Construction experience	Insufficient durability, needs to be repaired every 3–4 years
Stability of the deformative properties of cement concrete under temperature changes	Lack of an up-to-date regulatory framework	Easy maintenance and repair	The dependence of properties on temperature
Increased load capacity of the road surface	Lack of qualified personnel	Increased surface roughness and increased traction of wheel tires on the roadway	Influence of shear loads, rut formation
Good light-reflection, high wear resistance, frost resistance of road concrete	Intensive peeling of the concrete surface after a period of winter maintenance under the influence of frost and anti-ice reagents	Damping, driving on the road is silent	Increased risk of cracking in the surface during the cold season

Despite the fact that the cement industry in the Russian Federation is able to provide high-quality materials necessary for the construction of roads with cement-concrete surface, today their share in the Russian Federation is about 2%, while in developed countries the percentage is more than 60 (Fig. 1) [6].

The construction of transport infrastructure facilities in a prefabricated version with a large length of roads, especially federal ones, is more labor-intensive. In this paper, we evaluated the effectiveness of testing the technology of laying monolithic transport infrastructure objects using a concrete paver and their operation in the city of Krasnoyarsk.
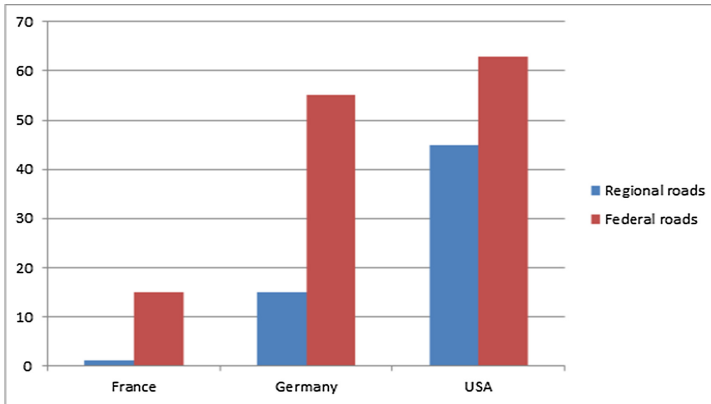
Fig. 1. Roads with cement concrete surface, %.

2   Methods and Materials

As the object of research, road drainage trays were selected, experimentally performed in 2015 with the use of a power Curb 5700-C concrete paver, located at a transport interchange near the village of Badalyk in the Krasnoyarsk territory. In winter, the road surface was treated with chemical reagents that fell on the structures under study [7, 8].

The survey of structures was performed according to the following scheme: visual field inspection of structures, determination of the general spatial position, type of structures; identification of defects and damages; assessment of the technical condition of building structures of the object; comparison of actual design solutions with the requirements of current regulatory documents [9, 10].

The presence of cracks was determined visually using a magnifying glass of 4 and 20 times magnification, the width of the opening of the MPB-3 microscope. The geometric dimensions of the sections were determined using a caliper SHTS-II-250–0.05.

Defects (cross-section dimensions of elements, gaps, cracks) of building structures were measured using steel tape measures with an accuracy of 0.5 mm and rulers with an accuracy of 0.5 mm, linear dimensions of building structures were measured using a Leica DISTO D2 laser distance meter.

The instrumental method was used to determine the actual dimensions of structures, the device of expansion joints, defects and damages [11].

3   Results and Discussion

The construction area is characterized by the following natural and climatic conditions (Table 2).

The Power Curber 5700-C concrete paver is equipped with a system for quick replacement of sliding forms with different profiles. The t-shaped traverse is movable and is designed to install these forms under the structure in any position, with a side formwork attachment and a conveyor installed in the rear of the machine. Vibration is

Table 2. Characteristics of natural and climatic conditions of the area of construction of monolithic road drainage trays.

Annual air temperature, ºC;	Average minimum temperature of the warmest month, ºC	Average temperature of the coldest period, ºC	Absolute maximum temperature, ºC	Absolute minimum air temperature, ºC
0.6	25.3	−22 º	36 º	−52

carried out in the front of the concrete compaction mold. Vibrators with automatic on and off function are activated with the movement of the machine. They are equipped with a hydraulic drive with an adjustable vibration frequency. The position of the vibrators is set using hydraulics for easy adjustment.

Experience in the construction of monolithic road drainage trays [12]. The method with sliding forms showed that the most important technological stages should be considered:

- Base preparation,
- laying of cement - concrete mix;
- care for freshly laid concrete;
- construction of expansion joints.

Quality control of these products can be divided into several types by time and place: production, input (by the consumer), and operational.

The technology of the base device provides for the preparation and testing of its surface. During the preparatory work, the following technological operations should be performed: the leveling layer should be profiled and compacted, a carbon string and reinforcement structures should be installed if necessary [13, 14].

The appearance of the object during the study period is shown in Figs. 2, 3.

Fig. 2. Appearance of the object when it was built in July 2015.

Fig. 3. Appearance of the object in August 2020.

As a result of visual examination, violations were detected in the construction of the base. The geometric dimensions of the sections determined using a caliper have a spread along the length of the bar. The evenness of the finished coating was checked in the longitudinal direction with a 3.0 m long rail.

The concrete surface in most of the timber is of proper quality, in accordance with the requirements of GOST. To assess the surface quality of monolithic concrete and reinforced concrete structures, four classes are used, determined by the maximum tolerances of straightness and local irregularities. The concrete surface class must be accepted at least A3, as on structures with straight surfaces, the requirements are specified in Table 3. Pits and cavities on the surface are not significant, the straightness tolerances correspond. No concrete damage caused by variable freezing and thawing was detected in the presence of de-icing salts. Concrete based on a rigid mix, laid using a Power Curber 5700-C concrete paver with sliding forms, is resistant to aggressive environments.

Table 3. Requirements for concrete surface A3 class.

Concrete surface class	Straightness tolerances for measured distances, mm			
	Local inequalities (0.1 m)	1 m	2 m	3 m
A3	2	4.5	7	9.5

No cracks were found in the area of the expansion joints. In some places, there is a grid of hair surface cracks - the opening width is less than 0.1 mm (Fig. 4).
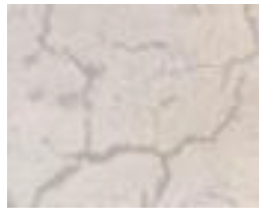
Fig. 4. Grid of hair surface cracks on the surface.

Determination of the actual strength of concrete drainage trays was performed by non-destructive direct method. The results are shown in Table 4.

Table 4. Determination of the actual strength and class of concrete.

№	Experiment data	The name and labeling of the samples (constructions)	Concrete design class	Actual strength of concrete, MPa	Actual concrete class according to GOST 18105–2010
1	20.08.2020	Concrete drainage element	V30	42.6	B34.1
2		Concrete drainage element (in the area of the crack grid)		39.3	B31.4

The resulting values are within the required values.

4   Conclusion

A survey of road trays made in 2015, located at the exit from the village of Badalyk in the Krasnoyarsk territory, was performed.

The identified defects do not affect the operational suitability of road trays, the identified violations are aesthetic and visual characteristics. The results of the survey showed that the actual concrete class of the drainage tray bar meets the requirements of current standards (GOST) for the concrete class index for compressive strength.

However, when studying the possibilities of using cement concrete surfaces in the city of Krasnoyarsk, it turned out that the issues of the regulatory framework, manufacturing technology and selection of concrete mix compositions taking into account local conditions were not sufficiently developed.

References

1. Trukhin, Yu., Budasov, O.S., Stolyarchuk, S.: Improving the technology of modern agro-industrial construction - a solution to the problems in the quality control system. In: VII international Scientific and Practical Conference, pp. 37–39 (2018)
2. Skrypnik, T., Pilipenko, R.: Features of the arrangement technology for rolled cement concrete surfaces of the hard road pavement. Bull. Automobile Highw. Inst. **2**(33), 55–61 (2020)
3. Olennikov, V.: Overview of modern constructions of parapet type road restraints. Siberian Transp. Univ. Bull. **1**(32), 22–24 (2015)
4. Vysotskaya, M., Shekhovtsova, S., Kosinova, A.: Roads with cement concrete surface - prospective direction in road construction. Sci. Almanac **2–3**(28), 38–40 (2017)
5. Petrova, T., Sorvacheva, Y.: Problems and perspectives of concrete road coverings construction in the Russian Federation. Bull. Civ. Eng. **3**(56), 149–155 (2016)
6. Skarkova, J.: Concrete pavements in the czech republic. Cem. Appl. **5**, 102–107 (2015)

7. Vo, K.-U.: Assessment of frost and freeze-thaw damage to concrete pavers (Part 2) | [Bewertung von Frost- und Frost-Tausalz-Sch?den an Betonpflastersteinen (Teil Z)]. Betonwerk und Fertigteil-Technik/Concrete Plant Precast Technol. **1**(86), 38–44 (2020)

8. Garrecht, H., Baumert, C., Hampel, S., Lisin, W., Lazik, P.: Challenges of uniform production of road concretes and possibilities of rheology-based mixing process control. Beton- und Stahlbetonbau **12**(114), 888–898 (2019)

9. Isakov, A., Olennikov, V.: Analysis of hydrophobic impregnations influence on the frost resistance of cement-concrete structures on novosibirsk region roads. Siberian Transp. Univ. Bull. **3**(46), 63–69 (2018)

10. Raman, S.: Utilizing and Optimizing Waste Resources in Paver Block. In: Shukla, S.K., Chandrasekaran, S., Das, B.B., Kolathayar, S. (eds.) Smart Technologies for Sustainable Development: Select Proceedings of SMTS 2019, pp. 407–416. Springer, Singapore (2021). https://doi.org/10.1007/978-981-15-5001-0_35

11. Linek, M., Nita, P., Zebrowski, W., Wolka, P.: Influence of operating media on the parameters of cement concrete intended for airfield pavements. J. Konbin **49**(4), 103–126 (2020)

12. Zhou, C., Lan, G., Cao, P., Tang, C., Cao, Q., Xu, Y., Feng, D.: Impact of freeze-thaw environment on concrete materials in two-lift concrete pavement. Constr. Build. Mater. **262**, 120070 (2020)

13. Pokorný, J., Šev, R., Šál, J.: The design and material characterization of reclaimed asphalt pavement enriched concrete for construction purposes. Materials **13**(21), 4986 (2020)

14. Melese, E., Baaj, H., Tighe, S.: Fatigue behaviour of reclaimed pavement materials treated with cementitious binders. Constr. Build. Mater. **249**, 118565 (2020)

Combined Method of Water Treatment for Sealing Gypsum Systems and Materials Based on Them

S. N. Lapteva$^{(\boxtimes)}$ and V. I. Pavlenko

Belgorod State Technological University named after V.G. Shukhov,
Belgorod, Russia
lapteval202@mail.ru

Abstract. The paper considers technologies for producing gypsum binders sealed with water that has passed through microwave (ultra - high-frequency) radiation, a permanent magnet field, and a combined processing method. Methods of mixing water treatment for gypsum binders are proposed, which provide high strength of gypsum systems, the introduction of substances of various concentrations improves the conductive properties of systems, reduces electrical resistance and increases electrical conductivity. The introduction of iron oxides of various degrees of oxidation contributes to the production of composite materials with a mixed type of conductivity. This paper uses the method of introducing low concentrations of iron chloride into the mixing water and treating the solutions with a microwave field and a magnetic field at different stages of the hardening process of a gypsum system based on iron oxides, which allows you to adjust the properties of the resulting gypsum matrix when using it. Methods of processing binders encapsulated in a gypsum matrix are analyzed, which in the future will make it possible to obtain structural composites with mixed electron-ion conductivity, which have high strength and controlled conductivity, in contrast to conventional gypsum systems used for the repair of construction objects.

Keywords: Ultra High Frequency (UHF) - field · Magnetic processing · Combined method · Permittivity · Tangent of the dielectric loss angle

1 Introduction

Microwave energy is becoming increasingly used in a number of energy-saving technologies. When a microwave field is applied to materials with low electrical and thermal conductivity, which include most oxide materials, electromagnetic energy is absorbed by the entire volume of the material, and the maximum effect is observed at the boundaries of media with different electrodynamic characteristics, which is impossible when heated by external heat sources [1–4].

Non-metallic materials for structural purposes, in the form of products, have a significant spread of physical and mechanical properties due to macro and microdefects, primarily at the phase boundaries [5, 6]. The creation of a new generation of non-metallic composite materials with improved strength and current-conducting

characteristics, as well as with the involvement of methods for effective management of the setting and structure formation phases, can be recognized as a promising and urgent problem today.

The paper scientifically substantiates the possibility of controlling the processes of hydration and structure formation of gypsum binders by microwave processing of components of gypsum systems [7, 8].

The fundamental basis for identifying patterns of behavior of systems with charge transfer in composite materials with a mixed type (electron-ion) conductivity is a physicochemical approach to understanding the mechanism of creating new materials based on iron oxides of different concentrations and different degrees of oxidation. Their principal feature is the presence of two types of carriers-electrons and ions and the interactions between them. Traditional methods for describing such properties of the system as a whole are reduced to the study of individual characteristics of its components, the additive component of which is usually taken as the final result, the processes in the considered area have not been studied [9–11].

To date, quite a lot of experimental data has accumulated that convincingly prove the effectiveness of the use of a magnetic field in various physical and chemical processes. Changes in the structural, optical, kinetic, magnetic, and other physical and chemical properties of the systems under study were recorded. At the same time, there is mainly an intensification of the process, although in some cases there are also qualitative changes. For example, it was shown in [12] that when exposed to a medium-strength magnetic field, not only the polymerization rate of styrene increases by a factor of 6–8, but also the molecular weight of the polymer increases.

Few literature data are available in the field of studying ultrahigh-frequency (microwave) radiation on water or water-containing objects. It should be noted that one of the important issues of the behavior of, for example, water under the influence of EHF or microwave signals is the choice of parameters for observations and, accordingly, the research method.

The most important result of the work is not the reliably measured increase in the conductivity of distilled water under low-power microwave irradiation, but the fact that the highest values of the increase in conductivity were achieved at low irradiation power.

In General, the results of work on ultra-high-frequency effects on the structure of water and aqueous solutions clearly show a significant impact on the physical and chemical state of systems. The mechanism of this type of action is not clearly described, although a number of hypotheses concerning the physics of microwave radiation have been put forward in [13].

There is no doubt that the activity of water and changes in its properties under the influence of weak influences are associated with the processes of structure formation [14].

Combined methods of low-energy activation of water-containing media are not fully reflected in the literature. As for the combined effect of electromagnetic radiation and the introduction of chemical additives of low concentrations, until recently, attention was mainly paid to the combination of high-energy electromagnetic fields such as gamma, ultraviolet, and laser radiation. For example, it was shown in [15] that the processes of structure formation of oxide systems are significantly accelerated, and the strength of the hardening structures increases significantly after pretreatment with

electromagnetic fields and radiation of low-concentration water-salt solutions. The combined combination of low-energy fields and low-concentration chemical additives is still practically unknown.

All of the above suggests that studies of the nature and mechanism of low-energy activation of the processes of structure formation of gypsum and oxide systems, as well as compositions based on them, are a very urgent problem in modern materials science and the construction industry.

2 Methods and Materials

The following standard devices and systems were used to test the developed materials, study the physical and chemical properties of systems, hydration processes, and structure formation of gypsum and composite materials: bridge E7-11; viscometer vpzh-2; meter R, L, C; pH meter pH-150MI with a combined pH electrode ESK-10603/7; photometer photoelectric KFK-3 "ZOMZ" BJ 2.853.021-02PS; flat capacitor; laboratory scales TVE-0.3-0.01, Michaelis device; press PSU-10.

Microwave oven SAMSUNG CE 101 KR with a frequency of 2.45 GHz and a power of 900 W; system consisting of permanent magnets, installation for microwave treatment of gypsum solutions (microwave generator-2450 MHz, waveguide, cell with polystyrene inserts).

The achievability of this goal was ensured by the features of technological techniques and methods based on the development of combined systems based on gypsum binders, which provided an increase in the conductive properties of the materials used.

The choice of calcium sulfate semihydrate as a material is due to its cheapness and ubiquity. Low-concentration metals and their solutions are used to regulate the conducting properties of composite systems.

To create a gypsum mixture with adjustable strength and electrophysical characteristics, combined methods of mixing water treatment (microwave and magnetic treatment) were used for the first time.

The source material for these studies will be calcium sulfate semihydrate of the Samara gypsum plant. The products of this plant are obtained by heat treatment of gypsum raw materials to obtain calcium sulfate, according to GOST 4013-82.

Gypsum of grade I and grade G-5 was used (5 MPa-compression limit and 2.5 MPa-bending limit), depending on the setting time, construction gypsum is normally hardening (index of hardening time B, i.e. the beginning of hardening, no earlier than 6 min, the end, no later than 30 min), gypsum II - medium grinding (the remainder on the sieve No. 2, calculated by the weight of the initial sample, is up to 14%).

3 Results and Discussion

Since the hydration process of gypsum binders is significantly affected by the properties of the mixing fluid, it is necessary to study its chemical and physical properties.

It is necessary to prepare solutions of iron chloride $FeCl_3$ of various concentrations of 0.01%, 0.1% and 1%.

Treatment with a permanent magnetic field of 130 MT for 2 min: a solution of various concentrations was placed in a chemical dish permeable to the magnetic field, and then in the field of action of a permanent magnet.

At the next stage, the electrical conductivity, viscosity, optical density, pH, and permittivity of the obtained solutions are studied.

The electrical conductivity of water was determined using an E7-11 bridge at a frequency of 1000 Hz in a Jones-type quartz cell calibrated with 0.1 and 1.0 N KCl solution. The value of the constant cell for 298 K is determined by a well-known formula. The kinematic viscosity of solutions is determined by a well-known method, according to GOST 10028-81 using a capillary viscometer.

Table 1 shows the dependence of the specific electrical conductivity on the concentration of solutions.

Table 1. Dependence of the specific electrical conductivity on the solution concentration.

	Concentration, %	Electrical conductivity gypsum binders, $10^{-3}Om^{-1}m^{-1}$	Electrical conductivity gypsum binders, $10^{-3}Om^{-1}m^{-1}$	Electrical conductivity gypsum binders, $10^{-3}Om^{-1}m^{-1}$
$FeCl_3$	0.01	2.47	15.33	4.79
	0.1	6.97	14.38	8.21
	1	9.58	14.38	32.86
$CuCl_3$	0.01	1.77	3.33	5.23
	0.1	3.90	4.42	9.58
	1	7.42	17.70	15.33
$CoCl_2$	0.01	1.28	1.97	3.19
	0.1	1.87	2.40	3.03
	1	2.88	10.00	6.39
$NiCl_2$	0.01	1.76	2.84	3.38
	0.1	2.42	5.90	5.00
	1	2.58	3.03	7.93
Cu $(NO_3)_2$	0.01	1.93	4.18	2.88
	0.1	3.54	4.18	6.57
	1	5.11	4.69	9.58
Co $(NO_3)_2$	0.01	1.80	1.68	1.69
	0.1	2.84	3.65	5.00
	1	4.69	5.48	5.48
Ni $(NO_3)_2$	0.01	1.72	2.42	2.71
	0.1	2.21	3.11	4.34
	1	3.49	3.59	5.00

The pH factor of solutions was determined using a pH meter: pH-150 MI with a combined PH electrode ESK-10603 with an accuracy of ± 0.02 pH.

The cell was made of organic glass, which contained steel electrodes located at a certain distance, necessary for measuring electrical conductivity.

A sample of the test solution was placed in this container and the value of the electrical capacity of the control sample of the solution (without treatment) C0 and the test CX (after treatment) was measured, the dielectric constant ε was determined by their ratio. Processing with a 900 W microwave field at 10% power over 10 s (2.7 kJ/mol of microwave energy).

Then a combined method is applied (magnetic + microwave) treatment of the mixing water. The specific electrical conductivity of the solution $\delta = 1 / p$ Ohms-1 m^{-1} was calculated using the formula (1).

$$\delta = k/R, \tag{1}$$

where R is the electrical resistance,
k is the cell constant that was calculated using the formula (2):

$$k = \frac{0.2765}{1.2 \cdot 10^{-3}} = 230\,\text{m}^{-1} \tag{2}$$

Treatment with a constant magnetic field of 130 MT was carried out for 2 min. Processing with a 900 W microwave field at 10% power for 10 s (2.7 kJ/mol of microwave energy).

The combined combination of microwave fields and magnetic fields, as well as chemical additives of metals with a low concentration of mixing water for gypsum binders is still not studied.

The proposed studies and the compiled dependence allow us to identify the most approximate solutions by electrophysical characteristics for the use of mixing water in the production of conductive gypsum systems.

It was found that the regularities of the action of the activated microwave field, magnetic field and combined method of water and solution treatment are particularly noticeable for iron chloride ($FeCl_3$), which significantly affected the features of the process of hydration and structure formation of gypsum binders.

At the next stage, the effect of these fields on the kinematic viscosity is analyzed. The kinematic viscosity of the solutions was determined using a time viscometer and calculated using the formula 3.

$$V = g/9.807 * t * k, \tag{3}$$

where k is the viscometer constant (0.03275 mm^2/s^2), g = 9.81 m/s^2.

Table 2 shows the results of the dependence of the kinematic viscosity of water on the treatment method.

Table 2. Dependence of kinematic viscosity on the concentration and method of treatment of solutions.

	Concentration, %	Without processing $*10^{-6}$	The processing by the magnetic field $*10^{-6}$	The magnetic field +microwave treatment $*10^{-6}$
$FeCl_3$	0.01	1.18	1.15	1.05
	0.1	1.18	1.18	1.02
	1	1.25	1.28	0.95
$CuCl_3$	0.01	1.25	1.25	1.08
	0.1	1.31	1.31	1.08
	1	1.25	1.41	1.12
$CoCl_2$	0.01	1.25	1.38	1.02
	0.1	1.31	1.05	1.12
	1	1.18	1.28	0.98
$NiCl_2$	0.01	1.21	1.25	1.12
	0.1	1.25	1.31	1.18
	1	1.18	1.25	0.98
Cu $(NO_3)_2$	0.01	1.28	1.28	1.02
	0.1	1.31	1.31	1.15
	1	1.31	1.31	1.12
Co $(NO_3)_2$	0.01	1.18	1.25	1.05
	0.1	1.31	1.21	1.12
	1	1.18	1.31	1.08
Ni $(NO_3)_2$	0.01	1.18	1.25	1.05
	0.1	1.31	1.21	1.12
	1	1.25	1.28	1.05

By changing the kinematic viscosity of solutions, it becomes possible to change not only the properties of the mixing water, but also to adjust the setting time and the processes of structure formation of oxide systems, and the strength of the hardening structures increases significantly after pre-treatment with magnetic fields and microwave fields.

Low-concentration water-salt solutions used to produce highly structural composites with a complex of properties, including high strength, have been studied.

4   Conclusion

Methods developed for exposure to microwave fields (2450 MHz), magnetic field (130 mTl) and combined treatment on the structure and properties of water and aqueous solutions depending on processing time, thereby contributing to the change of physico-chemical parameters (conductivity, dynamic viscosity, dielectric constant and pH-factor). The possibility of regulating the rate of physical and chemical processes, the duration of individual periods, the setting time, and the structure formation of calcium sulfate dihydrate is revealed. The dependence between the energy-activation characteristics of the water of the mixing and the values of technological processes is revealed. These techniques will help maintain the necessary thermal balance for the corresponding wall and floor coverings, as well as the durability of these coatings made of relatively inexpensive and environmentally friendly materials based on gypsum binders.
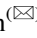
References

1. Gladkikh, Y., Yadykina, V.V., Zavrazhina, V.I.: Improving the quality of quartz aggregate by irradiation. J. Construc. Mater. **6**, 32–33 (1986)
2. Pavlenko, V.I., Gladkikh, Y., Lapteva, S.N.: Effect of activated tempering water and filling the aggregate surface on the hardening kinetics of gypsum blends. Int. J. Pharm. Technol. **8**(4), 24760–24769 (2016)
3. Lapteva, S.N.: Method of microwave processing of dielectric substances (variants) Patent 2570293 Russian Federation. BSTU named after V.G, Shukhov (2016)
4. Gorlenko, N.P., Mokrousov, G.M.: Fluid Motion in crossed magnetic and electric fields. Bull. Tomsk Polytech. Univ. **306**, 72–74 (2003)
5. Pavlenko, V.I., Lapteva, S.N., Barbanyagre, V.D.: Influence of microwave irradiation of tempering water on the process of crystallization of calcium sulfate dihydrate. Phys. J. **60**(7), 1243–1247 (2017)
6. Maslov, A.F., Gladkikh, Yu.P., Kulikova, S.N.: Influence of Water Treated With Microwave Irradiation on the Kinetics of Gypsum Hardening. VSTU Publishing House, Voronezh (2007)
7. Zavrazhina, V.I., Gladkikh, Y.: On the hydroxylation of the surface of calcium sulfates in aqueous media and their hardening processes. J. Appl. Book **2**, 184–187 (2010)
8. Klimenko, V.G., Hasanov, S.K., Kashin, G.A., Mamin, S.N.: Hypsomagnetite composites for protection from ionizing radiation. Bull. BSTU Named After V. G. Shukhov **9**, 100–105 (2017)
9. Lesovik, V.S., Absemetov, M.V., Elistratkin, M.Yu., Pospelova, M.A., Shatalova, S.V.: On the issue of studying the features of structure formation of composite binders for non-autoclave gas-concrete. Construc. Mater. Products **2**(3), 41–47 (2019)
10. Slesarev, V.I., Shabrov, A.V.: Influence of water structure on its static and dynamic properties. Fund for development of new medical technologies "Aires", Moscow (2002)

11. Vaks, V.L., Domrachev, M.A., Rodygin, Y., Selivanovsky, D.A., Spivak, E.I.: Dissociation of water under the action of microwave radiation. Izv. Higher educational. Radiophysics **37**, 149–153 (1994)
12. Klimenko, V.G.: Multicomponent Activators of Hardening of Composite Anhydrite Binders. Monograph. BSTU named after V.G. Shukhov, Belgorod (2018)
13. Cherevatova, A.V., Zhernovskaya, I.V., Alyokhin, D.A., Kozhukhova, M.I., Kozhukhova, N.I., Yakovlev, E.A.: Theoretical aspects of creating a composite nanostructured gypsum binder of increased heat resistance. Construc. Mater. Products **2**(4), 5–13 (2019)
14. Pavlenko, V.I., Lapteva, S.N.: Study of the hardening process of gypsum binders closed with water activated by an ultrahigh-frequency electromagnetic field. Chem. Chemical Technol. **60**(8), 47–52 (2017)
15. Lapteva, S.N., Pavlenko, V.I., Gladkikh, Yu.P.: Microwave treatment of surface-modified quartz sand and its effect on the hardening and strength of gypsum sand compositions. Bull. BSTU Named After V.G. Shukhov **12**, 152–154 (2016)

Sorption Extraction of Zn^{2+} Ions from Aqueous Environment with Zoo Compost of Black Soldier Fly

S. V. Sverguzova [ID], I. V. Bomba [ID], and E. A. Pendyurin[(✉)] [ID]

Belgorod State Technological University named after V.G. Shukhov,
Belgorod, Russia
pe@intbel.ru

Abstract. The paper presents the results of experimental studies to determine the possibility of sorption extraction of zinc ions (Zn^{2+}) from aqueous environment using the zoo compost of the Black soldier fly (Hermetia illucens). The indicators of zoo compost on the content of biogenic elements in it are given. The adsorption of zinc ions was studied on model solutions using a static method at a temperature of 20 °C and a sorption interaction time of 24 h. The concentration of Zn^{2+} ions in the initial and purified solutions was determined photocolorimetrically at a wavelength of λ = 213.8 nm. The obtained values of the concentrations of zinc ions in solutions before and after the adsorption process were used to determine the sorption capacity of the material (A). It was found that the maximum sorption capacity of the zoo compost for zinc ions is 0.149 mmol/g. To determine the mechanism of the process, the resulting adsorption isotherm was processed using the Langmuir, Freundlich, and Dubinin-Radushkevich models. It is established that the adsorption process is well described by the Langmuir isotherm, which indicates the course of monomolecular adsorption. The necessary constants and thermodynamic parameters are calculated. The Gibbs energy of the adsorption process is determined, the negative value of which indicates the spontaneous flow of the process.

Keywords: Zoo compost · Zinc ions · Adsorption

1 Introduction

According to the UN, currently the world's population stands at more than 7.6 billion and will reach 10 billion by 2050. Population growth is associated with the need to produce more and more food.

In this regard, the production of protein from insects is considered promising for use in aquaculture, poultry farming, and in the production of feed for agricultural and non-productive animals. At the same time, in many countries, the technology of producing a large amount of protein feed additives from the larvae of the black soldier fly is widely used at minimal cost. The larva of the black soldier fly develops for three weeks and increases its mass more than 1000 times during its life cycle. According to literature sources [1] the larvae of the black soldier fly can process any organic waste.

The waste of the larva of the black soldier fly (Hermetia illucens) is zoo compost. Zoo compost is a loose organic substance with a particle size of 1–3 mm of dark brown color with a very weak smell of ammonia, which has a high moisture capacity and moisture resistance. It is poorly clod, can be used as a lifter.

In addition, the zoo compost contains humic substances that are known to be able to bind heavy metal ions into chelate complexes [2].

In this paper, the possibility of using zoo compost as a sorption material for extracting Zn^{2+} ions from aqueous environment and binding them to poorly soluble and inactive compounds in order to reduce the content of Zn^{2+} ions in soil solutions is studied.

We used zoo compost "Germetsia" provided by LLC "EcoProtein" (Moscow region).

2   Materials and Methods

Generalized indicators of zoo compost and the content of biogenic elements in it, previously studied by Pendyurin E.A., Rybina S.Yu., et al. [3], are presented in Table 1.

Table 1. Content of biogenic components in the zoo compost.

Sample	Nitrates, (NO_3^-), mg/kg	Nitrites (NO_2^-), mg/kg	Ammonium ion (NH_4^+), mg/kg	Total nitrogen (N), mg/kg	Sorg., %	Humus,%	P_2O_5, mg/100 g	Fe_2O_3, mg/100 g
1	656.2 ± 28.06	2.66 ± 0.20	8178.7 ± 1795.4	6871.15 ± 1473.9	17.20 ± 0.27	29.65 ± 0.27	120.33 ± 28.00	26.00 ± 2.63
2	582.03 ± 62.72	2.42 ± 0.16	7882.1 ± 1196.9	6602.2 ± 985.8	18.27 ± 1.03	31,50 ± 1,03	31.50 ± 1.03	25.43 ± 1.73

A solution containing zinc ions (Zn^{2+}) in concentrations from 10 to 50 mg/dm^3 was prepared by dissolving the $ZnSO_4 \times 7\ H_2O$ (ch.p.) reagent in distilled water.

The biocompost was dried to a constant weight at a temperature of 105 °C in a drying cabinet of the IT-4610 brand.

The adsorption of Zn^{2+} ions by zoo compost was studied by a static method at a temperature of 20 °C and a sorption interaction time of 24 h. The volume of the solution taken for research, in all cases, was 100 cm^3, the mass of the added zoo compost was 0.5 g. After the end of shaking, the contents of the reaction flasks were filtered through a paper filter.

The concentration of Zn^{2+} ions in the initial and purified solutions was determined by the photocolorimetric method at a wavelength λ = 213.8 nm, using a KFK-3 "ZOMZ" photocolorimeter. The obtained values of the concentrations of zinc ions in solutions before and after the adsorption processes were used to determine the sorption capacity of the material (A) using the formula (1):

$$A = \frac{C_{init} - C_{comp} \times 100}{0.5 \times 1000} \qquad (1)$$

where C_{init} – initial concentration of zinc ions, mg/dm^3; C_{comp} – equilibrium concentration of zinc ions, mg/dm^3; 0.5 – weight of the sorption material added to the solution, g; 1000 – transition from cm^3 to dm^3.

3 Results

Based on the obtained data, we construct the adsorption isotherm (Fig. 1).
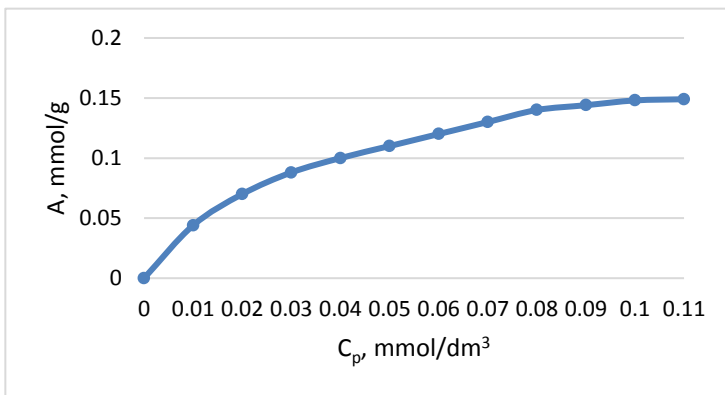
Fig. 1. Adsorption isotherm of Zn^{2+} ions with the zoo compost of the black soldier fly (Hermetia illucens). (Color figure online)

Based on Fig. 1, it is obvious that the adsorption isotherm of zinc ions on the surface of zoo compost particles belongs to type I isotherms according to the BDDT classification (Brunauer, Deming, Deming, and Teller) and describes monomolecular adsorption. The maximum sorption capacity in this case is 0.149 mmol/g or 9.69 g/g.

Zinc is a highly toxic substance, it is included in the group of substances belonging to the I hazard class of chemicals [4] and has a negative effect on humans and animals [5]. It leads to a decrease in crop yields, worsens the quality of products, violates immune barriers, which leads to the damage to plants of diseases and pests. In addition, zinc significantly inhibits enzymes in the soil.

It is known that heavy metals can be found in soils in the form of ions, organic compounds, or mineral salts. The part of heavy metal compounds that is contained in the soil solution is the most mobile and accessible to plants. The amount of metal ions entering the soil solution determines the toxicity of a particular metal in the soil [6–9].

In small concentrations, zinc increases plant resistance to dry and hot weather conditions, bacterial and fungal diseases [10–13]. The accumulation of excess zinc in the soil affects negatively most soil processes: causes changes in the physical and physical-chemical properties of soils, reduces their biological activity [14, 15].

To reduce the mobility of zinc in soils, it is possible to use the processes of formation of poorly soluble zinc compounds: hydroxide, basic salts, chelate complexes, as well as its binding by sorption materials.

There are known methods for adsorption of metal ions by various inorganic and cellulose-containing industrial and crop waste [16–21].

To determine the adsorption mechanism, the resulting isotherm was processed using the Langmuir, Freundlich, and Dubinin-Radushkevich adsorption models. The results of processing the isotherm in the framework of these models are shown in Figs. 2, 3 and 4. The Langmuir, Freundlich, and Dubinin-Radushkevich constants are given in Table 2, 3 and 4.
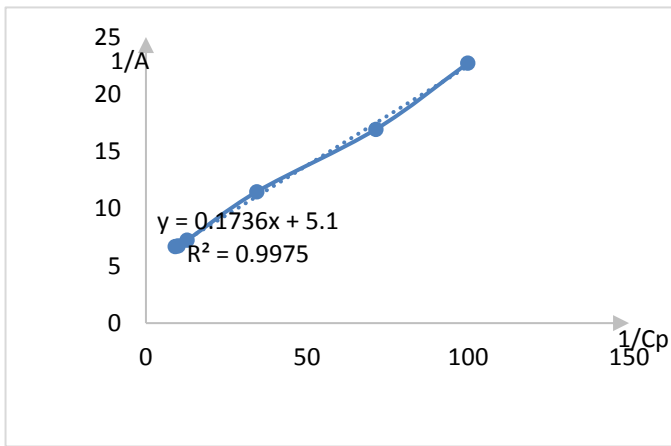
Fig. 2. Langmuir Isotherm.

Table 2. Langmuir constants.

$1/A = 1/A\infty + 1/(KLA\infty Cp)$			
$y = 5.1 + 0.1736x$			
$1/A\infty=$	5.099991	$1/(KLA\infty)=$	0.173597
$A\infty=$	0.196079	$KL=$	29.37837
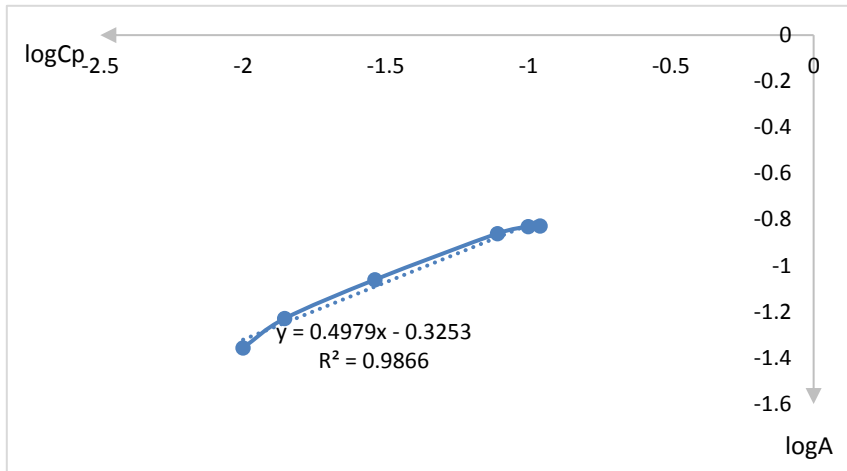
Fig. 3. Freundlich isotherm.

Table 3. Freundlich constants.

logA = logKF + 1/n logCp			
y = − 0.3253 + 0.4979x			
logKF=	−0.3253	1/n =	0.497878
KF=	0.472824	n=	2.008523
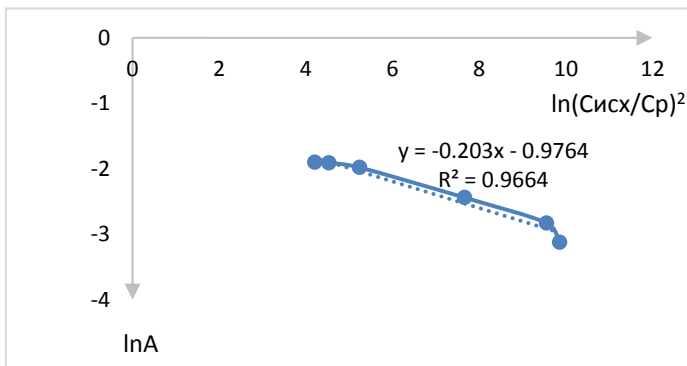
Fig. 4. Dubinin-Radushkevich isotherm.

Table 4. Dubinin-Radushkevich constants.

lnA = lnA∞ −(R*T/E)2 * (ln(Cinit/Cp))2			
y = − 0.9764 – 0.203x			
lnA∞=	−0.97642	(R*T/E)2=	0.20298
A∞=	0.376657	E=	5499.463

It follows from the calculations that the best description of the adsorption process is the Langmuir isotherm (R^2 = 0.9975), which indicates the course of monomolecular adsorption of Zn^{2+} ions on the zoo compost. The sorption energy determined using the Dubinin-Radushkevich equation (E, J/mol) is equal to 5499.463 J/mol or 5.499 kJ/mol, which indicates the physical nature of adsorption.

Using the Langmuir constant (KL), the Gibbs energy, ΔG_o, J/mol, was determined by Eq. (2):

$$\Delta G_0 = -RTlnKL, \tag{2}$$

where R – universal gas constant, 8.13 J/mol × K; T – temperature in Kelvin degrees; KL – Langmuir constant, in our case KL = 29.378.

ΔG_o = − 8.13 × 298 × 3.38 = − 8188.86 J/mol or −8.19 kJ/mol.

A negative value of ΔG_o indicates a spontaneous process.

4   Conclusion

Thus, in the course of research, it was found that the zoo compost of the black soldier (Hermetia illucens) fly larva has sorption properties, the maximum sorption capacity is 0.149 mmol/g, and its addition to soils reduces the proportion of mobile forms of zinc compounds.

References

1. Sapronova, Zh.A., Shaykhiev, I.G., Sverguzova, S.V., Danshina, E.P.: Valuable properties of Hermetia illucens fly larvae and possible products of their processing. Bull. Tomsk Univ. Biol. Sect. **54**(2), 316–325 (2020)
2. Vasilenko, M.I., Goncharova, E.N., Serykh, E.Yu.: Zoo compost of Hermetia illucens larvae as a type of biocompost. In: International Scientific Conference "Rational Use of Natural Resources And Processing of Technogenic Raw Materials: Fundamental Problems of Science, Materials Science, Chemistry And Biotechnology". BSTU, Belgorod, pp. 300–305 (2020)

3. Pendyurin, E.A., Rybina, S.Yu., Smolenskaya, L.M., Shaporov, M.V.: Zoo compost of the black soldier as a fertilizer. In: International Scientific Conference "Rational Use of Natural Resources and Processing of Technogenic Raw Materials: Fundamental Problems of Science, Materials Science, Chemistry and Biotechnology". BSTU publishing house. Belgorod, pp. 316–319 (2020)

4. Belous, N.M., Shapovalov, V.F., Moiseenko, F.V., Draganskaya, M.G.: Influence of various fertilizer systems on the accumulation of heavy metals in agricultural products. Bull. Bryansk State Agric. Acad. 22–29 (2006)

5. Alekseev, Yu.V.: Heavy Metals in Soils and Plants. Agropromizdat, Moscow (1987)

6. Medvedev, I.F., Derevyagin, S.S.: Heavy Metals in Ecosystems. Rakurs, Saratov (2017)

7. Dubovik, D.V., Dubovik, E.V.: Heavy Metals in the Slope Agricultural Landscape. RRIASPE, Kursk (2016)

8. Ovcharenko, M.M.: Heavy Metals in the Soil-Plant-Fertilizer System. Proletar. Svetoch, Moscow (1997)

9. Sokolova, O.Ya., Sryapkov, A.V., Antimonov, S.V., Solovykh, S.Yu.: Heavy metals in the system element-soil-grain crops. Bull. OSU **4**, 106–110 (2006)

10. Andrievskaya, L.P.: Accumulation of heavy metals in agricultural landscapes of the Lower Volga region. Fundamentals of achieving sustainable agricultural development. VSAA, Volgograd (2004)

11. Zborishchuk, Yu.N: Average content of B, Mn Co, Cu, Zn, Mo, and J in soils of the European part of the USSR. Agrochemistry **3**, 88–94 (1974)

12. Ilyin, V.B.: On the development of MPC of heavy metals in soils. Agrochemistry **11**, 94–101 (1985)

13. Kovalsky, V.V.: Microelements in the soils of the USSR. Moscow (1970)

14. Protasova, N.A.: Microelements (Cr, V, Ni, Mn, Zn, Cu, Co, Ti, Zr, Ga, Be, Sr, Ba, B, I, Mo) in chernozems and gray forest soils of the Central Chernozem region. Voronezh (2003)

15. Chernykh, N.A.: Ecotoxicological aspects of soil contamination with heavy metals. Puschino (2001)

16. Stepanova, S.V., Shaykhiev, I.G., Sverguzova, S.V.: Purification of model effluents containing heavy metal ions by wheat husk. Bull. BSTU named after V.G. Shukhov **6**, 183–186 (2014)

17. Sverguzova, S.V., Sapronova, Zh.A., Shaykhiev, I.G., Sapronov, D.V.: Use of corn processing waste for cleaning water media from the dye "Methylene blue". Bull. Kazan Technol. Univ. **17**(5), 173–175 (2014)

18. Sverguzova, S.V., Sapronova, Zh.A., Shaykhiev, I.G., Valiev, R.R.: Use of gabbro-diabase processing waste for wastewater treatment. Bull. Kamchatka State Technol. Univ. **45**, 6–11 (2018)

19. Sverguzova, S.V., Sapronova, Zh., Hunadi, L., Spesivtseva, S.E.: Extraction of the dye "methylene blue" from an aqueous solution by sorption materials from peanut shells. Bull. BSTU named after V.G. Shukhov **23**(1), 79–83 (2020)

20. Sverguzova, Zh.A., Elnikov, D.A., Sverguzova, S.V.: On the possibility of using sugar industry waste for wastewater treatment. Bull. BSTU named after V.G. Shukhov **3**, 128–133 (2011)

21. Sverguzova, S.V., Sapronova, Zh.A., Svyatchenko, A.V., Otiti, T.: Adsorption of spindle oil by native and thermo modified leaf litter of chestnuts. Constr. Mater. Prod. **1**(1), 4–11 (2018)

Porous Magnesia Compositions
with Various Fillers

O. A. Miryuk[(✉)]

Rudny Industrial Institute, Rudny, Kostanay Region, Kazakhstan
psm58@mail.ru

Abstract. The paper presents the results of studies of magnesia compositions of porous structure. The possibility of pore formation in the structure of magnesia materials by various technological methods is shown. It was found that the high adhesive capacity of magnesia binders allows the use of fillers of various origins in compositions. The characteristics of magnesia compositions containing an ash microsphere, expanded polystyrene, expanded granules based on liquid glass, and porous magnesia granules are determined. A combination of porization methods is proposed for the formation of low-density magnesia compositions. A comparative analysis of the mechanical and thermal properties of porous magnesia compositions of various preparations is carried out. The advantages of complex porization of magnesia compositions due to a combination of mechanisms of foaming, gas formation and insertion of fillers of a porous structure are revealed. Magnesia compositions containing integral fillers of various shapes and origins are proposed. Multi-component compositions are characterized by a density of 540 kg/m^3 and a compressive strength of 4.1 MPa. The impact of the method of preparing the molding mixture on the strength of porous structures is established. Porous raw materials were developed to produce granulated magnesia aggregate based on caustic magnesite and wood particles. Magnesia aggregate granules are used to obtain granular-cellular and coarse-pore structure of compositions.

Keywords: Magnesia compositions · Granular porous aggregate · Molding properties · Swelling · Porous structure

1 Introduction

Magnesia binders are an effective type of low-energy materials characterized by intensive hardening and high strength indicators. The advantages of a magnesia binder are determined by the low energy consumption of production; the ability to harden intensively; high strength and wear resistance; adhesion to any type of aggregate, especially organic; resistance to oils, alkalis, and salts. In many properties, magnesia binder is superior to Portland cement: it does not require a wet environment when hardening; it is decorative and environmentally friendly; provides high fire resistance and low thermal conductivity; has a neutral composition of hardening products; due to a significant amount of chemically bound water, it is suitable for biological protection [1–10].

The combination of caustic magnesite with natural and technogenic materials expands the range and increases the volume of production of magnesia cements. Advantages of mixed binders are in improving physical and mechanical characteristics while saving magnesia cement and rational use of natural and technogenic silicates [1, 6, 7].

Analysis of scientific and technical information indicates the active development of the technology of magnesia composite materials with different structures and characterized by a wide range of properties.

The aim of this work is to study porous magnesia compositions with fillers of various origins.

2   Materials and Methods of Research

To obtain magnesia compositions, caustic magnesite of the PMK – 75 brand with a content of 80–85% of active MgO was used. Characteristics of the binder: fineness of grinding – 5% of the residue on the sieve № 008; normal density 40–45%; setting time: beginning 20 min; ending – 2 h 40 min. On the basis of caustic magnesite, mixed binders were prepared, into which a technogenic fine ground filler was inserted – refuse magnetite ores. Chemical composition of technogenic filler, wt%: $SiO_{2-4}1$; Al_2O_3 – 13; Fe_2O_3 – 16; CaO – 12; MgO – 6; SO_{3-4}; R_2O_{3-3}; other – 2; p.o.i. – 3. Calcium silicates and aluminosilicates form the mineral basis of refuse magnetite ore.

Magnesium chloride solution with a density of 1230 kg/m^3 was used for mixing magnesia compositions. To form the porous structure of magnesia materials, a protein-based foaming agent was inserted; the gas-forming agent was an aqueous solution of hydrogen peroxide H_2O_2 with a concentration of 40%.

Materials of various origin are used as aggregates of magnesia compositions: ash microspheres, expanded polystyrene, granules based on liquid glass and magnesia granular particles.

Microspheres of energy ash are hollow solid particles of small size: particles with a diameter of 100–250 microns make up almost 75%; particles smaller than 100 microns– up to 15%; other spheres with a diameter of 250–500 microns. The bulk density is 400 kg/m^3.

Granular polymer aggregate – expanded polystyrene – granules up to 5 mm in size, obtained by breaking down used foam packages with a bulk density of 15 kg/m^3.

Swelling granules based on liquid glass (Fig. 1). – a porous aggregate synthesized by thermal expansion of a mass based on liquid glass and a silica-containing filler (for example, broken glass, gaize rock, oil shale, and others).
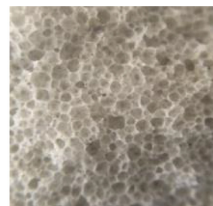
appearance   structure

Fig. 1. Swelling granules based on liquid glass.

Expanded granules of 5–10 mm fraction with a bulk density of 200 kg/m^3 were used Granulated magnesia aggregate – particles of 5–10 mm in size with a bulk density of 500 kg/m^3 (Fig. 2).

<div align="center">appearance   structure</div>

Fig. 2. Granulated magnesia aggregate.

The aggregate is obtained from a molding mass containing a magnesia binder, wood particles and a pore-forming agent.

3   Results and Discussion

The insertion of an ash microsphere into the magnesia mixture is accompanied by a decrease in the density of the composite material (Table 1). The strength of the compositions depends on the fraction of the ash microsphere and decreases as the structure is saturated with hollow particles, which is obvious for the systems under study. The properties of the compositions are largely determined by the composition of the mixed binder. The content of the ash microsphere should be limited to 20%, as an increase in the proportion of porous particles causes a shortage of binder for binding the microsphere.

Table 1. Influence of microspheres on the properties of magnesia compositions.

Content of technogenic filler in the binder, %	Content of the microsphere, %	Average density, kg/m^3	Tensile strength at compression, MPa
0	0	1879	67
0	5	1750	60
0	10	1578	48
0	15	1616	45
0	20	1441	37
0	30	1384	32
30	10	1768	53
50	10	1796	49
50	5	1956	55

The use of mixed binders is advisable with a limited content of the porous component in order to avoid a sharp deterioration in the technological properties of the molding mass.

The nature of the influence of the microsphere concentration does not differ in principle for binders of different material composition (Fig. 3). High strength of compositions with microspheres is due to the effect of magnesium chloride on the surface of aluminum silicate particles.

The insignificant solubility of the microspheres material in the medium of the chloride-magnesia matrix initiates the appearance of fibrous forms of aluminosilicate new formations on the surface, which contribute to increased adhesion to the matrix of the binder stone.
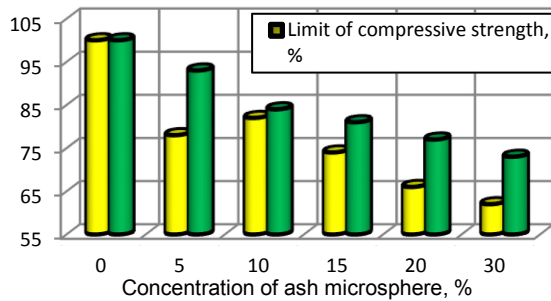
Fig. 3. Influence of the ash microsphere content on the composition properties.

An effective porous technogenic aggregate is expanded polystyrene granules formed during the destruction of used containers. Expanded polystyrene granules are one of the lightest concrete aggregates.

Expanded polystyrene granules are inserted to reduce the consumption of the binder, as well as to improve the thermal insulation characteristics. Practical implementation of the developments will lessen the cost of production and reduce environmental tensions in the regions.

To obtain a homogeneous technological molding mixture, a mobile mass of binder is required, enveloping light polystyrene granules. For this purpose, it is advisable to porize the binder paste, the density of which significantly exceeds the similar characteristic of expanded polystyrene. The uniformity of distribution of expanded polystyrene granules in the structure of compositions increases when using foam mass. To form stable magnesia foam mass, it is necessary to introduce 2.5–3.0% of the foaming agent.

Masses with different amounts of expanded polystyrene granules were studied (Table 2). Preparation of the molding mixture involves: at the first stage, foam mass is obtained in a mixer for 2.5 min, at the second stage, expanded polystyrene granules are added and mixed together until a homogeneous state is obtained. The porizing components complete each other, creating a composite with a density of 300 kg/m^3 or less.

To make the molding mass, a solution of magnesium chloride with a density of 1230 kg/m^3 was poured into the mixing container, a protein foaming agent was added, and then the mixed binder was filled in. The resulting suspension was foamed in a blender type mixer.

The insertion of expanded polystyrene granules significantly reduces the density and strength of magnesia samples.

Table 2. Influence of expanded polystyrene on the properties of the foam-magnesium composition.

Amount of expanded polystyrene, %	Density, kg/m^3	Strength at the age of 7 days, MPa
0	520	5.8
4	330	3.4
7	200	1.2
10	150	0.8

These compositions are appropriate as a heat-insulating part (central) in three-layer composite products, which must have a low density, heat-protective qualities and adhesion of foam mass with granules.

Expanded polystyrene granules together with foam mass can provide an effective combined structure with a low density.

For the formation of low-density magnesia compositions, a combination of porization methods is proposed (Table 3).

Table 3. Comparative characteristics of magnesia compositions.

Method for forming a porous structure	Density, kg/m^3	Thermal conductivity, W/ (m·^{0}C)	Compressive strength, MPa
Foam formation	525	0.07	4.3
Gas formation	650	0.09	4.6
Foam formation + gas formation	390	0.05	2.2
Foam formation + microsphere	435	0.08	3.6
Foam formation + expanded polystyrene granules	285	0.05	1.0
Foam formation + swelling granules on the liquid glass basis	350	0.05	3.2
Foam formation + gas formation + expanded polystyrene granules	220	0.04	0.8

When hydrogen peroxide is added to foam mass in the composition of the formed pores of different types: large cells and small gas pores of the foam, located in partitions between large are formed (Fig. 4). The possibility is shown of additional pore foam mass and the combined framework by 5–20% porous granules. When inserting expanded polystyrene granules into the foam mass, the density decreases by 1.8 times.

To create a cellular-granular structure, swelling granules of liquid glass were inserted. It is possible to reduce the density of the compositions by 33%.
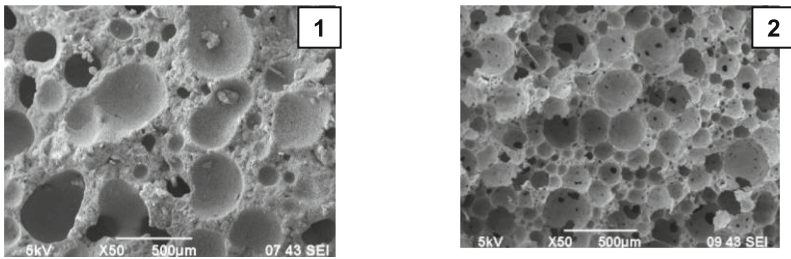
1 – gas formation; 2 – foam formation + gas formation + 15 % microspheres

Fig. 4. Microstructure of magnesium compositions with different porization.

Compositions based on a mixed magnesia binder and integral aggregate "expanded polystyrene – wood particles – ash microsphere" are proposed. Optimization of the particle ratio makes it possible to obtain a combined structure that is maximally "packed" with different pores. The compositions are characterized by a density of 350–650 kg/m^3 and a compressive strength of 1–7 MPa.

A rational method for preparing the molding mass is determined, which provides for the initial contact of the binder with a solution of magnesium chloride; then the addition of step-by-step fillers. The method will provide increased strength, uniform distribution of components. As a fibrous component, substandard wool and waste from the production of mineral wool were used. Technogenic fibre (2%) provide hardening of interporous partitions of aerated structure.

To obtain porous compositions, a granulated magnesia aggregate was used, which was inserted into the molding foam mass at a ratio of "binder: filler" – 30:70%. The resulting magnesia concrete is characterized by a density of 540 kg/m^3 and a compressive strength of 4.1 MPa (Fig. 5).

1 – porous structure;   2 – large-pore structure

Fig. 5. Structure of compositions with porous magnesia aggregate.

Granulated magnesia aggregate can be used in coarse-pored concrete with a density of 510 kg/m^3 and a strength of 2.2 MPa.

4   Conclusion

The possibility of creating porous compositions based on mixed magnesia binders and aggregates of different composition and structure is proved. The expediency of combining the mechanisms of foam and gas formation for the formation of a cellular structure is shown. The conditions and advantages of combined structures due to the combination of cellular, granular and fibrous porosity are determined.

References

1. Chen, L., Wang, L., Daniel, C.W., Tsang, V., Chi, M., Poon, S.: Efficacy of green alternatives and carbon dioxide curing in reactive magnesia cement-bonded particleboards. J. Clean. Product. **258**, 120997 (2020)
2. Xu, B., Ma, H., Hu, C.: Influence of curing regimes on mechanical properties of magnesium oxychloride cement-based composites. Constr. Build. Materials **102**, 613–619 (2016)
3. Ba, M., Xue, T., He, Z., Wang, H., Liu, J.: Carbonation of magnesium oxysulfate cement and its influence on mechanical performance. Constr. Build. Mater. **223**, 1030–1037 (2019)
4. Zhu, H., Yu, H., Ma, H., Yang, S.: Uniaxial compressive stress-strain curves of magnesium oxysulfate cement concrete. Constr. Build. Mater. **232**, 117244 (2020)
5. Ruan, S., Unluer, C.: Influence of supplementary cementitious materials on the performance and environmental impacts of reactive magnesia cement concrete. J. Clean. Product. **159**, 62–73 (2017)
6. Kumar, S., Sonat, C., Yang, E.-H., Unluer, C.: Performance of reactive magnesia cement formulations containing fly ash and ground granulated blast-furnace slag. Constr. Build. Mater. 232, 117275 (2020)
7. Miryuk, O.A.: Properties of magnesium composite materials based on technogenic raw materials. ARPN J. Eng. Appl. Sci. **2**(13), 545–558 (2018)
8. Mitina, N.A., Revva, I.B., Ditts, A.A., Simonov, D.V.: Waterproof magnesia binder for composite. Mater. Key Eng. Mater. **712**, 182–187 (2016)
9. Miryuk, O.A.: Porous magnesia compositions of a combined structure. IOP Conf. Ser. Mater. Sci. Eng. Mod. Build. Mater. **365**(3), 032052 (2018)
10. Xiangming, Z., Zongjin, L.: Light-weight wood-magnesium oxychloride cement composite building products made by extrusion. Constr. Build. Mater. **27**, 382–389 (2012)

Correction to: Strengthening of the Adhesive Joint in the Production of Glued Beams

S. I. Ovsyannikov ⓘ, A. A. Suska ⓘ, D. A. Levkin ⓘ, and O. L. Rudenko ⓘ

In the original version of the book, the following correction has been incorporated: In Chapter 33, Reference 17 has been updated as Benvenuti, E., Orlando, N., Gebhardt, C., Kaliske, M.: An orthotropic multi-surface damage-plasticity FE-formulation for wood: Part I – Constitutive model. Computers & Structures 240 (2020).

Author Index